LBL-28594

Lawrence Berkeley Laboratory
UNIVERSITY OF CALIFORNIA

EARTH SCIENCES DIVISION

Feasibility Analysis and Development of Foam Protected Underground Natural Gas Storage Facilities

P.A. Witherspoon, S. Benson, P. Persoff,
K. Pruess, C.J. Radke, and Y.-S. Wu

February 1990

Prepared for the U.S. Department of Energy under Contract Number DE-AC03-76SF00098.

LOAN COPY
Circulates
for 2 weeks
Bldg. 50 Library.
Copy 2
LBL-28594

DISCLAIMER

This document was prepared as an account of work sponsored by the United States Government. While this document is believed to contain correct information, neither the United States Government nor any agency thereof, nor the Regents of the University of California, nor any of their employees, makes any warranty, express or implied, or assumes any legal responsibility for the accuracy, completeness, or usefulness of any information, apparatus, product, or process disclosed, or represents that its use would not infringe privately owned rights. Reference herein to any specific commercial product, process, or service by its trade name, trademark, manufacturer, or otherwise, does not necessarily constitute or imply its endorsement, recommendation, or favoring by the United States Government or any agency thereof, or the Regents of the University of California. The views and opinions of authors expressed herein do not necessarily state or reflect those of the United States Government or any agency thereof or the Regents of the University of California.

FEASIBILITY ANALYSIS AND DEVELOPMENT OF FOAM PROTECTED UNDERGROUND NATURAL GAS STORAGE FACILITIES

FINAL REPORT
(January 1986 - June 1989)

Prepared by
Paul A. Witherspoon, Sally Benson, Peter Persoff,
Karsten Pruess, Clayton J. Radke and Yu-shu Wu

Earth Sciences Division
Lawrence Berkeley Laboratory
University of California
Berkeley, California 94720

For
Gas Research Institute
GRI Contract Number 5086-271-1160

GRI Project Manager
Yusuf A. Shikari
Manager, Storage Research

February 1990

Legal Notice

This report was prepared by Lawrence Berkeley Laboratory, operated by The Regents of the University of California (UNIVERSITY) on behalf of the U. S. Department of Energy (DOE), as an account of work sponsored by Gas Research Institute. Neither DOE, GRI, members of GRI, the University, LAB, nor any person acting on behalf of those parties:

''a. Makes any warranty or representation, express or implied, with respect to the accuracy, completeness, or usefulness of the information contained in this report, or that the use of any information, apparatus, method, or process disclosed in this report may not infringe privately owned rights; or

''b. Assumes any liabilities with respect to the use of, or for damages resulting from the use of, any information, apparatus, method or process disclosed in this report.''

Table of Contents

List of Figures vii

List of Tables ix

NTIS Report Documentation Page xi

Research Summary xiii

1.0. EXECUTIVE SUMMARY 1

1.1. Introduction 1
1.2. Experimental Approach 3
1.3. Experimental Findings 5
1.4. Foam Flow Modeling 6
1.5. Field Experiment Design 8
1.6. Recommendations 9

2.0. INTRODUCTION 11

2.1. Foam Protected Storage Concepts 12
2.2. Project Objectives 14

3.0. DESIGN AND CONSTRUCTION OF LABORATORY EQUIPMENT 21

3.1. Laboratory Facility for High-Pressure Foam Flow Experiments 21

4.0. LABORATORY INVESTIGATIONS 29

4.1. Surfactant Solution Screening and Formulation 30
4.1.1. Stable Foamer Solution Development 30
4.2. Foam Rheology in Porous Media 38
4.2.1. Foam Flow Experiments 38
4.3. Permeability Reduction by Foam 43
4.4. Foam Blocking Experiments 44
4.4.1. Blocking Trials Results 46

5.0. NUMERICAL SIMULATOR DEVELOPMENT 51

6.0. FIELD EXPERIMENT DESIGN 55

6.1. Proposed Field Experiment 56
6.2. Objectives 58

6.3. Field Operations 61
6.4. Budget 62

7.0. DISCUSSION AND CONCLUSIONS 71

8.0. REFERENCES 75

9.0. APPENDICES 77

A. Literature Survey Results A1

B. Summary of Experimental Data B1

C. Feasibility Analysis and Development of a Foam-Protected Underground Natural Gas Storage Facility C1

D. On PVT-Data, Well Treatment, and Preparation of Input Data for an Isothermal Gas-Water-Foam Version of MULKOM D1

E. A Laboratory Investigation of Foam Flow in Sandstone at Elevated Pressure E1

F. Aqueous Foams for Control of Gas Migration and Water Coning in Aquifer Gas Storage F1

G. Displacement of a Newtonian Fluid by a Non-Newtonian Fluid in a Porous Medium G1

List of Figures

Figure 2.1.	Schematic of gas injection with and without mobility control.	13
Figure 2.2.	Single well ''foam protected'' storage facility.	15
Figure 2.3.	Skirt well ''foam protected'' storage facility.	16
Figure 2.4.	Spill-point lowering with a ''foam-barrier''.	17
Figure 2.5.	Use of foam to seal fractures intersecting a mined cavern.	18
Figure 3.1.	High-pressure foam-flow apparatus (schematic).	22
Figure 3.2.	High-pressure foam-flow apparatus (photograph).	26
Figure 4.1.	Static foam longevity measured in drop tests, 1% Shell Enordet AES 911-2.5S in synthetic Mt. Simon brine, with varying amounts of Neodol 91.	34
Figure 4.2.	Static foam longevity measured in drop tests, 1% Shell Enordet AES 1213-6.5S in synthetic Mt. Simon brine, with varying amounts of Neodol 25.	34
Figure 4.3.	Static foam longevity measured in drop tests, 1% Shell Enordet AES 1215-9S in synthetic Mt. Simon brine, with varying amounts of Neodol 25.	35
Figure 4.4.	Static foam longevity measured in drop tests, 1% Shell Enordet AES 1215-3S in synthetic Mt. Simon brine, with varying amounts of Neodol 25.	35
Figure 4.5.	Duplicate tests of static foam stability, 1% Shell Enordet AES 1213-6.5S in synthetic Mt. Simon brine, with 0.1% Neodol 25.	36
Figure 4.6.	Duplicate tests of static foam stability, 1% Shell Enordet AES 1213-6.5S in synthetic Mt. Simon brine, with 0.2% Neodol 25.	36
Figure 4.7.	Duplicate tests of static foam stability, 1% Shell Enordet AES 1213-6.5S in synthetic Mt. Simon brine, with 0.35% Neodol 25.	37

Figure 4.8.	Grain size distribution of Ottawa Flint shot 3.0 sand used in foam rheology and blocking studies.	39
Figure 4.9.	Apparatus for foam rheology study in sandpacks, schematic.	43
Figure 4.10.	Foam rheology in sandpack. Plot of gas and liquid flow rates, gas injected at controlled pressure and liquid at controlled flow rate.	42
Figure 4.11.	Apparatus for forming foam blocks in sandpacks, schematic.	45
Figure 5.1.	The concept of reducing water coning in gas storage withdrawal well by means of a foam lens placed near the gas-water contact.	53
Figure 5.2.	Numerically simulated water rates of a typical gas withdrawal well with and without protective foam lens.	53
Figure 5.3.	Saturation distributions for one-dimensional displacement of brine (Newtonian fluid) by foam (non-Newtonian power law fluid).	54
Figure 6.1.	Location of proposed storage project at Los Medanos Field, Contra Costa County, California.	57
Figure 6.2.	Structure map, top of Nortonville sand, showing location of wells Gino-1 and Grif-1.	59
Figure 6.3.	Partial log of well Gino-1, showing Nortonville and Domengine formations.	60

List of Tables

Table 4.1.	Brines used for foamer solutions.	31
Table 4.2.	Results of foam blocking experiments in 60-cm long Ottawa Flint shot 3.0 sandpacks (90-110 darcy).	47
Table 6.1.	Phase I Proposed Test Program at Grif 1, PG&E Los Medanos Field.	63
Table 6.2.	Phase IIa Proposed Test Program at Grif 1, PG&E Los Medanos Field.	64
Table 6.3.	Phase IIb Proposed Test Program on Water coning in an Aquifer Gas Storage Field.	65
Table 6.4.	Direct Costs for Phase I Field Experiment.	67
Table 6.5.	Direct Costs for Phase IIa Field Experiment.	68
Table 6.6.	Direct Costs for Phase IIb Field Experiment.	69

50272-101

REPORT DOCUMENTATION PAGE	1. REPORT NO.	2.	3. Recipient's Accession No.

4. Title and Subtitle FEASIBILITY ANALYSIS AND DEVELOPMENT OF FOAM PROTECTED UNDERGROUND NATURAL GAS STORAGE FACILITIES Final Report	5. Report Date February 1990 6.
7. Author(s) P. A. Witherspoon, et al.	8. Performing Organization Rept. No.
9. Performing Organization Name and Address Earth Sciences Division Lawrence Berkeley Laboratory Berkeley, California 94720	10. Project/Task/Work Unit No. 11. Contract(C) or Grant(G) No. (C) (G)
12. Sponsoring Organization Name and Address Gas Research Institute 8600 West Bryn Mawr Avenue Chicago, Illinois 60631	13. Type of Report & Period Covered 14.

15. Supplementary Notes

Additional support was provided by the U. S. Department of Energy under Contract No. DE-AC 03-76SF00098 to the Lawrence Berkeley Laboratory of the University of California

16. Abstract (Limit: 200 words)

Two causes of poor recoverability of gas stored in aquifers are migration of gas far from the injection well and upward coning of water into withdrawal wells. Laboratory experiments and numerical simulations were conducted to study the possible use of aqueous foams to block the flow of gas or liquid to ameliorate these problems. Experiments in sandstone cores at simulated reservoir conditions showed that foam reduces the permeability to gas and liquid by typically three orders of magnitude. The rheology of foam was also investigated. It was found that steady-state pressure gradients for foam are practically independent of gas velocity but increase nearly linearly with increasing liquid velocity. This flow behavior is rationalized in terms of changes in bubble texture. A numerical simulation study showed that water coning could be significantly delayed by placing a horizontal foam lens just above the gas-water interface. Also discussed in the report are conditions for forming foam in situ, the feasibility of emplacing a foam bank, and the durability of permeability reduction. Laboratory experiments and numerical simulation indicate the potential for significantly improving the efficiency of aquifer gas storage with aqueous foams. A field trial of foam to diminish water coning is recommended.

17. Document Analysis a. Descriptors

Blocking sandstone
Foam
Gas storage
Surfactants
Two-phase flow

b. Identifiers/Open-Ended Terms

Foam flow
Gas permeability
Liquid permeability
Permeability reduction
Water coning

c. COSATI Field/Group

18. Availability Statement	19. Security Class (This Report)	21. No. of Pages 323
	20. Security Class (This Page)	22. Price

(See ANSI-Z39.18) See Instructions on Reverse OPTIONAL FORM 272 (4-77) (Formerly NTIS-35) Department of Commerce

1. RESEARCH SUMMARY

Title: Feasibility Analysis and Development of Foam Protected Underground Natural Gas Storage Facilities.

Contractor: Earth Sciences Division; Lawrence Berkeley Laboratory; University of California; Berkeley, California 94720

GRI Contract Number: 5086-271-1160

Principal Investigators: Paul A. Witherspoon, Clayton J. Radke, and Karsten Pruess

Report Period: January 1, 1986 - June 30, 1989

Objective: The general objective of the project is to evaluate the feasibility of using foam to improve the efficiency of underground gas storage operations. By using the ability of foam to impede and block undesired gas flow, gas mobility can be controlled to reduce the base-gas requirement. Specific objectives include the development of stable and brine-compatible foamer formulations, the measurement of foam rheology at reservoir conditions, the measurement of reduction of permeability to gas and liquid and the duration of such reduction, and the development of mathematical models to predict foam flow in porous media.

Technical Perspective: Underground storage of natural gas has been practiced for over 40 years as a cost-effective means of meeting peak demand. The process has limitations, however, in that much of the stored gas cannot be recovered. Reasons for incomplete gas recovery include possible migration of gas away from withdrawal wells, formation of isolated gas bubbles not in communication with injection/withdrawal wells, and watering-out of withdrawal wells before all of the gas has been recovered. These occurrences result from the fact that the injected gas has higher mobility than the water it displaces. Historically these issues have been dealt with by injecting a large amount of "base gas" which is not recovered during the withdrawal period. Controlling the mobility of the stored gas can sharply reduce the base-gas requirement for future storage facilities. Foam has been used as a mobility control agent in enhanced oil recovery, and the ability of foam to block the flow of gas in porous media has been well documented. The Earth Sciences Division of Lawrence Berkeley Laboratory is investigating the possibility of using foam to control the mobility of stored gas, and to assess the feasibility of "foam protected" gas storage. Several concepts for application of foam to underground storage were identified. These included the use of a foam barrier to block gas migration or reservoir capacity by lowering a spill point, the use of foam to block gas flow through fractures, and the use of foam to delay upward coning of water into gas withdrawal wells.

Results: Several concepts for application of foam to underground gas storage were identified. Those included the use of a foam barrier to block gas migration or to increase reservoir capacity by lowering a spill point, the use of foam to block gas flow through fractures, and the use of foam to delay upward coning of water into gas withdrawal wells. A brine-compatible foamer solution was developed that extends the longevity of foam, as measured in a modified Ross-Miles pour test, from 2 days to 4 months. This solution was used in experiments to measure the rheology of foam in porous media, to demonstrate and

measure the ability of foam to block the flow of gas or liquid in porous media (permeability reduction measurements), and to demonstrate foam emplacement and removal techniques. The experiments were conducted in specially fabricated apparatus at elevated pressure in sandstone cores of 1300 and 190 millidarcy permeability. The most important finding of this work was that foam in a sandstone core reduces the permeability, both to gas and liquid, typically by two to three orders of magnitude. The permeability to gas only very gradually increases, but the foam can be regenerated by injection of additional slugs of foamer solution. The second important finding from this work was a simple description of the steady-state rheology of foam in sandstone. The formation of a foam barrier spaced away from the injection well, and the intentional breaking of foam by injecting a solution of isopropanol, were also demonstrated. Concurrent with the experimental studies a relatively low-level effort was made to develop a numerical simulation capability for the flow of gas, water, and foam in porous media. An existing multiphase simulator, MULKOM, previously developed at LBL, was modified to accommodate the peculiar flow and blocking properties of foam. An important finding from our simulation studies is that a relatively small horizontal foam lens placed near the gas-water contact can substantially reduce and delay water coning in gas withdrawal wells. As part of this project we developed a program for a field test to demonstrate the emplacement of a foam bank and to test its ability to block gas or water.

Technical Approach: There are several essential elements for assessing the feasibility of using foam to improve the efficiency of aquifer gas storage operations. These include establishing the feasibility of creating and emplacing a foam barrier in the storage aquifer, ensuring that the foam will remain effective at blocking undesired gas or liquid flow for the required length of time, and demonstrating foam emplacement, regeneration, and intentional destruction. To address the issues, laboratory experiments and mathematical modeling studies were conducted. The laboratory experiments included screening surfactants for brine compatibility, evaluating the effect of chemical additives on the stability and strength of foam, and measuring both the rheology of foam and its ability to block gas and liquid flow in typical sandstones at reservoir conditions. Mathematical modeling activities included developing and validating codes for numerical simulation studies of foam emplacement and its application to delay water coning.

Project Implications: The results of the laboratory and simulation studies indicate that suitably placed foam banks would be effective in controlling gas migration (e.g., lowering of a spill point), and in delaying and diminishing water coning. A field trial using a modest sized foam plume (diameter ≈ 70 ft) to combat water coning is recommended as a promising and relatively low-cost application. Evaluation of economic feasibility should be done after a field trial.

Based on the input received from the gas industry advisors and experts, GRI has decided to defer a field experiment of this technology until a suitable well site can be located and substantial cofunding from a prospective field experiment participant can be obtained.

GRI Project Manager:
Mr. Yusuf A. Shikari
Manager, Storage Research

1.0. EXECUTIVE SUMMARY

1.1. Introduction

The storage of natural gas in aquifers has become a very effective and economical method of storing energy underground. There are large areas in the United States where depleted oil and gas fields are not present, such as in the Midwest from Indiana to Minnesota, and it is in these areas that aquifer storage is now widely used. There are, however, a number of constraints still limiting the use of aquifers that, if they could be solved or mitigated, would further enhance this method of energy storage.

One of the major constraints, especially in aquifers of low permeability, is relatively large base gas requirements. The pressures that are sometimes required to develop and then recharge the storage volume on an annual basis can cause gas migration into outlying areas where the gas is difficult to recover. In some cases these outlying gas volumes become isolated during production periods and are not an effective part of the storage system. This increases the base gas required to support some desired volume of working gas, that is, the total gas that can be produced and reinjected each year. A blocking agent, such as foam, that can be properly placed in the right regions of the structure should be able to combat this problem (Radke et al., 1983).

A related problem is that of increasing the depth of the structural closure and thereby increasing the potential storage volume of the project. This would require using foam to construct a vertical curtain that can act as a barrier at the location of the spill point. By lowering the spill point, a significant increase in working storage volume would be possible. An extension of this same idea could be applied to a monocline, or theoretically, to a flat structure as well.

A different application of the blocking properties of foam is possible in handling individual well problems. Leakage of gas up the annulus of a cased hole can become very troublesome in some cases, and the appropriate injection of foam should be able to eliminate, or reduce, this

undesired gas migration. A related problem concerns the leakage of gas that can occur through some geologic migration path. The problems of accurately locating such paths are well known, but if the emplacement of foam can be carried out in an effective and economical manner, this is yet another possible application of this blocking agent.

A completely different kind of wellbore problem can occur in aquifer storage when coning brings water prematurely into the producing well during periods of gas withdrawal. This is more often a problem in formations of low permeability, and the loss of productivity can be serious. Here, the application of foam in the form of a horizontal barrier that can impede vertical water movement is another potential application of the blocking property of foam.

The variety of possible applications for foam in aquifer gas storage, and the potential for significant benefits to the gas industry and consumers, served as the impetus for the present project. The main objectives of this project were:

(1) to investigate the physics of foam behavior in porous media, and

(2) to determine whether or not this behavior could be used to develop an effective methodology for foam-protecting aquifer storage operations so as to increase their efficiency and reduce base gas requirements.

Investigations on foam physics involved a number of important questions. What are the requisite conditions for creating a foam in the formation under the reservoir conditions that are typical for aquifer storage? How stable are such foams and what longevity can be expected? Can foam emplacement be manipulated to achieve specified geometric configurations? Does foam provide a sufficient reduction in permeability to gas to provide the desired blocking action? If necessary, can the foam barrier be broken and the surfactant chemicals be dispersed to restore the formation to its original condition?

These questions have been pursued with a program consisting of:

(1) a comprehensive literature search,

(2) the development of a procedure to screen various chemicals to determine their capa-

bilities for forming foams, and to assess their compatibilities to formation brines,

(3) the construction of a specialized apparatus in which the physics of foam behavior in sandstone cores can be investigated systematically, and

(4) the development of a numerical model that can incorporate the unusual physical behavior of foams and provide a means of investigating how these foams can affect aquifer gas storage.

(5) the development of a plan for field-testing the proposed concept.

Major results of the 3-year research effort have been presented in a number of scientific papers and reports that are included as appendices to this final report. The following paragraphs summarize the major findings.

1.2. Experimental Approach

Experiments were done to measure both the rheology of foam in sandstone (i.e., the relationship between pressure gradient permeability and flow rate) and its ability to block the flow of gas or liquid. Understanding of the rheology of foam is needed to design emplacement of foam barriers underground without exceeding the allowable injection pressure. The ability of foam to block gas or liquid flow is measured by a reduction in permeability, compared to unfoamed conditions.

To ensure that experimental conditions were representative of field conditions, foamer solutions were prepared with salinity and hardness typical of actual brines encountered in gas storage operations. All experiments were conducted at elevated back pressure (typically 700 psia), and sandstone cores of 1300 and 190 millidarcy (mD) permeability were used.

The experimental flow apparatus is fully described in Chapter 3, Design and Construction of Laboratory Equipment. Gas or liquid can be injected either separately or simultaneously into a 2-inch diameter, 24-inch long core of Boise or Berea sandstone; gas is injected either at controlled pressure or controlled mass flow rate, and liquid is injected at constant volumetric flow rate. Both pressure and liquid saturation are measured at several locations along the length of the

core. All measurements are computer-controlled and data are automatically recorded. Back pressure is maintained by a dome-loaded regulator. The measurement of both pressure and saturation profiles, especially during the transient phase of foam propagation, are unique capabilities. Results of the laboratory experiments are reported in Chapter 4 and Appendices E and F. Appendices E and F are reprints of papers that were presented at industrial symposia, and constitute a discussion of the most useful data; Chapter 4 includes a summary of all the laboratory work that was done for this project. A complete compilation of experimental data is presented in Appendix B.

A synthetic brine simulating Mt. Simon brine, with 5400 mg/L Ca, 18000 mg/L as $CaCO_3$ hardness, and 60000 mg/L TDS was used in the experiments. Initial screening of surfactants showed that alkylethoxysulfate (AES) surfactants are compatible with this brine.

Because foam stability is critical for the use of foam for blocking gas flow, the inclusion of cosurfactants to improve foam stability was investigated. Observations of decay of a bulk foam showed that addition of 0.2 wt % long-chain alcohol to the surfactant solution increased the life of the foam from 2 days to 4 months (Witherspoon et al., 1987). The foamer solution used in the experiments was 1 wt % active Steol 7N (commercially available AES) with 0.2 wt % n-dodecanol.

With an effective foamer solution developed, the behavior of foam was evaluated in sandstone cores. In all experiments the core was initially saturated with foamer solution, and foam was formed in the core by simultaneous injection of gas (N_2) and liquid or by injection of gas only into the liquid-saturated core. Transient displacement of liquid by foam was monitored by liquid saturation and pressure measurements. In foam-rheology experiments, the flow rates of gas and liquid were varied stepwise to achieve successive steady states. In other experiments, after foam had propagated through the core, the permeability to gas or liquid was measured to determine the degree of flow reduction; permeability measurements were continued over two weeks to monitor foam deterioration. Long-term foam-survival measurements were conducted in separate experiments in sandpacks.

1.3. Experimental Findings

The most important finding of this work was that foam in a sandstone core reduces the permeability, both to gas and liquid, by typically two to three orders of magnitude. Foam was formed in all experiments in which gas was injected (with or without simultaneous injection of liquid) into a core initially saturated with surfactant solution. The formation of foam is indicated by both reduction of liquid saturation to 30-35% (compared with connate water at 25%), and increased pressure gradients that are much steeper than those observed for the same gas and liquid flow rates without foam. Despite high gas saturation, the permeability to gas of a foamed core is extremely low (typically 0.1 mD), apparently because most of the gas exists as trapped bubbles and most gas flow paths are blocked by metastable lamellae (liquid films). If surfactant solution is injected along with the gas, the permeability stays very low. If no liquid is injected, or if injection of surfactant solution is stopped, the permeability to gas increases very gradually. Typically a value of 1 or 2 mD is reached after two weeks without liquid flowing; this value was the same for 1300 mD Boise and 190 mD Berea sandstone. The gradual increase in permeability presumably results from rupture of some blocking lamellae. It was found that injection of another slug of foamer solution causes rapid formation of additional lamellae and again reduces the permeability; this regeneration can be repeated indefinitely. Foam blocks in 20-darcy sandpacks reduced gas permeability to 1 mD for as long as 60 and 200 days in duplicate experiments without regeneration.

Because of the low liquid saturation in foamed sandstone, the permeability to liquid is also reduced. In one experiment 30 liquid volumes of surfactant-free brine were injected into a foamed core before the liquid saturation and liquid permeability increased.

The second important finding from this work was a simple description of the steady-state rheology of foam in sandstone. To form a foam barrier, foam must be driven to some distance from a foam-injection well, and the need to limit the injection pressure to avoid fracturing the overburden requires an understanding of how pressure gradients vary with the gas and liquid flow rates. In experiments in which the gas and liquid flow rates were varied independently, a very

simple relationship was found between foam flow resistance, calculated from the measured pressure gradients, and gas and liquid flow rates. These findings are discussed in detail in a paper by Persoff et al. (1989a) which is included here in Appendix E.

Other experiments were done to demonstrate practical aspects of foam barrier formation and controlled destruction. Controlled breakage of foam was demonstrated by injecting 0.1 PV of 50% isopropanol into a foamed core. Within 6 hours, during which 7.8 PV of gas were injected, the foam was broken in the inlet region where the isopropanol displaced surfactant solution (slightly less than half the core), but remained intact in the rest of the core.

One possible method of storing gas within a peripheral foam barrier could be realized by forming a foam barrier spaced some distance away from an injection-withdrawal well. The formation of such a spaced foam block was experimentally demonstrated by displacing foamer solution with brine and then injecting gas. The gas fingered through the brine until it reached the foamer solution, where it formed foam. This indicates that gas could be mobile near the injection well and immobile where foam has been emplaced, with both foam emplacement and gas injection being done through the same well.

In summary, it has been demonstrated that foamer solutions can be made using hard, saline water; that foam reduces the permeability of sandstone to both gas and liquid to approximately 1 mD; that such permeability reduction lasts long enough to be practical or can be restored as needed; and that the foam can be destroyed reliably if needed. Insight was also gained into the dynamics of foam formation and flow in porous media which indicate that foam emplacement is feasible without using excessive injection pressure.

1.4. Foam Flow Modeling

Concurrent with the experimental studies a relatively low-level effort was made to develop a numerical simulation capability for the flow of gas, water, and foam in porous media. Such a capability was deemed useful for the design and analysis of the laboratory experiments, and it would be essential for the study of field-scale processes.

At the present time there is no satisfactory theory for explaining and predicting the behavior of foam in porous media from basic fluid dynamics principles. A phenomenological approach was adopted in which the gas-water-foam system is represented as a three-phase mixture. An existing multiphase simulator MULKOM, developed at the Lawrence Berkeley Laboratory (LBL) with funding mostly from the DOE geothermal program, was modified to accommodate the peculiar flow and blocking properties of foam. The modifications involved mostly the PVT properties of foam (non-Newtonian flow behavior, compressibility); furthermore, capabilities were developed for simulating production and injection wells operating under a variety of pressure and rate constraints. The development of the model is described in Chapter 5 and the code MULKOM-GWF is fully documented in Appendix C.

A number of test cases were developed to verify the performance of the simulator and to study the dynamics of gas-water-foam flow. The classical solution of Buckley and Leverett for two-phase immiscible displacement was extended to non-Newtonian flow, and close agreement between analytical and numerical predictions was obtained. This work is presented in Appendix G. The simulator was applied to the design and analysis of the laboratory experiments. A number of issues relating to field application of foam in aquifer gas storage were also explored.

An important finding from the simulation studies is that a relatively small foam plume placed near the gas-water contact would substantially delay water coning in gas withdrawal wells. It was also found that, because of the high degree of permeability reduction caused by foam, prohibitively large pressure gradients may be needed to inject gas and liquid simultaneously to form foam banks on the scale required for gas storage. A practical approach for foam applications in gas storage reservoirs would, therefore, involve injecting a slug of surfactant solution first, followed by gas injection.

The code MULKOM-GWF is applicable for simulations of gas-water-foam flow in porous media from laboratory to field scale. Any of the three phases (gas, water or foam) can be absent, so that conventional aquifer gas storage systems involving only gas and water can also be modeled. At the present state of development the simulator is a useful research tool, and it is

being made available to the gas industry for this purpose.

1.5. Field Experiment Design

Laboratory experiments have demonstrated that foam blocks the flow of gas or liquid, and can be driven in-situ to where this blocking ability is needed. A pilot field experiment is now needed to test whether foam can be applied under actual operating conditions. Such an experiment would address issues that cannot be addressed in the laboratory, such as reservoir heterogeneity and the feasibility of driving foam long distances.

As part of this project a program was developed for a field experiment to show that a foam bank can be emplaced in an underground formation, that the foam bank is sufficiently stable to reduce permeability for the required length of time, and that the foam bank can be intentionally destroyed by injecting a foam breaker. Further field work would then demonstrate the application of foam to gas storage.

Pacific Gas and Electric Company (PG&E) was approached about conducting a field experiment at the Los Medanos gas storage field, and PG&E expressed willingness to cooperate with such a test. The experiment was planned for the Nortonville sand, a thin (50 ft) formation above the Domengine sand in which gas is actively stored. Advantages of this test site include: high pressure (1600 psi) gas stored in the Domengine is available for injection; depth of the formation (1800 ft) permits injection pressures necessary to drive foam; experiments in the Nortonville should not affect PG&E's operations in the Domengine; the shallow thickness of the Nortonville sand is appropriate for a test program; the site is continuously manned by PG&E for safety and security; and location is near LBL facilities to enable intensive monitoring. This first phase of the test program was scheduled to last 5 months. A second phase was also contemplated that was designed to study the possibility of developing a storage volume inside a foam blocked region. The detailed test program was presented to the Gas Research Institute's Gas Storage Steering Committee in 1988, and is further discussed in Chapter 6.

1.6. Recommendations

To date, the results of our research have indicated that foam has promise for improving the efficiency of aquifer gas storage operations. To further investigate this possibility and to attest the viability of potential applications, the following recommendations, listed in order of priority, are made:

(1) Carry out a field experiment to show that a controllable foam barrier can be created in a typical aquifer used for gas storage. This experiment could be conducted either in an easily accessible aquifer or in an active gas storage field. In the latter case, the experiment could be used to examine the technical feasibility and economic viability of a specific application of foam such as to combat water coning problems during the gas withdrawal cycle. Preliminary designs for several field experiments have been prepared, including experiments to evaluate a single-well foam block, a spaced foam block, and minimization of water coning. Several gas storage operators have expressed interest in cooperating with such field experiments.

(2) Conduct additional laboratory experiments to improve the understanding of the fundamental mechanisms of foam generation, displacement, and stability. The extensive laboratory experiments conducted to date have already revealed some important insights into the fundamental nature of foam flow in porous media. These insights are crucial to developing a successful approach for employing foam in gas storage operations. Areas which yet remain to be addressed include determination of the minimum gas velocity needed to form foam, factors controlling bubble size and its effect on foam rheology, and the range of conditions over which the quantity,

$$\left[\frac{dp}{dx}\right]\frac{k}{\mu_{liq}v_{liq}}$$

is constant, where μ_{liq} and v_{liq} are the liquid viscosity and velocity, respectively, k is the permeability of the formation, and (dp/dx) is the pressure gradient in the direction of flow.

(3) Calibrate and validate the foam-flow simulator MULKOM-GWF to improve its ability to model accurately foam generation and displacement. Data from numerous laboratory column experiments are now available for calibrating and validating the foam-flow simulator. By history matching these data with the foam flow simulator, the rheological properties of foam could be parameterized for both steady-state and transient flow. The validity of the calibrated model could then be tested by comparing simulated results to additional experimental data.

(4) Prepare a verified, validated, and well-documented version of the foam flow simulator for use by the gas industry. Technical and economic decisions regarding the applicability of a new technology often rely heavily on the preliminary modeling studies. The availability of a reliable and accurate model will facilitate these decisions. In addition, a foam flow model will be helpful in the design and evaluation of various schemes for foam-assisted aquifer gas storage operations.

2.0. INTRODUCTION

The transmission and distribution segments of the gas industry in the United States share a common interest in gas storage. To meet peak loads and to ensure dependable delivery of gas to all end users, gas storage has become a vital link in the supply, transport, and distribution network. Of the various forms of natural-gas-storage technologies adopted, large-scale seasonal storage by utilities in underground formations is perhaps the most prevalent.

Two problems associated with underground storage of natural gas -- migration of gas beyond the designated storage area during the gas injection cycle and water coning into wells during the withdrawal cycle -- are addressed in this study. During the formation of the initial storage volume in an aquifer, some of the injected gas fingers away from the main bubble, sometimes for long distances, because of the extremely adverse mobility ratio between water and gas.

For underground storage in aquifers, gas must displace water from the porous medium. Unfortunately, gas does not invade a water-saturated zone in a uniform piston-like fashion. Rather, the gas front breaks up and "fingers" through the water, leading to a very inefficient displacement mechanism. Also, because of its low density, the gas tends to rise to the top of the system where it migrates as a thin layer (gravity override). More importantly, high mobility of gas, compared to that of water, results in formation of thin gas zones far from the main bubble. During gas withdrawal, these far-removed zones can be trapped as off-site and isolated gas which is practically unrecoverable.

Another aspect of gas storage operation pertains to a typical wellbore problem in aquifer gas storage where water coning during gas withdrawal significantly reduces the deliverability (or well productivity). Elimination or significant delay of water coning in the production zone is, thus, highly desirable during the withdrawal season.

In the past, these problems have been dealt with by injection of large volumes of gas (typically twice as much as the working gas, with the proportion being larger in specific reservoirs), but long-term increases in both interest rates and the value of natural gas have impelled a search for methods to control gas migration and water coning. One possible solution to these problems is the use of aqueous foam as a mobility control agent. The basic idea of foam-protected gas storage is to emplace a suitable foam barrier in an aquifer that would confine the stored gas in a compact volume around the injection wells (Witherspoon et al., 1987).

2.1. Foam-Protected Storage Concepts

The ability of foam to control the mobility of the injected gas and to block undesired gas flow can be used to improve the efficiency of underground gas storage operations with several different concepts. The earliest documentation of the concept of using foam for this purpose was presented by Bernard (1967), who proposed to take advantage of the ability of foam to block undesired gas flow and to create better closure of the natural structure of the storage aquifer. Later, Bernard and Holm (1970) proposed that foam be used to block gas flow to seal natural leaks in the storage facility. In the present study, we have investigated the potential for exploiting the ability of foam to achieve mobility control and block undesired gas flow to improve the efficiency of gas storage operations. The general concepts for foam protection were outlined by Radke, et al. (1983), and are reviewed briefly below.

The first of these concepts, which is illustrated in Figure 2.1, relies on the ability of foam to achieve mobility control during the injection phase of the storage operation. By injecting a slug of surfactant solution before the gas is injected, a foam blanket is formed between the initially water-filled aquifer and the gas behind it. The foam blanket acts to stabilize the interface between the gas and water during the injection phase, thereby improving the displacement efficiency, minimizing gravity override, and counteracting the effects of geologic heterogeneity. This concept can be used to achieve a deeper, more compact gas bubble around the injection well, which would result in improved gas recovery during the withdrawal phase.

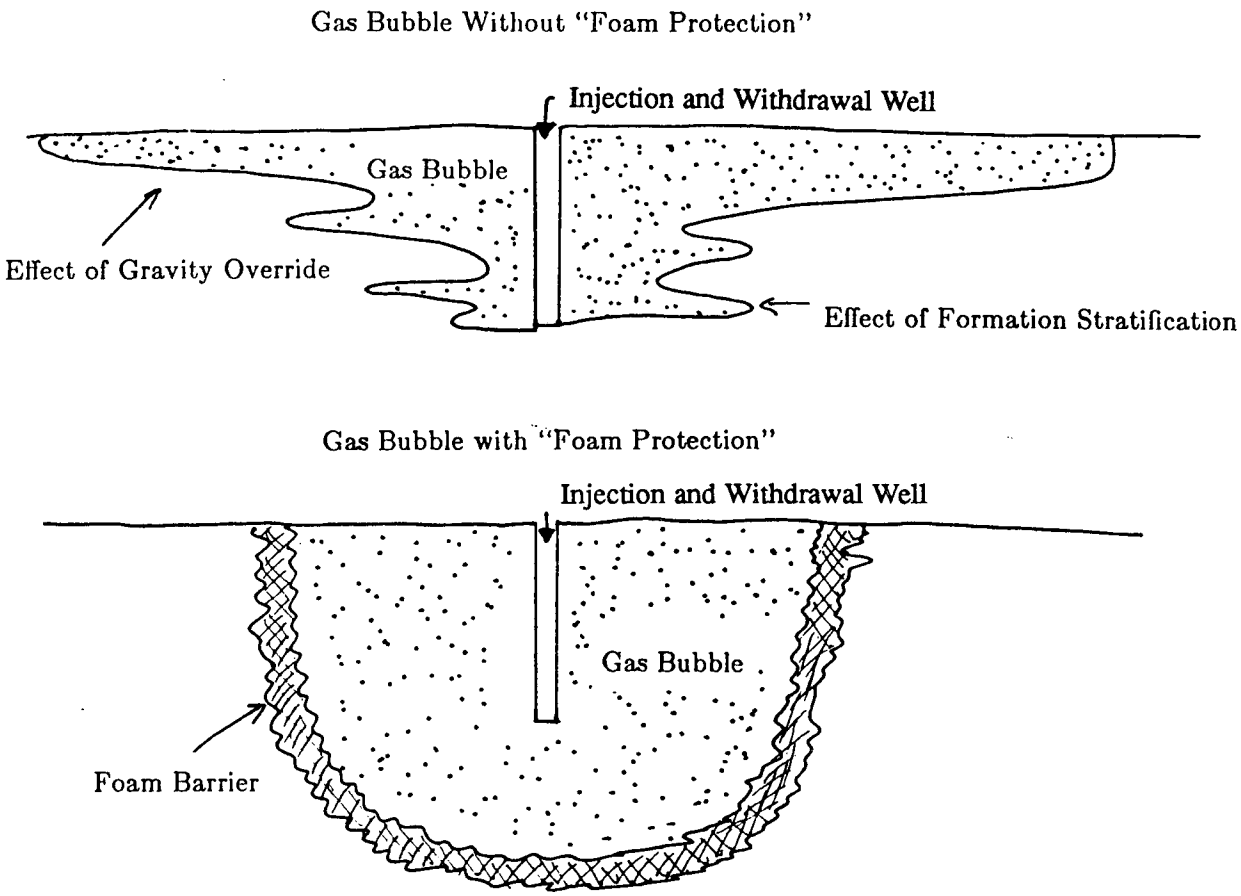

Figure 2.1. Schematic of gas injection with and without mobility control.

A more elaborate version of this concept (illustrated in Figure 2.2), which provides even better "protection" of the stored gas, could be achieved by creating a permanently emplaced "foam barrier" spaced away from the injection well. The barrier would be created by injecting surfactant solution, injecting surfactant-free water to space the slug of surfactant solution away from the well, and then injecting gas to form a hollow cylindrical foam barrier. This procedure creates a cylindrical, water-free storage volume that can be used for repeated injection and withdrawal cycles.

A continuous foam curtain can be created by injecting surfactant solution followed by gas (or alternating slugs of surfactant solution and gas) through several wells so that the foam plumes merge to form a continuous "curtain." Such a multi-well barrier can be used to lower the "spill point" in an existing storage aquifer, as shown in Figure 2.3, thereby creating a larger storage volume and preventing leakage of gas beyond the designated storage volume. This concept could also be extended to provide gas storage capacity in formations that do not have natural closure, by extending the foam curtain to compltely surround the designated storage volume, as shown in Figure 2.4.

Another potential application of foam for underground gas storage would be to seal leaks in caverns mined in hard rock. Along the eastern seaboard of the United States, where geologic formations suitable for gas storage are absent, gas could be stored in mined caverns. The problem here is to control leakage of gas through fractures that intersect the cavern. Just as foam blocks gas flow in porous media, it may do so as well in fractures, which would make the use of mined caverns for gas storage feasible. This application of foam is illustrated conceptually in Figure 2.5. As shown in this figure, foamer solution would be injected through boreholes parallel to the walls of the cavern, and gas escaping through fractures would form foam. Additional foamer solution could be injected as needed to regenerate the foam.

2.2. Project Objectives

The general goal of this project was to assess the feasibility of improving the efficiency of underground gas storage by the use of foam. Specific goals were to develop brine-compatible

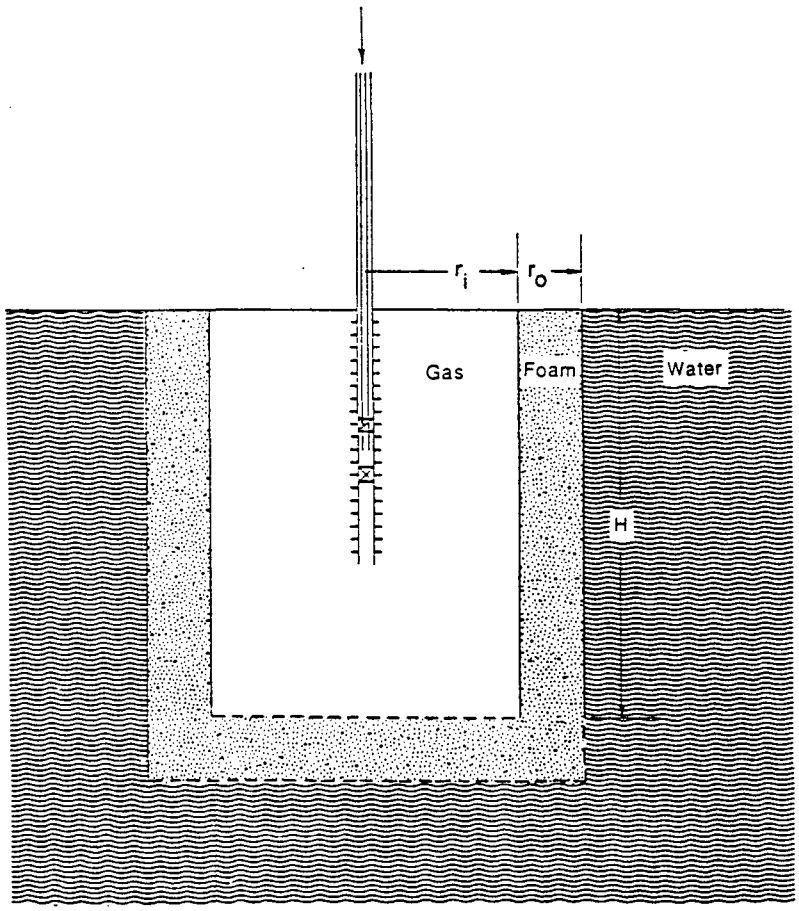

Figure 2.2. Single well "foam protected" storage facility.

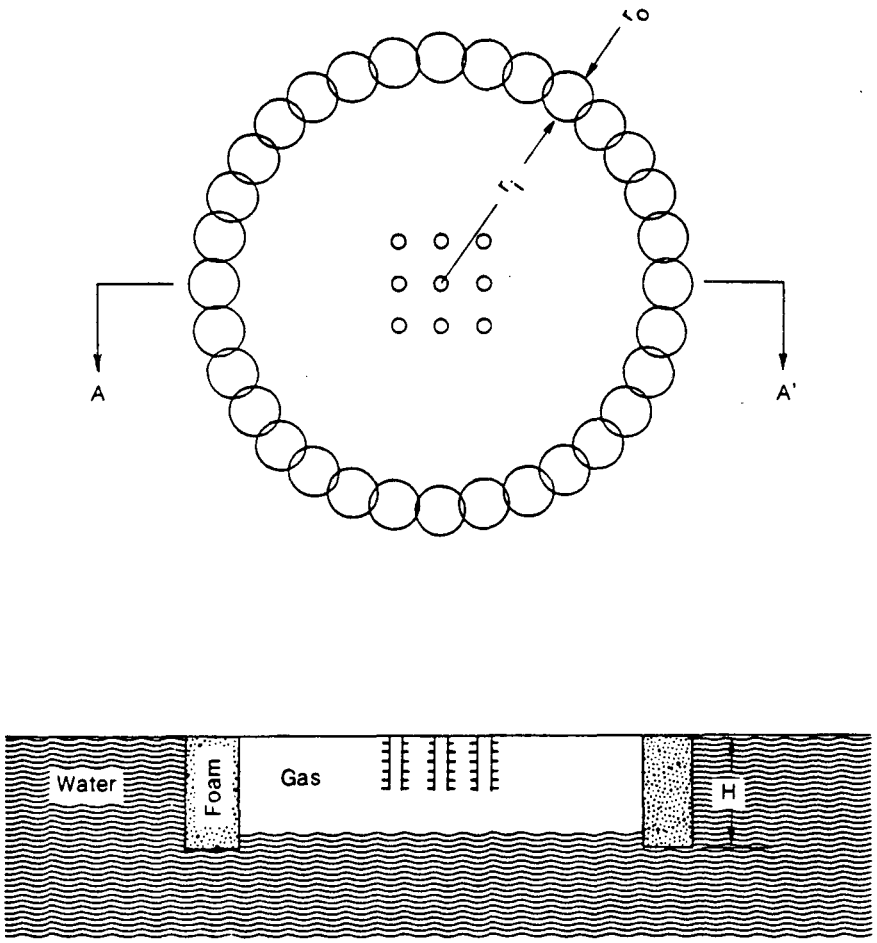

Figure 2.3. Spill-point lowering with a ''foam-barrier''.

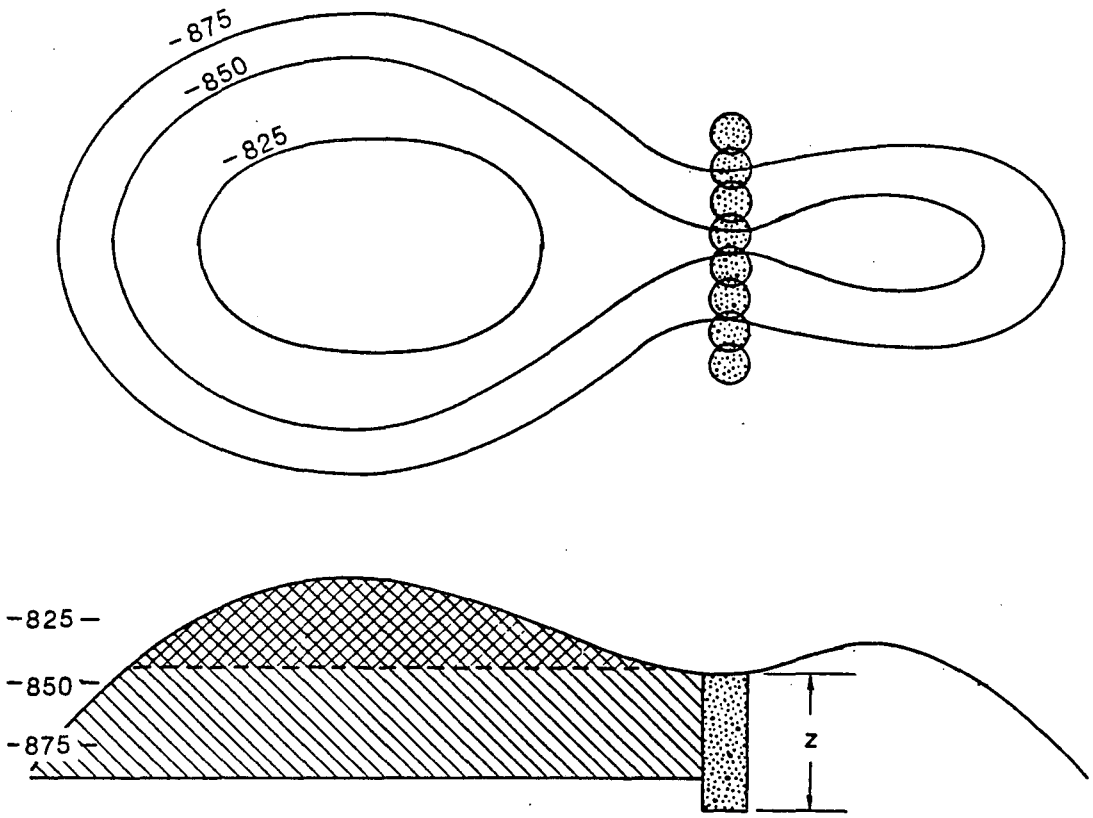

Figure 2.4. Skirt well ''foam protected'' storage facility.

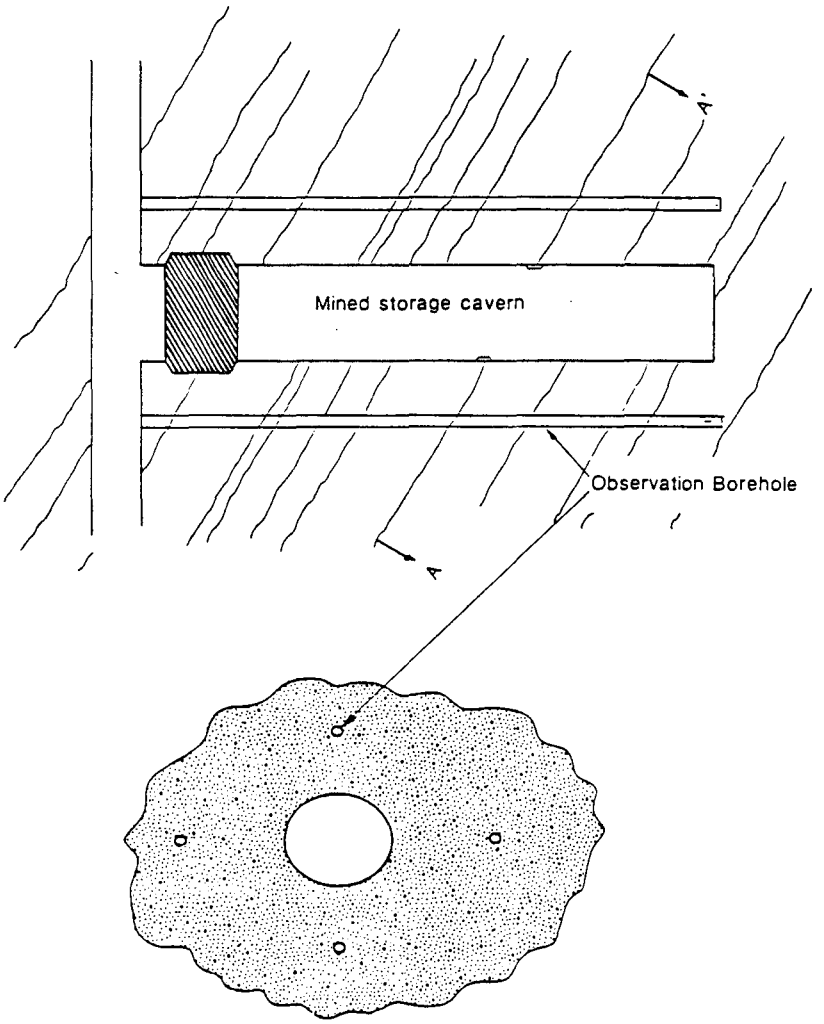

Figure 2.5. Use of foam to seal fractures intersecting a mined cavern.

stable foamer solutions, to understand foam rheology in porous media by means of controlled laboratory experiments under selected reservoir conditions, to measure the ability of foam to block gas and liquid flow in porous media, to determine the relationship betwen pressure gradient, permeability, and gas and liquid flow rates for foam flow in sandstone, to develop a numerical simulator capable of accurately simulating the experiments and field projects, and to design a field experiment. The laboratory equipment designed and constructed for this project is described in Chapter 3. The experiments done on this project are described in Chapter 4 and in Appendices E and F. Appendices E and F discuss the most important results, while Chapter 4 summarizes all the experimental work that was done for this project. Appendix B presents a summary of all experimental data.

The numerical simulator has been developed as a research tool, as described in Chapter 5. A guide to input data preparation is presented in Appendix C. As part of the simulator development, analytical solutions were developed for displacement of general (Newtonian or non-Newtonian) fluids in porous media, and used to check the simulator. These analytical solutions are presented in Appendix G.

Finally, a proposed field experiment is described in Chapter 6.

3.0. DESIGN AND CONSTRUCTION OF LABORATORY EQUIPMENT

3.1. Laboratory Facility for High-Pressure Foam Flow Experiments

For this project we fabricated a laboratory facility for studying the behavior of foams at simulated reservoir conditions. The purpose of the experiments was to demonstrate and measure foam flow, foam blocking of gas and liquid flow, and intentional foam breakage in sandstone. Experiments were conducted in 2-in. × 24-in. cores of Boise sandstone (1300 millidarcy permeability and 25% porosity) and Berea sandstone (190 millidarcy permeability and 19% porosity).

A schematic of the experimental apparatus is shown in Figure 3.1. The core holder was a tube of 316 stainless steel, with a 2.25-inch i.d. and 5/8-inch wall, designed for 2200 psi. Pressure taps were drilled through the core holder and tapped to accommodate Swagelok O-ring seals. The 2-inch diameter core was epoxy-mounted into the core holder. The epoxy used was 301-AD resin (Castall, Weymouth Industrial Park, MA) with 4% RT-1 curing agent and 4% toluene to reduce the viscosity. First the sides and end of the core were painted with two coats of the epoxy to prevent any epoxy from entering the pores of the sandstone during the subsequent vacuum-filling procedure. Then the core was mounted co-axially in the core holder by tacking it with three spacers at each end. The spacers were made of cured 301-AD resin; any material could have been used as long as it was not harder than the resin. The spacers were held in place with a quick-setting "5-minute" epoxy. The annular space between the core and the core holder had to be completely filled with epoxy resin to avoid any short-circuiting. To accomplish this the pressure taps were sealed and O-ring temporary end caps were made to seal the ends of the core holder. The core holder was then evacuated, and the uncured epoxy liquid was admitted to fill the evacuated space. After curing for 3 days, the end caps were removed (they were previously sprayed with a teflon mold release to facilitate removal), the ends of the sandstone core were exposed by machining away the cured epoxy, and the pressure taps were opened by drilling

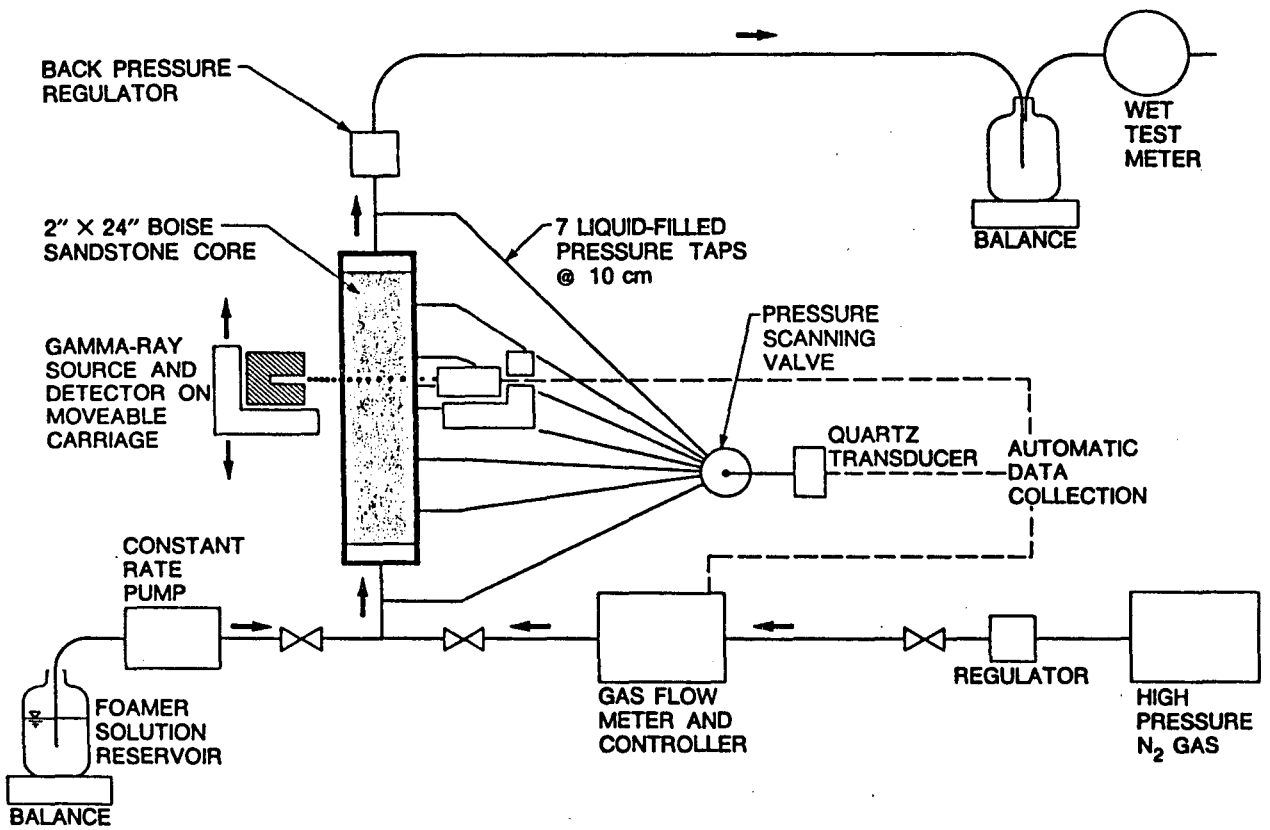

Figure 3.1. High-pressure foam-flow apparatus (schematic).

through the epoxy to the sandstone. Gas permeability measurements of the core were then made to check that the epoxy seal was good.

End caps for use during experiments were sealed to the core holder using O-ring piston seals with split-ring clamshell retainers to keep them in place against internal pressure. The end-caps were originally made large enough to accommodate an in-line foam generator of the same sandstone material, but eventually these were replaced by endcaps with minimum dead volume. The flow behavior of the foam was not affected by the presence or absence of the foam generator.

Gas was delivered at a constant mass flow rate through a Brooks 5850-TRP mass flow controller (Emerson Electric, Hatfield, PA). Gas flow rates could be pre-programmed or operator-varied through the computer, or the controller could be overridden to allow gas injection at constant pressure. For foams in which the gas phase dissolves minimally in the liquid phase and does not condense or react with any component of the liquid phase, the composition of the gas phase does not influence foam behavior. For safety, therefore, nitrogen gas was used both to form the foam and represent the stored natural gas. Liquid was delivered at a pre-set constant flow rate by an LDC minipump (Milton Roy Co., Riviera Beach, FL), which is a dual piston pump that can deliver up to 20 mL/min with a precision of 0.2 mL/min at pressures up to 6000 psi.

The LDC minipump delivers a pulsing flow, and when pumping liquid through a liquid-saturated core, the pressure wave could be detected at all the pressure taps. When injecting liquid into a partially-saturated core, however, the comparatively large gas compressibility damped out pulsations. During one experiment, the LDC minipump was replaced by a high-pressure syringe pump (ISCO, Lincoln, NE) which delivered the same flow rate without pulsations, and no difference in foam rheology was detected.

Back pressure in the core was maintained by a Mity-mite dome-loaded back-pressure regulator (Grove Valve and Regulator, Emeryville, CA). This device throttles the flow through an orifice which is nearly sealed by a teflon diaphragm. Regulated gas pressure (the "load") on the other side of the diaphragm controls the backpressure in the core. This device cannot shut off flow completely so a certain minimum flow through the regulator is necessary for accurate back-

pressure control. When an ordinary high-pressure gas regulator was used to load the dome, daily temperature changes caused cycling of the back pressure. This difficulty was resolved by using a spring-loaded relieving regulator that vented some of the gas when the load exceeded the spring setting.

All flow rate, pressure, and liquid saturation data were automatically recorded by a Hewlett Packard measurement system. Pressures were measured by a Paroscientific, Inc. (Redmond, WA) piezoelectric temperature compensated quartz crystal transducer. During an experiment, the pressure transducer was sequentially connected to each of the pressure taps by a Scanivalve (San Diego, CA) 12L7 multiplexing valve. The multiplexing valve scanned not only the seven pressure taps but also two reference pressures, so that checking transducer performance and multiplexing valve position was automatic. Each cycle took about 2 minutes. Use of a single transducer to measure pressure at each point eliminated error due to variability between instruments and allowed good definition of the pressure profile in the core.

The pressure taps connecting the core to the multiplexing valve were filled with the foamer solution, i.e., brine with surfactant. To prevent corrosion of the multiplexing valve by the brine in the experiment, the valve was filled with silicone oil. In the operation of the multiplexing valve, the transducer is connected sequentially to different pressures. If a lower pressure is sensed before a higher pressure, when the transducer is connected to the higher pressure, liquid in the pressure tap will expand into the transducer. Because during an experiment the transducer continuously scans pressures in sequence many times, this accumulated liquid transfer could result in transfer of brine into the interior of the multiplexing valve. To minimize this, all air bubbles were carefully excluded from the multiplexing valve and the pressure taps, but even the compressibility of the silicone oil (about twice that of water), could result in transfer of more than 5 mL during an experiment. Each channel of the multiplexing valve was therefore connected to 8 inch long 1/4-inch diameter stainless steel tubing which acted as a reservoir of silicone oil, and each reservoir was connected to the respective pressure tap, which was 1/8-inch stainless steel tubing filled with brine. The silicone oil buffer prevented transfer of brine into the

interior of the multiplexing valve. Also, the pressures were always scanned in order from highest to lowest pressure, so that the transfer of liquid was always out of the core and into the next pressure tap, and the last pressure tap (no. 1) was always connected to a pressure lower than the lowest pressure in the experiment, so it alone received fluid. Tap no. 1 was fitted with an extra-large reservoir, so that only silicone oil was actually transferred into the multiplexing valve.

In one experiment, pairs of pressure taps were drilled, one inch apart, at the same distance from the inlet of the core. A consistent bias was observed in that whichever tap was sensed first read 0.05 psi lower than the other. This bias remained even when the pressure taps were switched and when the pressure was allowed to stabilize for as long as 400 sec before being recorded. This discrepancy, and observations of atmospheric pressure, suggest that pressure measurements have an error of ±0.1 psi.

Liquid saturation was measured by gamma-ray densitometry. A 200 mCi ^{137}Cs gamma source emits a collimated beam of photons with an energy level of 662 keV, which penetrates the core holder and core. The attenuated beam was detected by a 8S8/2 scintillation detector with NB15X plug-on preamplifier (Harshaw Chemical Company, Solon, OH) and counted by a 917 multichannel buffer with a 990 digital spectrum stabilizer (EG&G Ortec, Oak Ridge, TN). Saturation was measured by comparing the intensity of the attenuated beam to reference measurements made at two different liquid saturations. Because of point-to-point variability in the sandstone core, it is critical that gamma ray intensity measurements be made at exactly the same location as the reference measurements. Precise reproducibility of location of the gamma-ray measuring system relative to the core was achieved by use of a stepper motor (Rapid-syn 42D-112-25D; driver Anaheim Automation DPF-107) and ball screw; the measuring system can be located to within ±0.02 mm. To ensure that cumulative errors in step counting do not result in drifting of the locations at which liquid saturation is measured, after each cycle of counting at the preselected stations, the step-counting is re-initialized by tripping a limit switch.

Figure 3.2 shows the apparatus as assembled. The vertical core holder is in the center of the picture. Stainless steel tubing pressure taps connect various locations to the multiplexing

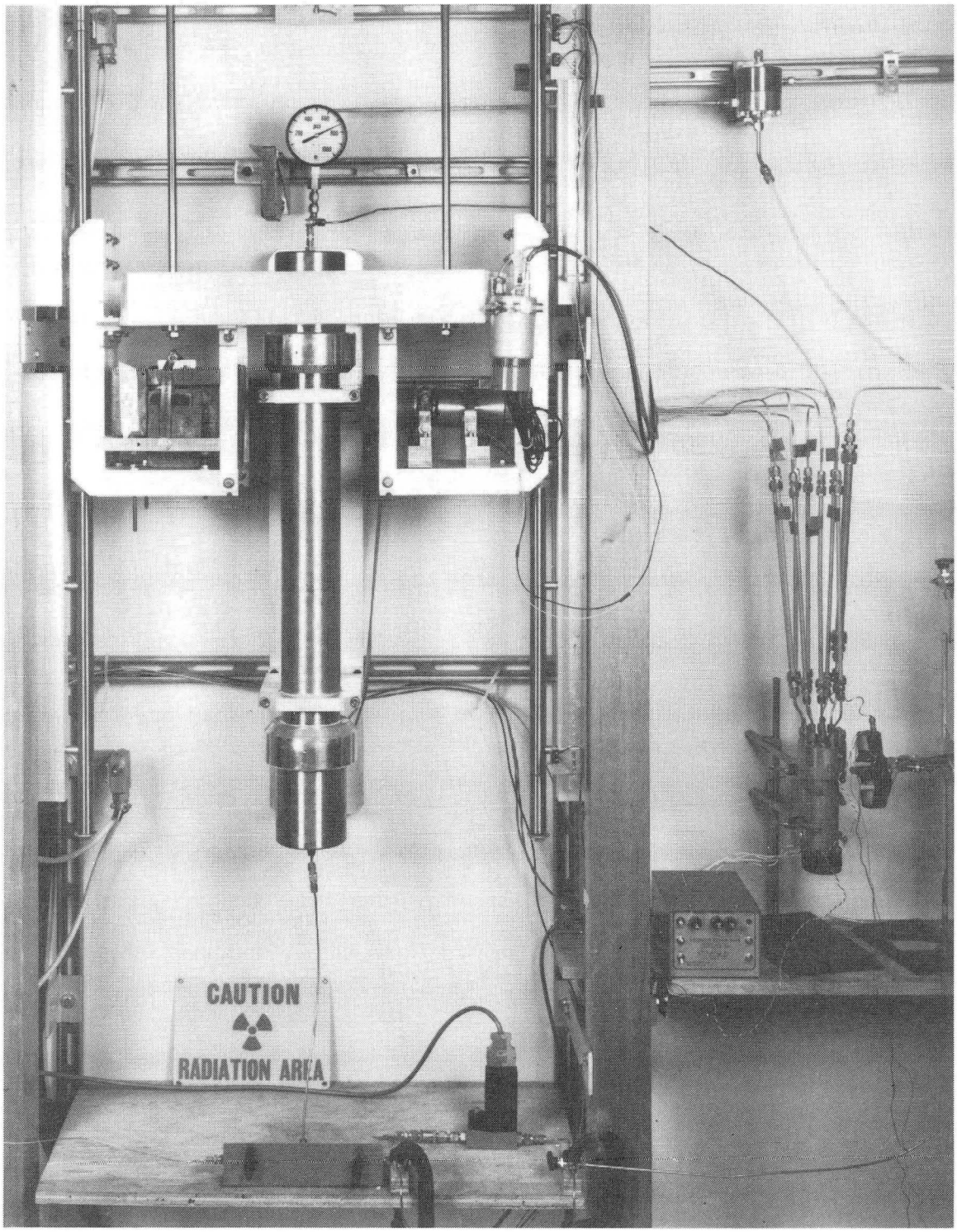

Figure 3.2. High-pressure foam-flow apparatus (photograph).

valve and pressure transducer. The gamma source and scintillation counter move vertically on a carriage, which is raised or lowered by the stepper motor located at the top of the frame (not shown in the Figure).

Gas-tracer measurements were made during some experiments to determine the fraction of gas in the core that was flowing. To accomplish the tracer measurements, the concentration of oxygen in the inlet gas was changed as a step function between 0 (pure nitrogen) and a constant concentration. Initially, the step was made between 0 and 20% (i.e., nitrogen to air), but this caused changes in the pressure gradient, as detailed in Appendix B, experiment 12. Therefore a metering valve was installed in the air line so that the concentration of oxygen could be varied between 0 and 2%. At the exit of the back-pressure regulator the gas was allowed to expand to atmospheric pressure, and oxygen content was monitored by means of a Beckmann model O260 oxygen analyzer. The average residence time of oxygen in the core was calculated by taking the first moment of the recorded oxygen concentration in the effluent (Smith, 1981).

This laboratory facility allowed systematic investigation of foam flow behavior, and reduction of gas and liquid permeability caused by foam, at simulated reservoir conditions. The separate control over both gas and liquid flow rates, and the measurement of local (rather than overall) liquid saturation allowed experiments to be conducted that led to a simple and consistent description of foam flow in porous media, presented in Appendix E. The substantial reduction of both gas and liquid permeability caused by foam in both 1300-millidarcy and 190-millidarcy sandstone cores was also measured, as detailed in Appendix F.

4.0. LABORATORY INVESTIGATIONS

The laboratory investigations for this project consisted of:

(1) Experiments to screen surfactants for brine compatibility and to formulate foamer solutions for maximum foam stability,

(2) Experiments to measure the rheology of foam in porous media,

(3) Experiments to verify and measure the ability of foam to block the flow of gas or liquid in porous media (permeability reduction measurements),

(4) Evaluations of alternative foam emplacement and removal techniques.

Screening and formulation of surfactant solutions is discussed in the Section 4.1 of this chapter.

Foam rheology experiments were conducted in a 90-darcy sandpack at one atmosphere back pressure and in 1300-mD and 190-mD sandstone cores at 700 psi back pressure. The experiment in the sandpack is reported in Section 4.2.1; those in the sandstone cores are reported in Appendix E. In the high-pressure experiments in the sandstone cores gas and liquid flow rates were varied by almost two orders of magnitude; foam rheology was found to follow a simple relationship as described in Appendix E: at steady state, with both gas and liquid flowing, the pressure gradient is approximately directly proportional to the liquid velocity, but essentially independent of the gas velocity. The observed pressure gradients can be explained by the observed liquid saturation and independently measured relative permeability relationships.

The ability of foam to block gas and liquid flow was proven and measured in 20- and 90-darcy sandpacks at one atmosphere back pressure and in sandstone cores at elevated back pressure (700 psi). The experiments in sandpacks are reported in Section 4.4 in this chapter and in Appendix F; those in the sandstone cores are also reported in Appendix F, with all experimental

data in Appendix B. Essentially, we found that the presence of foam in a sandstone core reduces the permeability to gas or to liquid by two or three orders of magnitude, and the permeability gradually increases with time.

The emplacement of a spaced foam block and intentional breaking of foam are also reported in Appendix F, with all experimental data in Appendix B.

4.1. Surfactant Solution Screening and Formulation

4.1.1. Stable Foamer Solution Development

Longevity of foam blocks in porous media is a key element in demonstrating the feasibility of foam-protected underground gas storage. It was first necessary to screen several surfactants to determine their brine compatibility. A test technique to measure static foam stability was then developed, and the effect of additives on foam stability was investigated.

Table 4.1 shows analyses of a typical brine from the Mt. Simon formation of Illinois, where several aquifer gas storage projects are located, and the synthetic brines used in this work. Four classes of oilfield surfactants were screened for brine compatibility, including Shell Enordet AOS (alpha olefin sulfonate), AE (alcohol ethoxylate), AES (alcohol ethoxysulfate), and Chevron Chaser (alkyl sulfonate) products. Of these, the AOS and Chaser products were eliminated because they formed precipitates with the synthetic Mt. Simon brine (although not with a Ca-free brine which had the same hardness level). The AES surfactants were selected for further screening because, being anionic, they were expected to have less sorption on mineral surfaces than the nonionic AE surfactants. Another advantage of using an anionic surfactant is the possibility of increasing foam life by adding a cosurfactant. Four AES products were tested: AES 911-2.5S, AES 1215-3S, AES 1215-9S, and AES 1213-6.5S. The AES surfactants are designated by the length of the ethoxy chain as follows: AES 1213-6.5S indicates a 12 to 13 carbon alkyl chain, with an average of 6.5 ethoxy groups on the hydrophilic end, terminating in a sulfate group with a sodium counter ion: $CH_3(CH_2)_{11-12}-(O-CH_2CH_2)_{6.5}-OSO_3^- Na^+$.

Combinations of surfactants have also been used to produce more stable foams than can be

Table 4.1. Brines used for foamer solutions

		Synthetic Brines		
	Mt. Simon brine[a]	Mt. Simon brine	Ca-free brine	SO_4-free brine
cations (mg/L)				
Na^+	18200±700[b]	18170	18170	18170
Mg^{++}	1310±110	1260	4500	1260
Ca^{++}	5360±130	5410	0	5410
anions (mg/L)				
Cl^-	39900±900	40000	40000	41360
$SO_4^=$	1760±100	1860	1860	0
hardness (mg/L as $CaCO_3$)	18800±600	18750	18750	18750
TDS (mg/L)	66200±1800	66700	64560	66200

[a]Average and standard deviation of eight analyses, Lexington Field, McLean Co., Illinois, 1970.
[b]Not reported -- estimated by charge balance.

produced with a single surfactant. The proposed mechanism of stabilization (Sharma, et al., 1982) is that the molecules of ionic surfactants align themselves like match-sticks at the gas-liquid interface (i.e., one layer at each side of a lamella). The ionic ends, being of like charge, tend to repel each other. This repulsive force makes the packing of molecules less dense. To relieve this, molecules of nonionic surfactants are added, which are hypothesized to pack between the molecules of the ionic surfactant. This diminishes the repulsive force and stabilizes the lamellae. Commonly used "cosurfactants" are long chain alcohols (Schick and Fowkes 1957). Foam stability is reported to be maximized at a specific concentration ratio of surfactant to cosurfactant, and best results are obtained when the alkyl chain lengths of the surfactant and cosurfactant are equal (Sharma, et al. 1984). In this work, the cosurfactants Neodol 91 and Neodol 25 were used. These cosurfactants are mixtures of straight chain alcohols from which the AES surfactants are synthesized. Neodol 91 contains C_9 to C_{11} alcohols, and Neodol 25, C_{12} to C_{15} alcohols.

The cosurfactants are insoluble in water. They can only be brought into solution by the action of the surfactants. The procedure used was to dissolve the AES surfactants (1.0% active, by weight) in synthetic Mt. Simon brine and warm this solution to 50° C. The alcohol cosurfactant was then added as a liquid (after melting if necessary), and the mixture was stirred at this temperature to produce a solution or emulsion. Alcohol was added at concentrations ranging from 0 to 1.0% by weight.

Mixtures with more than 0.2% alcohol were turbid, suggesting that the capacity of the surfactant solution to dissolve the alcohol had been exceeded. Excess surfactant appeared as an emulsified separate phase. The threshold cosurfactant concentration for formation of the emulsion approximately coincided with the optimum cosurfactant concentration, as discussed below. With AES 1215-3S, the emulsified droplets were buoyant (the density of the alcohol is about 0.85 g/cm^3) and rose to form a separate layer at the top of the liquid, occupying as much as three-quarters of the total volume. In these cases separate foaming tests were done on the buoyant layer and the main layer; little difference was noted between the two.

A test method was devised to screen surfactants for foam stability. The method is a variant of the Ross-Miles pour test and is based on ASTM method D-1173. First, 35 cm^3 of the foamer solution is placed in a standard 250-cm^3 graduated cylinder and the cylinder is tilted and rotated to coat the walls. Then 50 cm^3 of foamer solution is dropped from a standard 50-cm^3 pipette into the cylinder. The tip of the pipette is 65.0 cm above the 35 cm^3 mark of the graduated cylinder. The height of the foam column formed is measured immediately and at intervals until the foam collapses. The top of the cylinder is covered with aluminum foil during this period to reduce evaporation. This test is not necessarily indicative of the stability of foam in a porous medium, but it is considered adequate to discriminate among foamer solutions in selecting those which produce longer-lasting foams.

Results of foaming tests with the four AES surfactants are shown in Figures 4.1 through 4.4. These figures show that addition of the appropriate long-chain alcohol produced a marked increase in static foam stability up to about a 1:5 alcohol:AES ratio. Beyond this level, additional alcohol increased the solution viscosity. Increased viscosity was inferred from an increase in the length of time needed to drain the liquid from the pipette during the drop test. Increased viscosity also reduces the height of foam initially formed in the Ross-Miles test.

With AES 911-2.5S, addition of Neodol 91 produced little increase in foam stability (Figure 4.1). With AES 1213-6.5S and AES 1215-9S (Figures 4.2 and 4.3), addition of increasing amounts of Neodol 25 increased foam stability up to a 0.2 weight ratio of alcohol to AES, but increasing the alcohol beyond this level only increased the viscosity, which reduced the volume of foam formed in the test. With AES 1215-3S, addition of Neodol 25 reduced the initial foam volume (Figure 4.4).

Figures 4.5 through 4.7 show the decay of foam volume with duplicate batches of foamer solutions. The tests shown in these figures were run at different times, while the tests shown in Figures 4.1 through 4.4 were run simultaneously. The lack of reproducibility shown in Figures 4.5 through 4.7 may have been caused by different conditions (temperature, bench vibration) existing during the tests. While reproductibility is only fair, the stabilizing effect of cosurfactant

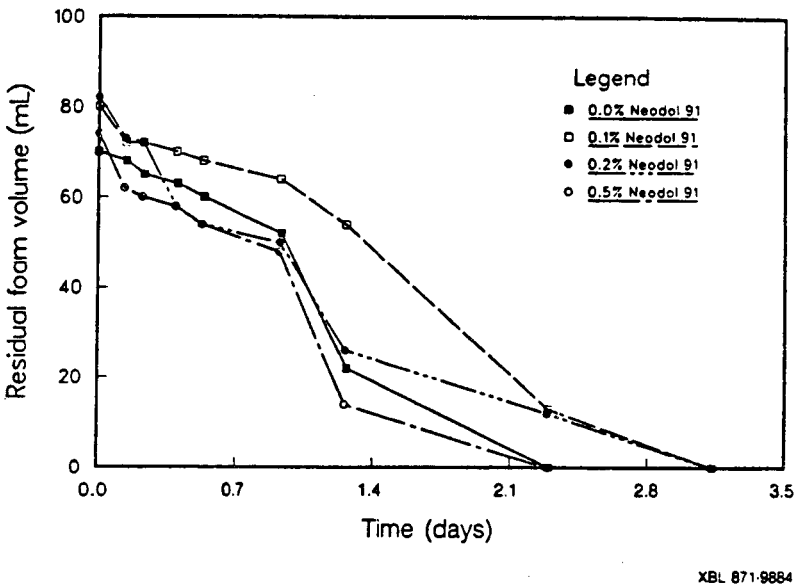

Figure 4.1. Static foam longevity measured in drop tests, 1% Shell Enordet AES 911-2.5S in synthetic Mt. Simon brine, with varying amounts of Neodol 91.

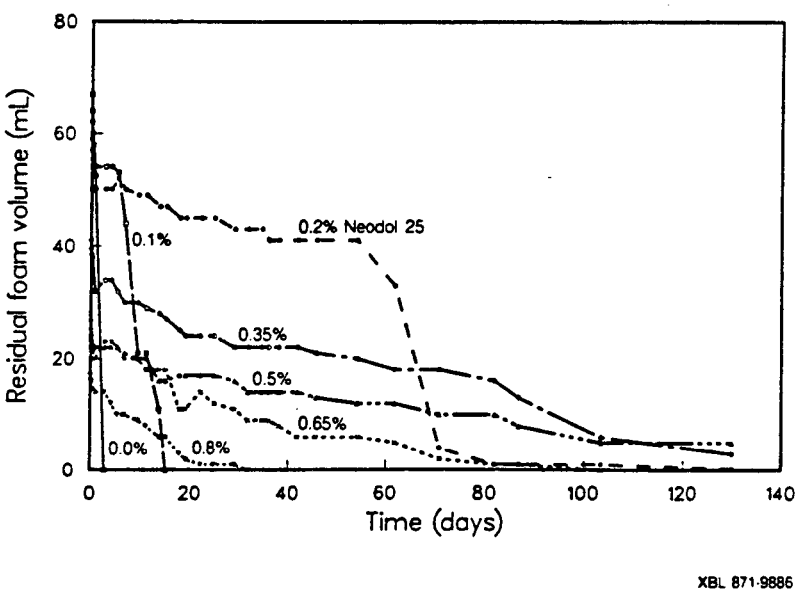

Figure 4.2. Static foam longevity measured in drop tests, 1% Shell Enordet AES 1213-6.5S in synthetic Mt. Simon brine, with varying amounts of Neodol 25.

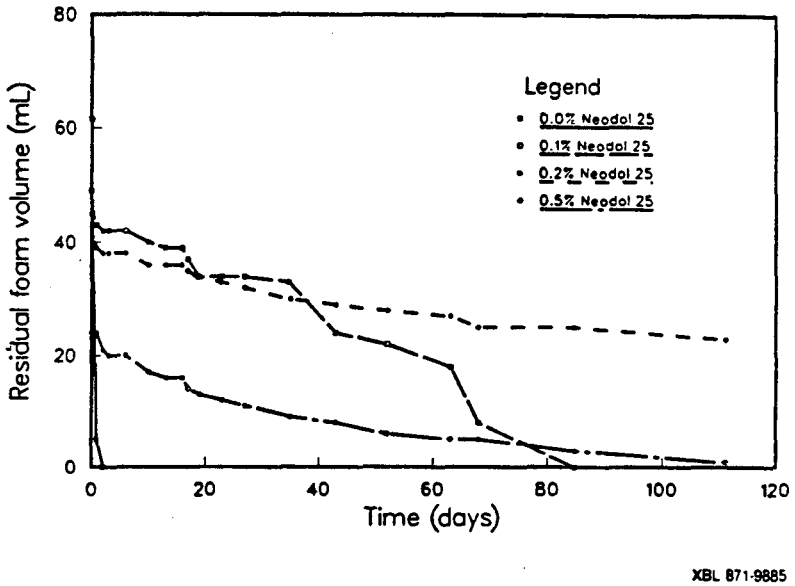

Figure 4.3. Static foam longevity measured in drop tests, 1% Shell Enordet AES 1215-9S in synthetic Mt. Simon brine, with varying amounts of Neodol 25.

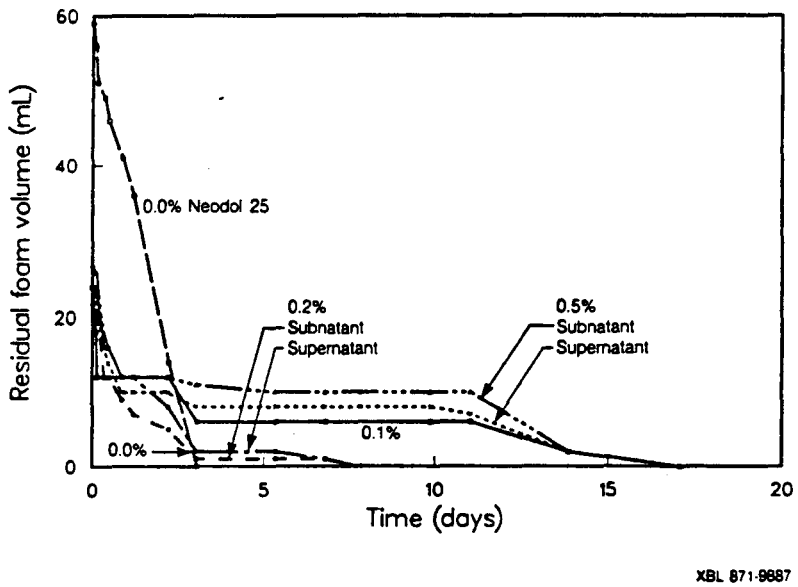

Figure 4.4. Static foam longevity measured in drop tests, 1% Shell Enordet AES 1215-3S in synthetic Mt. Simon brine, with varying amounts of Neodol 25.

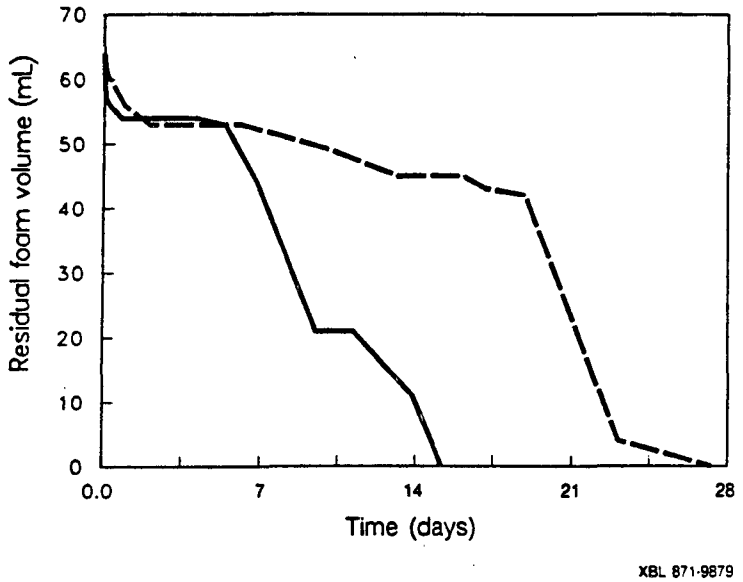

Figure 4.5. Duplicate tests of static foam stability, 1% Shell Enordet AES 1213-6.5S in synthetic Mt. Simon brine, with 0.1% Neodol 25.

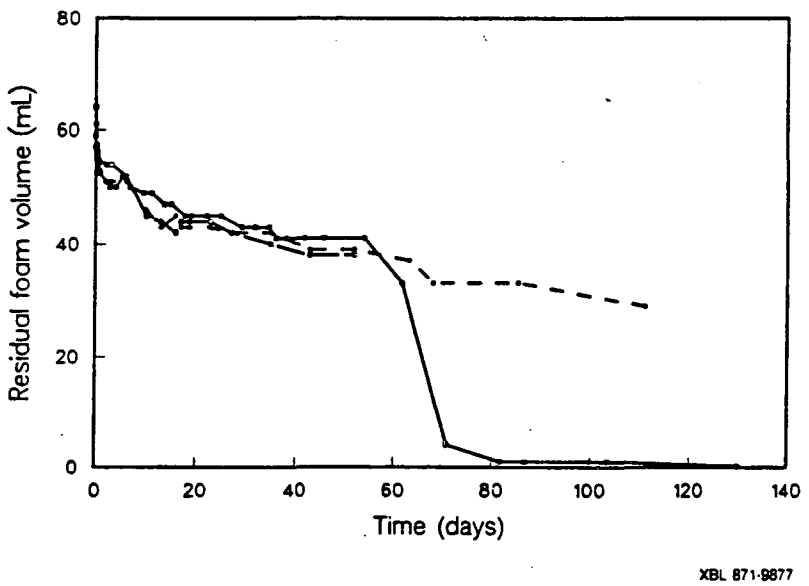

Figure 4.6. Duplicate tests of static foam stability, 1% Shell Enordet AES 1213-6.5S in synthetic Mt. Simon brine, with 0.2% Neodol 25.

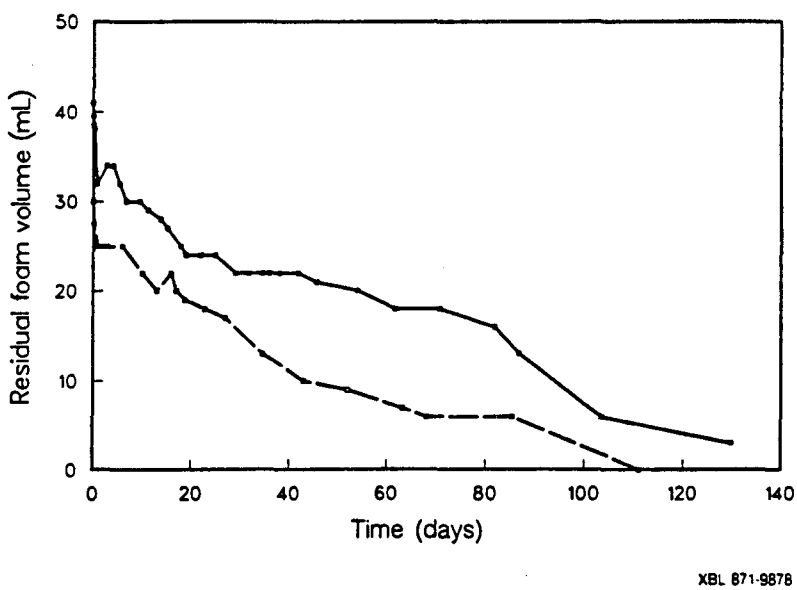

Figure 4.7. Duplicate tests of static foam stability, 1% Shell Enordet AES 1213-6.5S in synthetic Mt. Simon brine, with 0.35% Neodol 25.

addition at the 1:5 concentration ratio is clear. Based on these results, a combination of 1% AES 1215-9S with 0.2% Neodol 25 in synthetic Mt. Simon brine was selected for foam-block experiments in sandpacks and in sandstone cores.

The Neodol AES surfactants were experimental batches and not available in sufficient quantity to complete this work. Therefore, for the high pressure experiments in sandstone cores Steol 7N, which is chemically similar to AES1215-9S and commercially available, was substituted. As a cosurfactant lauryl alcohol was used.

4.2. Foam Rheology in Porous Media

Two experiments were done to measure the rheology of foam in porous media. In these experiments, gas and liquid were injected simultaneously into a sandpack or a sandstone core, and the resulting pressure gradient was measured.

The first experiment was done at one atmosphere back pressure in a sandpack, as reported in Section 4.2.1 in this chapter. The second experiment (actually a series of experiments) was done at simulated reservoir conditions, i.e., in sandstone cores at elevated back pressure. Those experiments are reported in Appendix E.

4.2.1. Foam Flow Experiments

The first set of experiments, using a foamer solution consisting of 1% Triton X-100 in distilled water, was conducted to measure the rheological properties of foam in a sandpack.

The sandpack was 1/2-inch (nominal) schedule 40 grey PVC pipe, packed with Ottawa flint shot 3.0 sand. The particle size distribution of this sand is shown in Figure 4.8. The permeability of the sandpack to gas was 92.6±2.5 Darcy. Endcaps were socket welded using grey PVC cement. All penetrations through the pipe walls and endcaps were 1/8-in. standard pipe thread, and threads were brushed with PVC cement. Bourdon-tube pressure gauges measured the gas injection pressure and the pressure at three locations along the sandpack and at the exit. As shown in Figure 4.9, liquid was injected at the bottom of the column and gas was injected through the side. Gas was actually injected at the center line of the sandpack, not at the wall.

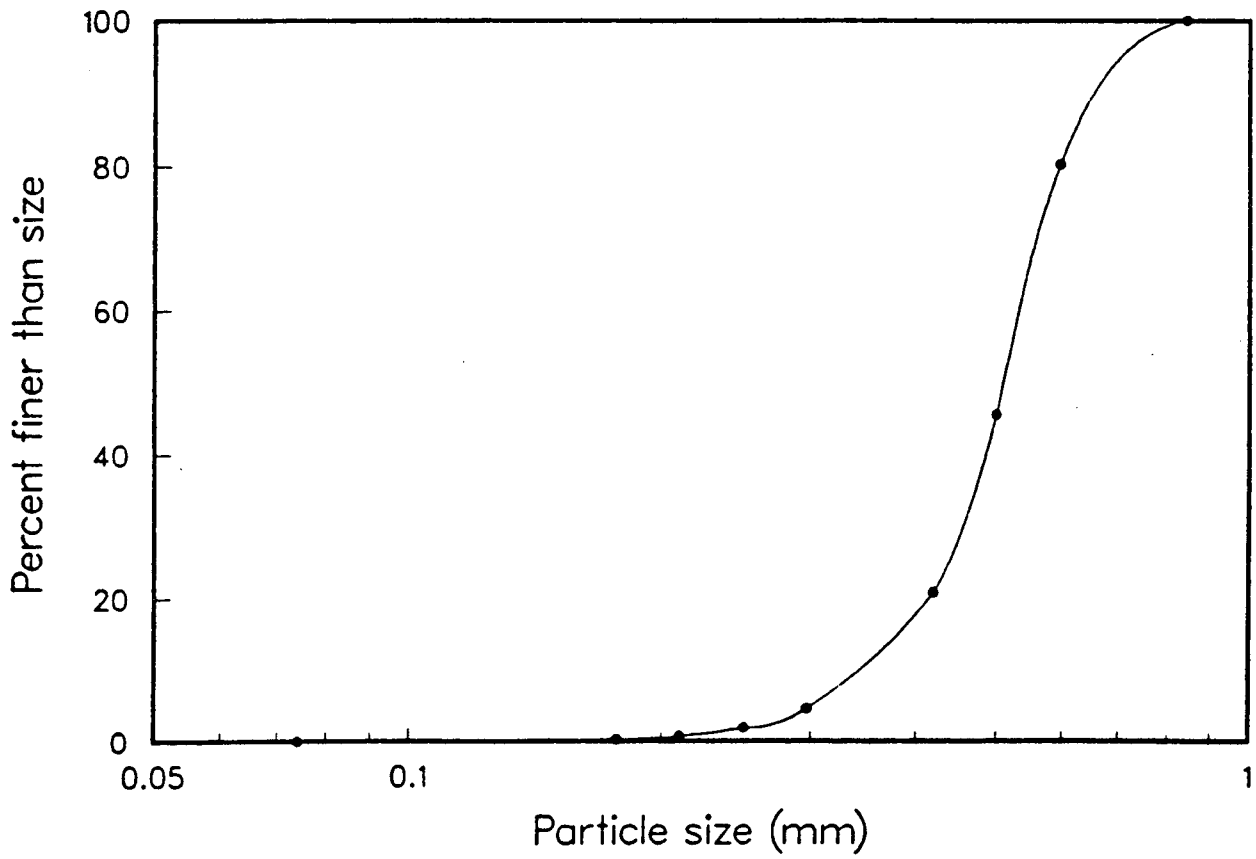

Figure 4.8. Grain size distribution of Ottawa Flint shot 3.0 sand used in foam rheology and blocking studies.

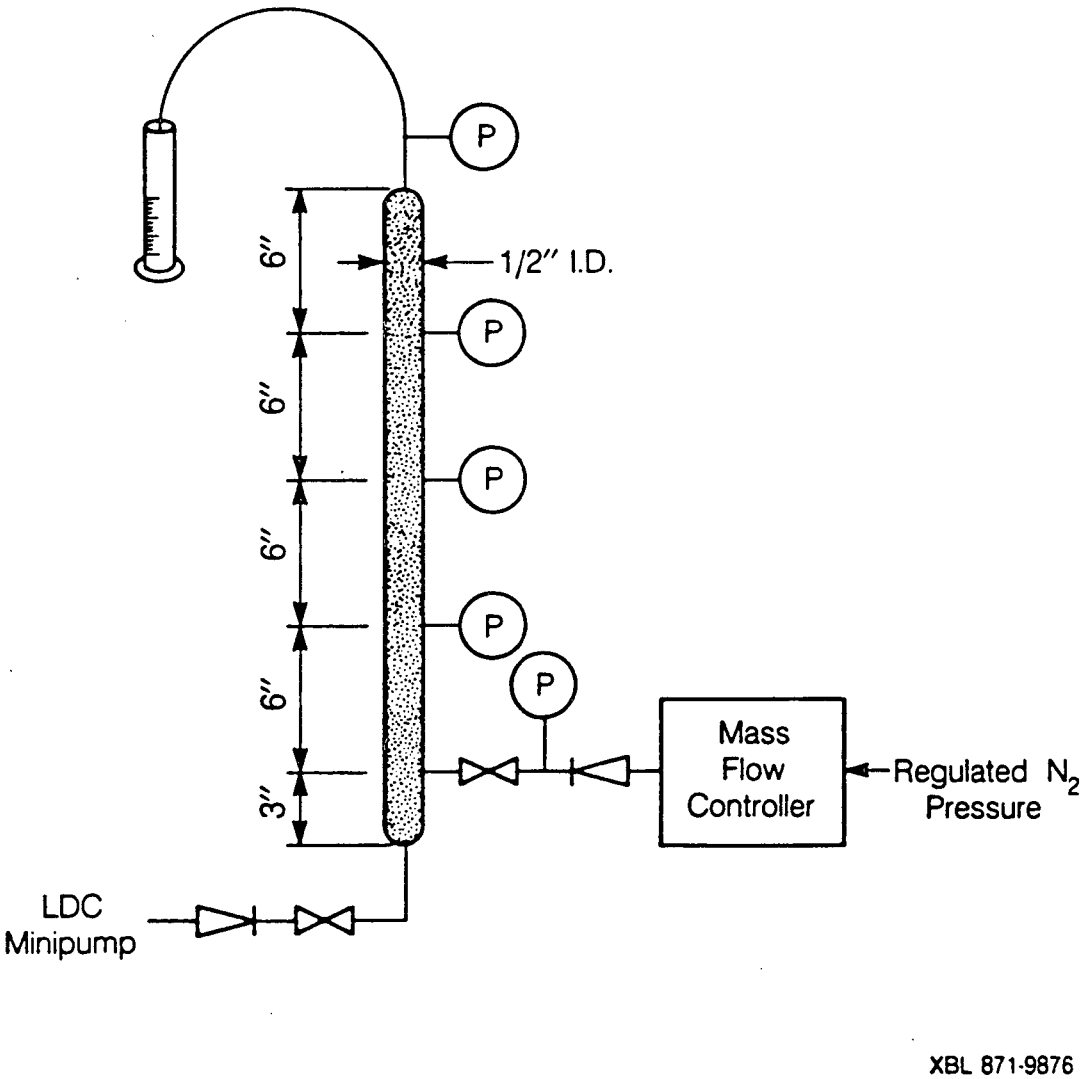

Figure 4.9. Apparatus for foam rheology study in sandpacks, schematic.

Before starting an experiment, the sandpack was evacuated and the air replaced with CO_2. The sandpack was then evacuated again and distilled water was pumped into the sandpack. The foamer solution was then pumped through the sandpack for 10 pore volumes. A simple shaking test showed that the liquid emerging from the sandpack had as much foamer solution as the influent, so it was assumed that the adsorptive capacity of the sand for surfactant had been satisfied. After saturating the sandpack with foamer solution, the experiment was started.

The experiment consisted of injecting gas at a controlled pressure while liquid was injected at a controlled volumetric flow rate. Pressures measured by the bourdon-tube gauges were recorded, and the flow rates of gas and liquid were measured by collecting the effluent foam into a pre-weighed graduated cylinder. The flow rates were calculated from the amount of time needed to fill the cylinder and the volume and weight of the collected foam. Gas flow rates were also measured by a Matheson mass-flow controller. The gas injection pressure was held constant while the liquid flow rate was increased in stages from 3 to 18 cm^3/min. Then the liquid flow rate was decreased to 3 cm^3/min and flow rates were remeasured before increasing the gas injection pressure for another sweep through the liquid flow rates. After each change of either gas injection pressure or liquid flow rate, pressure and flow rates stabilized quickly. Five minutes at each set of conditions were adequate to assure steady state. Results of the experiment are shown in Figure 4.10. Excellent reproducibility of conditions was obtained, with no observable hysteresis or effects of flow history. For example, after sweeping from point C to point D, the liquid flow rate was reduced and point C′ was measured; similarly for points E and E′. After reaching point H, gas injection was switched from injection pressure control to injection rate control, using the mass-flow controller. Then both gas and liquid rates were reduced by one-third, to point I, and then by another one-third, to point J, while the gas injection pressures were measured. The injection pressures, as shown in Figure 4.10 (points I and J), agreed with the relationship between injection pressure and fluid flow rates that was established by points A through H. The experiment was stopped, and restarted on the following day with points K through L and M through N. Again excellent reproducibility was observed.

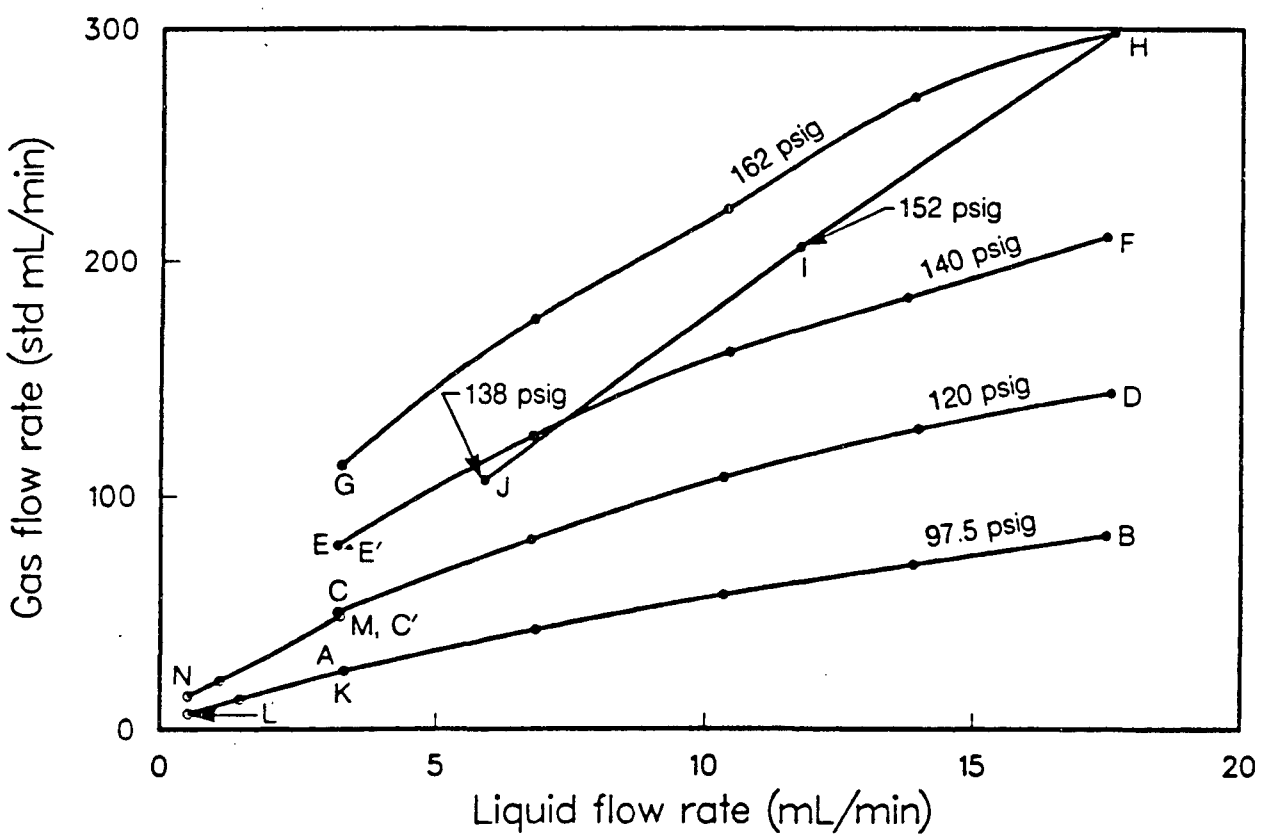

XBL 871-9888

Figure 4.10. Foam rheology in sandpack. Plot of gas and liquid flow rates, gas injected at controlled pressure and liquid at controlled flow rate.

The results shown in Figure 4.10 are counterintuitive, in that when liquid flow rate was increased at constant gas injection pressure, the gas flow rate also increased. Without foam, the gas flow rate would have decreased. At a particular gas injection pressure, the ratio of gas to liquid flow rate was nearly constant. To a large degree, the ratio of the gas to liquid flow rate was determined by the gas injection pressure, and the flow rates of both gas and liquid was determined by the liquid flow rate.

4.3. Permeability Reduction by Foam

Several experiments were conducted to verify and measure the ability of foam to reduce the permeability of a porous medium to gas or to liquid. In experiments in sandpacks at one atmosphere back pressure, complete blocking of gas flow, but of variable duration, was produced; in experiments in sandstone cores at elevated back pressure, it was not possible to block gas flow completely but a reduction in the permeability to gas by factors of 100 to 1000 was achieved. This difference appears to result not from the difference in porous media, but rather from the difference in back pressure. When the outlet pressure of the system is small compared to the inlet pressure, a large expansion of bubbles can be caused by reducing the gas injection pressure. This apparently causes rearrangement of lamellae in the pores to a configuration that completely blocks gas flow. Section 4.4 of this chapter describes experiments in which complete, but temporary, blocking of gas flow was achieved in sandpacks by reducing the gas injection pressure, using a foamer solution consisting of synthetic brine, 1% AES 1213-6.5S surfactant, and 0.2% Neodol 25 cosurfactant. Appendix F provides details on additional experiments in which 0.5% guar (a natural polymer) was added to the foamer solution, making the liquid more viscous and improving the durability of the foam. It also has a report on experiments in sandstone cores at elevated back pressure. These experiments are more relevant to field conditions. It was found that the foam reduced the permeability of both 1.3-darcy Boise sandstone and 0.19 darcy Berea sandstone to approximately 1 millidarcy, and this permeability gradually increased with time as gas was continuously injected through the core. Appendix F also presents data to show that the foam can be regenerated by injection of additional slugs of liquid. It also shows data on the

reduction of permeability to liquid, which is important for application of foam to delay water coning into gas withdrawal wells.

4.4. Foam Blocking Experiments

Sandpack experiments were done to gain insight into the foam blocking mechanism. In early foam blocking experiments by Bernard and Holm (1964) and by Albrecht and Marsden (1970), foam was formed by injecting gas into a sandpack previously saturated with foamer solution. A difficulty with this type of experiment is that although foam forms in the sandpack, the system is never at steady state because liquid is continuously leaving the sandpack while none enters. It was felt that forming foam at steady state would permit better control of experiments. Foam was formed in sandpacks by simultaneously injecting gas and liquid through check valves (Figure 4.11). Gas was injected at a constant pressure and liquid at a constant flow rate; gas and liquid flow rates were measured by timing and weighing foam exit flow into a graduated cylinder. The foamer solution was 1% AES 1213-6.5S with 0.2% Neodol 25 in either synthetic Mt. Simon brine or sulfate-free brine. Two-foot-long sandpacks of Ottawa Flint Shot 3.0 sand were used. The permeability of the sandpacks ranged from 90 to 110 darcy. The sandpack was first saturated with the foamer solution and 10 or more pore volumes were flowed through it to reach adsorptive equilibrium with the sand, and then gas injection was started. Foam was formed and flowed through the sandpack at steady state conditions for a measured period of time (generally about 1 hr).

A simple preliminary experiment was done to determine whether gas injected into a sandpack saturated with foamer solution would block itself by forming foam as it entered. Using the apparatus shown in Figure 4.11, the sandpack was initially saturated with the foamer solution, and gas pressure was applied at 10 psig. The rate of gas injection was monitored by observing the rate of liquid forced out of the sandpack by entering gas. This rate was initially fast, but rapidly decreased to a low level, suggesting that foam was being formed, reducing the permeability of the sandpack. However, gas broke through within a few minutes. This suggested that for blocking to occur, foam must be formed and then the gas pressure must be reduced below the

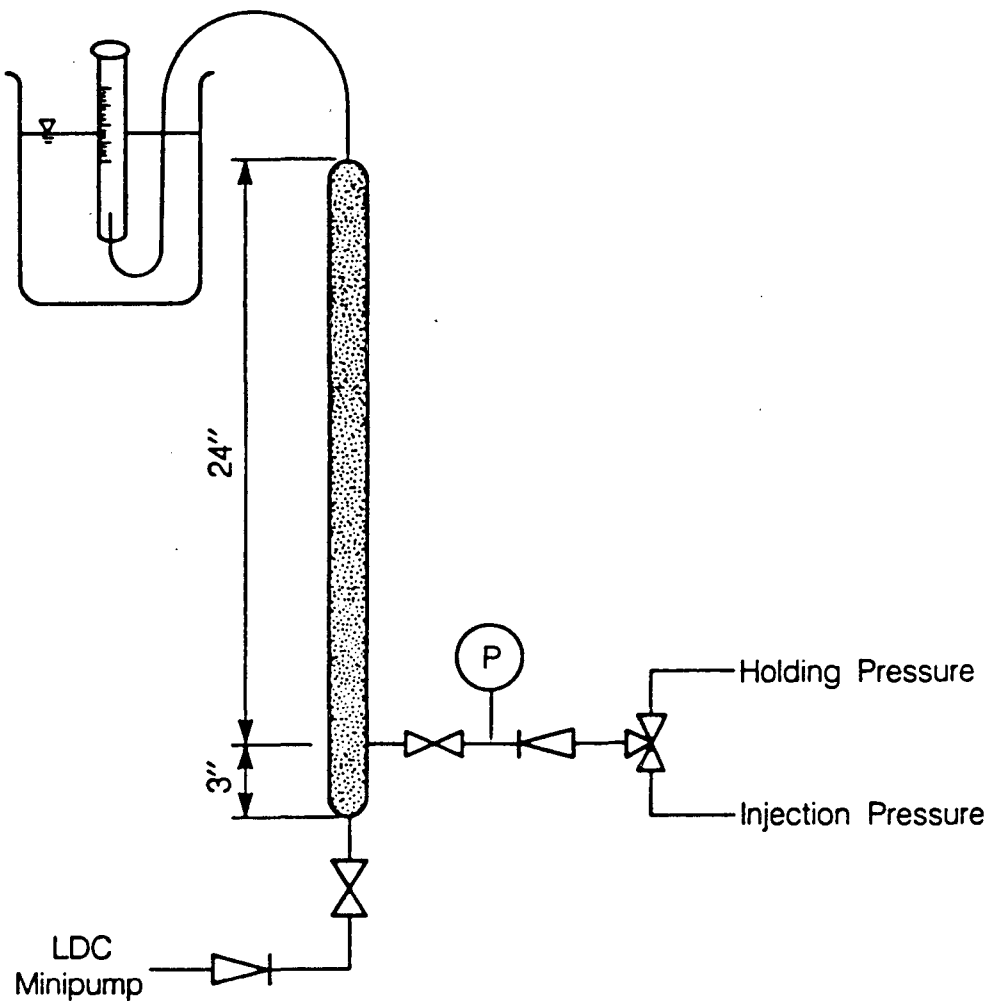

XBL 871-9875

Figure 4.11. Apparatus for forming foam blocks in sandpacks, schematic.

pressure at which the foam was formed.

In subsequent experiments, foam blocks were formed by rapidly reducing the gas injection pressure from the "injection" pressure to the "holding" pressure. Liquid injection was stopped at the same time. In a few minutes, flow of foam from the sandpack stopped, indicating that gas flow was blocked. After blocking occurred, any further gas emerging from the sandpack was collected by displacing water in an inverted graduated cylinder. In this way both the time of first breakthrough and the flow rate at breakthrough were monitored.

4.4.1. Blocking Trials Results

As shown in Table 4.2, foam was formed by injecting foamer solution at rates ranging from 1.5 to 18.9 mL/min and gas at injection pressure ranging from 16 to 143 psig. Blocking was achieved in all cases when the absolute holding pressure was less than 74% of the absolute injection pressure.

The time to breakthrough ranged from less than one day in several runs to over a month. This variability in the breakthrough time was noted even in replicate runs. Such variability suggests that either the breakthrough time is very sensitive to small variations in experimental procedure, or that it is controlled by random processes such as spontaneous rupture of lamellae.

These results prompted an investigation of various methods to produce blocking in an effort to extend the time to breakthrough and improve the reproducibility of these times. Blocking apparently results from expansion of gas bubbles in pores. As the injection pressure is reduced to the holding pressure, the available pressure gradient to force bubbles through pore throats decreases, while at the same time the pressure gradients needed to force them through pore throats increases. As mentioned, a reduction of 26% was always sufficient to cause blocking. The results summarized in Table 4.2 show that reduction greater than 26%, while still causing blocking, did not increase the time to breakthrough.

Rapid expansion of bubbles during the blocking phase of the experiment may have caused rupture of some of the lamellae in the sandpack and adversely affected the ability of the foam

Table 4.2. Results of foam blocking experiments in 60-cm long Ottawa Flint shot 3.0 sandpacks (90-110 darcy).

Run no.	Gas inj. press. (psig)	Liq. flow rate (mL/min)	Gas flow rate (std mL/min)	Exit quality (%)	Free liq.[a] (%)	Blocking pressure (psig)	Blocking duration (time)	Permeability after breakthrough[b] (Darcy)
15	69	15.6	32.9	71.6	16.1	16	8 d	-
16	69	14.9	25.5	66.9	15.2	17	21 h	0.5 (16 psig) 0.2 (10 psig)
16A[c]	16	14.9	-	low	high	10	33 d	0.4 (for 2 d)[g]
19	115	18.4	80.3	81.4	0	100	did not block	-
20	122	19.8	78.4	80.7	0	10	48 d	-
21	111	18.9	90.3	82.7	0	10	113 h	0.15 (init) 5 (2 d)[h]
23	116	18.9	92.0	83.0	0	10	6 h	0.96
25	113	19.1	101.6	84.0	0	10	1 d	-
27	40	15.6	3.7	19.0	85.3	30	5 min	-
27A[d]	16	1.5	-	low	high	10	<18 h	-
28	50	1.5	-	low	high	10	<18 h	-
30	143 red. to 30[e]	18.0	198 red. to 0	91.7 red. to 0	varied	10	>7 h, <20 h	0.005 (init) 1.7 (2 d)[i]
31	140 red. to 50	18.9 red. to 2	167 red. to 0	89.8 red. to 0	varied	50 red. to 10[f]	4.5 d	0.5

[a] For foams of exit quality less than 70%, the collected foam appears as bubbles forming a head over continuous liquid. Free liquid is the fraction of liquid which is continuous liquid, not foam.
[b] Permeability increased with time after breakthrough. In run 16, permeability at breakthrough was measured at two values of injection pressure.
[c] After run 16 broke through, restarted liquid flow and then gas flow until gas emerged, then reduced gas pressure to block.
[d] After run 27 broke through, restarted liquid flow and then gas flow until gas emerged, then reduced gas pressure to block.
[e] During foam formation, gas injection pressure was reduced from 143 to 30 psig.
[f] Initial blocking was at 50 psig, then holding pressure was reduced in stages to 10 psig.
[g] 0.4 darcy after breakthrough, and continuing for 2 days; then experiment was discontinued.
[h] 0.15 darcy after breakthrough increased to 5 darcy 2 days later, then experiment was discontinued.
[i] 0.005 darcy after breakthrough increased to 1.7 darcy 2 days later, then experiment was discontinued.

bank to support a pressure gradient. Two experiment runs were made in which gradual reduction of gas injection pressure was used to minimize this effect and in one of these two runs the holding pressure was gradually reduced after initial blocking. These modes of operation did not produce any consistent increase in the time to breakthrough.

Two additional runs were made using different techniques that require description apart from Table 4.2. In the first run (Run No. 29, not shown in Table 4.2), foam was formed by injecting both gas and liquid at controlled injection rates. Initially, gas was injected at 160 standard cm^3/min, and liquid at 18.3 cm^3/min. The gas and liquid injection rates were both reduced in proportion, to reduce gradually the flow rate of foam, and cause blocking. However, the expected decrease in gas injection pressure did not result, because of the non-Newtonian flow behavior exhibited by foam as shown in Figure 4.10. As the flow rate is reduced, the apparent viscosity increases, requiring the same pressure drop to move a smaller flow rate of foam through the sandpack. In the second run (Run No. 35, also not shown in Table 4.2), foam was formed and then blocked in five cycles, with injection pressures increasing from 80 to 160 psig, and keeping the holding pressure constant at 10 psig. After forming foam at an injection pressure of 140 psig, reduction to a holding pressure of 100 psig did not cause blocking. After the last cycle, at a gas injection pressure of 160 psig, flow was blocked at a holding pressure of 70 psig, but gas broke through after one hour. In all runs, when gas first broke through, the measured permeability to gas was always less then 0.5% of the intrinsic permeability of the sandpack. With time this permeability increased.

The following qualitative description of breakthrough is consistent with the data. In blocked conditions, each flow path in the sandpack must contain some minimum number of lamellae. In time, lamellae along a path rupture, either spontaneously because they are metastable, or systematically because of a change in the local pressure gradient, or because gas diffusion drives two lamellae together. As fewer of the original lamellae remain, the overall gas pressure drop that can be supported by the remaining lamellae decreases. Breakthrough occurs when too few lamellae remain to support the imposed pressure drop. Less-permeable porous

media, having finer pores and more pore throats along a flow path, should therefore be more durable, and similarly so should longer porous media. This was observed by Bernard and Holm (1964) without explanation.

5.0. NUMERICAL SIMULATOR DEVELOPMENT

As part of this project, a numerical simulation tool was developed that can model simultaneous flow of several fluid phases in a porous medium. This chapter briefly summarizes the current status of the three-phase gas storage reservoir simulator "MULKOM-GWF," which was developed under this project for simulation of flow of gas, water, and foam by suitable modification of an existing general-purpose multiphase simulator MULKOM (Pruess 1983, 1988). It should be emphasized that MULKOM is a research tool which continues to evolve. A technical description of the novel features of MULKOM-GWF and a guide for preparation of input data are presented in Appendix C. Analytical solutions that were used to test the code accuracy for displacement of Newtonian fluids by non-Newtonian fluids are presented in Appendix G. In this chapter the approach and formulation used in MULKOM-GWF is briefly summarized.

MULKOM-GWF is a member of the MULKOM family of multiphase flow codes. It is designed to simulate the flow of gas, water, and foam in porous media, using concepts borrowed from "black oil" simulation. The flow of each of the three phases is represented by means of a multiphase extension of Darcy's law. The peculiar non-Newtonian flow properties of foam are described with an effective viscosity that varies as a function of the pressure gradient. In applications of MULKOM-GWF it is not necessary that all three phases be present; the code can also simulate conventional aquifer gas storage operations by simply setting foam saturation to a very small value.

The formulation used in MULKOM-GWF emphasizes stability and robustness. All flow terms are calculated fully implicitly, and the mass balance equations for gas, water, and foam are solved in a fully coupled simultaneous manner. Because these equations tend to be highly nonlinear, an iterative Newton-Raphson process is used. The linear equations arising at each iteration step are solved with a sparse version of LU-decomposition and backsubstitution. The PVT

properties of the water and gas phases are calculated from empirical correlations, assuming that the liquid and gas consist of pure water and pure methane, respectively. Foam density is represented by the real gas law. Effects of capillarity and relative permeability are described as is customary in black oil simulators, with foam taking the place of the oil phase (wettability intermediate between water and gas). Special provisions are available to treat sharp displacement fronts. Production and injection wells can flow under a combination of pressure and rate constraints, with arbitrary user-specified schedules.

An unconventional aspect of MULKOM-GWF is the space discretization, which is based on an "integral finite difference" (control volume) technique. This avoids any reference to a global system of coordinates, and thus offers the flexibility of being applicable to regular or irregular grid systems in one, two, or three dimensions. When regular grid systems are used the method is completely equivalent to conventional finite differences.

The simulator has been applied to model injection into and production from gas storage reservoirs, water coning at gas withdrawal wells, emplacement of foam plumes in aquifers, and one-dimensional laboratory displacement experiments involving gas, water and foam. Figure 5.1 illustrates the concept of reducing water coning in gas withdrawal wells by means of a foam lens emplaced near the gas-water contact in a gas storage reservoir. Figure 5.2 shows the predicted water production rate for a gas well flowing at the rate of 5 MMCF/D. Four cases were modeled with the simulator, one with no foam lens and three cases where the foam was located at the gas-water contact and 5m above and 5m below. The formation permeability was assumed to be 37 md, and it was assumed that foam lens could reduce this by a factor of 100. The foam lens was cylindrical with a diameter of 30 m and a height of 10m. It can be seen that water production rates can be significantly delayed by the emplacement of the foam lens, and the best result was obtained when the foam was placed 5m above the gas-water contact. Figure 5.3 shows results for a Buckley-Leverett type one-dimensional immiscible displacement problem, in which the displacing phase is a non-Newtonian power law fluid. The numerical simulation agrees very well with an exact analytical solution that was derived for this case and is presented in Appendix G.

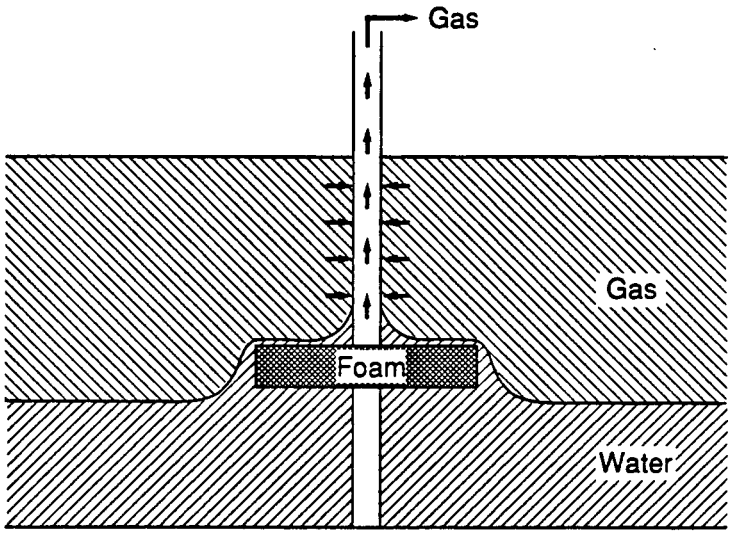

Figure 5.1. The concept of reducing water coning in gas storage withdrawal wells by means of a foam lens placed near the gas-water contact.

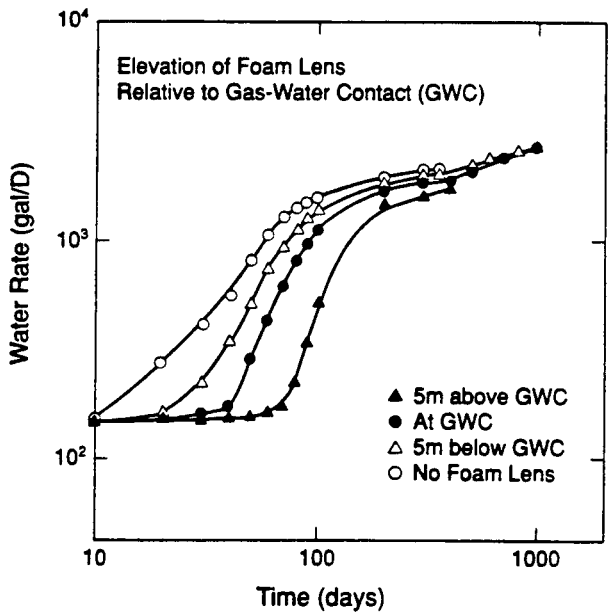

Figure 5.2. Numerically simulated water rates of a typical gas withdrawal well with and without protective foam lens. Three different elevations of the foam lens relative to the gas-water contact were examined.

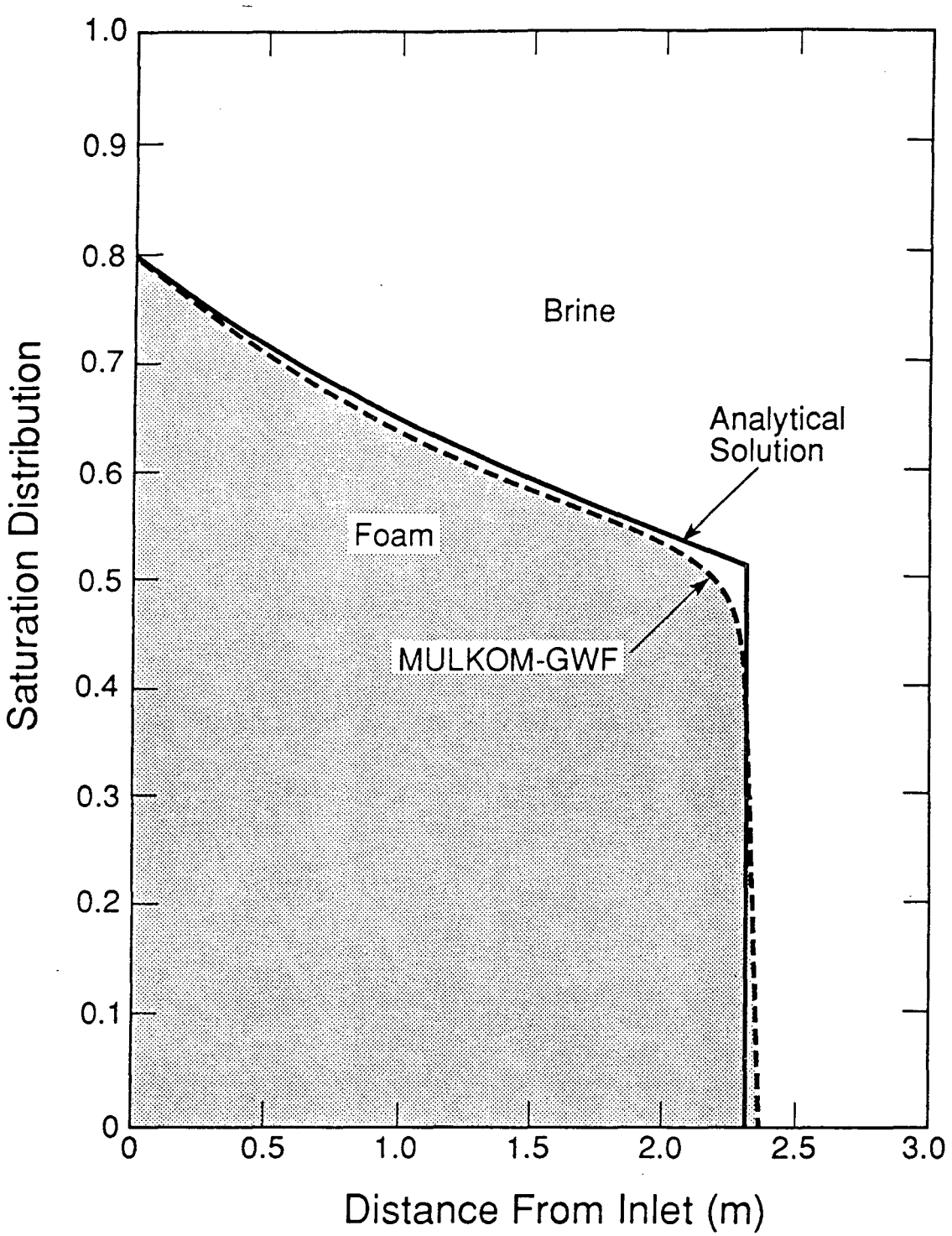

XBL 894-7540

Figure 5.3. Saturation distributions for one-dimensional displacement of brine (Newtonian fluid) by foam (non-Newtonian power law fluid).

6.0. FIELD EXPERIMENT DESIGN

The results of laboratory experiments presented in Chapter 4 and in Appendices B, E, and F showed that foam could be generated in cores of representative sandstones at reservoir conditions, that the pressure gradient in foam flow could be controlled by the liquid injection rate, that the foam would block the flow of gas or water and degrade slowly, and that it could be regenerated. But however much can be learned from laboratory experiments, they cannot assure success in a field operation where certain factors may be important that cannot be simulated in the laboratory. These include

- natural heterogeneity of the formation, which may prevent foam from being formed uniformly around a well
- radial flow in an aquifer, which causes flow velocities to decrease inversely with the distance from the well
- effectively infinite extent of saturated aquifer beyond the foam barrier
- likelihood of initial saturation being less than 100%
- uncontrolled chemical and biological conditions of a field site
- need to measure permeability reduction and longevity under field conditions.

As originally planned, this project was to include a field test in a shallow aquifer during the third year. However, laboratory results revealed a strong sensitivity of foam behavior to the ratio of injection pressure and back pressure, and showed that a test at actual reservoir conditions would be more useful. Therefore it was necessary to plan a field experiment to be carried out at substantial depth below the ground surface. Because of the much larger cost involved in a deep field experiment compared with the originally proposed shallow one, the field work was not carried out during this project. However, a field test remains an essential next step to the eventual application. The design of a proposed field experiment, with schedules and costs, is described below.

6.1. Proposed Field Experiment

The field experiment is planned to be carried out in two phases. The objectives of the first phase are to verify that a foam bank can be emplaced in an underground formation, that the foam bank is sufficiently stable to provide permeability reduction for the required length of time, and that the foam bank can be intentionally destroyed by injecting a foam breaker. In the second phase, foam would be used to create an enclosed storage volume and/or assess the ability of foam to reduce water coning during the withdrawal cycle in an operating storage field.

The proposed location for the first phase of the test program is the Los Medanos gas-storage field, operated by the Pacific Gas and Electric Company (PG&E). The Los Medanos gas field was discovered in 1958, and, after depletion, was acquired in 1972 by PG&E for underground storage, and put in full operation in 1980. It is a dry gas field, i.e., there is no water drive. The location of the field, near Concord, Contra Costa County, California, is shown in Figure 6.1. The field has 14 directional injection/withdrawal wells drilled from 4 pads and completed in the Domengine sand. The operating surface pressure of the field ranges between 600 and 1600 psig, and the maximum delivery at 1600 psig is approximately 290 MMCF/D. The working volume is approximately 14 BCF out of a total of 21 BCF gas in storage.

It is proposed that the experiment be done in the Nortonville sand, a thin (50 ft) sand formation above the Domengine sand in which gas is actively stored. Advantages of this test site include: high pressure (1600 psig) gas stored in the Domengine is available for injection; the depth of the formation (1800 ft) permits pressures representative of field conditions; experiments in the Nortonville should not affect PG&E 's operations in the Domengine; the shallow thickness of the Nortonville sand is appropriate for a test program; the site is continuously manned by PG&E for safety and security; and the location convenient to LBL permits intensive monitoring. Another attractive feature is the existence of a plugged well, Gino-1, which was used to drain gas from the Nortonville when the field was being depleted. During phase IIa, this well will be

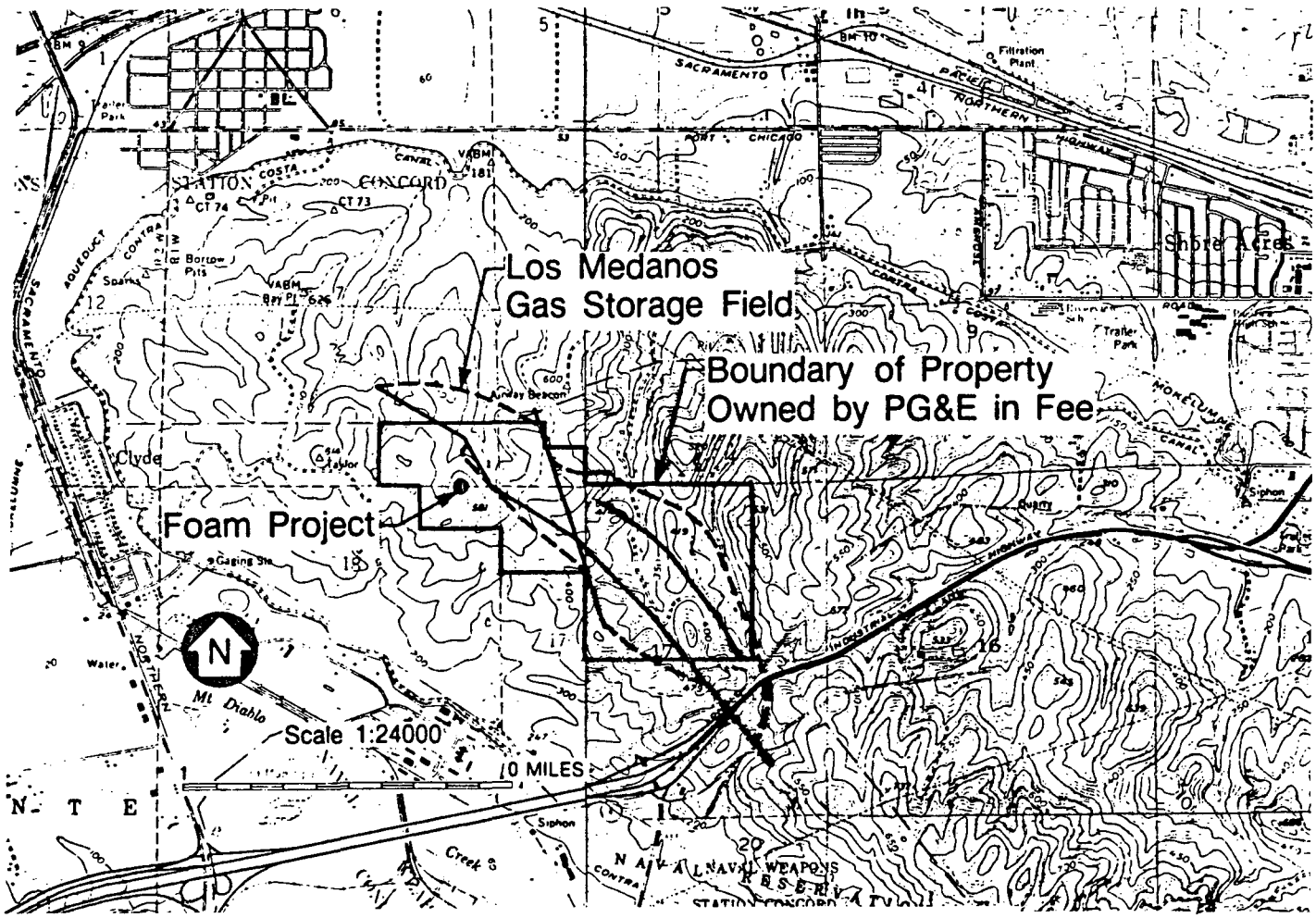

Figure 6.1. Location of proposed storage project at Los Medanos Field, Contra Costa County, California.

recompleted for use as an observation well. Figure 6.2 is a structure map of the top of the Nortonville sand, showing the location of the wells to be used in phases I and IIa. Figure 6.3 is a partial log of Gino-1.

The second phase is proposed to be conducted at the Los Medanos field in California and/or at a typical aquifer gas storage field.

6.2. Objectives

The general objective of this project is to assess at pilot scale the technical feasibility of the application of foam to underground gas storage. Specific objectives include:

Phase I

1. Verify ability to create a foam plume of modest size (r=10 ft) around an injection well, which suppresses gas permeability by a large factor (e.g. 1000).
2. Evaluate the stability (longevity) of the foam plume by monitoring the decay of wellbore pressure, and by means of gas pulse injection tests.
3. Assess ability to break foam in-situ by injecting a suitable foam breaker.

Phase IIa

1. Verify ability to create a foam "ring" (barrier spaced away from the injection well) by injecting a slug of surfactant solution, followed by water injection to space it away from the injection well, then by gas injection to form foam. This would be important for practical applications where it is desired to have a foam barrier some distance away from a well without incurring the cost of surfactant to foam the entire region from the well to the outer radius of the barrier.
2. Directly show the existence of, and monitor the permeability reduction resulting from, a foam barrier using an observation well.
3. Operate the region inside the foam barrier as a storage reservoir.

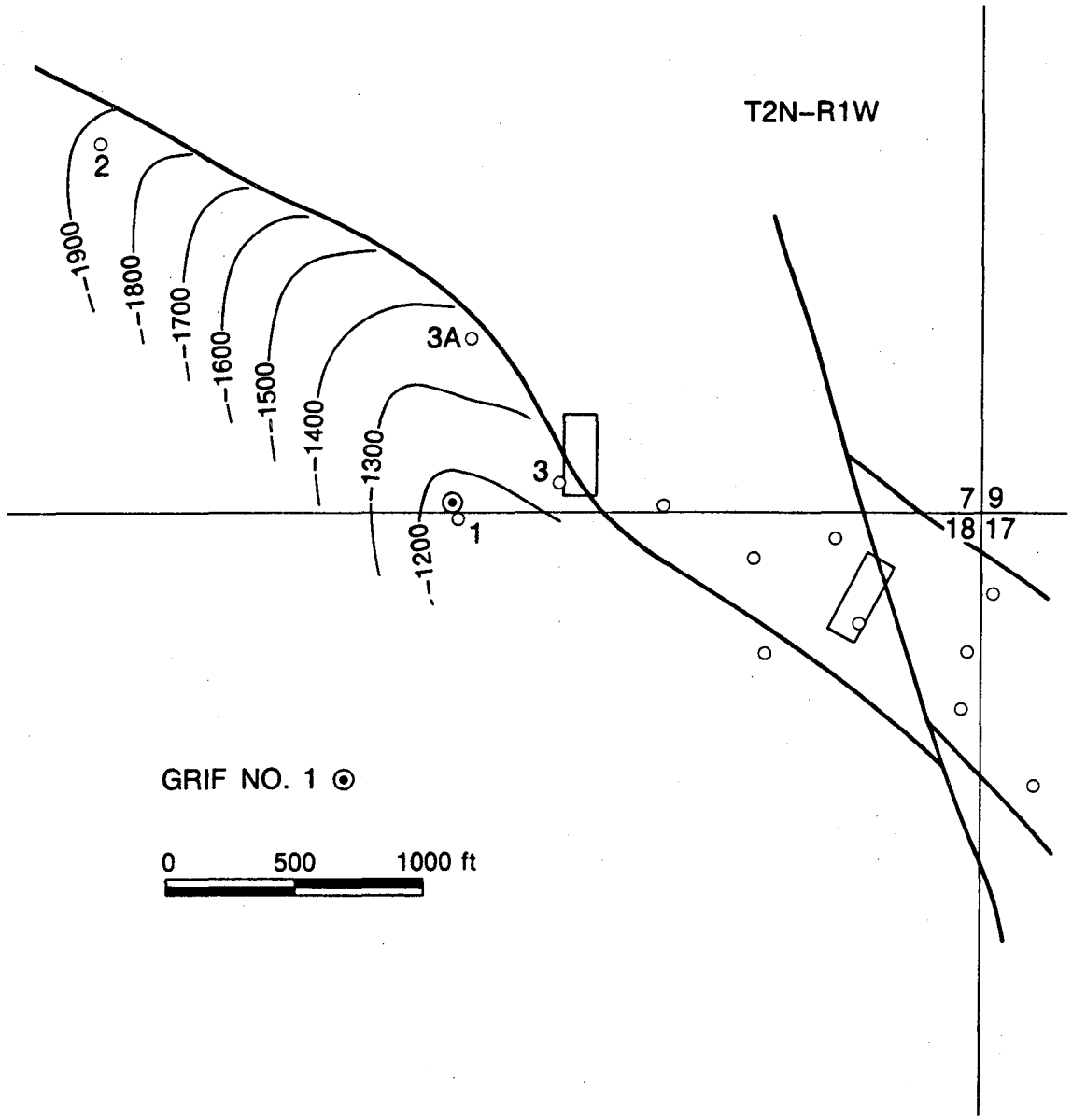

APPROXIMATE CONTOURS OF TOP NORTONVILLE SAND
(feet below mean sea level)

XBL 882-10044

Figure 6.2. Structure map, top of Nortonville sand, showing location of wells Gino-1 (labelled "1") and Grif-1 (bullseye).

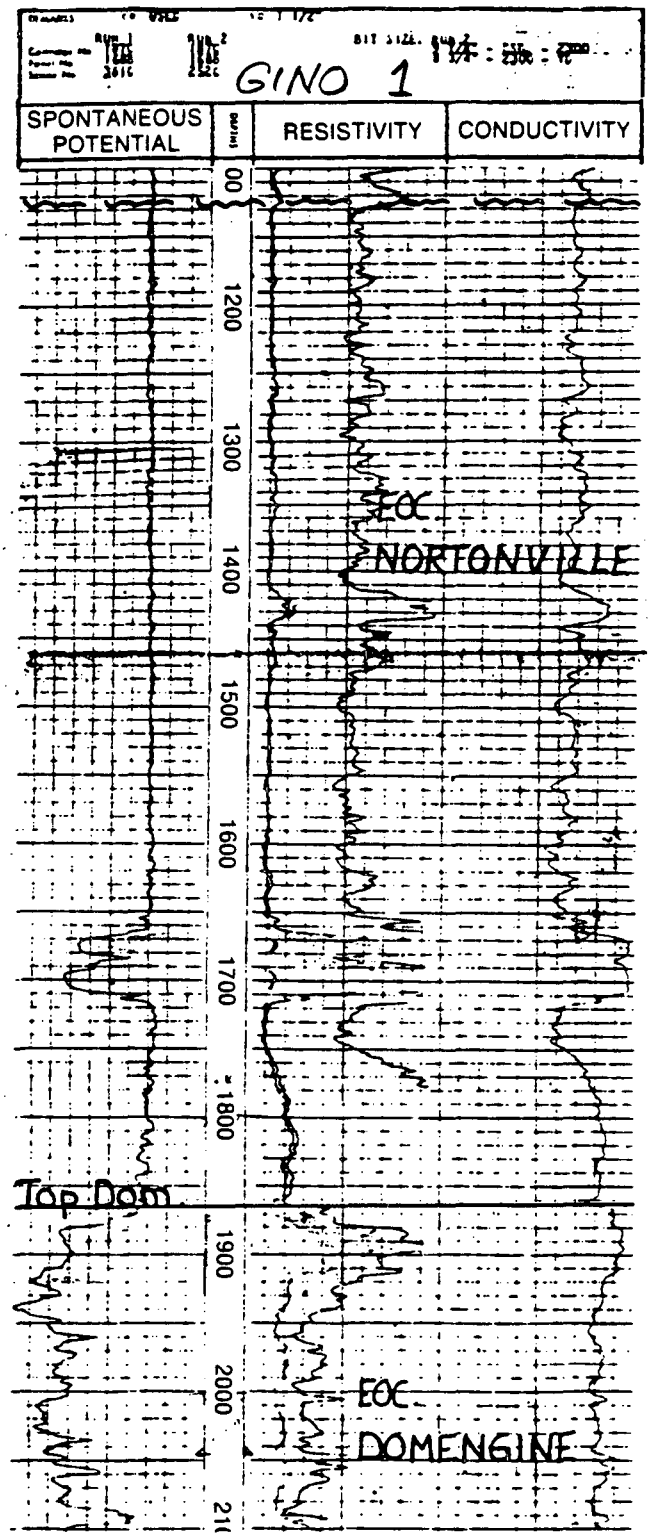

Figure 6.3. Partial log of well Gino-1, showing Nortonville and Domengine formations.

Phase IIb

1. Assess the ability to inject a foam "blanket" at the gas-water contact below a withdrawal well, which delays water coning during the withdrawal cycle.

2. Examine the ability to break the foam blanket by injection of foam breaker.

6.3. Field Operations

The following filed operations are planned to accomplish the stated goals:

Phase I: Form a foam bank in situ, measure its ability to block gas and its longevity.

a. Drill an injection well ("Grif-1"), completed in the Nortonville sand. Evaluate the formation by gas pressure transient testing. Perform laboratory studies to design surfactant and test cores.

b. Inject surfactant solution into Grif-1, followed by gas to form foam. Run neutron logs to determine gas saturation before and after gas injection. Successful generation of a foam plume would be verify by pressure tests which would indicate a large reduction in gas permeability (factor of 1000, based on laboratory tests).

c. Monitor pressure decline in the foam bank. Periodically conduct pressure pulse tests to monitor foam stability.

d. Break foam by injecting foam breaker. Breaking of foam would be indicated by a recovery of gas permeability.

Phase IIa: Recomplete observation well, flush out formation with brine, form a ring of foam 80 ft from the injection well, and store gas in the interior of the ring.

a. Recomplete existing well Gino-1 for observation.

b. Inject brine to flush the surfactant and foam breaker out of the test region.

c. Inject surfactant solution, water, and gas in that order to create a foam "ring" spaced away from the injection well.

d. Operate as a gas storage reservoir. Inject and withdraw gas over a six month period. Monitor pressures at both the observation and active wells. Run gas logs in both wells.

Phase IIb: Emplace foam barrier at existing well to prevent water coning.

a. Run preliminary test ("flow prover") on existing well.

b. Perforate well for foam injection.

c. Inject foam to foam horizontal blanket.

d. Run withdrawal cycle, monitor pressure and flow.

e. Retest well (run flow prover).

f. Break foam if required.

6.4. Budget

The proposed field experiment is planned in two phases. In Phase I (budgeted at $325,000 and scheduled for 160 days), the formation and stability of foam in an gas sand are to be established. After review of Phase I results, a decision to proceed with Phase IIa and/or Phase IIb could be made. Phase IIa, where foam would be used to contain stored gas, is budgeted at $525,000 and scheduled for 220 days. Phase IIb, where foam would be used to delay water coning in an operating storage field, is budgeted at $232,000 and scheduled for 240 days. The proposed schedule of field operations for phases I, IIa and IIb are presented in Tables 6-1 through 6-3, respectively. The budgets for phases I, IIa and IIb are presented in Tables 6-4 through 6-6, respectively. All budgets are in 1988 dollars.

Table 6.1.

Phase I Proposed Test Program at Grif 1

PG&E Los Medanos Field

Experiment 1 - Foam Injection around Wellbore

(1) Measure shutin wellhead pressure and run temperature survey.

(2) Test well productivity (or injectivity) to establish data base of formation properties. Run flow test and determine velocity profile with spinner survey.

(3) Install packer above perforated interval with 2-7/8'' tubing and connect up to foam injection equipment.

(4) Inject about 7000 barrels of untreated water (no surfactant) to develop a water-saturated zone around well bore out to about 40 feet. Run flow injection test to determine permeability and spinner survey for injection profile.

(5) Inject about 700 barrels of water containing 1% Steol 7N (Stepan Chemical Co.) surfactant to create a surfactant zone out to about 10 feet from well bore. Run spinner survey.

(6) Inject natural gas at controlled rate and pressure(s) to develop foam bank out to about 20 feet from well bore.

Experiment 2 - Foam Bank Properties and Longevity

(1) Run GRN log to determine foam distribution along borehole.

(2) Measure initial shutin pressure and determine initial permeability of foam bank.

(3) Monitor shutin pressure with time over a two-month period. Make periodic permeability measurements.

(4) If there is evidence of premature foam decay, inject a volume of water containing 1% Steol 7N that is about 10% of the first treatment and follow with gas to create a second foam treatment. Check velocity profile with spinner survey.

(5) Repeat (3) and (4) as necessary.

Experiment 3 - Foam Removal

(1) Measure permeability of foam bank to untreated water. Run spinner survey.

(2) Inject 140 barrels of 50% isopropanol solution to break foam bank.

(3) Displace isopropanol solution with untreated water and determine permeability to untreated water. Compare with pre-foam measurement (Experiment 1, step 4). Run spinner survey.

(4) Repeat (2) and (3) if necessary.

(5) Determine need for gas injection test to provide additional measure of post-foam conditions in formation.

Field Work Evaluation

(1) Analyze results and prepare report.

(2) Make a go/no-go decision for Phases IIa and IIb.

Table 6.2.

Phase IIa Proposed Test Program at Grif 1

PG&E Los Medanos Field

Experiment 1 - Reservoir Continuity between Grif-1 and Gino-1

(1) Measure shutin pressures in Grif 1 and Gino 1.

(2) Test Gino 1 well productivity (or injectivity). Run flow test and determine velocity profile with spinner survey.

(3) Run interference test to establish level of communication between wells in Nortonville sand.

(4) Set packer above perforated interval in Gino 1 with 2-7/8'' tubing and equip for pressure and temperature observation.

Experiment 2 - Develop Foam Bank near Gino 1

(1) Inject from 10,000 to 20,000 barrels of untreated water in Grif 1 to build a water-saturated zone that extends part way over to Gino 1.

(2) Inject about 9000 barrels of water containing surfactant and displace with about 28,000 barrels of untreated water so that the surfactant water occupies an annular ring from 60 to 70 feet from Grif 1.

(3) Inject natural gas at controlled rate and pressure 9S0 to develop foam bank from 80 to 100 feet from Grif 1. Monitor Gino 1 for first appearance of foam. Run GRN log to locate foam. This should also develop a significant gas volume around Grif 1.

Experiment 3 - Test Foam Bank and Gas Storage Volume

(1) Change pressures at Grif 1 and monitor effects at Gino 1.

(2) Run GRN log at Grif 1 to locate gas/water conditions around well.

(3) Inject gas to raise pressure at Grif 1 in steps of 50 psi and monitor effects at Gino 1. Maximum pressure should probably not be more than 1000 psi.

(4) Shutin both wells at maximum pressure and monitor system for evidence of foam decay.

(5) Withdraw gas and measure percent recovery.

Field Work Evaluation

(1) Analyze results and prepare report.

Table 6.3.

Phase IIb Proposed Test Program on Water Coning in an Aquifer Gas Storage Field

Experiment 1 - Determine Reference Well Condition

(1) Run Gamma Ray Neutron (GRN) log in selected well at end of withdrawal period.

(2) After allocated storage gas volume has been injected, run flow prover test to determine well productivity.

(3) Pull tubing and run spinner survey with one or more injection rates to determine velocity profile.

Experiment 2 - Prepare Well and Treat with Foam

(1) Run GRN log to determine location of Gas-Water contact.

(2) Select 10-foot interval just above G-W contact. If necessary, perforate with 4 shots per foot.

(3) Set packer just above 10-foot interval.

(4) Run tubing and connect to packer.

(5) Treat 10-foot interval with acid flush.

(6) Inject water containing selected surfactant to create a treated water zone extending 20 to 50 feet from well.

(7) Inject gas at pressures up to maximum permissible pressure (to be determined by NIGAS) to create foam bank.

Experiment 3 - Foam Bank Properties and Longevity

(1) Run GRN log to determine foam distribution along borehole.

(2) Measure initial shutin pressure and determine initial permeability of foam bank.

(3) Monitor shutin pressure with time and make periodic permeability measurements until start of withdrawal.

(4) If there is evidence of premature foam decay, give well second foam treatment and repeat (2) and (3) until start of withdrawal.

Experiment 4 - Effect of Foam Bank on Coning

(1) Disconnect tubing from packer and raise tubing to original location for normal injection/withdrawal operations.

(2) Withdraw gas at rates similar to that of previous year and measure pressures and flow rates of gas and water daily.

(3) Run GRN log and, if possible, spinner survey from bottom of tubing to top of packer.

(4) If decision is made to remove foam, lower tubing to connect to packer and extend GRN log to bottom hole.

Table 6.3 (continued)

Experiment 5 - Foam Removal

(1) Measure permeability of foam bank to untreated water. Run spinner survey.

(2) Inject sufficient volume of isopropanol solution to break foam bank.

(3) Displace isopropanol solution with untreated water and determine permeability to untreated water. Run spinner survey.

(4) Repeat (2) and (3), if necessary.

(5) Disconnect tubing from packer and raise tubing to original setting for normal injection/withdrawal operations.

Experiment 6 - Evaluate Well Injectivity/Productivity

(1) Measure injection rates and pressures for comparison with previous years records.

(2) After allocated storage gas volume has been injected, run flow prover test to determine well productivity for comparison with pre-foam result.

(3) Run GRN log for comparison with pre-foam result.

Field Work Evaluation

(1) Analyze results and prepare report.

Table 6.4. Direct Costs for Phase I Field Experiment

Action	Cost (1000$)	
Drill injection well and evaluate formation		
Permitting (incl. bond)	12	
Drill, complete, and log Grif No. 1	185	
Site supervision	10	
Abandonment and cleanup	30	
Install gas line and choke	15	
Install meter	15	
Site supervision	3	
Gas	1	
Miscellaneous	4	
Subtotal		275
Foam emplacement around wellbore		
Water to pre-saturate formation	1	
Surfactant	6	
Pump rental, 1 mo. minimum	5	
Operator, 3 days injecting	2	
Gas	1	
Two neutron logs	8	
Miscellaneous	2	
Subtotal		25
Foam bank properties and longevity		
Gas	1	
One neutron log	4	
Subtotal		5
Foam Removal		
Foam breaker	11	
Water	1	
Pump rental	5	
Gas to pressure test	1	
Miscellaneous	2	
Subtotal		20
Phase I total		325

Table 6.5. Direct Costs for Phase IIa Field Experiment

Action		
Recomplete Gino No. 1 as observation well and test reservoir		
Permitting	2	
Bond	10	
Open, recomplete, and log Gino No. 1	110	
Abandonment and cleanup	30	
Pressure test	5	
Miscellaneous	3	
Subtotal		160
Develop foam bank near Gino No. 1		
Pump rental	5	
Operator, 14 days	10	
Water, 75000 bbl = 2.9 MMgal	45	
Log observation and injection wells	10	
Inject water 0.37 MMgal	10	
Surfactant	60	
Water to displace foamer solution	40	
Pump rental (included above)	0	
Operator 14 days	10	
Gas	50	
Engineering	10	
Log 2 wells	10	
Miscellaneous	20	
Subtotal		280
Test foam bank and gas storage volume		
Gas	1	
One neutron log	4	
Gas	40	
Operator	30	
Log 2 wells	10	
Subtotal		85
Phase IIa total		525

Table 6.6. Direct Costs for Phase IIb Field Experiment

Action		
Determine reference well condition		
GRN log (spring)	14	
Flow prover	1	
Pull tubing and tubescope	20	
GRN log (fall)	15	
Miscellaneous	5	
Subtotal		55
Prepare well and treat with foam		
Perforate well	10	
Packer	10	
Wireline unit	5	
Acid flush	5	
Run tubing	17	
Surfactant and water	16	
Gas	7	
Labor	10	
Compressor	7	
Miscellaneous piping	10	
Tank rental	5	
Miscellaneous	10	
Subtotal		112
Evaluate foam bank properties and effect on coning		
GRN log	15	
Flow prover	1	
10% contingency	2	
Subtotal		18
Foam removal		
Foam breaker	25	
Pump breaker	5	
Labor	10	
Miscellaneous	5	
Subtotal		45
Phase IIb total		**230**

7.0. DISCUSSION AND CONCLUSIONS

The purpose of this project was to investigate the use of foams to improve underground gas storage operations. This involved a number of technical questions relating to the physics of foam, the mechanism of flow blocking in porous media, and the feasibility of using foams in underground gas storage. These questions include:

- How is foam formed in porous media? What conditions (e.g. flow rates, liquid saturation) are necessary for the formation of foam?
- How can foam best be emplaced in a formation?
- By what mechanism does foam reduce the permeability of a porous medium to gas and to liquid? What is the degree of permeability reduction?
- How long does the permeability reduction last? How can it be made to last longer?
- What is the most effective way to use foam for underground gas storage?
- How can foam be broken, if desired?

Our experiments, while not answering all the questions, have given favorable results to suggest that foam can be applied effectively to increase the efficiency of underground gas storage.

The theoretical arguments and experiments of Radke and Ransohoff (1988) indicate that there is a critical gas velocity that must be exceeded for generation of a strong foam. Lamellae are formed when gas invades individual liquid-filled pores, so the critical velocity presumably refers to the gas pore velocity, which is always greater than the superficial velocity. The difference between the two velocities may be large because the porosity and gas saturation are both less than unity, and some or most of the gas in the core may be trapped and immobile. The critical pore velocity in our experiments has not been determined, except to observe that it was exceeded in one-dimensional experiments when the superficial gas velocity was 1 m/day.

If foam is to be formed by injecting gas from a well in radial flow, the superficial gas velocity, and possibly also the gas pore velocity, will decrease at large distances from the well. This may limit the distance at which foam can be generated in situ. Therefore better definition and measurement of the critical velocity is needed. In any case, generation of foam near a wellbore is certainly feasible.

The question of emplacement is essentially a question of how far gas can be injected above the critical velocity without exceeding the allowable injection pressure. The gas permeability of a foam-filled formation, the allowable injection pressure, the critical velocity for snap-off, and the viscosity of the liquid phase all combine to set a limit on the distance to which foam can be driven in situ. Spacing the foam bank away from the wellbore reduces the injection pressure, but also makes it more difficult to regenerate. Note also that as gas displaces liquid, the liquid is driven ahead of the foam, and its pressure drop must be added to the pressure drop through the foam. If a polymer is used in the liquid, this could also become significant.

Although one-dimensional laboratory experiments in homogeneous media have shown large reductions in gas and liquid permeability, it is necessary to determine whether this degree of permeability reduction can be achieved and sustained in the field. Radial flow may cause gas velocities to be too slow to form a strong foam at distances from the wellbore, and natural heterogeneity may interfere with emplacement of a foam bank.

The results shown in Figure 5 of Appendix F suggest that for a gas-blocking application, some provision must be made to regenerate the foam. The cost of the project will depend upon the needed frequency of regeneration. It appears that additional slugs of liquid would be injected whenever the permeability of the foam block exceeds a certain limit, and the higher this limit is set, the less frequently regeneration would be needed. But even if the foam were allowed to decay, the gas saturation in the designated storage volume would be greater and more uniform than if foam had not been used, so improved recoverability of injected gas should result.

The rate of foam decay shown in Figure 5 of Appendix F is likely pessimistic due to the test method. The gas injected in all these experiments was dry, and liquid saturations below connate

measured during the later stages of each experiment near the inlet region indicate that liquid was removed from the core by evaporation. Low liquid saturation is known to be detrimental to foam stability (Khatib et al. 1988). The method used to conduct the experiment is therefore a severe test of foam block durability. The observation that inclusion of guar in the foamer solution increased the durability of the blocked condition might be explained by more stable lamellae being formed or by higher liquid saturation in those experiments due to greater viscosity of the displaced liquid.

Pilot-scale field testing is now needed to confirm these results in practice. The most promising application for a field trial appears to be control of water coning. Such a field trial could be done at a well where coning has been experienced in the past (the control experiment has already been done), and the foamer solution could be injected through the existing well and followed with gas. Another attractive prospect for a field trial would be the use of foam to seal a known leakage path of limited area, such as a fault zone or casing leak.

Application of foam to underground gas storage need not be limited to conventional underground storage in aquifers. Where demand is present but suitable geologic formations are absent, mined caverns in hard rock could be used as storage reservoirs. Here leakage through fractures intersecting the cavern might be controlled by foam. Another area where foam technology could be applied is compressed-air energy storage in aquifers. By controlling gas migration and water coning, foam could prevent leak-off of pressure and loss of stored energy, and ensure deliverability. Because the cycle in this application would be daily, rather than annual, requirements for foam stability might be reduced.

The results of the experiments conducted during the course of this research effort support the following conclusions:

1. Foam reduces the gas permeability of a porous medium by 2 or 3 orders of magnitude. The permeability gradually increases as lamellae decay, but foam can be regenerated by injection of additional slugs of foamer solution.

2. Inclusion of 0.5 weight % guar in the foamer solution appears to enhance the stability of a foam block in a porous medium.

3. The pressure drop in foam flow through a porous medium varies directly with the liquid flow rate. Therefore, where injection pressure must be limited, the most effective way to form a foam bank is to saturate the formation with surfactant solution, and then inject gas. Alternating slugs of surfactant solution may be used to make a stronger foam.

4. Foam effectively blocks liquid flow because the liquid saturation is low. When liquid is pumped through a foam-filled core, the liquid saturation remains low as long as the surfactant concentration is not diluted. When the surfactant concentration is diluted, trapped gas is released, and liquid saturation and liquid permeability increase. The results of the laboratory experiment indicate that approximately 17 pore volumes of water were pumped through the core before the permeability increased significantly.

5. The most effective location for placement of a foam bank to prevent water coning is just above the gas-water contact.

6. Formation of a foam bank spaced away from an injection well may be feasible by injecting foamer solution, displacing it with brine, and then injecting gas. The location of the foam bank reflects displacement both by the brine and by injected gas.

7. Foam can be broken by injection of a 50 weight % isopropanol solution.

Based on the results of the experimental and theoretical studies, it is concluded that application of foam to improve the efficiency of aquifer gas storage appears to be technically feasible. The logical next step would be a field trial. The most promising field trial would be an attempt to control water coning by means of a relatively small foam lens emplaced beneath the feed zone of a gas withdrawal well.

8.0. REFERENCES

Albrecht, R. A., and Marsden, S. S., 1970. "Foams as Blocking Agents in Porous Media," *Society Petroleum Engineers Journal, 51*, March.

Bernard, G. G. and Holm, L. W., 1964. "Effect of Foam on Permeability of Porous Media to Gas, *Society of Petroleum Engineers*, September.

Bernard G. G. and Holm, L. W., 1970. "Model Study of Foam as a Sealant for Leaks in Gas Storage Reservoirs," *Society of Petroleum Engineers Journal*, 9-16, March.

Khatib, Z. I., Hirasaki, G. J. and Falls, A. H., 1988. "Effects of Capillary Pressure on Coalescence and Phase Mobilities in Foams Flowing through Porous Media," *SPE Reservoir Engineering, 3*, (3), 919-926.

Persoff, P., Radke, C. J., Pruess, K., Benson, S. M. and Witherspoon, P. A., 1989a. "A Laboratory Investigation of Foam Flow in Sandstone at Elevated Pressure," presented at 1989 California Regional SPE Meeting, Bakersfield, CA, April 5-7, (SPE-18781) submitted to SPE Reservoir Engineering.

Persoff, P., Witherspoon, P. A., Pruess, K., Shikari, Y. A., Radke, C. J., Benson, S. M. and Wu, Y. S., 1989b. "Aqueous Foams for Control of Gas Migration and Water Coning in Aquifer Gas Storage," abstract submitted for presentation at 1989 International Gas Research Conference, November 6-9, 1989, Tokyo.

Pruess. K., 1983. "Development of the General Purpose Simulator MULKOM," Annual Report 1982, Earth Sciences Division, Report LBL-15500, Lawrence Berkeley Laboratory.

Pruess, K., 1988. "SHAFT, MULKOM, TOUGH: A Set of Numerical Simulators for Multiphase Fluid and Heat Flow," *Geotermia, Rev. Mex. Geoenergia, 4*, 185-202 (also Lawrence Berkeley Laboratory Report LBL-24430).

Radke, C. J., King, M. S. and Witherspoon, P. A., 1983. "Foam-Protected Natural Gas Storage Reservoirs," Proceedings Second Underground Storage Session, American Gas Association Transmission Conference, Seattle, Washington, May 2-4.

Ransohoff, T. C. and Radke, C. J., 1988. "Mechanism of Foam Generation in Glass-Bead Packs," *SPHERE*, 573-585, May.

Schick, M. J., and Fowkes, F. M., 1957. "Foam Stabilizing Additives for Synthetic Detergents. Interaction of Additives and Detergents in Mixed Micelles," *Jour. Phys. Chem, 61*, 1062-1068.

Sharma, M. K., Shah, D. O. and Brigham, W. E., 1982. "The Chain Length Compatibility and Surface Properties of Foaming Solutions in Relation to Fluid Displacement Efficiency in Porous Media," paper presented at the SPE Sixth International Symposium on Oilfield and Geothermal Chemistry, Dallas, Texas, January 25-27.

Sharma, M. K., Shah, D. O. and Brigham, W. E., 1984. "Correlation of Chain Length Compatibility and Surface Properties of Mixed Foaming Agents with Fluid Displacement Efficiency and Effective Air Mobility in Porous Media," *I&EC Fundamentals, 23,* 213-220.

Smith, J. M., 1981. *Chemical Engineering Kinetics,* McGraw-Hill Book Co., New York, 3rd ed., 275-279.

Witherspoon, P. A., Radke, C. J., Shikari, Y. A., Pruess, K., Persoff, P., Benson, S. M. and Wu, Y. S., 1987. "Feasibility Analysis and Development of Foam-Protected Underground Natural Gas Storage Facility," Proceedings AGA Operating Section, paper #87-DT-110, p. 539-549.

9.0. APPENDICES

A. Literature Survey Results

B. Summary of Experimental Data

C. On PVT-Data, Well Treatment, and Preparation of Input Data for an Isothermal Gas-Water-Foam Version of MULKOM

D. Feasibility Analysis and Development of a Foam-Protected Underground Natural Gas Storage Facility

E. A Laboratory Investigation of Foam Flow in Sandstone at Elevated Pressure

F. Aqueous Foams for Control of Gas Migration and Water Coning in Aquifer Gas Storage

G. Displacement of Newtonian Fluid by a Non-Newtonian Fluid in a Porous Medium

Appendix A. Literature Survey Results

In this Appendix the major results of numerous articles and patents found in the open literature are summarized. The review is separated into topics, including: the physics of foam formation, mobility reduction and blocking by foam, proposed applications of foam in porous media, laboratory observations of foam blockage, stability of foam, use of foam for mobility control, foam rheology, and economics. Within each topic, the articles are reviewed chronologically.

Table of Contents

A-1. Physics of Foam Formation A5
A-2. Mobility Reduction and Blocking by Foam A6

A-2.1. Theory A6
A-2.2. Applications of Foam in Porous Media A7
A-2.3. Laboratory Observations of Foam Blockage A9
A-2.4. Foam for Mobility Control A12

A-3. Stability of Foam A18

A-3.1. Stability Enhancement A19
A-3.2. Combinations of Surfactants to Enhance Foam Stability A19
A-3.3. Polymers and Gels to Enhance foam Stability A21

A-4. Theory of Foam Rheology A23
A-5. Rheological Measurements on Bulk Foam A25
A-6. Foam Rheological Measurements in Porous Media A29
A-7. Controlling Emplacement of Foam Banks A32
A-8. Delayed Foams A34
A-9. Experience in Field Applications A35

A-9.1. Water Floods A35
A-9.2. Thermal Floods; In-Situ Combustion A35
A-9.3. Steam Flooding A36
A-9.4. Sealing Gas Leaks A38

A-10. Economics A38

A-10.1. Need to Reduce Base-Gas Requirement A38

A-11. Bibliography A41

A-1. Physics of Foam Formation

Roof (1970)*

This paper discusses the formation of bubbles when gas is driven into a liquid-saturated porous medium. Bubbles will not form in uniform channels. The formation of bubbles is described as a snapping-off phenomenon occurring when gas (or any non-wetting phase) intrudes through the axis of a pore throat. As it proceeds into the next pore body, a retrograde flow of liquid (wetting phase) forms a collar in the pore throat which, under certain conditions, can completely close off the pore throat, causing a bubble to snap off. Additional gas following after the first snapped-off bubble will repeat the process, causing a train of bubbles to be formed. The pore diameter be at least twice the throat diameter for snap-off to occur (the Roof criterion). If this criterion is not met, gas will flow as a thread-like continuous phase, not separated by lamellae. Bubble sizes expected for foams formed in situ must be on the order of pore body sizes. This supports the observation that foams formed in porous media are non-bulk foams.

Ransohoff and Radke (1988)

This work defined the conditions necessary for foam generation in porous media. Pore bodies separated by relatively narrow throats (meeting the Roof criterion) are referred to as "generation sites." To form foam, generation sites must be invaded by gas. The authors report a critical velocity or pressure drop necessary to form a foam in uniform glass bead packs. At a high enough gas velocity, snap-off was visually observed in the transparent beadpack, but not below this velocity. This suggests that in-situ foam generation would require a minimum gas injection pressure.

The authors argue that the Roof criterion must be met before a pore-throat/pore-body pair can serve as a foam generation site. Further, the gas must penetrate into the pore throat to initiate

*Complete literature citations are presented in the Bibliography at the end of this Appendix.

snap-off. It is the second event that is velocity-dependent. This work needs to be extended to more realistic porous media.

A-2. Mobility Reduction and Blocking by Foam

For intelligent design of foam blocks, it is necessary to understand the mechanisms by which blocking occurs; if foam blocks are to be formed in situ, it is also necessary to understand the mechanisms by which bubbles and lamellae are formed in porous media. Several theoretical and experimental studies at the pore level have contributed to theories of these phenomena.

A-2.1 Theory

Gardescu (1930)

This paper describes two mechanisms by which bubbles at rest in a porous medium can support a gas pressure gradient without flowing. The bubbles must be large enough to fill the pores, i.e., the foam must be non-bulk foam. Both mechanisms result from the fact that the radius of curvature of the gas-liquid interface is different at the front and rear of the bubble. By Young's and Laplace's equations, this causes a pressure difference across the bubble which must be balanced by the external liquid for static conditions and must be overcome for bubble movement. The first mechanism is the Jamin effect, and occurs in uniform or nonuniform capillaries where the solid phase is not wetted by the liquid. Gas bubbles and liquid slugs alternate. Because of hysteresis in the wetting of the pore walls by the liquid, the advancing and receding ends of the bubble have different contact angles, and therefore different radii of curvature. The second mechanism is occurs in wetted capillaries of nonuniform cross section. Here the radii of curvature are different because of the different pore radius at the two ends of the bubble. The bubble is pear-shaped and becomes wedged in a pore throat such that the pressure gradient across the bubble exactly matches the available gas pressure gradient. To squeeze the bubble through the pore neck requires additional work equal to the product of the surface tension and the additional sur-

face area created when the bubble is deformed. This mechanism is more important in porous media.

See also Falls et al. 1986 reviewed under Foam rheology.

A-2.2. Applications of Foam Blocking in Porous Media

Beeson (1963) (pat. no. 3,100,524)

The discovery disclosed in this patent is claimed to improve the efficiency of gas-driven solvent flooding for enhanced oil recovery. Solvent flooding recovers residual oil by diluting it and reducing its viscosity so it can flow from smaller pores into larger, more permeable pores. But the solvent does not invade the smallest pores because it tends to flow in the larger pores. Additional solvent invasion is obtained when the surfactant solution changes the reservoir rock from water-wet to oil-wet. Foam is not mentioned in the patent, but Marsden (1986), in reviewing it, suggested that formation of foam (from the surfactant solution and injected gas) was the actual cause of improved recoveries.

O'Brien (1967) (pat. no. 3,306,354)

To prevent gas from escaping either around a well bore or through cap rock fractures, the region around the wellbore or above the cap rock is injected with a surfactant solution. Escaping gas is supposed to form a foam and seal itself.

Bernard (1967) (pat. no. 3,330,352)

This is the first patent to propose the use of foam to increase the efficiency of underground gas storage. It is proposed that a viscous, aqueous slug containing a foaming agent first be injected, and then followed by the gas to be stored. The idea is that the foam fills the larger pores, causing gas to displace water from smaller pores which otherwise would remain saturated with water. In this way the storage capacity of the reservoir is increased. "Furthermore, the foam forms a wall or envelope which contains the gas... Alternatively, the foam forming solution

can be injected about the periphery of the storage zone.'' This is suitable where closure is inadequate. Foam is not to be injected as foam, but rather formed in situ. Periodically additional foamer might need to be injected. Use of a carbonated brine to release gas to form the foam in situ is also claimed. No experimental data to support the concept was reported.

Heuer et al. (1968) (pat. no. 3,368,624)

In oil recovery, water or gas may be produced along with the oil. This invention is supposed to reduce the water cut or gas cut in an oil production well, by forming a foam block in either the water- or gas-producing cone. First a slug of brine is injected, then a slug of surfactant solution, then another slug of brine, and then (if into the water cone, but not if into the gas cone), a final slug of gas. When the well is returned to production, the final gas slug or gas cone is supposed to form foam which blocks the flow of either water or gas to the production well.

Laboratory and field experimental data are supplied to support the claim. A 6-ft. long core of Berea sandstone was saturated with brine, then flooded with kerosene, and then air-driven for 24 hours to a condition similar to that of a gas sand. A brine ''spearhead'' was introduced, followed by a slug of surfactant solution, and then gas flow was resumed. A foam block formed which was ''98% effective for 15 days and 95% effective for 28 days.'' Another example is cited for a well. Following treatment, the gas flow was initially 1% of the rate before treatment; the gas flow rate increased steadily for 4 days, and then gas broke through. This patent also describes some preferred foaming agents.

Leach (1969) (pat. no. 3,460,623)

In enriched gas drives for enhanced oil recovery, the enriched gas dissolves in the oil, making it more mobile. A problem is that with layers of varying permeability, excess costly enriched gas is injected into more-permeable zones before the less-permeable zones have been adequately treated. A temporary plugging agent is needed to divert the enriched gas into the less-permeable zones. Foam is used here for mobility control, to ensure that penetration of the enriched gas is

more piston-like than would occur without the foam. After the enriched gas treatment, the foam must break in the presence of oil so that the enriched gas can effectively contact the oil. A test method is described to screen surfactants for oil-sensitivity. For this application, a surfactant that is moderately oil-sensitive is desired.

A-2.3. Laboratory Observations of Foam Blockage

Bernard and Holm (1964)

This is the first demonstration of the ability of foam to block gas flow in porous media. The effect is described as a reduction in the relative permeability of the porous medium to gas: at a given gas saturation, the permeability to gas is less if the gas is present as a foam than if gas is present as a free gas phase. Under some conditions, the relative permeability to gas is zero, which can be interpreted as blocking. The relative permeability to gas was measured by the "Penn State method" in which surfactant solution and gas are injected simultaneously. Below 40% gas saturation there was no flow of gas; it is not clear how gas was injected into the core if permeability was zero. At gas saturations greater than 40%, permeability was reduced much below the gas permeability of the dry porous medium (specific or absolute permeability). The greater the specific permeability of the porous medium, the less its permeability to gas at gas saturations greater than 40%. Orders of magnitude reduction in permeability were observed.

Additional experiments were conducted to measure how long the permeability reductions would last. Foam was formed in 1-ft long sandpacks by first saturating the sandpack with foamer solution and then injecting gas at constant pressure. In all cases the permeability increased with time; after several hours the permeability appeared to stabilize at a value less than 1% of the specific permeability. Similar experiments were done with 30-ft long sandpacks. These results showed the foam blocks lasting up to 30 days. Reduced permeability lasted longer in longer sandpacks and in less-permeable sandpacks. The pressure gradient needed to cause a foam block to "break down" was greater for low-permeability sandpacks. All these trends suggest to us that

during these experiments the foam block was failing continuously from the inlet end toward the outlet end. For long-term stability, continuous injection of surfactant is recommended.

Bernard et al. (1965)

In this work, foam banks were produced in porous media and the relative permeability to water was measured. In previous work it had been discovered that the relative permeability to gas, at a given gas saturation, was much less in the presence of foam than in the absence of foam. Regarding the relative permeability to water, the presence or absence of foam made little difference. The reduction of permeability to water was found to be dependent only on the water saturation in the porous medium. Water flowed through pore channels not invaded by gas.

Bernard and Holm (1970)

This is the first study directed at evaluating the use of foam to seal leaks in gas storage reservoirs. The reservoir was modeled by a horizontal slab of Berea sandstone. Initially the slab was saturated with brine. Then gas was driven in at one end at 15 psi to reduce the water saturation to 30-35%. The slab was then in the condition of a gas storage reservoir. Gas injection was continued at 15 psi, and gas was driven out of the other end of the reservoir, simulating a leak. Liquid (either brine or surfactant solution) was injected into the slab at three points along a line perpendicular to the direction of flow, simulating efforts to stop the leak.

When brine was injected, gas flow was reduced from an effective permeability of 207 mD to 26 mD (due to a reduction in gas saturation), but the permeability rapidly increased and was back up to 200 mD only 36 hours after cessation of brine injection. Depending upon the rate and amount of brine injected, the permeability could be temporarily reduced almost to zero, but in all cases it recovered rapidly.

When foamer solution was injected, permeability reduction was greater, but recovery of permeability was still rapid. Failures were ascribed to adsorption of surfactant of the sandstone and incomplete "sweeping" of the foamer solution across the entire cross-section of the model.

Screening of surfactants for adsorption identified another surfactant (not specified) which was more effective in reducing leaks. By injecting a solution of this surfactant, permeability to gas was reduced from 294 to 15 mD and maintained at that level for over 1000 hours, suggesting that foam blockage or at least reduced permeability can be maintained for months in low-permeability rocks.

Albrecht and Marsden (1970)

This work related the blocking pressure gradient to flowing pressure gradient. The experiment started with a porous medium (sandpack or sandstone core) initially saturated with foamer solution, and gas was injected at constant pressure. Foam emerged from the outlet of the porous medium. When "steady state" was reached, the gas injection pressure was reduced (not to zero), until foam flow stopped, i.e., a blocked condition existed. (With foam emerging from the porous medium and no liquid entering, true steady state could not have existed.) With sandpacks (beach sands, apparently with narrow particle size range), only a small decrease in injection pressure was needed to block flow, but in sandstones (presumably with a wider range of pore sizes) a larger decrease in injection pressure was needed to stop the flow of foam. No measurements of how long the blocked condition lasted are reported. The proposed mechanism of blocking is consistent with Gardescu's explanation: with decreased pressure, the bubbles expand in the pores until the pressure gradient needed to push them through the pore throats exceeds the available gradient.

Minssieux (1974)

This work reports experiments in which a nonionic surfactant solution (Triton X 100 in water) and gas were simultaneously injected into glass-bead-packs (permeability = 4.5 darcy). Liquid was injected at a constant flow rate (not reported, but apparently between 0.6 and 2.5 cm^3/min for a liquid darcy velocity of 0.63 to 2.63 cm/min), while gas was injected at a constant pressure (also not specified, but possibly at a gas pressure gradient of 108 psi/ft). Under these

conditions, foam was formed in and flowed from the beadpack, but during a period of one to two hours, the gas flow rate dropped to zero, while liquid flow continued. This gas-blocking effect continued at a pressure gradient of 108 psi/ft. The investigator did not determine how long it would last without liquid flowing. This gas-blocking effect was observed with most surfactants, but not those which produced "less elastic and less resilient" lamellae. The reduction of gas flow was attributed to accumulation of gas in the beadpack. As the foam quality in the beadpack increased, the viscosity of the foam was also supposed to have increased. The viscosity of higher-quality foams measured in coaxial viscometers was greater.

This is the first use of X-ray attenuation to measure liquid saturation in foam flow experiments. $BaCl_2$ was added to the brine to make it "denser" to the X-rays. The liquid saturation was greatest at the upstream end of the core and then was almost uniform over most of the core length.

Taber and Fulton (1976)

This report describes work that was done to control methane release from fractures ("cleats") in coal mines. Foam was either formed in fractures or injected as foam. Blocking pressure gradients as high as 160 psi/ft were measured. A two-week life was estimated for a 12-foot thick foam block formed in a fracture. The recommended surfactants were sodium lauryl sulfate combined with lauryl alcohol at a ratio of 0.2% to 0.044%; or Tide commercial laundry detergent.

A-2.4 Foam for Mobility Control

Bond and Holbrook (1958) (pat. no. 2,866,507)

This is the first patent to disclose a process wherein foam is used as the displacing fluid in an enhanced oil recovery process. The authors demonstrated by laboratory experiments in sand packs that secondary recovery in gas drive was improved if the gas is preceded by a small amount of aqueous surfactant solution. No discussion of foam mobility was included, but it is

generally understood that foam drive works because foam has a higher viscosity than either its gas or its liquid phase, and therefore it has low mobility which is desired for a displacing fluid.

Fried (1961)

This was the first study of foam drive for enhanced oil recovery. Sandpacks were saturated with water and then flooded with oil to produce a condition representative of an oil sand. Oil was then recovered from the sandpack by successive water and gas drives until the water-oil ratio or gas-oil ratio reached economic limits. At this point, foam drive was initiated and, in most runs, additional oil was recovered. In most experiments foam was formed externally and injected as bulk foam. Enhanced oil recovery was also observed when gas was injected following a surfactant-solution flood. The increased oil recovery was explained as follows. After secondary recovery by water drive, residual oil remains in the smallest pores. In foam drive, foam fills and blocks the larger pores, causing foam then to invade and displace oil from the smaller pores.

Foam viscosity was measured in both rotational and capillary viscometers. In rotational viscometers apparent viscosity decreased with increasing foam drainage and with increasing rotor speed, but little effect of surfactant concentration was observed in the range 0.16 to 1.25% surfactant. In capillary viscometers, the apparent viscosity increased with increasing capillary radius. Results were correlated by plotting the dimensional group ($\mu F_x/r$) against linear flow velocity where μ = apparent viscosity, F_x = expansion factor (volume of foam/volume of liquid), and r = capillary radius. This group increased with increasing F_x and decreased with increasing flow velocity.

In some tests, foam blocking was observed. This was associated with the use of foams which were qualitatively more stable. After injection as foam, bubbles were observed (in transparent Pyrex sandpacks) to redivide. In more stable foams redivision occurred more rapidly than foam decay, causing increased resistance to flow, and in some cases blocking, without any decrease in foam injection pressure. This blocked condition lasted for days in some cases.

Blocking was considered undesirable as it prevented the flow of foam and driving of oil.

In some experiments foam was injected and followed by gas. The gas drove the foam bank as a buffer fluid behind the driven oil bank. Sometimes gas broke through the foam bank; this was remedied by repeating foam injection or increasing the stability of injected foam.

Bernard (1963)

In this work, gas drive was used to remove oil, water, or oil and connate water from a sandpack. Effectiveness was judged based on how much liquid was driven out of the sandpack by the foamed gas. In some experiments, the water or oil initially in place contained the foaming agent; in others, a small slug of surfactant solution was injected prior to the gas drive. Oil recovery was increased threefold when gas drive was preceded by a slug of foamer solution.

Bennett (1964)

The effect of the presence of foam on gas-liquid deplacement was studied experimentally by using two separate linear vertical and horizontal flow systems, each consisting of a naturally consolidated sandstone core. The vertical core was used to study the effect of surfactant concentration on recovery. The horizontal core was used to investigate the manner in which slug size affected recovery and in-situ foam generation.

The results of this work show that it is possible to generate a foam in a porous medium by introducing the proper volume and concentration of surfactants into the sandstone and driving it by air. The presence of a foam bank between the driving air and the brine being displaced improves not only breakthrough recovery but also ultimate recovery. Use of a gas-driven foam appeared very promising as an aid to the storage of natural gas in aquifers or in watered-out oil or gas reservoirs. No positive conclusion was obtained about whether externally generated foam can be injected into a consolidated sandstone. In addition, the common electrical conductivity measurement technique was found to be of little value for detecting foam saturation in porous media.

Kolb (1964)

Foam-drive experiments were conducted in a sandstone core containing water or brine. An attempt was made to correlate displacement efficiency with properties of the surface-active solution. The conclusions are as follows: the breakthrough recovery of an air-drive displacement can be improved as much as 50% in a brine-saturated sandstone core if a surfactant is present in the brine. Recovery increases as slug size and surfactant concentration increase. Loss of the surfactant solution through dilution and adsorption causes the early breakdown of the foam bank. Foaming ability was determined to be the major factor in improved displacement efficiency, with foam stability and surface tension effects of minor importance.

Deming (1964)

Three specific properties of foam—ability to form foam, foam stability, and surface plasticity—were studied in this paper in relation to the foam-drive process. Experiments were done on cores of sintered glass beads. High foaming ability favors high displacement efficiency. (Foaming ability is a measure of the amount of interfacial area generated by a standard input of energy, such as the Ross-Miles pour test.) In contrast, high foam stability did not appear to be a major factor in foam-drive performance. Surface plasticity appeared to be deleterious to the foam-drive process, and displacement efficiency in the experiments decreased with increasing surface plasticity of the solution. (Surface viscosity is defined as the ratio of surface shearing to shearing stress. If the two are not linearly related, and a finite shearing stress does not cause shearing, that value of shearing stress is defined as the surface plasticity.) In addition, displacement efficiency appeared to be unaffected by the static surface tension of the soap solution.

Some basic properties of foam are summarized and a brief review of literature relevant to foam drive is given.

Craig and Lummus (1965) (pat. no. 3,185,634)

This patent claims improved mobility control for enhanced oil recovery by using foam as a buffer fluid between oil and the driving fluid, which can be gas or water. The minimum foam quality is 67%; below that foams are unstable. However, use of gels in the foam can allow the use of lower quality foams although the advantage of this is not clear. Gelled foams require greater pressure drop to move them. Greatest recovery is achieved when the foam is injected rather than generated in situ. Laboratory results are presented to show improved oil displacement by foam compared with surfactant solution or water.

Holbrook and Bernard (1965) (pat. no. 3,207,218)

This patent discloses a method to reduce the gas cut in a well which is producing both gas and liquid. When gas breaks through into an oil-producing well, it is proposed that production be halted. Then oil containing an oil-soluble foaming agent is injected 1 to 10 ft into the formation. In the oil-producing layer, the oil and surfactant are produced with along with new oil, but in the gas-producing layer, the gas forms a foam, blocking gas flow. The use of foam is also mentioned in connection with preventing losses from gas storage reservoirs. However, the foam is not to be used to prevent loss of stored gas, but rather to prevent gas from coning downward into wells which are used to inject or withdraw water from the water table beneath the stored gas to vary the storage volume. For this application it is recommended that an aqueous solution of surfactant be injected to prevent gas (not water) coning. A screening test for surfactants is also described.

Rai and Bernard (1967) (pat. no. 3,323,588)

This patent discloses a method of successive foam drives which is claimed to result in better oil recovery than is possible with a single foam drive. First an "oxygenated hydrocarbon" (i.e., an alcohol) is injected, followed by a slug of anionic surfactant and gas to form a foam, then followed by a cationic surfactant and gas to form a foam; then a drive fluid. This is claimed to cause greater recovery of oil than is possible by a single foam drive. The reason for the improve-

ment was not known.

Bernard and Holm (1967) (pat. no. 3,342,256)

This patent claims the use of foam to improve sweep efficiency in CO_2 flooding. A small amount of surfactant is incorporated in the CO_2, or the surfactant can precede the CO_2 slug.

Kamal (1970)

In this study, miscible displacement of oil by a micellar solution was combined with foam drive to investigate enhanced recovery. The experimental apparatus consisted of a vertical plexiglass sandpack, filled with brine initially, then saturated with oil. For the secondary or tertiary recovery process, a micellar solution slug was used (a) without prior waterflooding (secondary recovery), (b) or following waterflooding down to the residual oil saturation (tertiary recovery). Air was injected to form foam with the micellar solution and to displace the slug.

The results showed that micellar solutions can be displaced by foam for secondary or tertiary oil recovery, resulting in considerable increase in oil recovery for the two methods. The flow rate of air injection should be controlled according to the volume of the slug.

Dilgren et al. (1978) (pat. no. 4,086,964)

This patent discloses an application of foam for use with steam drive in reservoirs which are not highly stratified. Here fluids are segregated by density. The foam is formed by injecting dilute surfactant and noncondensible gas along with the steam. The composition is adjusted so that the foam increases the resistance of the steam channel but does not block it entirely. The object is to prevent steam from overriding the oil and to sweep a wider "steam channel."

Dilgren and Owens (1979) (pat. no. 4,161,217)

This patent is similar to that of Dilgren et al. (1978); the principal difference is that here the foam consists of hot water, surfactant, and noncondensible gas. By avoiding the use of steam, the foam can be formed at higher pressures. The viscosity of the hot foam is controlled to avoid plugging. The foam is used both as a drive fluid and to transfer heat to the oil.

A-3. Stability of Foam

Stable foams are required to produce long-lasting foam blocks. The effectiveness of foam blocks in preventing gas flow has been demonstrated but the lifetimes of foam blocks have not been long. Indeed, in many cases only a temporary blocking effect was desired. The stability of foams has in most cases been studied in connection with bulk foams. Where results apply to individual lamellae, the principles should be applicable as well to non-bulk foams.

De Vries (1958)

This is a review on the subject of foam stability. The research was undertaken in connection with foam rubber manufacture, in which a gas-in-liquid foam must remain stable at high temperatures while the liquid cures. Foams are always unstable in the thermodynamic sense. Spontaneous collapse is due to two processes: diffusion of gas under a pressure gradient from small bubbles to large, and hydrodynamic collapse of lamellae.

For the first mechanism, surface tension produces a pressure difference between bubbles of differing diameters (Laplace's law). This pressure difference produces a chemical potential which drives gas diffusion from small to large bubbles. Measurements of bubble growth and shrinkage showed that the presence of a surface surfactant layer did not retard diffusion through the lamellae. Liquid in lamellae drains to Plateau borders; as the lamellae become thinner, the probability of spontaneous rupture becomes greater. Drainage proceeds until lamellae reach a certain "limiting thickness" which may be as thin as 120 Angstroms. When lamellae rupture, a hole appears at a thin spot. Formation of a thin spot requires an increase in surface area, so a certain activation energy must be overcome before the lamellae can rupture. This activation energy is proportional to the square of the film thickness; greater surface viscosity also stabilizes lamellae against rupture.

A-3.1. Stability Enhancement

Raza (1970) (pat. no. 3,491,832)

This patent discloses that foam blocks last longer if they are made by injecting alternating slugs of gas and foamer solution. In a laboratory study, a foam block was formed by injecting a single slug of surfactant solution followed by gas. The foam block reduced but did not completely stop the flow of gas. After a short time, gas flow increased. Another foam block was formed by slugging in 1/4 pore volume of foamer solution, followed by a "small amount" of nitrogen gas, until gas flow almost stopped. Then, after an unspecified amount of time, gas flow increased, and the treatment (1/4 pore volume of liquid followed by gas) was repeated. Again gas flow increased after an unspecified period of time. After a third treatment, the return of gas flow was slower than after the first two treatments. Gas flow was never completely blocked. Reduced gas flow rates were measured up to two days following the third treatment. The recommended application of the process is rather than to alternate slugs of liquid and gas waiting until gas flow resumes before repeating the treatment. This experiment started with an oil-saturated sandpack. Since oil is usually detrimental to foams it was believed that the improved results were probably due to the lower oil content after the first treatment.

A-3.2. Combinations of Surfactants to Enhance Foam Stability

Schick and Fowkes (1957)

This is the first paper to discuss combining surfactants for greater foam stability. Addition of lauryl ethanolamide (a foam stabilizer) to sodium 2-n-decylbenzene sulfonate (a detergent) reduced the critical micelle concentration (CMC), up to about a 16% ratio of stabilizer to detergent. Additives with branched chains did not reduce the CMC as much as additives with straight chains. Greater reduction of the CMC was correlated with greater improvement in foam stability.

Dauben and Raza (1970) (pat. no. 3,530,940)

This patent discloses that the stability of foams can be increased by including film-forming water-soluble polymers in the foam. This stabilizes the foam against the effects of high temperature and oil. Examples of polymers are polyvinyl alcohol and polyvinyl pyrrolidone. A surfactant, a polymar, and glycerine, each 2% by weight, can be used. The polymer is supposed to form a film; no crosslinking is used. The glycerine is included as a "plasticizer."

Laboratory data are presented to demonstrate the stabilizing effect. An 18-in long, 3000 millidarcy (mD) sandpack was saturated with the aqueous solution of foaming agent(s), and nitrogen gas injected at 7.5 psig at the upstream end. The time for gas breakthrough was greater with polymer than without by a factor of 2 in one case, and by a factor of 8 in another. The greatest breakthrough time reported was about 10 hours.

Sharma et al. (1982)

Sodium dodecyl sulfate and various straight chain alcohols were combined in 10:1 molar ratio, and various properties measured. When the alkyl chain lengths of the two compounds were equal, the CMC was least, surface viscosity was greatest, fluid displacement in sandpacks was greatest, bubble size was smallest, and time to breakthrough in sandpack experiments was greatest. Surface viscosity was suggested to be the most important property causing lamellae to resist rupture.

Sharma et al. (1984)

This paper reports essentially the same results as the preceding. Additionally, the observation that the optima occur when chain length of alcohol and surfactant are equal is explained by the thermal motion of the excess chain length (if chain lengths are unequal) causing the molecule to occupy a greater area at the interface.

Dellinger et al. (1984)

This is a study of the use of foam to reduce the mobility of CO_2 used to drive oil. Foam stability was recognized as an important property. Stability was measured by using a blender with a graduated cylinder container to form the foam, and measuring the decay of the height of the foam column. The best single surfactant (best initial foam height as well as fair stability) was Alipal CD-128, an ammonium AES compound (GAF Corp.). When this was combined in a 10:1 ratio with the ethanolamide. Monamid 150, foam stability increased. The stabilized foam lost 34% of its volume in the first 20 minutes. Data cited in this paper indicate that Alipal CD-128 degrades at low pH; the chemical half life may be 2 to 20 months. Degradation at low pH would not be expected to impact gas-storage applications; it is important where CO_2 foams are formed. Other cosurfactant systems were also investigated, but did not result in improvement.

A-3.3. Polymers and Gels to Enhance Foam Stability

A gel is a colloid in which the dispersed phase forms a structure incorporating the continuous phase (water), giving it stiffness. Although gels and foams have been used separately, the two have rarely been combined in porous media (see Freeman, 1986). Yet gelling the continuous phase of a gas-in-liquid foam after foam has formed may be a powerful means to impart stability to the foam.

One of the factors which was identified by De Vries (1958) as contributing to foam instability is the drainage of lamellae. The rate of lamellae drainage is reduced when the viscosity in the liquid phase is increased. One way to increase viscosity of the liquid phase is to include in the liquid phase polymers such as guar or carboxymethylcellulose. It appears that such viscosity increase would retard drainage, but after lamellae reach their ultimate thinness, no further benefit would accrue unless the ultimate thinness is thicker than without polymer.

Greater increases in viscosity can be achieved if the polymers are crosslinked, forming a

gel. The gel can be thought of as water with a skeleton. Crosslinked gels have been investigated in the oil field as a means to plug high permeability streaks. The use of crosslinked gels in foam was reported by Freeman et al. (1986) as a means to increase the proppant-carrying capacity of fracturing foam. The variety of polymers that can be dissolved in water or brine to increase its viscosity was reviewed by Chatterjee and Borchardt (1981). Typical gelling reactions involve reaction of a polyvalent metal ion with active sites on more than one polymer molecule, thus causing crosslinking. An apparent difficulty in applying this technology to foams is the adverse sensitivity of surfactants to the high concentrations of metal ions typically used. One possible solution to the problem of high metal concentrations is the use of chelated metals which are slowly released at controlled pH and which react rapidly to form gels, so that metal ion concentrations are never high. Another is the use of borate crosslinkers, in which no polyvalent metal ion is believed to be involved in the crosslinking. Another difficulty is the requirement for the polymer solution not to gel until the foam is formed in situ, or driven to its desired location, and yet gel quickly enough that the foam does not collapse before the gel sets.

Hayashi and Goring (1965)

This is a study on the rate of setting of chrome-lignin gels, which are formed by the reaction of sodium lignosulfonate with sodium dichromate. The tests were done in beakers. The mixture (13% lignosulfonate, 3.8% sodium dichromate, 6% acetic acid in water) was initially a Newtonian fluid. During the initial reaction period, the viscosity increased, but the yield stress was still zero. During the second stage, the yield stress and the viscosity (now defined as the slope of the shear stress vs. shear rate plot) both increased at a constant rate. During the third stage, both these quantities increased at a higher constant rate, until the gel had set. The break between the second and third stage occurred at the same time as the liquid began to behave as a gel. Acetic acid was included because "it is known to enhance the gelling reaction." It was not determined whether the acid was necessary; Felber and Dauben (1977) did not include it. Gel-

ling was most rapid at pH 4-5; and slowed down markedly as the pH increased. The concentration of sodium lignosulfonate was critical; below about 12%, crosslinking did not occur (the molecules were too far apart). Increasing the ionic strength by adding NaCl increased the rate of the reaction. At higher temperatures, gellation was inhibited.

Felber and Dauben (1977)

This paper reports the development of a slow-setting chrome-lignin gel. Lignosulfonate is inexpensive because it is a waste product from paper manufacturing, but dichromate is expensive. This work showed that the gel time could be controlled (gel times from 10 to 1000 hours were measured) by varying the dichromate concentration, and that costs could be reduced by replacing up to 80% of the dichromate by sodium or calcium chloride. Variability among batches of lignosulfonate was a problem; TREX-LTA (Scott Paper Co.) was adequately uniform.

Huang et al. (1986)

This study compared the rate of gellation of polyacrilamide with Cr^{+3} in beaker tests to the rate observed in cores. The gels set up faster when they were sheared. The gel time increased sharply as the initial pH was increased from 3 to 6.

A-4. Theory of Foam Rheology

Lord (1981)

An equation of state relating pressure, volume, and temperature of compressible foam is presented. It is shown how this equation of state of foam can be used in an isothermal, steady-state mechanical energy balance equation for compressible foam static and dynamic behavior. A computational procedure for the description of foam flow is given, based on the equation of state and the energy balance. As an illustration of injection-pressure predictions, a case history of a foam fracturing treatment for well stimulation is presented.

Hirasaki and Lawson (1985)

This paper develops a theory for the apparent viscosity measured when foam flows in smooth capillaries. Whether foam is flowing as bulk foam or as a series of lamellae, the most important variable affecting the apparent viscosity is bubble size. Resistance to flow in smooth capillaries is taken to be the sum of three contributions: (1) viscous drag by flow of liquid slugs between bubbles; (2) deformation of interfaces against the restoring force of surface tension at the front and back ends of the bubble; (3) gradients of surfactant concentration caused by expansion of the interface at the front end of the bubble, and compression of it at the back end of the bubble. Experiments were done to confirm the theory and measure two adjustable parameters in the model.

Falls et al. (1989)

This work expanded the theory developed for smooth capillaries in the preceding paper to include two effects of flow in porous media: capillary pressure and constricted flow paths. Experiments in homogeneous beadpacks were done to confirm the extended theory. Foam texture was still the most important factor determining apparent viscosity; this is consistent with the idea that most of the resistance occurs at lamellae. For foams where lamellae are widely separated compared to constrictions, a relationship is presented for the blocking pressure gradient (Eq. 23 of that paper).

Hatziavramidis (1986)

This is a theoretical study in which the mobility of fine-textured dispersions is represented as a function of the mobilities of the continuous and dispersed phases, and the quality. The analysis does not relate specifically to gas-in-liquid foams. The bubbles (spheres of dispersed phase) are assumed to be small compared to the pores; i.e., the analysis could only be applied to bulk foams. For a foam with mobility of the dispersed phase 100 times as great as the mobility of the continuous phase, and quality greater than 0.5, the mobility of the dispersion is approximately

1.5 times as great as the mobility of the continuous phase. No experimental work was reported.

A-5. Rheological Measurements on Bulk Foam

Most rheological measurements on foams have been done on bulk foams. These results may be applicable to foams flowing in porous media but only if they are flowing as bulk foams, i.e., if the bubble size if smaller than the pore size.

Marsden and Khan (1966)

In this work, foam was formed in graded sandpacks and flowed through various short porous media, and then viscosity was measured on the bulk foam after it exited the porous medium. In agreement with other reported results, the apparent viscosity increased approximately linearly with foam quality, and decreased with increasing shear rate in a modified Fann VG viscosimeter (i.e., the foams were pseudoplastic). Where the following porous medium was coarser than the generator, it had no effect on the foam texture; but when the following porous medium was finer than the generator, it changed the foam texture to smaller bubbles. Apparent viscosity depended upon foam quality, but not upon foam texture. Viscosity varied only slightly as surfactant concentration varied from 0.1 to 1%; below 0.1% foams were too unstable to measure. It was stated that both liquid and gas moved through the same pores simultaneously. The mobility of foam in the porous medium was calculated from the permeability of the porous medium and the apparent viscosity measured outside the porous medium. Mobility was calculated for liquid and gas (assuming them to be flowing in separate channels, although this was not believed to be the case) and for foam (considering it as a single fluid). Surprisingly, for all three fluids the mobility increased with liquid saturation. Estimated viscosity of the foams in the porous media were in the range 30 to 100 cP.

Holcomb et al. (1981)

In this laboratory study, foams were generated using various concentrations of surfactants. The foam quality was maintained at 88%, and microscopic observations were made of the foam

while it was flowing under pressure. A subjective "bubble quality" scale was used to rate the foams; a "stable foam [with] bubbles too small to measure" was considered the best foam. Foam bubble quality increased with increasing surfactant concentration up to the critical micelle concentration; beyond that, increasing the surfactant concentration did not improve the bubble quality. Foam viscosity was measured from pressure drop and velocity through a 19-ft capillary viscometer coil (1/16" o.d.). Foam viscosity increased with surfactant concentration. Viscosities less than 1 cP were measured.

Patton et al. (1983)

This laboratory study was undertaken to measure the rheology of foams to be used to reduce channeling of CO_2 used for enhanced oil recovery. Nitrogen gas and an alcohol ethoxy-sulfate surfactant in brine were used. Foams were generated in a bead pack (0.1 to 0.5 mm glass beads), and then flowed through capillary tubes of various lengths and diameters (diameters ranged from 0.69 to 4.95 mm). The shear stress and shear rate were measured and the data were fitted to an Ostwald-de Waele model:

$$\eta = \kappa\dot{\gamma}^{n-1}$$

where

η = apparent viscosity
κ = a constant
n = a constant
$\dot{\gamma}$ = shear rate (sec^{-1})

This relationship is empirical only; the results unfortunately depended upon the diameter and length of the capillaries. Extrapolation of the data to infinitely long capillaries and then to capillaries 15 to 70 μm in diameter showed that, at shear rates of 0.5 to 4.0 sec^{-1}, the expected apparent viscosity would be about 80 cP. This was supposed to represent reservoir conditions. The value of n ranged from 0.6 to 0.8, indicating a pseudoplastic (shear-thinning) fluid. Apparent viscosity increased with foam quality.

Harris (1985)

This paper reports "pipeline loop viscometer" measurements. The principal factors controlling the apparent viscosity of foam circulating in pipelines were the bubble size (mean and size distribution) and the viscosity of the continuous phase.

Reidenbach et al. (1986)

This work deals with bulk foams. The authors reviewed the previously-published data on foam rheology and noted that despite much disagreement among the previous investigators, it was generally agreed that foam exhibited a yield stress, and that rheology depended upon foam quality. From theoretical considerations, it was argued that the wall stress exerted by foam flowing in a pipe would be a function of two dimensionless groups: foam quality and $\frac{D_e}{D_b}$, the ratio of "foam element diameter" (the pipe diameter for foam flowing in a pipe) to bubble diameter. Different relationships were proposed for laminar and turbulent flow. For laminar flow, the foam is described as a yield-pseudoplastic fluid fitting the Herschel-Bulkley model; the power-law index for the foam is the same as for the liquid phase, and the two other constants (yield point and consistency index) are functions of the dimensionless groups. Experiments were conducted with CO_2 and N_2 gas and water with and without hydroxypropyl guar. Experiments were conducted in tubes, covering both laminar and turbulent flow regimes. Water foams were Bingham fluids; so-called gelled-water foams (containing 0.48% hydroxypropyl guar but not crosslinked) were Herschel-Bulkley fluids. For both types of foam, the yield stress varied linearly with foam quality up to quality = 0.6, and exponentially with foam quality above that value. Laboratory data and field wellhead pressure data both fit the model well.

Freeman et al. (1986)

This paper reports the only work with foamed gels. The gels were "delayed crosslinked;" the gel time was on the order of minutes. The polymer was carboxymethylhydroxypropyl guar. This work was done in connection with foam-fracturing, where the foam is to transport a

proppant. By gelling the foam, high viscosities can be achieved with low foam quality. This combination of properties is needed in foam fracturing applications to achieve high both high viscosity and high proppant concentrations in the fracture.

Bulk foams were studied. The authors measured the apparent viscosity of foamed gels, both linear and cross-linked. For foams where the bubbles are small compared with the tube diameter, they used a power-law relationship (same as the Ostwald de Waele model used by Patton et al, 1983). The behavior index, n , is 1 for Newtonian fluids. For crosslinked foams, n was less than 1 at high quality and increased as quality decreased. Crosslinked foams also exhibited higher apparent viscosity than "linear" gel foams. This allows lower foam quality to be used, an advantage in transporting high concentrations of proppant.

Assar, Nutt and Burley (1988)

Foam was generated by flowing gas at constant volumetric flow rate into a sand-packed foam generator, initially saturated with foamer solution. Six gas flow rates were used. Gas broke through as foam, with the quality of the effluent foam continuously increasing. The quality at breakthrough was 30 or 40%, and gas flow was continued until the quality was 100% (i.e., no more liquid produced). A capillary tube (2.54 mm i.d.) viscometer with a differential pressure transducer, immediately downstream of the foam generator, was used to measure the viscosity continuously, while continuous weighing of the effluent was used to monitor quality. The viscosity was plotted against flow rate and quality. The results indicate that foam viscosity decreases with increasing shear rate, especially at higher foam quality; and increases with foam quality, especially at low shear rates. Foam viscosity measured ranged from 15 to 300 mPa-sec.

A-6. Foam Rheological Measurements in Porous Media

Holm (1968)

This study was conducted to determine the mechanism of gas and liquid flow in porous media in the presence of foam. Foam viscosities were not calculated. Application of the technology to gas storage is mentioned in this paper. In previous studies, foam had been considered to flow as bulk foam through channels, or gas and liquid had been thought to flow through separate channels. Conclusions from this work were that gas flows through the foamed porous medium by breaking and reforming lamellae; the resistance to gas flow is proportional to the number of lamellae per unit length of flow path. Liquid flows through lamellae and through small pore channels not invaded by gas.

Treinan et al. (1985)

In this work, the apparent viscosity of foam was measured from flow rates and pressure drop through a sandpack. The foam was formed in a sandpack and then flowed through another sandpack, longer but of the same material. Apparent viscosity was found to increase with foam quality, provided there was adequate surfactant, but the increase in apparent viscosity with foam quality was less than had been reported by other workers who had measured the viscosity in viscosimeters. The apparent viscosity was found to decrease with increasing flow velocity through the sandpack (i.e., the foam was pseudoplastic). Also, flow history was observed to have an effect on the observed apparent viscosity: a foam flowed at a 28 ft/day and then reduced to 2.8 ft/day had a higher viscosity than a foam flowed at 2.8 ft/day without a more rapid flow rate preceding. This was reported but not explained; we suspect that it may have been the result of texture alteration.

Casteel and Djabbarah (1988)

Surfactants were screened by shaking tests in hard, saline water. Ammonium salts of alkylethoxysulfates were judged best. To evaluate foam-assisted CO_2 flooding, parallel

coreflood experiments were conducted in cores of 24 and 154 mD permeability, previously waterflooded. CO_2- foam floods were performed, and compared with unfoamed CO sub 2 and CO sub 2 - WAG tests. The best results were obtained when CO_2 was injected, followed by foamer solution, then additional CO_2. Unfoamed CO_2 recovered all the oil from the more permeable core and none from the less. Three WAG floods produced up to 9% of the oil from the less permeable core. Possible additional improvements in WAG are suggested. When the foamer solution was injected before CO_2, the more permeable core plugged up and 100% recovery was obtained from the less permeable core. The best results were obtained when CO_2 was injected first, then foamer, and then additional CO_2. This got all the oil from the more permeable core and 80% from the less permeable core.

De Vries and Wit (1988)

Foam is modeled as gas flowing through a bundle of parallel capillaries. If the quality of foam (fractional flow of gas) is above a certain value, all pores not filled with foam are filled with gas; below that value, all pores not filled with foam are filled with liquid. At the "break point" all pores are filled with foam. From this model, with several assumptions, the pressure gradient is predicted to increase with increasing gas velocity up to the break point, and thereafter be approximately constant; at any gas flow rate the pressure gradient is predicted to increase with the liquid flow rate. The location of the break point varies; at greater liquid velocity both the gas velocity and pressure gradient at the break point increase. Experimental data are presented for experiments in a sandstone core and in a sandpack; the constancy of pressure gradient with gas flow rate above the break point is evident, but the location of the break point and behavior below the break point are obscured by experimental errors. In-situ liquid saturation measurements by gamma ray attenuation showed that liquid saturation was constant at 18.1% through changes in flow rates. (This may mean 18.1 saturation units above connate).

Lau and O'Brien (1988)

Foam can not propagate through a formation faster than the surfactant, so retardation of surfactant transport by adsorption or by reaction with calcium ions slows the rate of foam propagation. Surfactant transport was measured in core flood experiments in which surfactant solution displaced brine. Increasing the amount of sodium in the surfactant solution caused displacement of exchangeable calcium, and reduced the retardation of surfactant breakthrough. But increasing the sodium also increased adsorption of the surfactant. A theory is presented to predict surfactant breakthrough.

Lee and Heller (1988)

In a laboratory study, dense CO_2 and foamer solution were flowed through Berea sandstone cores. In the experiments, foam quality was held constant and total velocity was varied. The foam mobility increased with decreasing surfactant concentration, with increasing foam quality, and, at high foam quality (90%), with increasing total velocity. The effect of surfactant concentration was observed with amphoteric and anionic surfactants, and was observed both above and below the critical micelle concentration. Pressure gradients calculated from the data were from 0.5 to 10 atm/cm.

Huh and Handy (1989)

In this laboratory study, gas and liquid relative permeabilities were measured during transient flow of gas into an initially saturated core, and during steady-state simultaneous flow of flow of gas and liquid. The liquid was brine with surfactant concentration ranging from 0 to 1 wt%. The gas was nitrogen injected at constant pressure. In both transient and steady state experiments, the dependency of liquid relative permeability to liquid saturation was approximately the same whether with or without surfactant, but gas relative permeability was lower by approximately an order of magnitude when foam was present. Gas broke through at lower gas saturation without surfactant than with it (15% compared with 30%).

A-7. Controlling Emplacement of Foam Banks

In applying foam technology in porous media, it may be necessary to form the foam in, or drive it to, a specific location. The following papers show how this can be done.

Hardy and Macarthur (1966) (pat. no. 3,269,460)

This patent describes a technique to improve the sweep profile when driving fluids through a stratified reservoir. A viscous mobile slug (which might be foam) is placed between the driving and the driven fluids. As fluid drive proceeds, the viscous mobile slug is displaced further in high permeability zones than in low permeability zones. Therefore the pressure gradient is steeper in the low permeability zones, and the displacement front adjusts itself to a more piston-like displacement front.

We note that in gas-storage applications, the piston-like displacement afforded by a foam buffer is advantageous because it prevents gas from fingering and penetrating far from the injection well. If base-gas were replaced by inert gas, as has been suggested, mixing between the stored natural gas and inert base gas would be enhanced by fingering, because this would increase the interfacial area between the two gases. Therefore foam could be used in conjunction with base-gas replacement both to reduce fingering and to act as a diffusion barrier between the two gases.

Bond and Bernard (1967) (pat. no. 3,318,379)

When foam is used as a buffer between a driving fluid (usually gas) and a driven fluid (usually oil), complete plugging, "making subsequent fluid injection impractical," may occur if the foam is formed immediately outside the wellbore in a region of steep pressure gradients. This patent describes a method to generate foam at a distance from the wellbore by first injecting a slug of surfactant solution (possibly non-aqueous), followed by a slug of foamer-free water to displace the foamer into an annular cylinder a certain distance from the wellbore. This is followed by a gas drive. The object of this invention was to improve tertiary oil recovery by

locating the foam at some distance from the wellbore where it would be easier to drive.

O'Brien and Sayre (1967) (pat. no. 3,335,792)

This patent discloses an improved method of driving a foam bank by a subsequent aqueous driving fluid. A slug of dilute surfactant is injected after foam generation in situ and before following it with the driving fluid. This was claimed to increase the stability of the foam bank and reduce the permeability further than if the surfactant buffer fluid were not injected. Improved oil recovery from foam flooding was also demonstrated in laboratory experiments.

Ferrell et al. (1968) (pat. no. 3,366,175)

In oil reservoirs in which gas overlays the oil, driving fluids may be displaced upward into the gas cap rather than toward a production well; similarly, oil displaced by a driving fluid may also be displaced upward into the gas cap and not recovered. This patent claims that a foam blanket (i.e., a horizontal foam block) can be formed at the oil-gas interface, thus directing the flow of driving fluids and recovered oil toward the production well. This patent and that of Heuer et al (1968) recommend a foaming agent comprised of 35% water, 50% alcohol ethoxysulfate, and 15% isopropanol. Others have also used isopropanol to break foams. The foam blanket cannot be formed by injecting foam through wells, nor can it be formed by injecting a surfactant solution followed by gas. Rather it can be formed by injecting a layer of surfactant solution between the oil and gas zones. Then the gas zone is pressurized and gas expands downward into the surfactant layer to form foam. The thickness of the foam blanket is supposed to be adequate to withstand a pressure differential of 100 psi without moving. A pressure differential between the oil and gas zones of 20 - 200 psi is supposed to be enough to get the gas to flow downward into the surfactant layer and form the foam. The thickness of foam blanket is not stated, but 0.05 lb of foaming agent per ft^3 of rock is estimated to be enough to form the foam. Laboratory examples are supplied: A 5-inch thick foam bank was formed in a Lucite cylinder sandpack, and the permeability to oil was reduced by 82 - 99%. The reduction lasted for 1.5 hour.

Bernard (1970) (pat. no. 3,529,668)

This patent describes a foam-drive process for enhanced oil recovery. A foam bank is formed in situ by injecting a slug of aqueous surfactant solution followed by gas and then driven by a combination of gaseous and aqueous fluids, in a volume ratio between 5:1 and 15:1, measured at reservoir conditions. The drive fluids can be alternating slugs or simultaneously injected. The original foam bank can also be injected as foam. In laboratory experiments, the optimum volume ratio of driving fluids to maximize displacement of residual oil was 10:1.

A-8. Delayed Foams

Because foam has high apparent viscosity and tends to plug formations, it is difficult to drive it to its desired location. To avoid having to drive foam, delayed foams have been proposed. These would be formed in situ after the ingredients were driven to the desired locations.

Clampitt (1976) (pat. no. 3,993,133)

This is a process to delay formation of foam by adding a chemically cross-linkable, water-dispersible polymer to the injected surfactant solution Foam is prevented from forming until the polymer thermally degrades. The gas phase is steam, so the foam collapses when the steam condenses. The foam is supposed to be temporary and self-destructive. The surfactants are prevented from foaming because they are "coated with" the polymers.

Richardson et al. (1980) (pat. no. 4,232,741)

This patent describes a process in which foam is generated in situ by formation of nitrogen gas which is the product of a delayed chemical reaction (reagents are disclosed in another patent). The reaction is delayed because it proceeds only at low pH and the injected solution contains an acid-yielding compound which degrades slowly. The nitrogen gas is formed when the pH drops below a threshold value. The intent is to temporarily seal high-permeability streaks.

A-9. Experience in Field Applications

A-9.1. Water Floods

Holm (1970)

This paper reports a field test at the Siggins oil field in Illinois of a water drive using foam as a mobility control buffer. The field had already been water-driven for secondary oil recovery prior to the test. Foam was formed by five cycles of alternating surfactant solution and gas injection, followed by simultaneous liquid and gas injection. The surfactant used was O.K. liquid (Procter and Gamble) at concentrations of 0.5, 1, and 1.5%. The total surfactant injection was 0.06 pore volumes at 1% equivalent concentration. No mechanical problems resulted from foam injection. Some corrosion occurred, but this was attributed to the large amount of air injected which was greater than necessary to form the foam. Injection of foam caused a reduction in water to oil ratio of produced fluid, from 15 to 12; in a control area the WOR increased from 20 to 28. Mobility reduction of air did not last beyond the period when surfactant solution was injected.

A-9.2. Thermal Floods; In-Situ Combustion

Elkins (1970) (pat. no. 3,504,745)

This patent claims the use of foam to prevent vertical gas flow during in-situ combustion of tar sands. In this case, when the tar is heated, it loses viscosity and no longer forms a seal around the well casing. Air injected for in-situ combustion then escapes around the well casing. A field test is described in which surfactant solution was injected outside and adjacent to the well casing, about 100 feet above the level of air injection. Foamer injection was continuous; after 45 days of injection it became difficult to inject more foamer solution but it was continued at a reduced rate. Because no air leakage was detected with this modification, foam formed in situ and stopped the air leakage. Continuous injection of surfactant was used to replace that which thermally degraded.

A-9.3. Steam Flooding

Doscher and Hammershaimb (1982)

The objective of this study was to demonstrate the use of foam for improving the efficiency of steam flooding projects. As part of the study, surfactants were screened for their foaming ability, their ability to block the gas flow, their sensitivity to the addition of corrosion inhibitors to the foaming solution, and their ability to form foam at elevated temperatures and pressures. As a result of the screening process, one of the foaming solutions appeared to have all the attributes required for successful application to a steam flood. Laboratory studies were then conducted with this surfactant to determine the most efficient way of injecting the foaming mixture. It was shown that steam alone, without the presence of a noncondensible gas is not a satisfactory gas for generating a foam. However, addition of nitrogen, at a concentration of 4%, creates the optimal foaming mixture. Various procedures for generating a foam block were investigated, including injecting sequential slugs of the foamer solution, steam and gas, and several combinations of these. No conclusion regarding the optimal procedure was reached.

A field pilot program was conducted to determine the feasibility of using foam under actual operating conditions. The reservoir chosen for the pilot consisted of lithologically heterogeneous sandstone, where stratification, as well as gravity override contributed to the poor performance of the conventional steam flood. After the creation of a foam bank in the reservoir, improved oil recovery and a lower water cut was observed, indicating that the foam bank at least partially alleviated the effects of gravity override and reservoir stratification.

Mohammadi, Van Slyke, Ganong (1989b)

This paper reports laboratory and field tests of steam-foam flooding. In laboratory studies, water and gas were injected with a gas-liquid volume ratio of 9:1 at standard conditions. During the experiment the liquid was changed to 0.5% AOS surfactant, and the pressure drop through a 2.3 darcy Dundee sandstone core increased. Pressure profiles showed that foam propagated as a

front, with a pressure gradient of 150 psi/ft behind the front. Field tests were done in a field that had been steam driven for 7 years with a declining production rate baseline. During two years, 60% quality steam was injected, with 0.5% active AOS surfactant (based on total water) and 19.6 scf nitrogen/bbl steam. Incremental production due to steam-foam (compared with steam only) was observed, and temperature logs showed expansion of the heated zone in observation wells, indicating that foam was effective in diverting steam from previously swept areas. ti +5i

Mohammadi, and McCollum, 1989a

This paper reports laboratory and field tests of steam-foam flooding. Laboratory tests were done to select a surfactant and to verify that foam drive could recover residual oil remaining after waterflooding. Resistance factors (defined as the ratio of pressure drop with foam to pressure drop with the same flow rates and no foam) varied between 20 and 28; with three surfactants and a gas-to-liquid ratio at standard conditions of 6:1. Foam flood experiments in parallel cores of 30 and 400 mD showed that additional 4.5% PV oil was recovered from the 400 mD core and additional 11% PV oil from the 30 mD core Based on these laboratory tests, three surfactants were injected into wells as ingredients in the liquid phase of steam. Noncondensible gas was also included in the steam foam. The apparent viscosity of the foam was estimated from plots of injection pressure against time (values not reported). Based on these field tests, formulated alkyl toluene sulfonate was selected for steam/foam flooding. 75% quality steam foam was injected into four wells at 600 psig injection pressure. The steam injection rate was 525 bbl/day water equivalent into each well, with 17.8 scf/bbl nitrogen. The surfactant concentration 0.5 wt% initially, later reduced to 0.1%. The concentration of surfactant was correlated with both injection pressure and the rate of pressure buildup. Incremental oil production was observed from some of the nine producing wells, but foam may have blocked flow channels to other wells, causing a decrease in production.

A-9.4. Sealing Gas Leaks

Anonymous (1960, 1961, 1963)

These three articles report a test of a water-curtain concept for storing gas under a cap rock with no closure. Although foam was not used in this test, it represents a concept similar to a proposed application of foam for gas storage. Eight wells were drilled, in a 1700-ft diameter circle, into a sandstone formation overlain by a flat caprock that provided no closure for gas storage. A well in the center of the circle was for gas injection and withdrawal, Water, continuously injected into the peroipheral wells, was to form a water curtain and prevent injected gas from migrating beyond the circumference of the circle. Initial difficulties were experienced with plugging of injection wells; after these were resolved 21 MMcf of air was injected into the reservoir. Upon withdrawal, only 1.35 MMcf were recovered before the withdrawal well watered out. The stored air apparently leaked through the cap rock, so the concept was not properly tested.

A-10. Economics

Papers reviewed here contain methodology used to determine the economic feasibility of inert gas replacement, another proposed technology for reducing base gas. While the break-even dollar figures are out-of-date and not relevant to foam protection, the methodology for calculation could probably be modified to for foam protection.

A-10.1 Need to Reduce Base-Gas Requirement

Base gas amounts to approximately 60% of all gas in underground storage (Loftness 1984). Problems of gas loss from aquifer storage are discussed by Mayfield (1981). In specific storage facilities, base gas amounts to as much as 80%. The Gas Research Institute is supporting research to reduce this base-gas requirement, which presently "consumes" underground 3.7 billion ft^3 of natural gas (Mayfield 1981). Future gas-storage and base-gas requirements were projected by Cimino and Morra (1980).

Mayfield (1981) describes problems of losses from gas-storage facilities. In two cases, gas losses were 0.0 and 1.2% of inventory, annually. Methods to calculate gas inventory in fields with and without water drive are presented.

Cimino and Morra (1980)

The object of this study was to determine the feasibility of replacing base gas with inert gas. In 1978 there were 3.2 Tscf (trillion = 10^{12} standard cubic feet) of natural gas in base gas. Of this, up to 40% is reported to be nonrecoverable (even at slow withdrawal rates). This base gas is needed to ensure access to 2.6 Tscf of working gas. It is not generally economic to recover the base gas due to the added costs of compression. In addition to existing storage facilities, new storage facilities also require base gas. If new storage facilities are located in 60% must be injected. One possibility for reducing the "consumption" of natural gas as base gas in new storage facilities is to substitute an inert gas. The decision to replace base gas with inert gas depends upon the expected degree of mixing between inert and natural gas. If withdrawn gas is below pipeline quality then the inert gas must be separated from the natural gas. Laboratory and field studies are cited which suggest that "first cycle mixing would be . . . 20% and that inerts would only be detected after most of the natural gas had been withdrawn." Despite this, interviews with operators showed concern about possible mixing. Likely candidates for replacement are cryogenic nitrogen and exhaust or flue gas. Nitrogen could be manufactured on site, but is only economical if there is another use for nitrogen nearby. Otherwise, after the required nitrogen has been manufactured (about 2 yr), the equipment must be sold for salvage value. Engine exhaust gas or boiler flue gas must be dewatered and treated before injecting to avoid corrosion problems. Replacement by cryogenic nitrogen was judged to be feasible if gas cost was $3.00±0.40 per Mcf if no mixing occurred in the reservoir, or $3.80±0.60 if gas mixing occurred. For replacement with exhaust gas, the break-even cost was $4.00 per Mcf.

Legatski and Katz (1967)

In this work, dispersivities were measured for argon displacing nitrogen or nitrogen displacing argon in sandstones. Dispersion causes gases to mix when one displaces another through a porous medium, even in the absence of fingering (i.e., even if displacement is piston-like). An equation is presented relating the dispersivity to the gas velocity raised to a power between 1 and 1.5. This relationship could be used to predict mixing of stored gas and inert base gas. The presence of an immobile phase (such as connate water) was shown to increase the dispersivity. Differences in properties between the two gases are not included in the equation; little difference was observed whether argon or nitrogen was the displacing gas.

A-11. Bibliography

References

Albrecht, R. A., and S. S. Marsden, (1970). Foams as blocking agents in porous media, *Society Petroleum Engineers Journal,* Vol. 51, March.

Anonymous, (1960). Will a wall of water hold stored gas? *Oil and Gas Journal 58(24)* June 13.

Anonymous, (1961). "Bubble" storage test delayed, *Oil and Gas Journal 59(23)* June 5.

Anonymous, (1963). "Bubble" gas-storage test hits a snag, *Oil and Gas Journal 61(5)* Feb. 4.

Assar, G. R., Nutt, C. W., and Burley, R. W. (1988). Viscosity/quality spectrum of foam flowing in straight capillary tubes, *Intl. Jour. of Engin. Fluid Mechanics 1* (4), 445-470.

Beeson, D. M., (1963). Recovery of oil from partially depleted reservoirs, U.S. Patent No. 3,100,524, issued August 13, 1963.

Bennett, G. S., (1964). A study of the foam-drive process for removal of brine from a consolidated sandstone core, Masters Thesis, The Pennsylvania State University, 97 pp.

Berkman, S., and G. Egloff, (1941). *Emulsions and Foams,* Reinhold Publishing Corporation, New York, 1941.

Bernard, G. G., (1963). Effect of foam on recovery of oil by gas-drive, *Producers Monthly,* pp. 18-21, January.

Bernard, G. G., (1967). Method for the subterranean storage of gas, U.S. Patent No. 3,330,352, issued July 11, 1967.

Bernard, G. G., (1970). Foam drive oil recovery process, U.S. Patent No. 3,529,668, issued September 22, 1970.

Bernard, G. G., and L. W. Holm, (1964). Effect of foam on permeability of porous media to gas, *Society of Petroleum Engineers,* September.

Bernard, G. G., and L. W. Holm, (1967). Method for recovering oil from subterranean formations, U.S. Patent No. 3,342,256, issued September 19, 1967.

Bernard, G. G., and L. W. Holm, (1970). Model study of foam as a sealant for leaks in gas storage reservoirs, *Society of Petroleum Engineers Journal* pp. 9-16, March.

Bernard, G. G., L. W. Holm, and W. L. Jacobs, (1965). Effect of foam on trapped gas saturation and on permeability of porous media to water, *Society of Petroleum Engineers,* pp. 296-300, December.

Bikerman, J. J., (1953). *Foams: Theory and Industrial Applications*, Reinhold Publishing Corporation, New York, 1953.

Bond, D. C., and G. G. Bernard, (1967). Foam formed in-situ away from the wellbore (flush with clean water), U.S. Patent No. 3,318,379, issued May 9, 1967.

Bond, D. C., and O. C. Holbrook, (1958). Gas drive oil recovery process, U.S. Patent No. 2,866,507, issued December 30, 1958.

Casteel, J. F., Djabbarah, N.F. (1988). Sweep improvement in CO_2 flooding by use of foaming agents, *SPE Reservoir Engineering 3*, (4), 1186-1192.

Chatterji, J., and J. K. Borchardt, (1981). Applications of water-soluble polymers in the oil field, *Journal of Petroleum Technology*, pp. 2042-2056, November.

Cimino, M., and F. Morra, (1980). Economic feasibility of inert cushions in underground gas storage, paper presented at the 55th Annual Fall Technical Conference and Exhibition of the Society of Petroleum Engineers of AIME, Dallas, Texas, September 21-24.

Clampitt, R. L., (1976). Selective plugging of formations with foam, U.S. Patent No. 3,993,133. issued November 23, 1976.

Craig, F. F., and J. L. Lummus, (1965). Oil recovery by foam drive, U.S. Patent No. 3,185,634, issued May 25, 1965.

Dauben, D. L., and S. H. Raza, (1970). Increasing foam stability in earth formations, U.S. Patent No. 3,530,940, issued September 29, 1970.

Dellinger, S. E., J. T. Patton and S. T. Holbrook (1984). CO_2 mobility control, *Society of Petroleum Engineers Journal*, pp. 191-196, April.

Deming, J. R., (1964). Fundamental properties of foams and their effects on the efficiency of the foam-drive process, Masters Thesis, The Pennsylvania State University, 72 pp.

DeVries, A. J., (1958). Foam stability, *Recueil des travaux chimiques des Pays-Bas, 77*, pp. 8-19, 109-223, 283-296, 383-399, 444-461; reprinted as *Rubber Chem. and Tech., 5*, pp. 1142-1196, 1958.

De Vries, A. S., and K. Wit, (1988). Rheology of foam in the quality range relevant to steam foam, SPE 18075, presented at the 63rd Annual Technical Conference and Exhibition of the SPE, Houston, TX Oct. 2-5.

Dilgren, R. E., G. J. Hirasaki, H. H. Hill, and D. G. Whitten, (1978). Steam-channel-expanding steam foam drive, U.S. Patent No. 4,086,964, issued May 2, 1978.

Dilgren, R. E., and K. B. Owens, (1979). Hot water foam oil production process, U.S. Patent No. 4,161,217, issued July 17, 1979.

Doscher, T. M., and E. C. Hammershaimb, (1982). Field demonstration of steam drive with ancillary materials, *Journal of Petroleum Technology*, pp. 1535-1542, July.

Elkins, L. E., (1970). Use of foam to prevent vertical flow in tar sands during in-situ combustion, U.S. Patent No. 3,504,745, issued April 7, 1970.

Falls, A. H., J. J. Musters, and J. Ratulowski, (1989). The apparent viscosity of foams in homogeneous beadpacks, *SPE Reservoir Engineering, 4* (2), 155-164, May.

Felber, B. J., and D. L. Dauben, (1977). Laboratory development of lignosulfonate gels for sweep improvement, *Society of Petroleum Engineers Journal*, pp. 391-397, December.

Ferrell, H. H., M. Felsenthal, and C. L. Jacocks, (1968). Secondary recovery process in a gas cap reservoir, U.S. Patent No. 3,366,175, issued January 30, 1968.

Freeman, E.R., D. M. Bilden, and M. Hossaini, (1986). Delayed crosslinked gels: Their role in aqueous foam fracturing, presented at the 56th California Regional Meeting of the Society of Petroleum Engineers, Oakland, CA, April 2-4.

Fried, A. N., (1961). The foam-drive process for increasing the recovery of oil, United Sates Department of Interior, Bureau of Mines Report of Investigations RI-5866.

Gardescu, I. I., (1930). Behavior of gas bubbles in capillary spaces, *Trans. Am. Inst. Mining Metallurgical Engineers, 86*, pp. 351-370.

Hardy, W. C., and B. W. Macarthur, (1966). Secondary recovery of petroleum, U.S. Patent No. 3,269,460, issued August 30, 1966.

Harris, P. C., (1985). Dynamic fluid-loss characteristics of nitrogen foam fracturing fluids, *Journal of Petroleum Technology*, October, pp. 1847-1852.

Hatziavramidis, D. T., (1986). The effective mobility of fine-texture dispersions flowing in porous media, *Journal Chemical Physics*, Vol. 84, (6), March, p. 3379.

Hayashi, A., and D. A. I. Goring, (1965). Studies on lignosulphonate (XVII), An investigation of gelling reaction of lignosulphonate with dischromate, *Pulp and Paper Magazine of Canada*, Convention Issue, pp. T-154-T-164.

Heuer, G. J., M. Felsenthal, and C. L. Jacocks, (1968). Control of gas-oil ratio in producing wells, U.S. Patent No. 3,368,624, issued February 13, 1968.

Hirasaki, G. J., and J. B. Lawson, (1985). Mechanisms of foam flow in porous media: Apparent viscosity in smooth capillaries, *Society of Petroleum Engineers Journal*, pp. 176-190, April.

Holbrook, O. C., and G. G. Bernard, (1965). Use of foam for plugging gas producing strata, U.S. Patent No. 3,207,218, issued September 21, 1965.

Holcomb, D. L., E. Callaway, and L. L. Curry, (1981). Chemistry, physical nature, and rheology of aqueous stimulation foams, *Society of Petroleum Engineers Journal,* August, pp. 410-414.

Holm, L. W., (1968). The mechanism of gas and liquid flow through porous media in the presence of foam, *Society of Petroleum Engineers Journal,* pp. 359-369, December.

Holm, L. W., (1970). Foam injection test in the Siggins Field, Illinois, *Journal of Petroleum Technology,* pp. 1499-1506, December.

Huang, C. G., D. W. Green, and G. P. Willhite, (1986). An experimental study of the in-situ gelation of chromium(+3)/polyacrylamide polymer in porous media, *SPE Reservoir Engineering, 1* (6), 583-592, November.

Huh, D. G, and L. L. Handy, (1989). Comparison of steady- and unsteady-state flow of gas and foaming solution in porous media, *SPE Reservoir Engineering 4,* (1), 77-84.

Kamal, M., (1970). Displacement of a miscible slug by foam, Masters Thesis, Stanford University, 13 pp.

Kolb, G. E., (1964). Several parameters affecting the foam-drive process for the removal of water from consolidated porous media, Masters Thesis, The Pennsylvania State University, 68 pp.

Lau, H. C. and S. M. O'Brien, (1988). Surfactant transport through porous media in steam-foam processes, *SPE Reservoir Engineering, 3* (4), 1177-1185, November.

Leach, R. O., (1969). Foams in enriched gas drives, U.S. Patent No. 3,460,623, issued August 12, 1969.

Lee, H. O. and J. P. Heller (1988). Laboratory measurements of CO_2-foam mobility, SPE/DOE 17363, presented at EOR Symposium, Tulsa, Apr. 17-20.

Legatski, M. W., and D. L. Katz, (1967). Dispersion coefficients for gases flowing in consolidated porous media, *Society of Petroleum Engineers Journal,* pp. 43-53, March.

Lord, D. L., (1981). Analysis of dynamic and static foam behavior, *Journal of Petroleum Technology,* pp. 39-45, January.

Marsden, S. S., (1986). Foams in porous media-Supri TR-49, Topical Report, DOE/SF/11564-15 (DE8600290), Technical Information Center, Office of Scientific and Technical Information, U.S. Department of Energy, July.

Marsden, S. S., and S. A. Khan, (1966). The flow of foam through short porous media and apparent viscosity measurements, *Society of Petroleum Engineers Journal,* pp. 17-25, March.

Mast, R. F., (1972). Microscopic behavior of foam in porous media, SPE 3997, presented at the Annual Fall Meeting, Society of Petroleum Engineers, San Antonio, Texas, 11 pp. October.

Mayfield, J. F., (1981). Inventory verification of gas storage fields, *Journal of Petroleum Technology*, pp. 1730-1734, September.

Minssieux, L., (1974). Oil displacement by foams in relation to their physical properties in porous media, *Journal of Petroleum Engineers*, pp. 100-108, January.

Mohammadi, S. S., D. C. Van Slyke, and B. Ganong, (1989b). Steam-foam pilot project in dome-tumbador, Midway-Sunset Field, *SPE Reservoir Engineering, 4* (1), 7-16, February.

Mohammadi, S. S., T. J. McCollum, (1989a). Steam-foam pilot project in Guadalupe Field, California, *SPE Reservoir Engineering, 4* (1) 17-23, February.

O'Brien, L. J., (1967). Foam to seal the permeable zone above a domed cap-rock, U.S. Patent No. 3,306,354, issued February 28, 1967.

O'Brien, L. J., and A. T. Sayre, (1967). Method for increasing oil recovery, U.S. Patent No. 3,335,792, issued August 15, 1967.

Patton, J. T., S. T. Holbrook, and W. Hsu, (1983). Rheology of mobility-control foams, *Society of Petroleum Engineers Journal*, June, pp. 456-460.

Ransohoff, T. C., and C. J. Radke, (1988). Mechanisms of foam generation in glass bad packs, *SPE Reservoir Engineering 3*, (2), 573-585, May.

Rai, C., and G. G. Bernard, (1967). Method of secondary recovery employing successive foam drives of different ionic characteristics, U.S. Patent No. 3,323,588, issued June 6, 1967.

Raza, 1970. Plugging formations with foam, U.S. Patent No. 3,491,832, issued January 27, 1970.

Reidenbach, V. G., P. C. Harris, Y. N. Lee, and D. L. Lord, (1986). Rheological study of foam fracturing fluids using nitrogen and carbon dioxide, *SPE Production Engineering*, January, pp. 31-41.

Richardson, E. A., R. F. Scheuerman, D. C. Berkshire, J. Reisberg, and J. H. Hybarger, (1980). Temporarily plugging a subterranean reservoir with a self-foaming aqueous solution, U.S. Patent 4,232,741, issued November 11, 1980.

Roof, J. G., (1970). Snap-off of oil droplets in water-wet pores, *Society of Petroleum Engineers Journal*, p. 85, March.

Schick, M. J., and F. M. Fowkes, (1957). Foam stabilizing additives for synthetic detergents. Interaction of additives and detergents in mixed micelles, Jour. Phys. Chem., Vol. 61, pp. 1062-1068.

Sharma, M. K., D. O. Shah, and W. E. Brigham, (1982). The chain length compatibility and surface properties of foaming solutions in relation to fluid displacement efficiency in porous media, paper presented at the SPE Sixth International Symposium on Oilfield and Geothermal Chemistry, Dallas, Texas, January 25-27.

Sharma, M. K., D. O. Shah, and W. E. Brigham, (1984). Correlation of chain length compatibility and surface properties of mixed foaming agents with fluid displacement efficiency and effective air mobility in porous media, *I&EC Fundamentals, 23*, pp. 213-220.

Taber, J. J., and P. F. Fulton, (1976). A study of the use of foam to control methane emission in coal mines, United States Department of Interior, Bureau of Mines Report report OFR 40-76, (NTIS No. PB 250 367).

Treinen, R. J., W. E. Brigham, and L. M. Castanier, (1985). Apparent viscosity measurements of surfactant foam in porous media-supri TR-48, Topical Report, DOE/SF 11564-13, U. S. Department of Energy, Bartlesville Project Office, Bartlesville, Oklahoma.

Appendix B. Summary of Experimental Data.

This appendix presents data from all experiments on foam flow and blocking in sandstone cores. The apparatus is described in Chapter 3. Each experiment is briefly summarized, and the data are presented in graphical form. All data are also available as formatted data files. The experiments are numbered in chronological order, but some numbers were assigned to "experiments" intended to check operation of equipment, and are not reported here. In all experiments (except as noted) the core was initially saturated with foamer solution and several pore volumes of foamer solution were pumped through the core to establish adsorptive equilibrium.

Experiments 3, 4, 6 (first part), 12, and 15 (second part) were conducted with gas and liquid flowing simultaneously, to determine the relationship between pressure gradient and flow rates. Steady-state data from experiments 3 and 12 and transient data from experiment 4 are discussed in the technical report provided in Appendix E. Transient data from experiment 3 and steady-state data from experiments 4, 6, and 15 also support the conclusions presented in Appendix E.

Experiments 5, 7, 8, 9, and 15 (first part) were conducted with gas flowing through a foam-filled core to measure the permeability to gas. These data are discussed in the technical report provided in in Appendix F.

Experiment 6 (second part) was conducted with liquid flowing through a foam-filled core to measure the permeability to liquid. These data are discussed in Appendix F.

Experiment 3

In experiment 3, liquid was injected at a constant rate (0.26 mL/min). Gas was injected at controlled mass flow rates increasing stepwise from 80 to 3700 scc/min, corresponding to gas velocities of 1 to 43 m/day. These flow rates corresponded to "flowing qualities at pressure" ranging from 82 to 99.5 %. An unexpected result was that the pressure gradient scarcely changed, expect for a transient increase, when the gas injection rate (equivalently: flowing quality) was changed. This is shown in Figure B-3.1 as small upticks at every step increase in the gas flow rate.

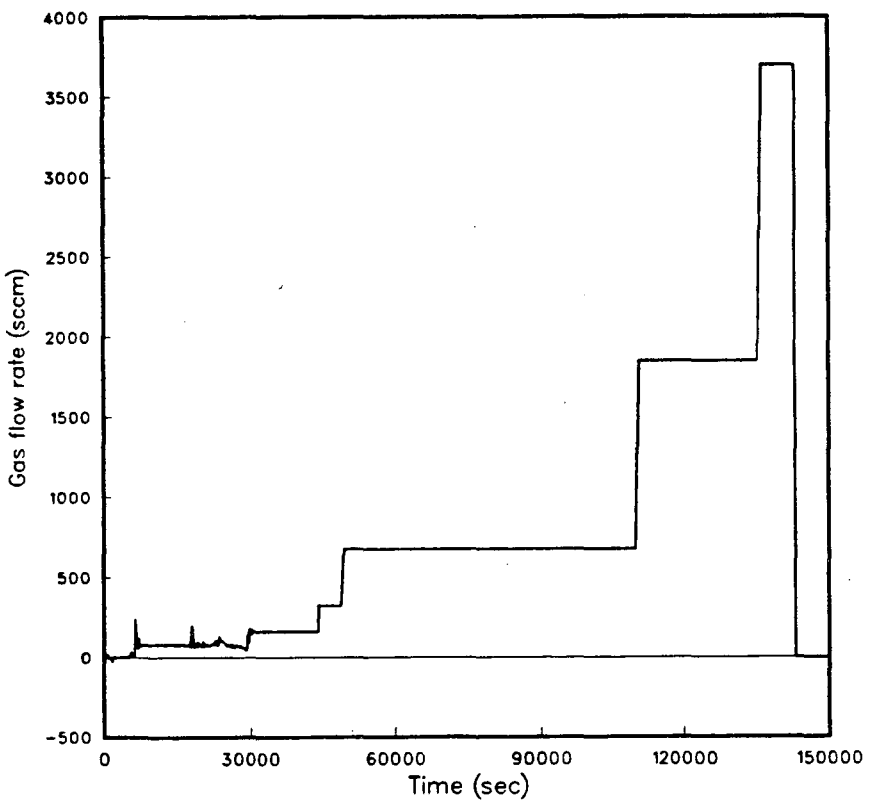

Figure B-3.1. Gas flow rate during Experiment 3. The liquid flow rate was 0.26 mL/min throughout this experiment (v_{liq} = 0.185 m/day).

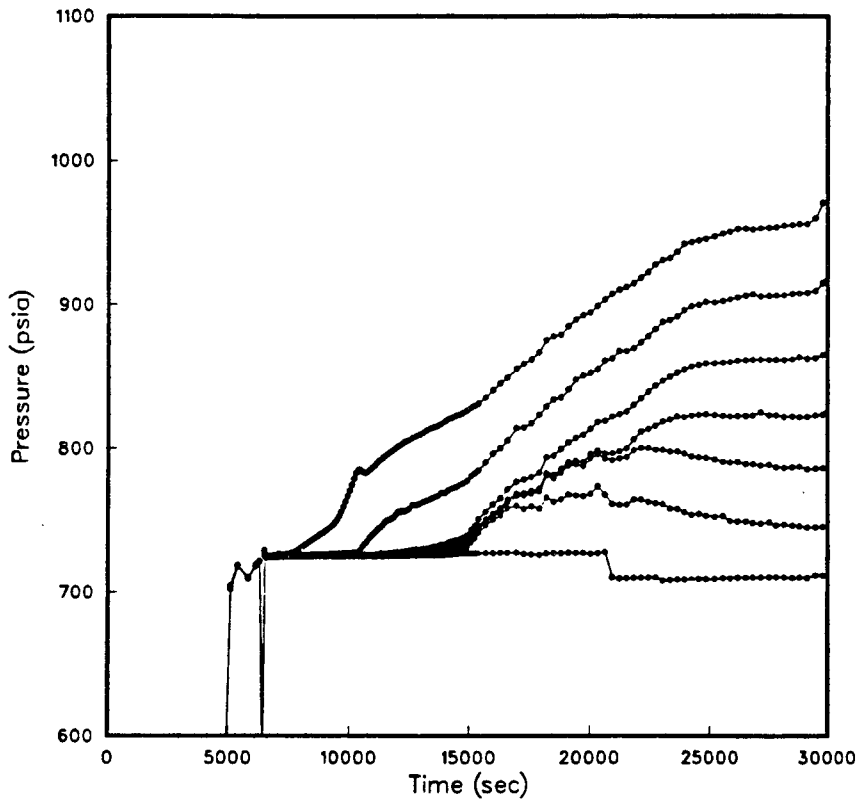

Figure B-3.2. Pressures recorded at taps 2 through 8 (60 cm = outlet to 0 cm = inlet) during initial foam propagation, experiment 3.

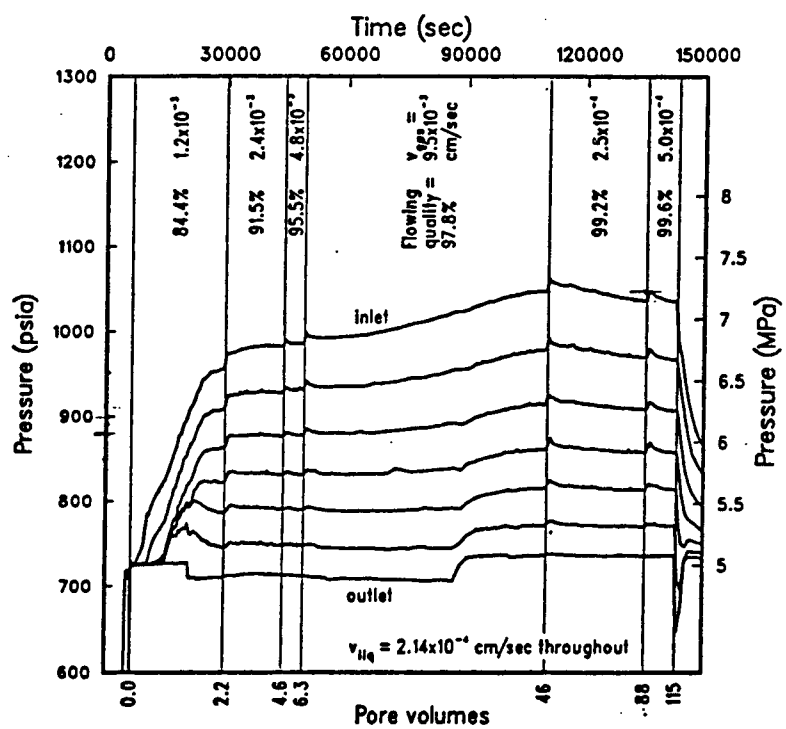

Figure B-3.3. Pressures recorded at taps 2 through 8 (60 cm = outlet to 0 cm = inlet) during changes in gas flow rate, experiment 3.

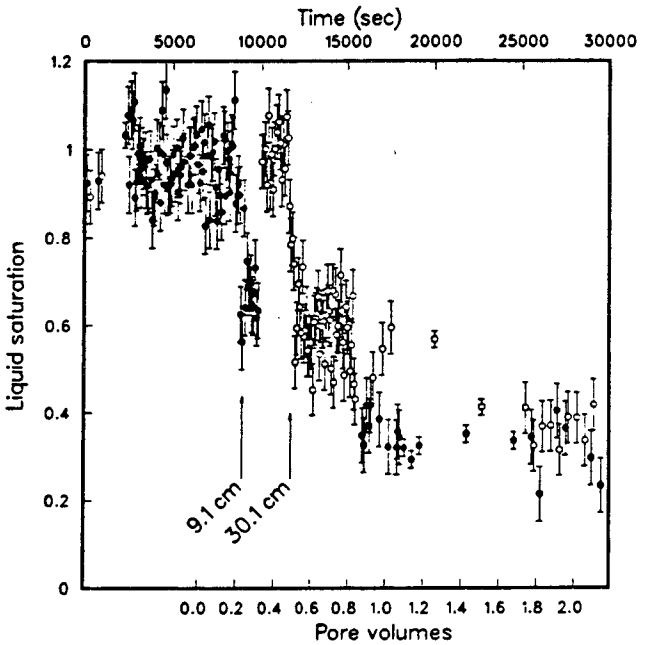

Figure B-3.4. Liquid saturation at 9.1 and 30.1 cm, showing passage of foam front, experiment 3.

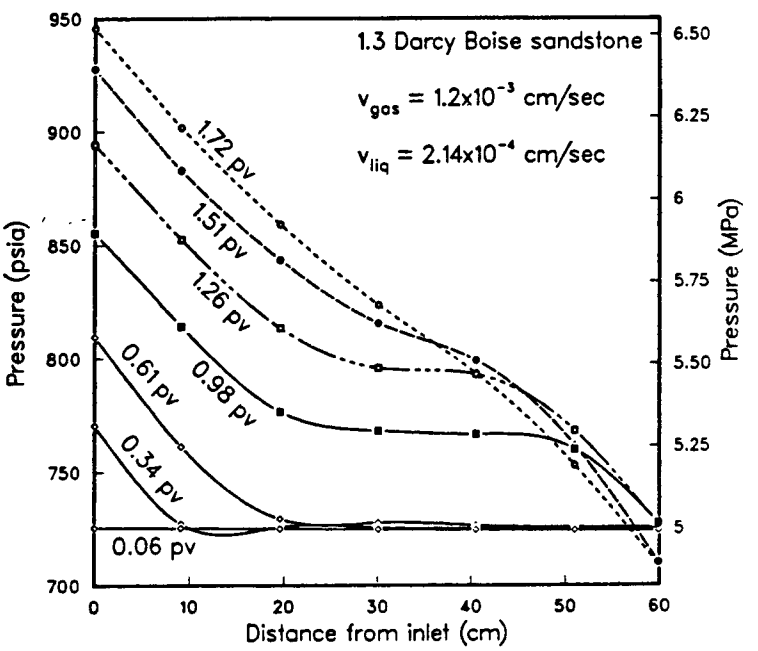

Figure B-3.5. Pressure profiles during transient displacement of foam, experiment 3. Times have been converted to pore volumes of fluid. Conversion to times for comparison with other plots: 0 pv = 6393 sec; 0.06 pv = 6997 sec; 0.34 pv = 10034 sec; 0.61 pv = 12950 sec; 0.98 pv = 16985 sec; 1.26 pv = 20042 sec; 1.51 pv = 22742 sec; 1.72 pv = 24851 sec. Note that pressure front did not pass uniformly from inlet to outlet but skipped over 20-40 cm. Compare with Figure B-3.6 through 11 to see correspondence between pressure gradient and liquid saturation discussed in Appendix E.

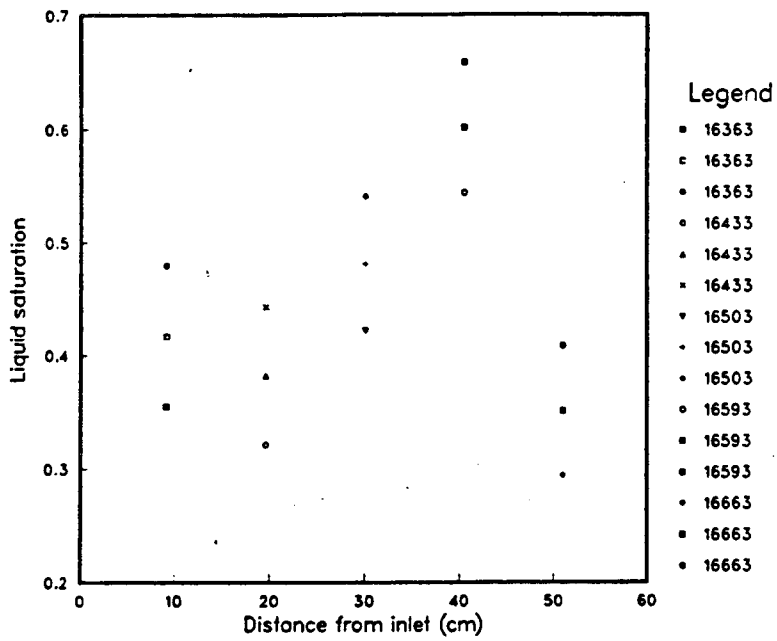

Figure B-3.6. Liquid saturation profile during transient displacement of foam, experiment 3, 16500 sec. Three values at each station represent best value and one standard deviation based on counting error. Times under "Legend" are the mid-count times for each measurement. Compare with Figure B-3.5.

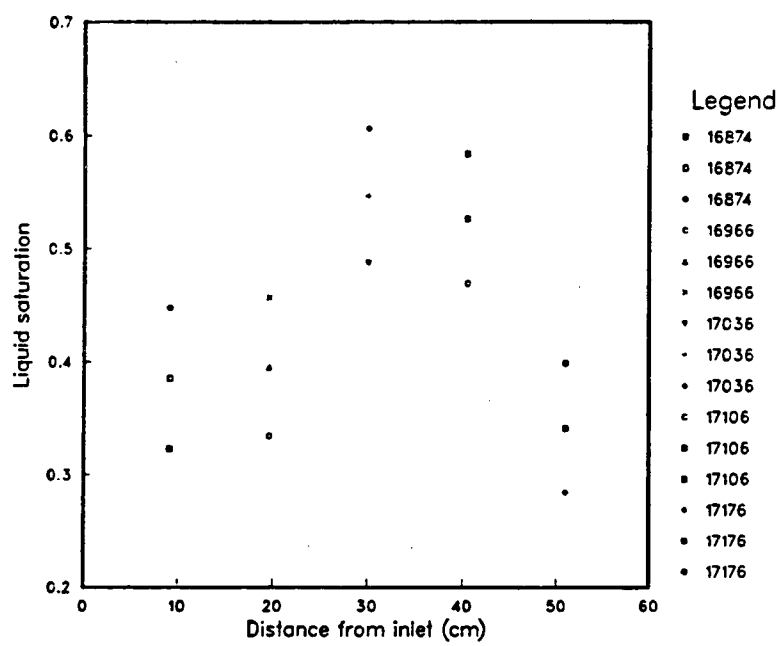

Figure B-3.7. Liquid saturation profile during transient displacement of foam, experiment 3, 17000 sec. Three values at each station represent best value and one standard deviation based on counting error. Times under "Legend" are the mid-count times for each measurement. Compare with Figure B-3-5.

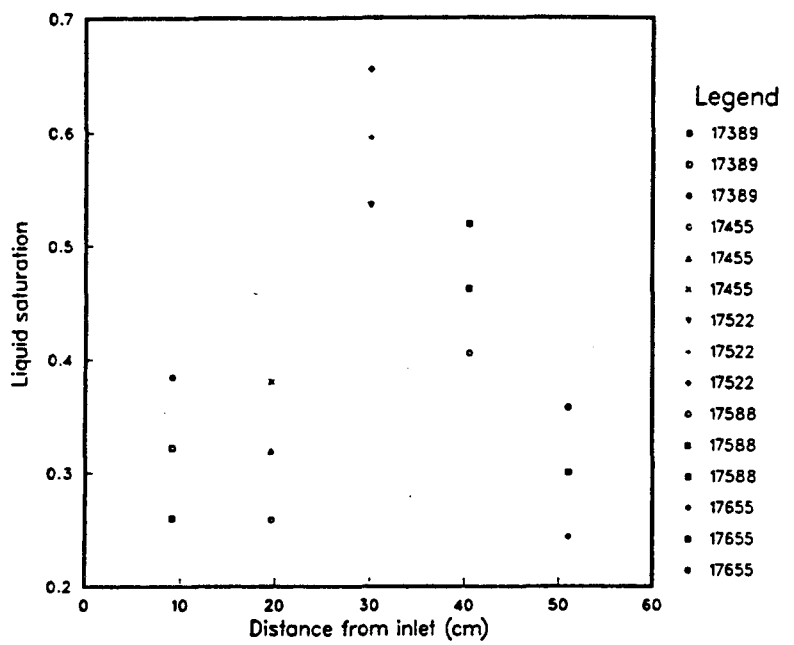

Figure B-3.8. Liquid saturation profile during transient displacement of foam, experiment 3, 17500 sec. Three values at each station represent best value and one standard deviation based on counting error. Times under "Legend" are the mid-count times for each measurement. Compare with Figure B-3-5.

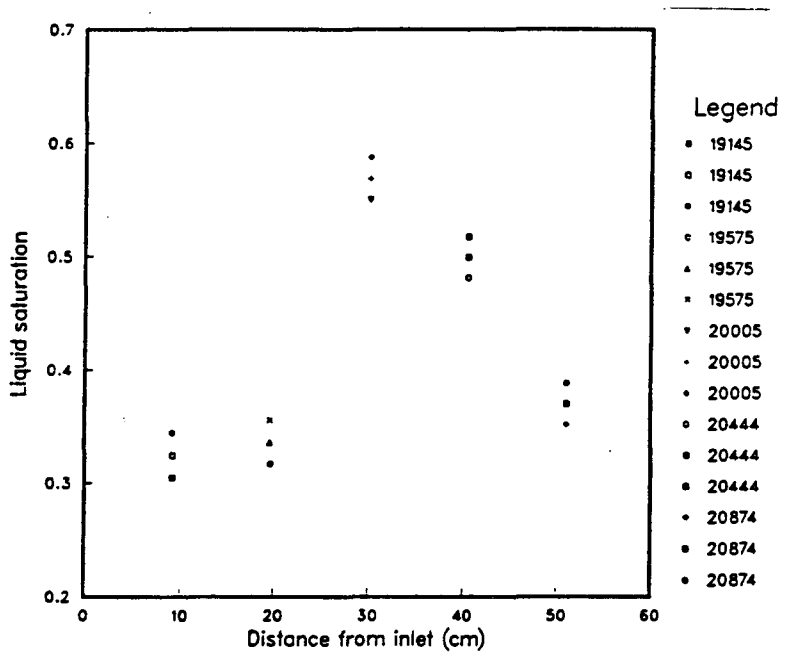

Figure B-3.9. Liquid saturation profile during transient displacement of foam, experiment 3, 20000 sec. Three values at each station represent best value and one standard deviation based on counting error. Times under "Legend" are the mid-count times for each measurement. Compare with Figure B-3.5.

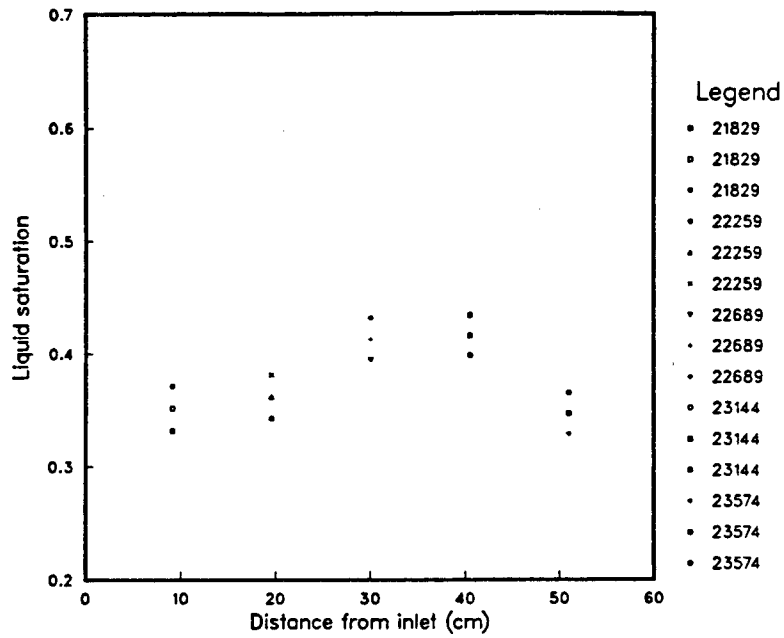

Figure B-3.10. Liquid saturation profile during transient displacement of foam, experiment 3, 22700 sec. Three values at each station represent best value and one standard deviation based on counting error. Times under "Legend" are the mid-count times for each measurement. Compare with Figure B-3-5.

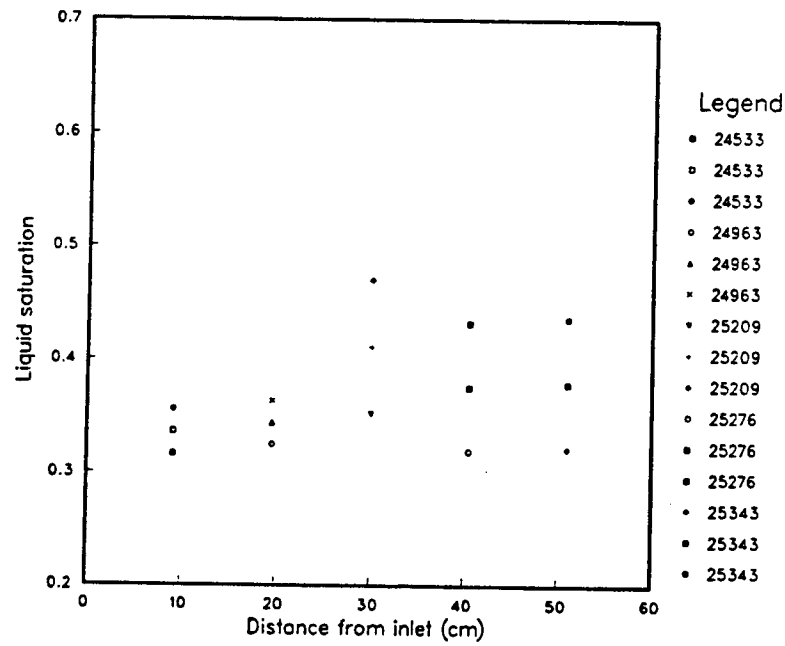

Figure B-3.11. Liquid saturation profile during transient displacement of foam, experiment 3, 25000 sec. Three values at each station represent best value and one standard deviation based on counting error. Times under "Legend" are the mid-count times for each measurement.

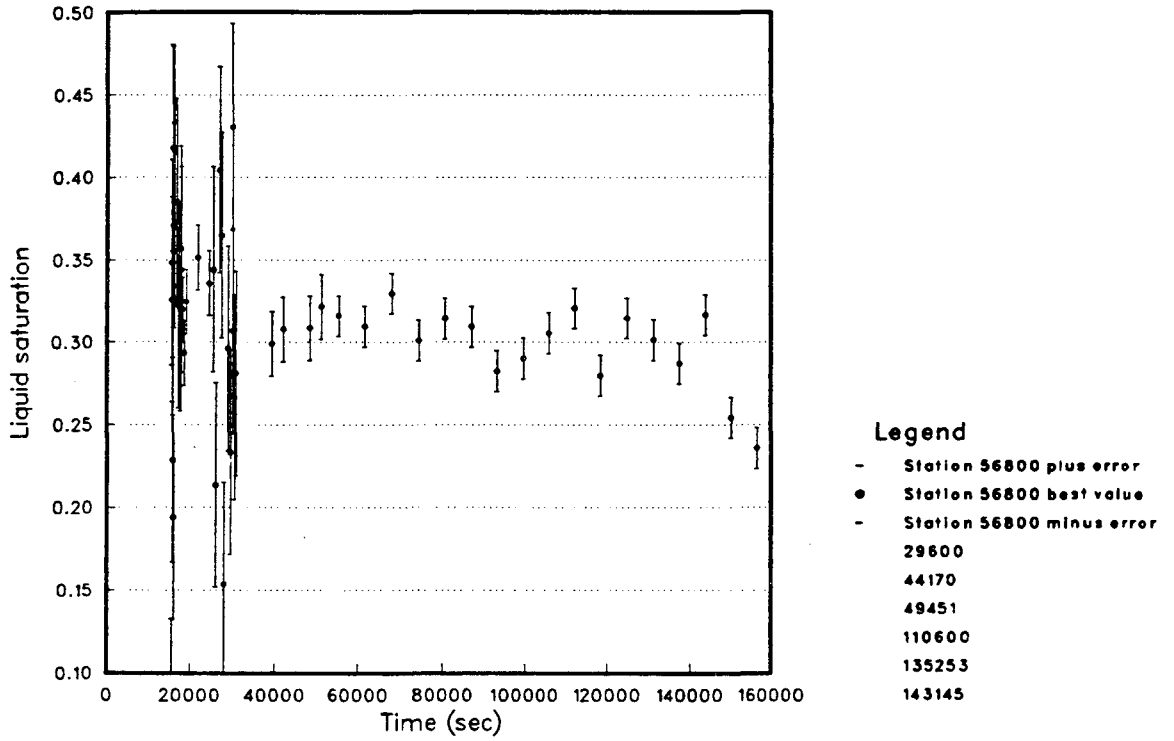

Figure B-3.12. Liquid saturation at 9.1 cm during stepwise changes in gas velocity. Compare with Figure B-3.1 and B-3.3.

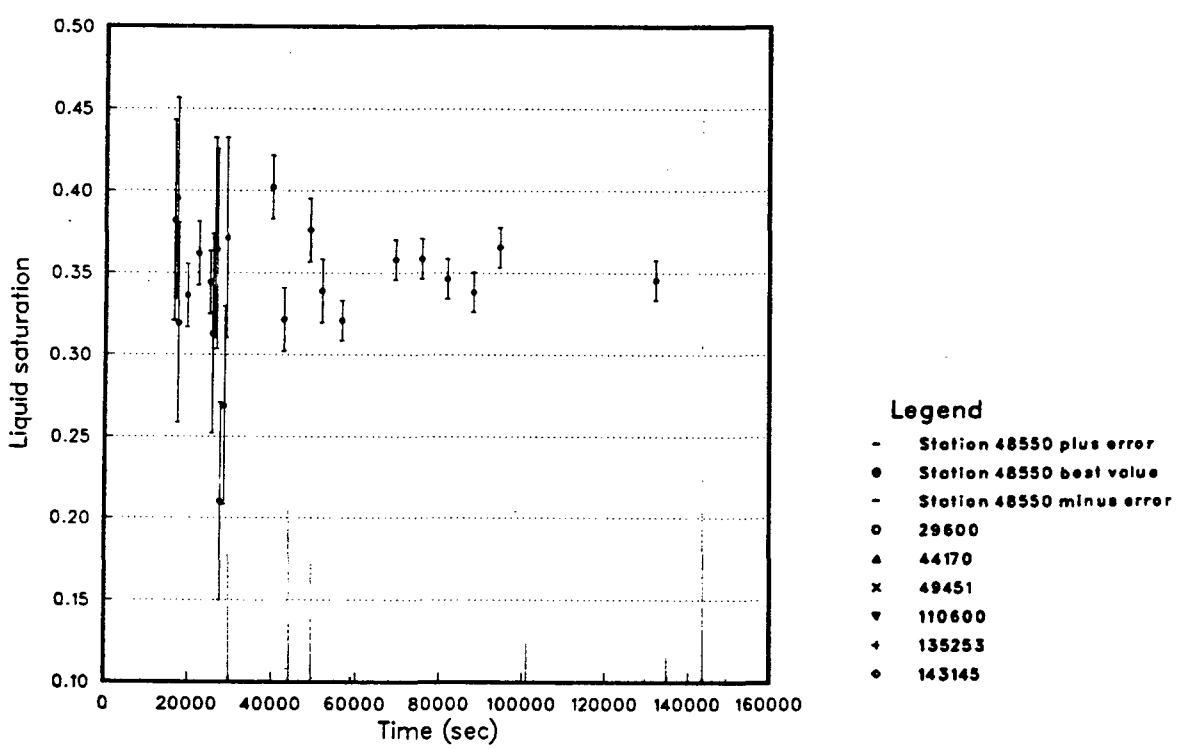

Figure B-3.13. Liquid saturation at 19.6 cm during stepwise changes in gas velocity. Compare with Figure B-3.1 and B-3.3.

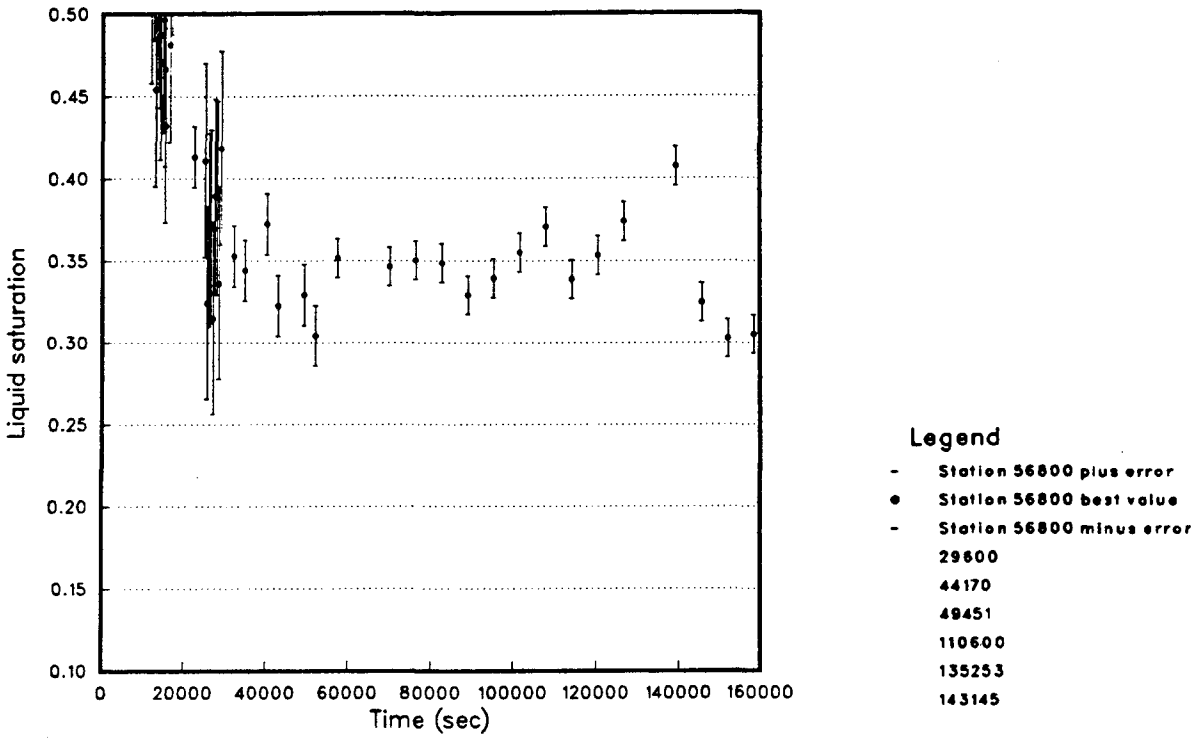

Figure B-3.14. Liquid saturation at 30.1 cm during stepwise changes in gas velocity. Compare with Figure B-3.1 and B-3.3.

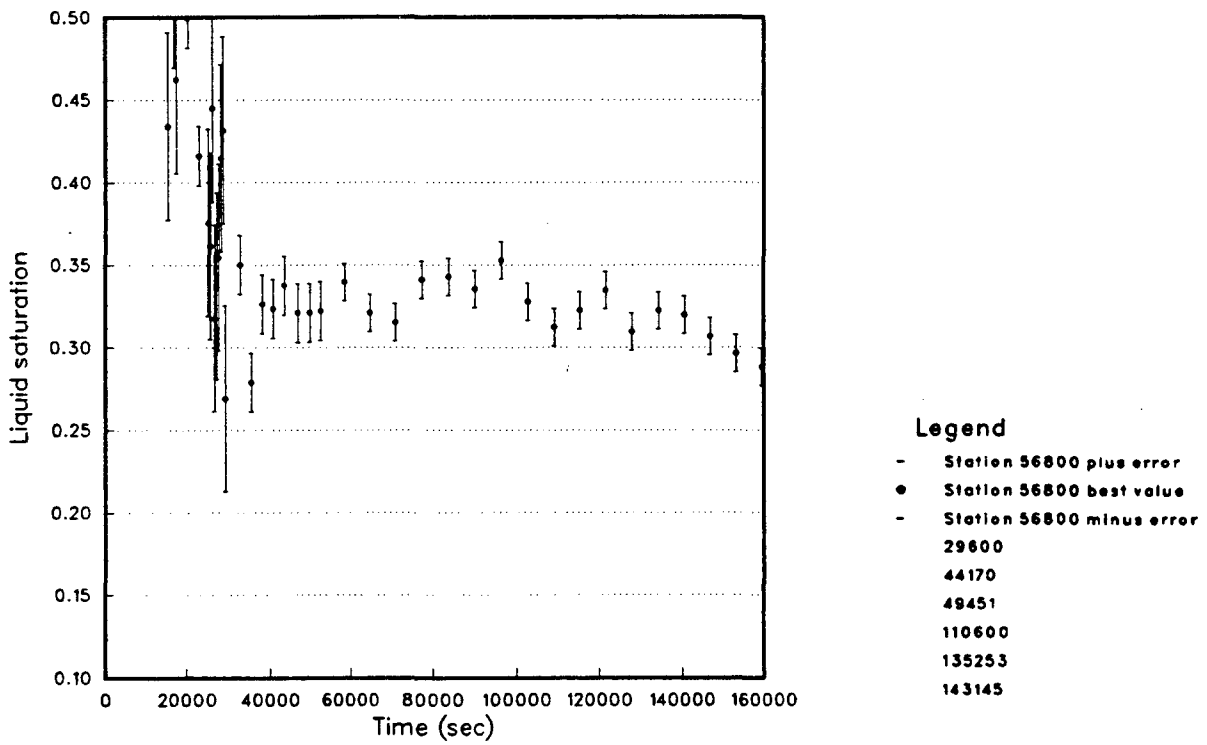

Figure B-3.15. Liquid saturation at 40.6 cm during stepwise changes in gas velocity. Compare with Figure B-3.1 and B-3.3.

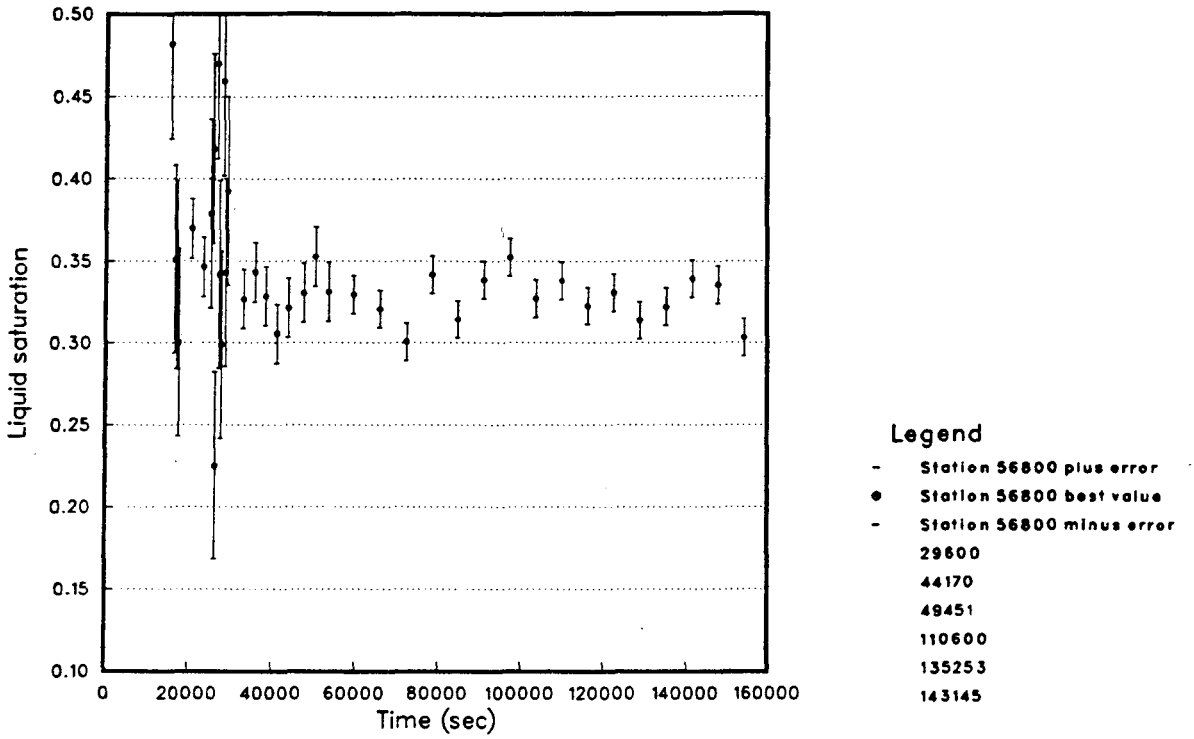

Figure B-3.16. Liquid saturation at 51.0 cm during stepwise changes in gas velocity. Compare with Figure B-3.1 and B-3.3.

Experiment 4

Experiment 4, like experiment 3, started with 100% liquid saturation. The liquid flow rate was the same as for experiment 3, but the gas flow rate was 323 scc/min (same as the 95% quality phase of experiment 3). The steady-state pressure and liquid saturation profiles during this experiment matched the results from experiment 3. This shows that the initial flow conditions do not determine the steady state of the core.

After experiment 4, attempts to cause complete blocking by reducing the gas injection pressure failed. There was always some gas flow, although at a reduced rate.

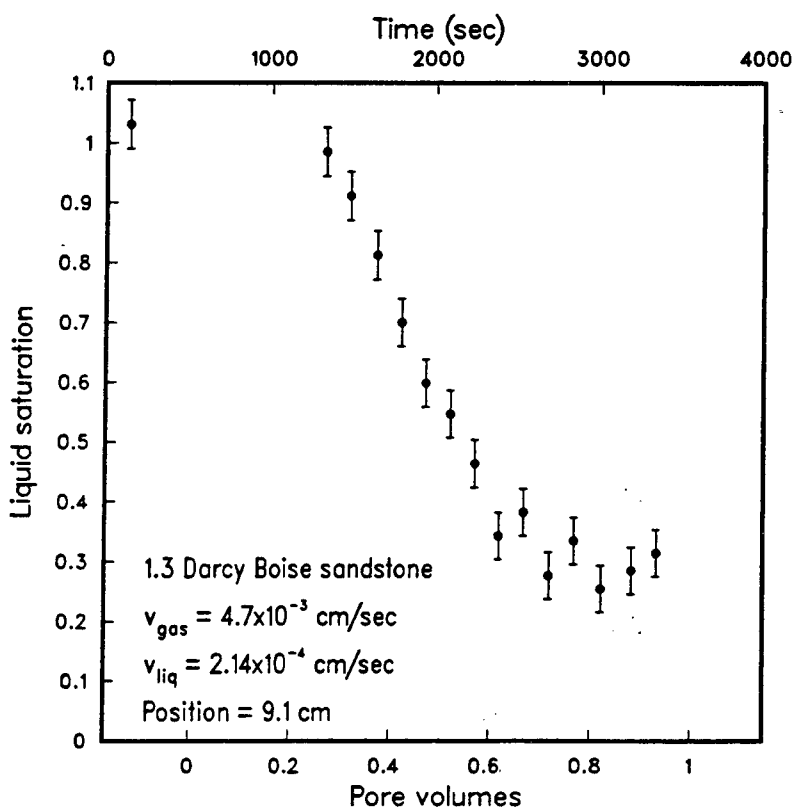

Figure B-4.1. Liquid saturation at 9.1 cm, showing passage of foam front, experiment 4.

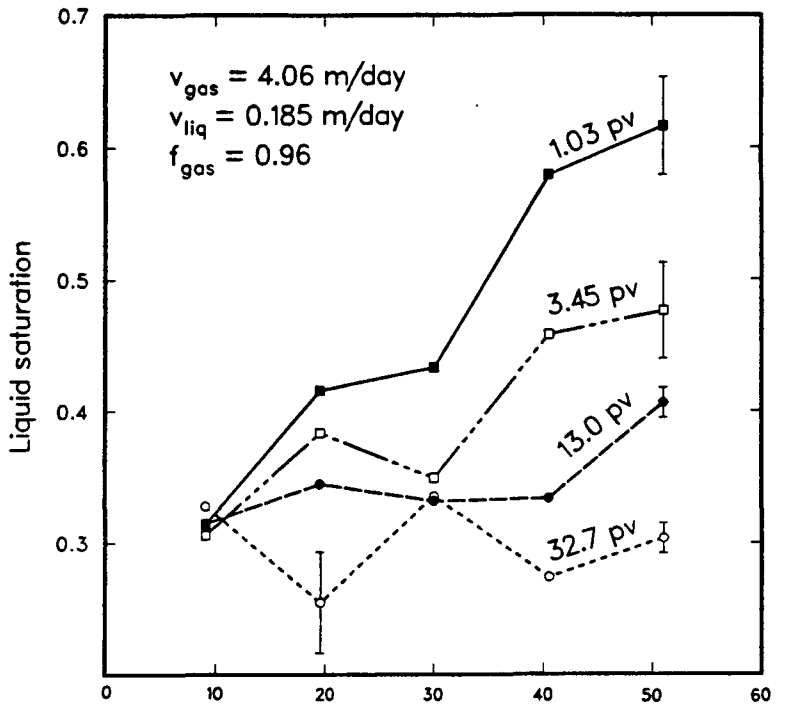

Figure B-4.2. Liquid saturation profiles during transient displacement of foam, experiment 4. Times have been converted to pore volumes of fluid. Conversion to times for comparison with other plots: 0 pv = 510 sec; 1.03 pv = 3650 sec; 3.45 pv = 11000 sec; 32.7 pv = 100000 sec.

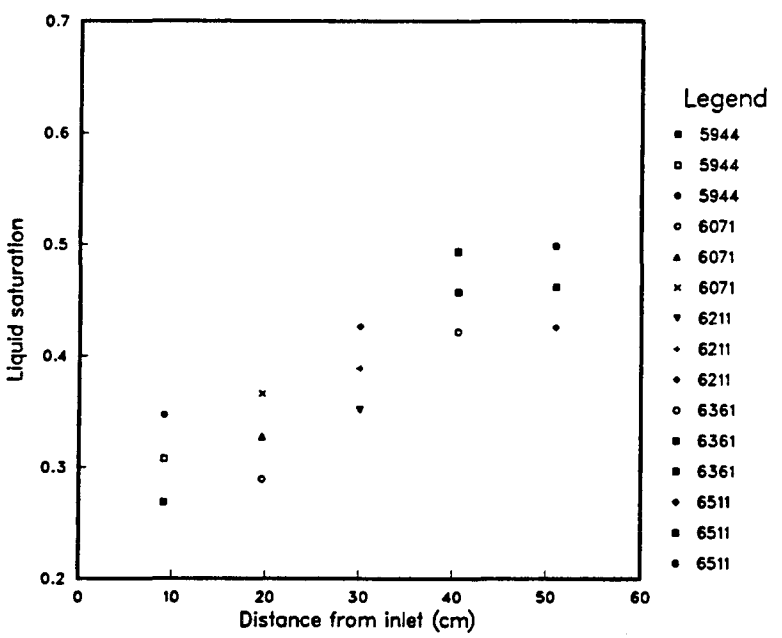

Figure B-4.3. Liquid saturation profile during transient displacement of foam, experiment 4, 6200 sec. Three values at each station represent best value and one standard deviation based on counting error. Times under "Legend" are the mid-count times for each measurement.

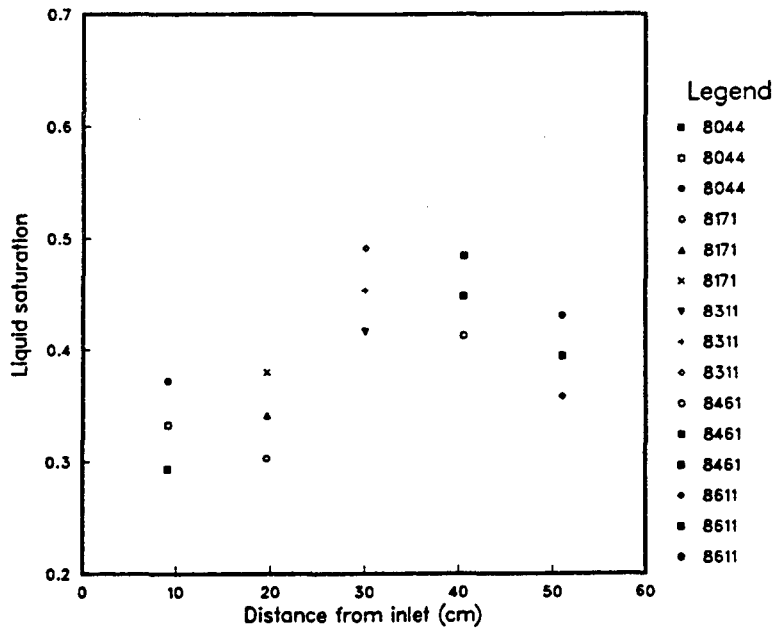

Figure B-4.4. Liquid saturation profile during transient displacement of foam, experiment 4, 8300 sec. Three values at each station represent best value and one standard deviation based on counting error. Times under "Legend" are the mid-count times for each measurement.

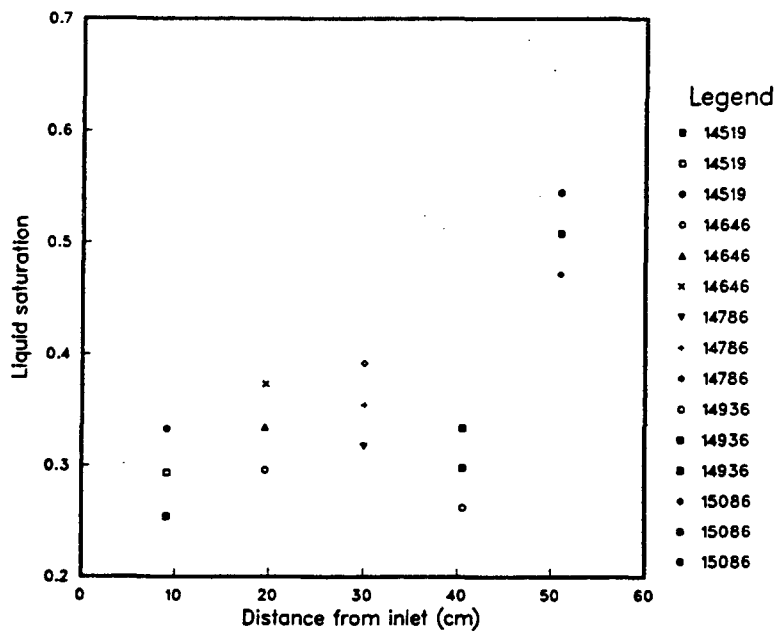

Figure B-4.5. Liquid saturation profile during transient displacement of foam, experiment 4, 14800 sec. Three values at each station represent best value and one standard deviation based on counting error. Times under "Legend" are the mid-count times for each measurement.

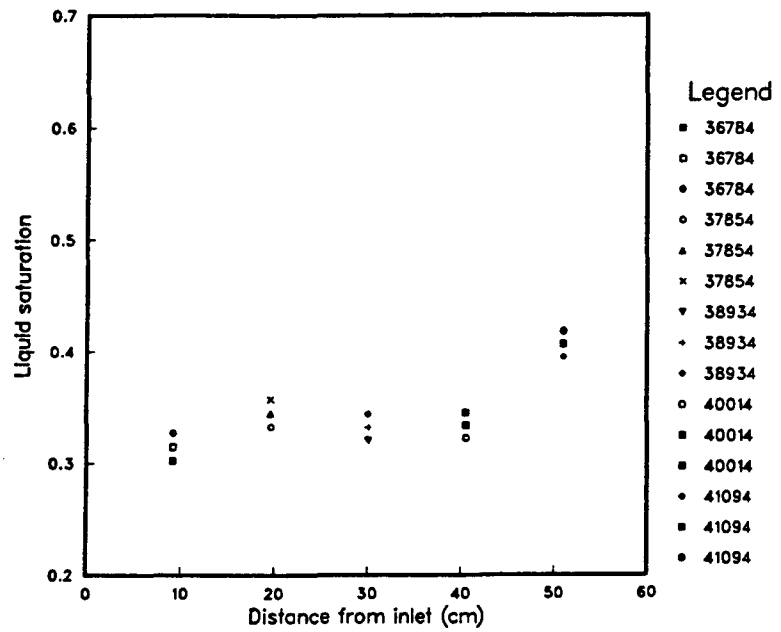

Figure B-4.6. Figure B-4-6. Liquid saturation profile during transient displacement of foam, experiment 4, 40000 sec. Three values at each station represent best value and one standard deviation based on counting error. Times under "Legend" are the mid-count times for each measurement.

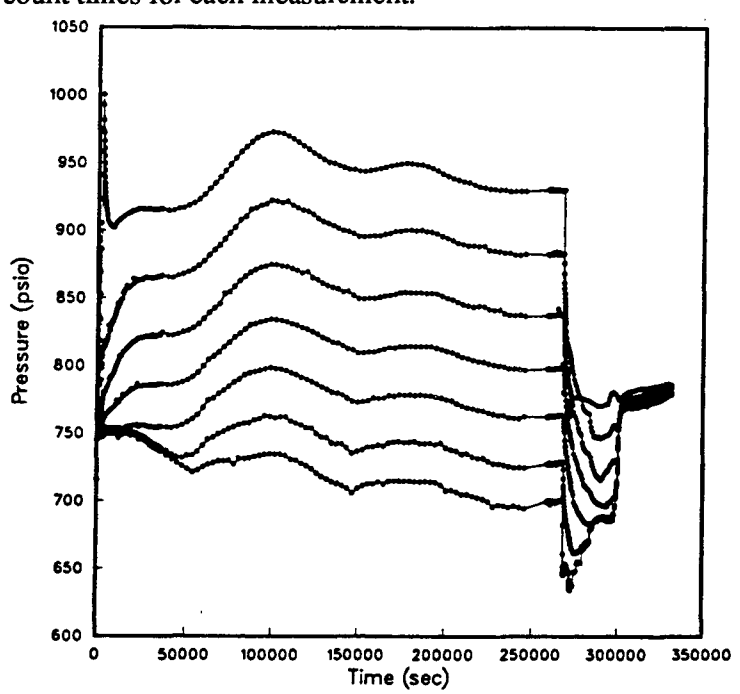

Figure B-4.7. Pressures recorded at taps 2 through 8 (60 cm = outlet to 0 cm = inlet) during initial foam propagation and steady state, experiment 4. The temporary pressure spike at tap 8 is real, but its cause is not known. Compare with Figure B-3.5.

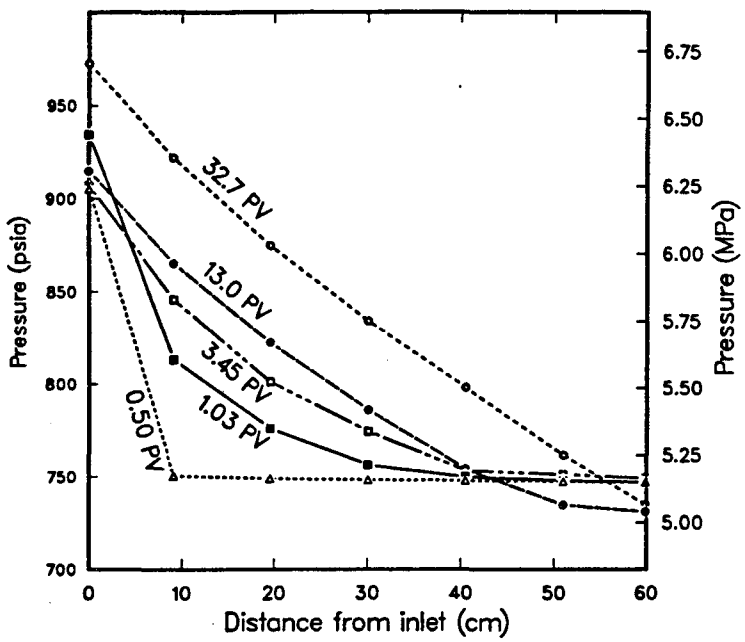

Figure B-4.8. Pressure profiles during transient displacement of foam, experiment 4. Times have been converted to pore volumes of fluid. Conversion to times for comparison with other plots: 0 pv = 510 sec; 1.03 pv = 3645 sec; 3.45 pv = 11056 sec; 32.7 pv = 100000 sec. Compare with Figure B-4.2 to see correspondence between pressure gradient and liquid saturation discussed in Appendix E.

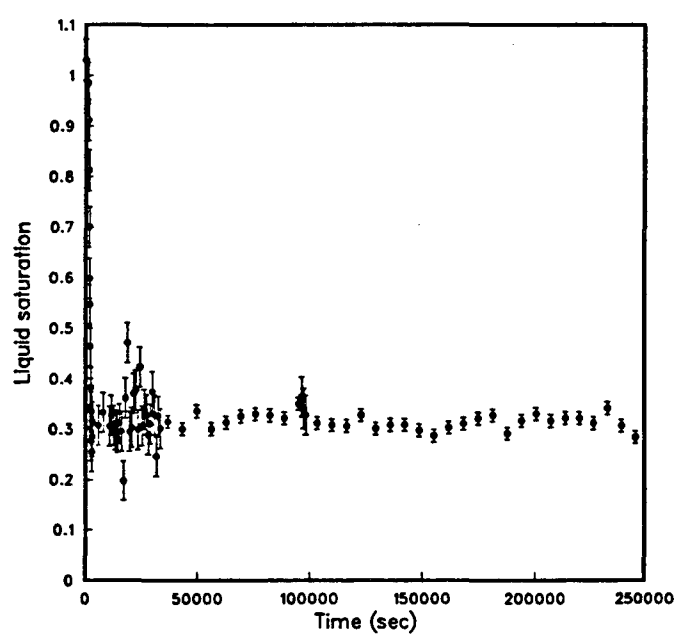

Figure B-4.9. Liquid saturation at 9.1 cm during experiment 4.

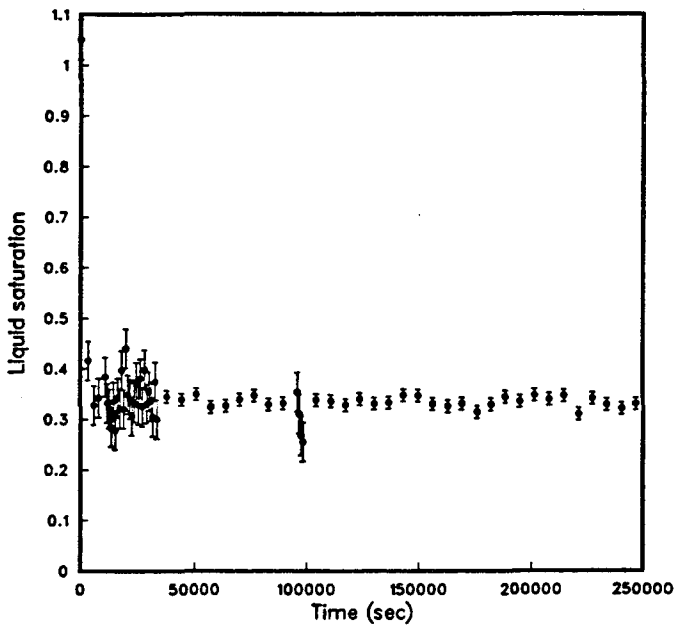

Figure B-4.10. Liquid saturation at 19.6 cm during experiment 4.

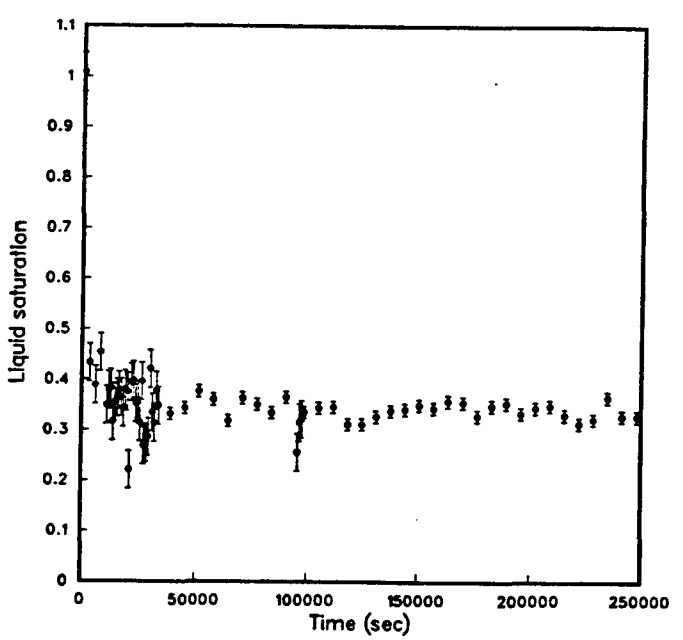

Figure B-4.11. Liquid saturation at 30.1 cm during experiment 4.

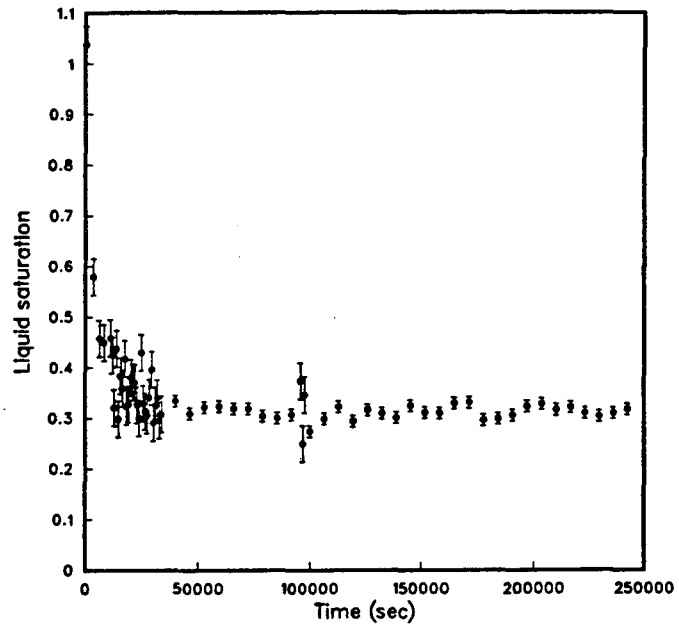

Figure B-4.12. Liquid saturation at 40.6 cm during experiment 4.

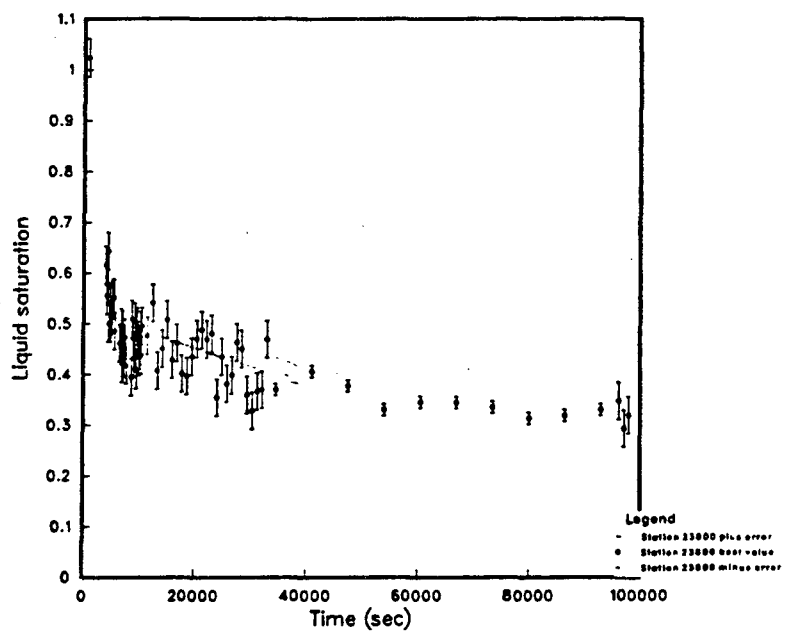

Figure B-4.13. Liquid saturation at 51.0 cm during experiment 4.

Experiment 5

After steady state was reached in Experiment 4, I attempted to produce a completely blocked state by stopping the liquid flow and reducing the gas injection pressure. This caused the gas flow rate to decrease but not to stop. Therefore I re-established the flow conditions of experiment 4 without resaturating. When the same steady state had been re-established, I reduced the gas injection pressure from 980 to 810 psi leaving a 60 psi differential pressure across the core. The pressure profile evolved as shown in Figure B-5.1, and the gas flow rate increased as shown in Figure B-5.2. Saturation profiles are shown in Figure B-5.3. Decreased saturation near the inlet is probably due to evaporation.

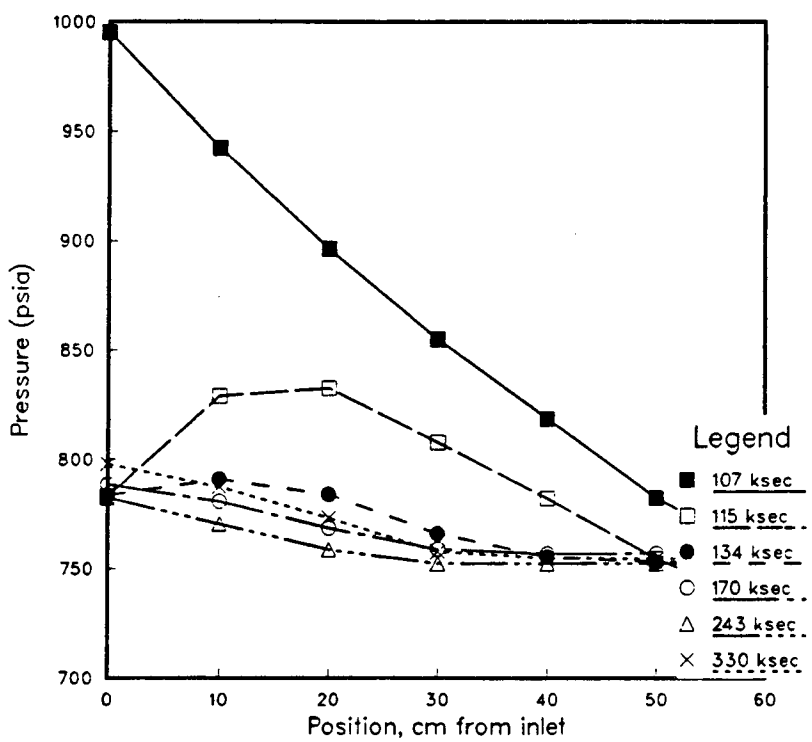

Figure B-5.1. Pressure profiles after reduction of gas injection pressure, experiment 5.

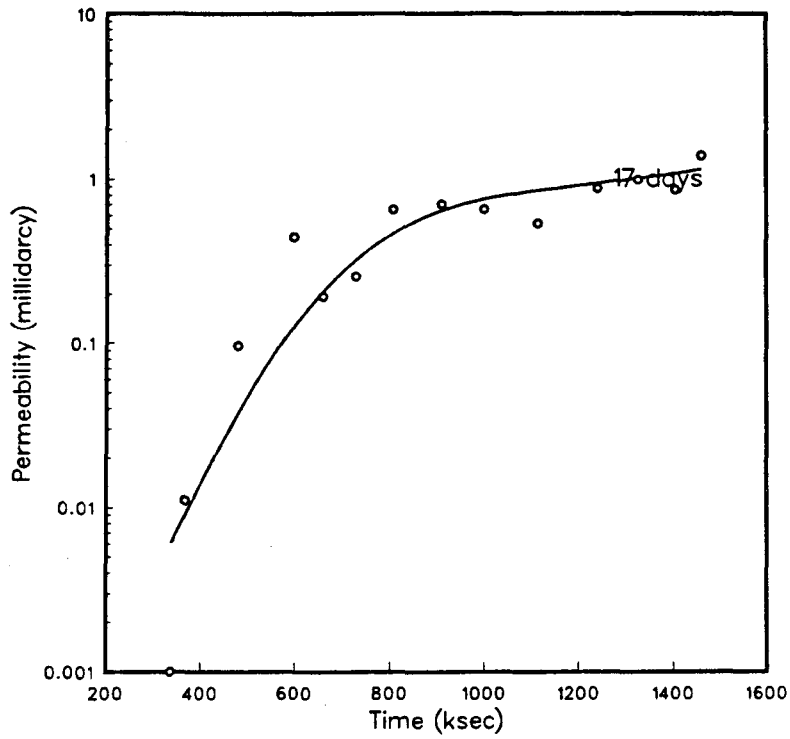

Figure B-5.2. Increase in gas permeability after reduction of gas injection pressure, experiment 5.

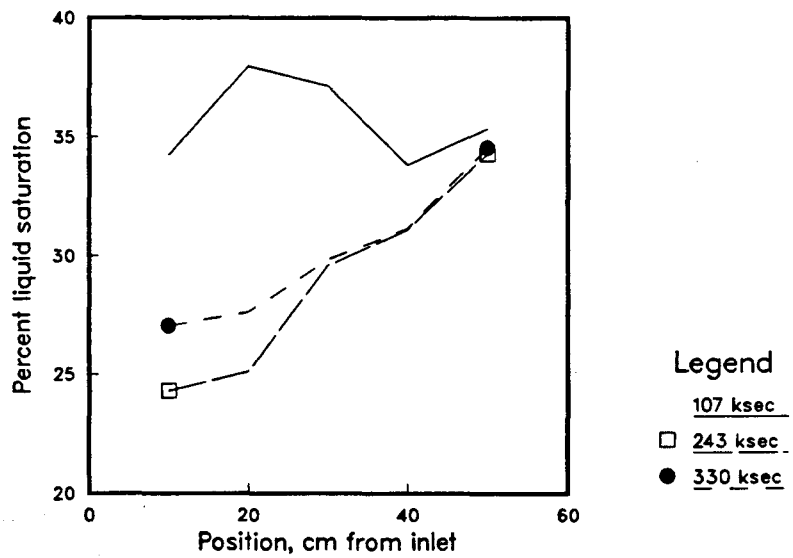

Figure B-5.3. Liquid saturation profiles before and after reduction of gas injection pressure, experiment 5.

Experiment 6.

This experiment was planned to complement experiment 3. In experiment 3 the liquid flow rate had been held constant and the gas flow rate varied; now the gas flow rate was held constant and the liquid flow rate varied. Then in the second part of the experiment the gas flow was shut off and the liquid flow was continued, to measure the permeability to liquid of the foam-filled core.

Because of experimental difficulties, the first part of the experiment was only qualitatively successful. Figure B-6.1 and B-6.2, respectively, show the gas and liquid flow rates during the experiment. Initially, liquid was injected at 0.25 mL/min, and gas at 320 sccm. Figure B-6.3 shows the pressures recorded at taps 2 through 8, respectively (60 cm to 0 cm). Figure B-6.4 shows the pressures measured during initial propagation of foam through the core. Figure B-6.3 shows that the pressure gradient did not reach a steady state. Because of this fluctuation, it was impossible to determine a quantitative relationship between liquid flow rate and pressure gradient as had been planned. However, it was possible to observe that the pressure gradient increased in response to the increase in the liquid flow rate. With the unexplained fluctuations, the inlet pressure sometimes became too great for gas to be injected at the set rate, so the gas rate also varied, as shown in Figure B-6.1.

A possible cause for the failure to reach steady state is separation of long chain alcohol from the foamer solution. In all experiments up to and including this one, gas and liquid were injected into an in-line foam generator. In this experiment very steep pressures gradients were observed across the foam generator. Inspection afterward showed that some of the long-chain alcohol had separated from the foam solution and formed a skin. In the future the foam generator was eliminated, and foamer solution was clarified by decanting before injection. The difficulty in achieving steady state, however, can not be entirely ascribed to this; because, as shown in Figure B-6.3, fluctuations in the pressure gradient occurred throughout the core, not only at the inlet.

The drift in pressure gradient also cannot be explained by changes in the liquid injection rate, as the liquid reservoir data show that the liquid flow rate the rate was relatively constant.

Several attempts were made to determine the increase in pressure gradient that would result from a step increase in the liquid flow rate. In most cases, when the liquid flow rate was increased, the pressure gradient became too steep for gas injection to continue at its set value. In these cases, the liquid flow rate was then decreased to its previous value to re-establish a quasi-steady state, and a smaller step increase in the liquid flow rate was made. Figure B-6-5 shows the transient pressure wave that followed a step increase in the liquid flow rate that was small enough that the pressure gradient did not become too steep to continue gas injection.

After 1.05 Msec, the gas flow was shut off, and the pressure gradient decreased. Liquid flow was continued, and pressure and liquid saturation measurements continued. Nine pore volumes (PV) of foamer solution were pumped through the the core; then the liquid was changed from foamer solution to surfactant-free brine. Data from this part of the experiment are presented in Appendix F.

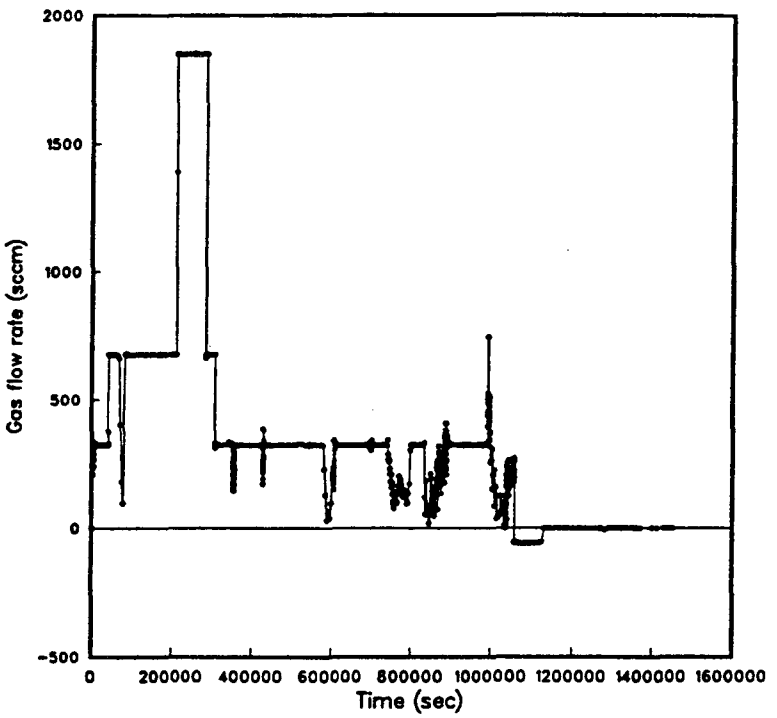

Figure B-6.1. Gas flow rate, experiment 6. Note times when gas delivery rate fell below set value, as described in caption for Figure B-6.3.

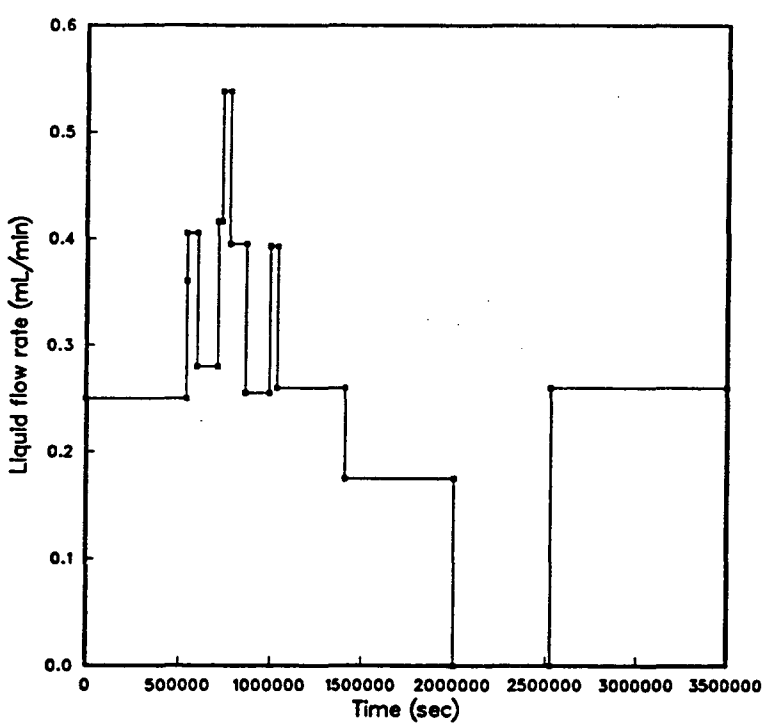

Figure B-6.2. Liquid flow rate, experiment 6. Step changes in liquid flow rate are reflected in changes in pressure gradient; see Figure B-6.1.

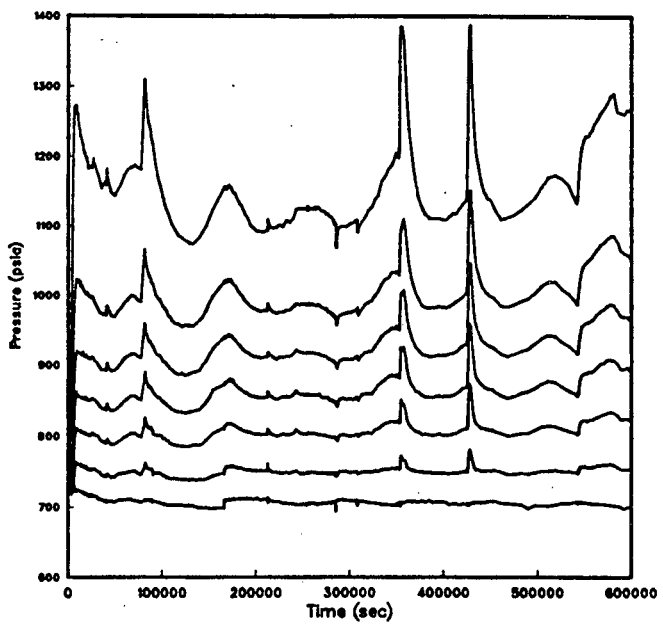

Figure B-6.3. Pressures recorded at taps 2 through 8, experiment 6. Variations over time in pressure gradient through core are unexplained. Pressure drop between taps 7 and 8 is approximately twice as steep as between other pairs of adjacent pressure taps; this appears to be a permanent damage to the core caused by filtration of long-chain alcohol from the foamer solution. Pressure ticks up at 40834 sec and at 212563 sec are due to step increases in the gas flow rate (see Figure B-6.1). Similar ticks down at 285439 sec and at 308124 sec are due to step decreases in the gas flow rate (see Figure B-6.1). With no change in either gas or liquid flow rate, pressure gradient through the core drifted. At 70490 it became so steep that the inlet pressure approached the gas delivery pressure, and the gas inflow rate decreased. At 81290 sec the gas delivery pressure was increased (spike) and the gas flow rate returned to its set value. The same thing happened between 353000 and 361000 sec. At 540000 sec the liquid flow rate was increased, causing an increase in the pressure gradient; but the presure gradient also continued to drift upward so that at 580000 the gas delivery rate again dropped below the set value.

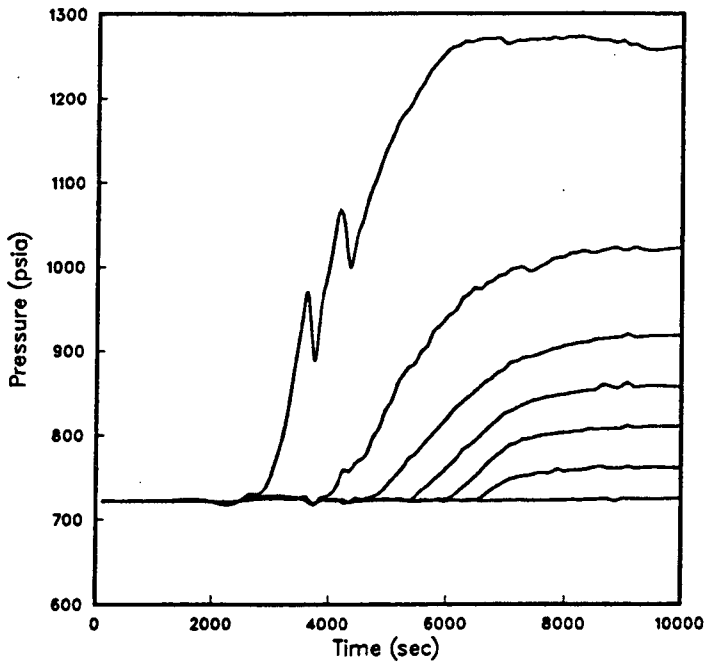

Figure B-6.4. Pressures recorded at taps 2 through 8 (60 cm = outlet to 0 cm = inlet) during initial foam propagation, experiment 6.

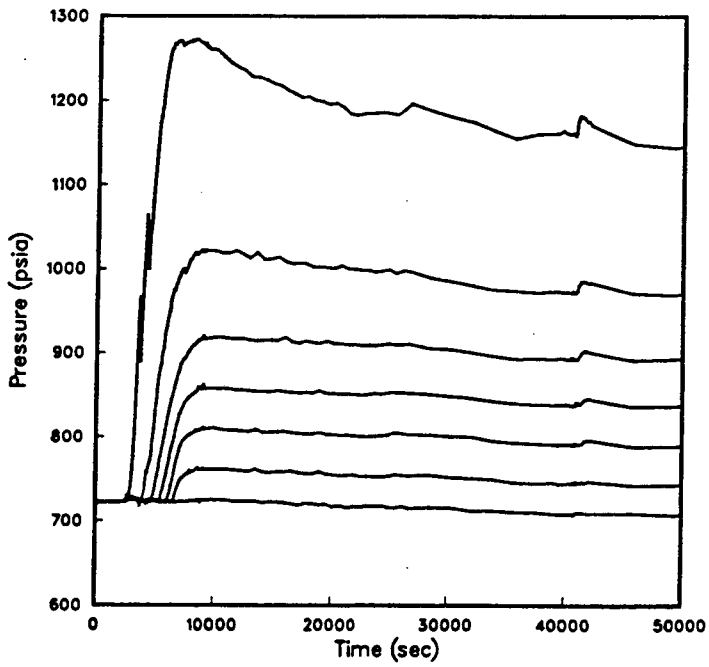

Figure B-6.5. Pressure wave following step increase in liquid flow rate; gas flow rate constant.

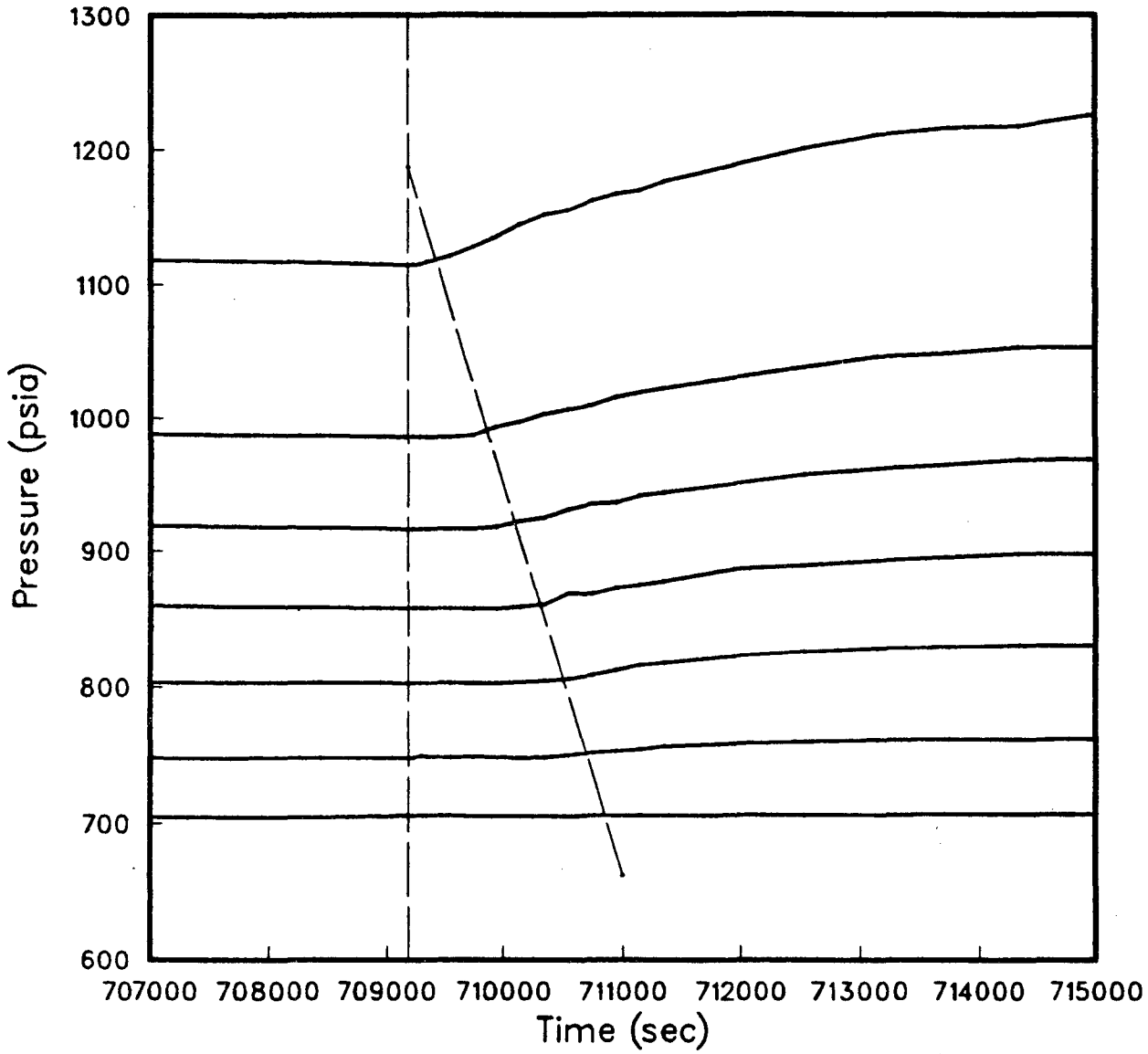

Figure-B.6. Transient response of pressure gradient to a step increase in the liquid flow rate. Pressure traces are shown for the seven taps located at the core inlet (top trace) and at 10 cm intervals to the outlet (bottom trace). The vertical dashed line indicates the time when the liquid flow rate was increased from 0.279 to 0.416 mL/min. The gas flow rate was maintained constant at 323 sec/min. The oblique dashed line indicates passage of the pressure wave.

Experiment 7

Experiment 6 showed that the pressure gradient was strongly influenced by the liquid flow rate, and it appeared that such steep pressure gradients might not be practical for field operations. Therefore, in experiment 7 foam was formed by pre-saturating the core with foamer solution and injecting only gas. Gas was injected at constant pressure, and the gas flow rate was observed but not controlled. In this experiment we also examined the effect of injecting additional slugs of foamer solution after foam had been formed. After three additional slugs had been injected, we observed the flow rate through the core at constant pressure for eight days, and then broke the foam by injecting a 50 % isopropanol solution.

As foam was formed in the core, the gas flow rate decreased. This caused a reduction in the pressure drop through the mass flow controller; consequently the pressure measured at tap 8 (the core inlet) increased. Figure B-7.1 shows the pressure profiles through the core during initial foam propagation. Figure B-7.2 shows the gas flow rate measured at during this time. Comparison of the two figures shows that the pressure at the inlet increased as the gas flow rate decreased. Figure B-7.3 shows the pressures after injection of the first additional slug of foamer solution; as the gas flow rate decreased sharply, the pressure at the inlet increased. There was also some loss of back-pressure control resulting from insufficient flow through the back-pressure regulator. Other figures, presented in Appendix E, show the results of injection of two additional slugs of foamer solution and a slug of foam breaker. Figure B-7.4 shows the gas permeability calculated from the observed pressures and gas flow rates. Figure B-7.5 through B-7.9 show the liquid saturation measured at five location in the core. Figures B-7.10 through B-7.13 show four transient liquid saturation profiles measured during initial foam displacement.

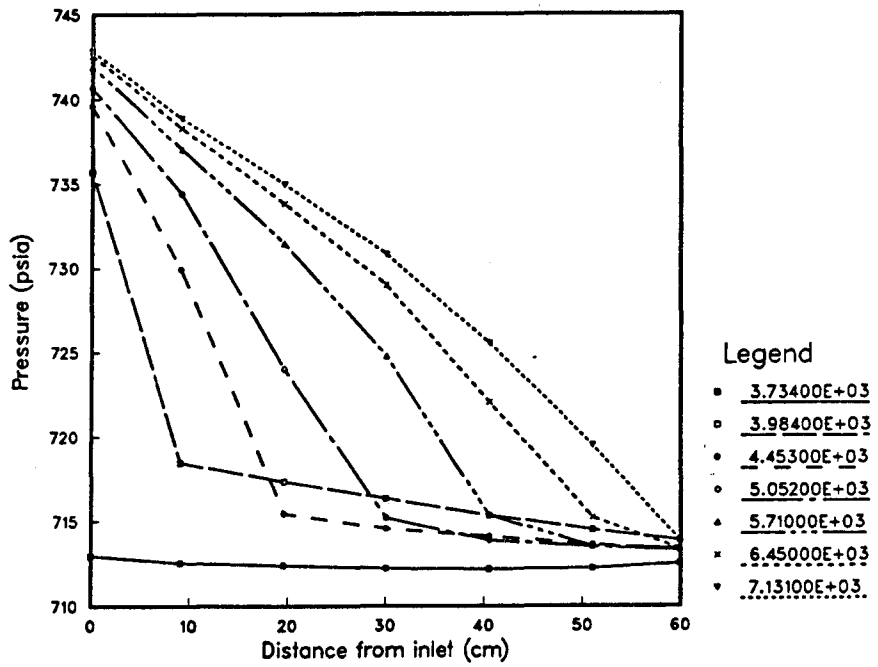

Figure B-7.1. Pressure profiles during initial propagation of foam, Experiment 7. Injection pressure is not actually constant because as the gas flow rate decreased due to the flattening of the pressure gradient, the pressure drop through the mass flow controller decreased.

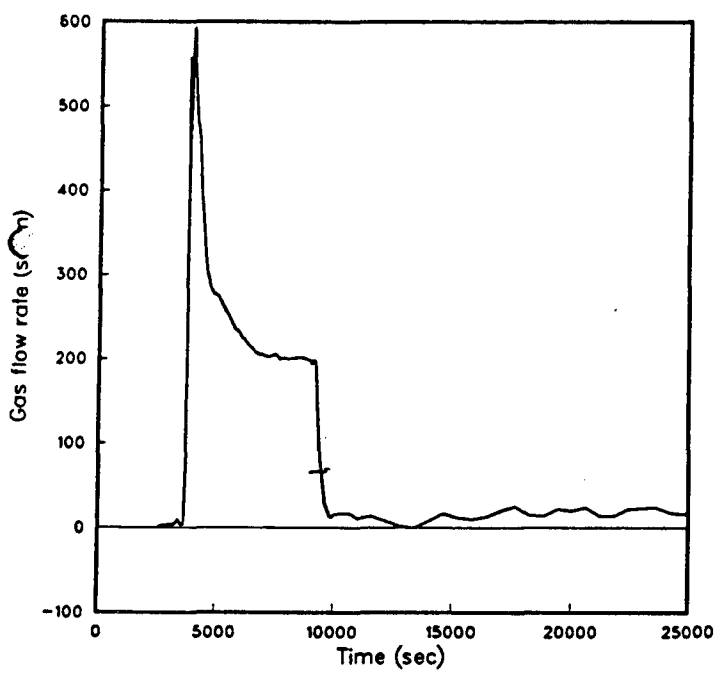

Figure B-7.2. Gas flow rate during initial propagation of foam, Experiment 7.

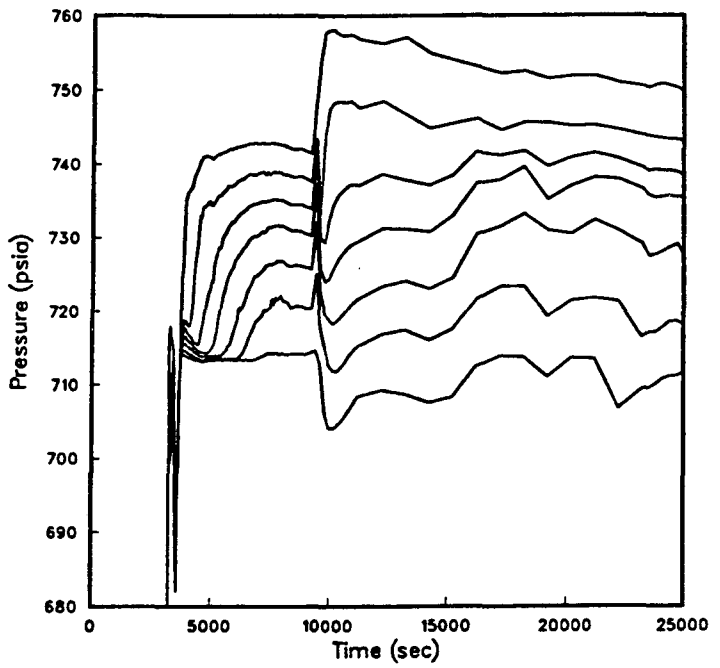

Figure B-7.3. Pressures measured during initial propagation of foam and after injection of an additional 0.03 PV slug of foamer solution, Experiment 7.

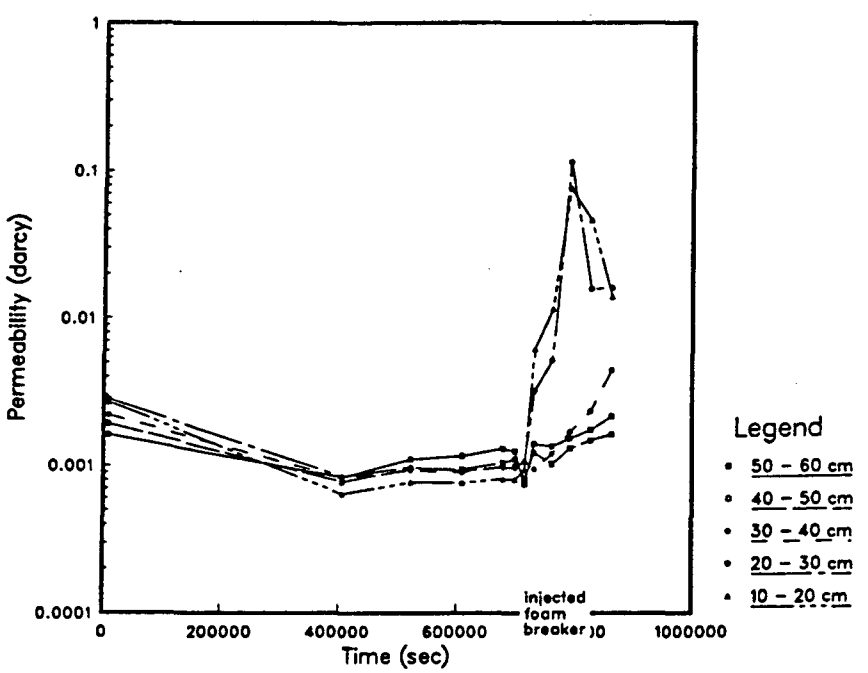

Figure B-7.4. Gas permeability calculated from pressure and gas flow rate measurements. After injection of foam breaker, the gas permeability between 0 and 30 cm increased as shown.

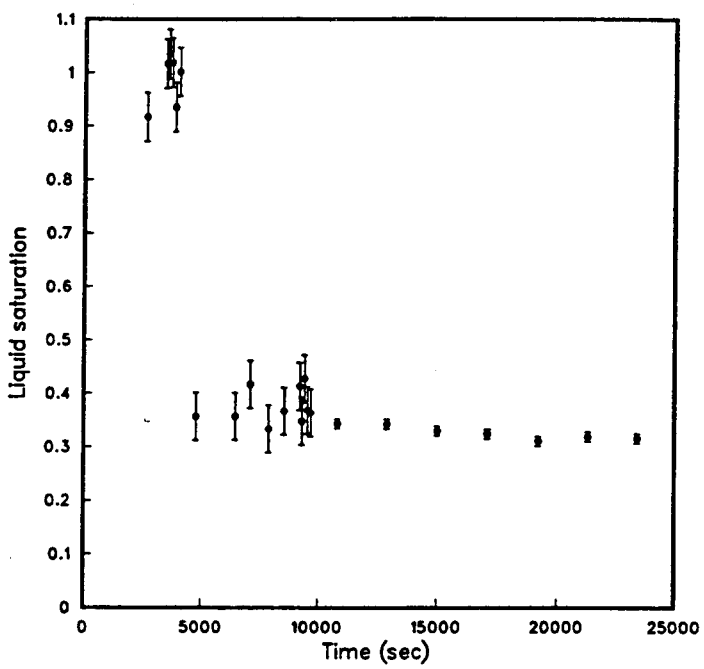

Figure B-7.5. Liquid saturation at 9.1 cm, showing passage of foam front, experiment 7.

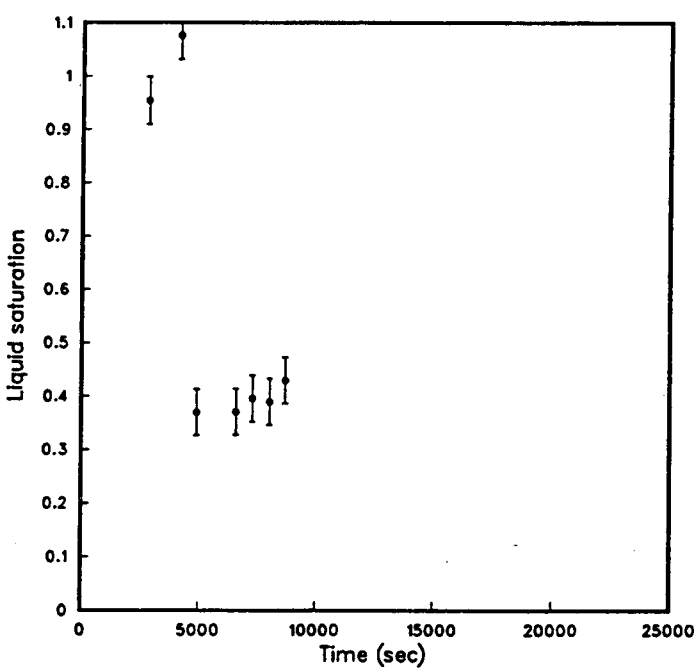

Figure B-7.6. Liquid saturation at 19.6 cm, showing passage of foam front, experiment 7.

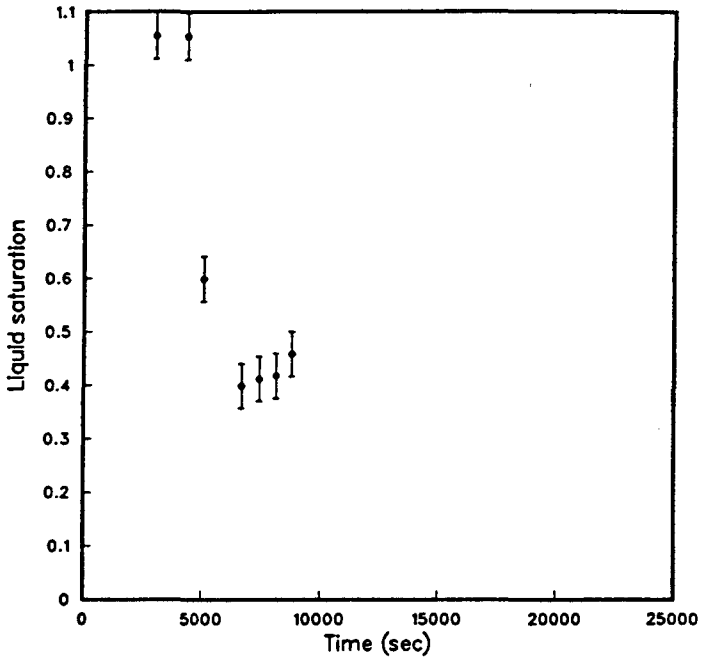

Figure B-7.7. Liquid saturation at 30.1 cm, showing passage of foam front, experiment 7.

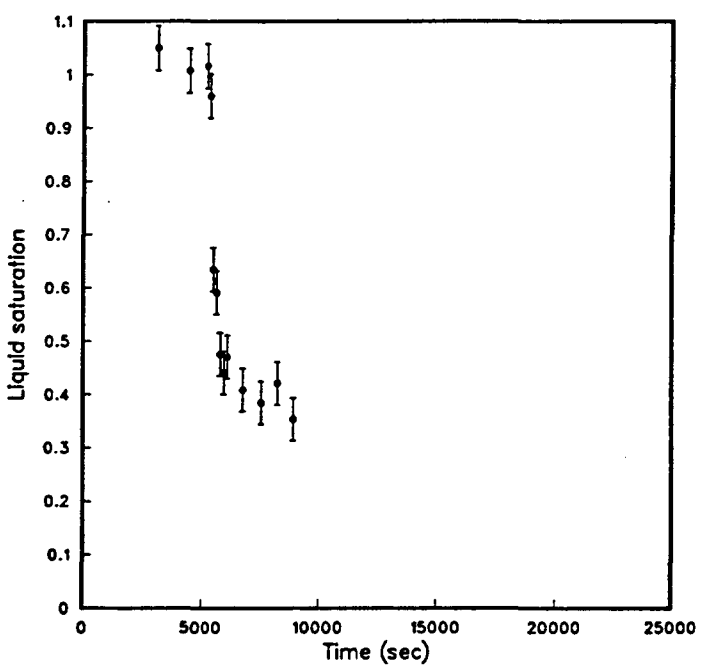

Figure B-7.8. Liquid saturation at 40.6 cm, showing passage of foam front, experiment 7.

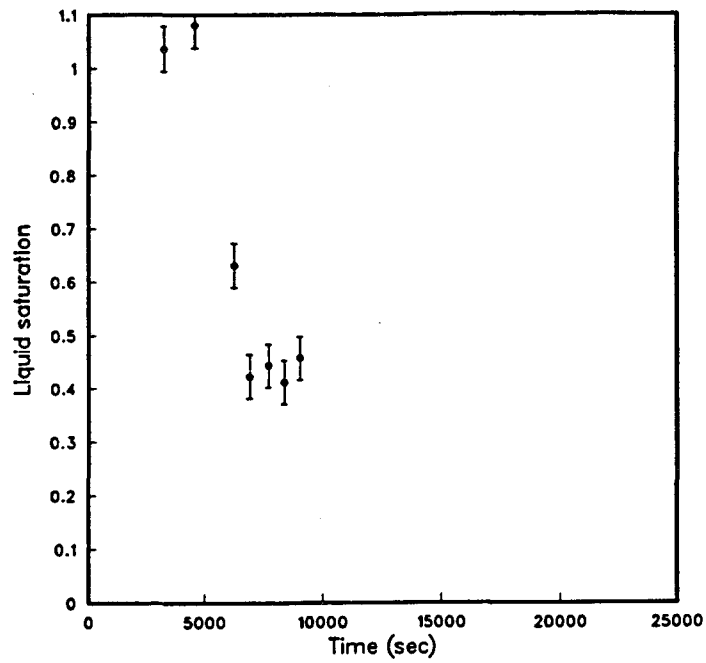

Figure B-7.9. Liquid saturation at 51.0 cm, showing passage of foam front, experiment 7.

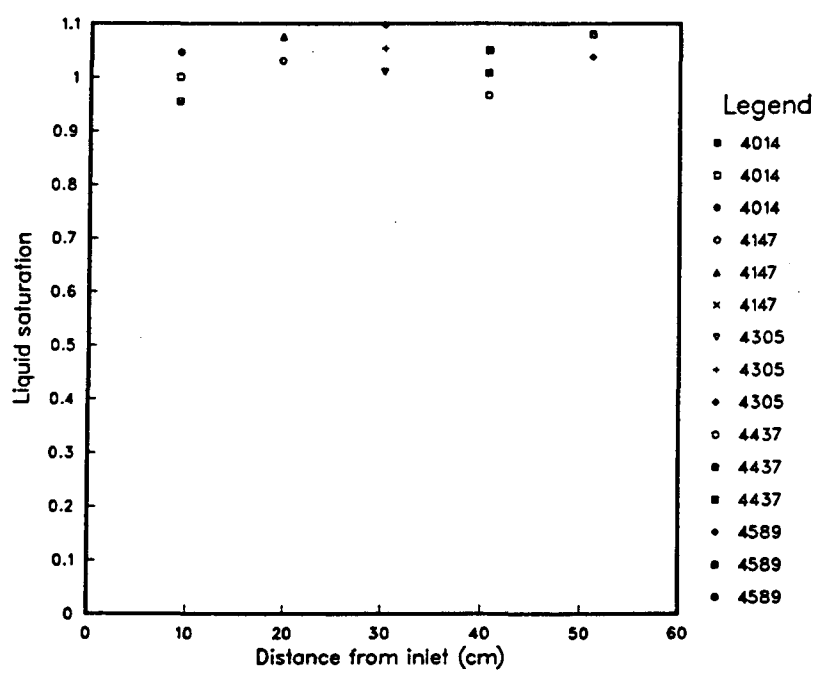

Figure B-7.10. Liquid saturation profile during transient displacement of foam, experiment 7, 4300 sec. Three values at each station represent best value and one standard deviation based on counting error. Times under "Legend" are the mid-count times for each measurement. Compare with Figure B-7.1.

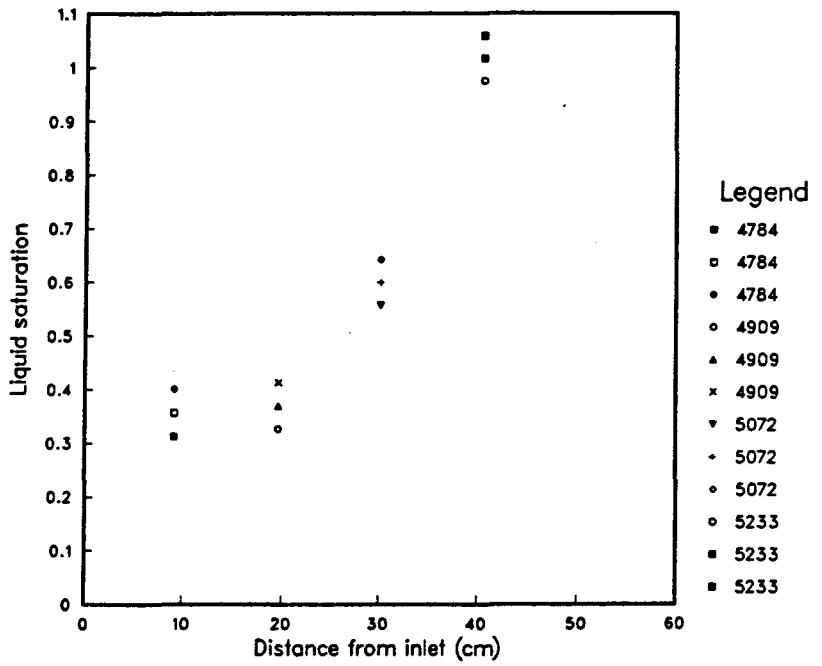

Figure B-7.11. Liquid saturation profile during transient displacement of foam, experiment 7, 5000 sec. Three values at each station represent best value and one standard deviation based on counting error. Times under "Legend" are the mid-count times for each measurement. Compare with Figure B-7.1.

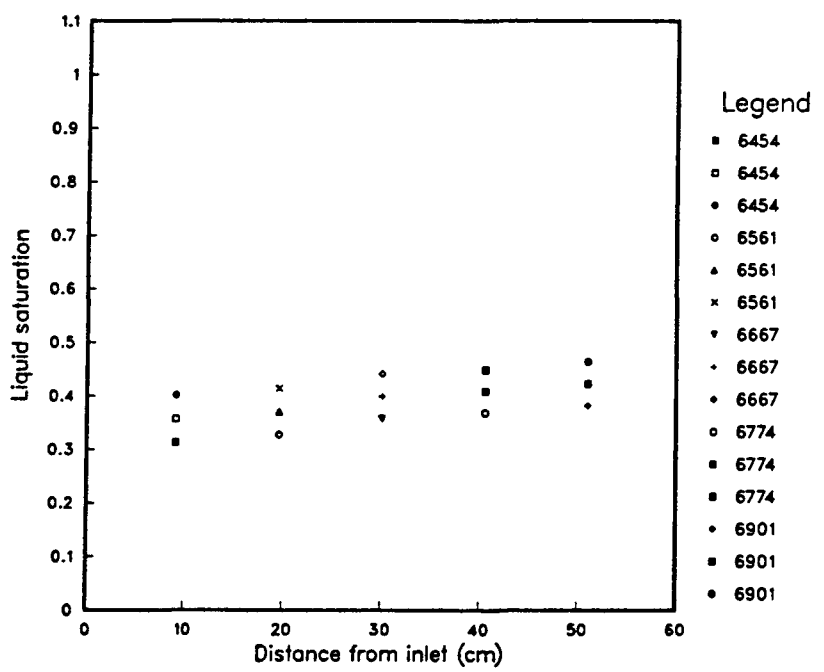

Figure B-7.12. Liquid saturation profile during transient displacement of foam, experiment 7, 6700 sec. Three values at each station represent best value and one standard deviation based on counting error. Times under "Legend" are the mid-count times for each measurement. Compare with Figure B-7.1.

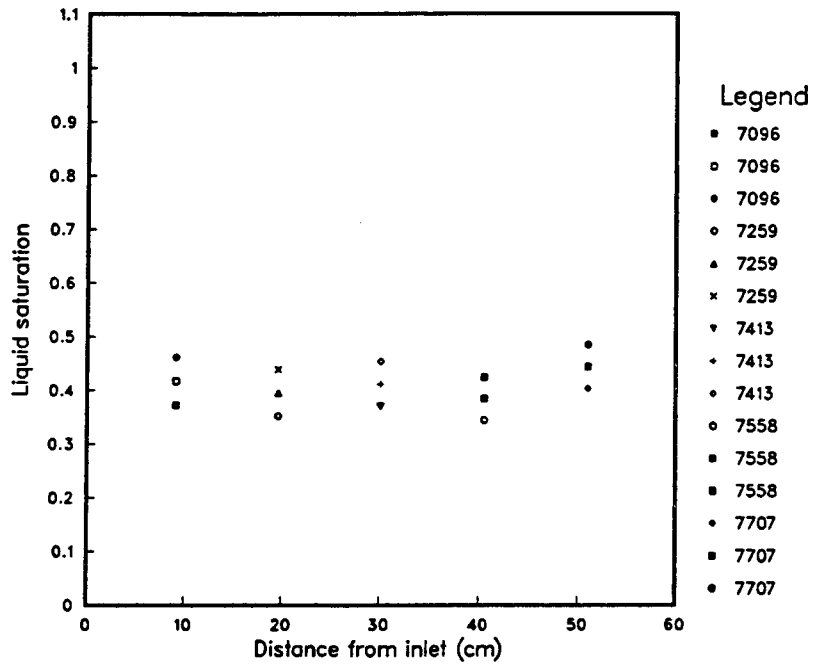

Figure B-7.13. Liquid saturation profile during transient displacement of foam, experiment 7, 7400 sec. Three values at each station represent best value and one standard deviation based on counting error. Times under "Legend" are the mid-count times for each measurement. Compare with Figure B-7.1.

Experiment 8

Experiment 8 was conducted to demonstrate formation of a spaced foam block. Initially the core was saturated with foamer solution. Brine was injected to displace the foamer solution from the first 25 cm of the core. Figure B-8.1 shows the core at the start of the experiment. Then gas was injected at 500 sccm. Pressure profiles measured during the experiment are shown in Figure B-8.2. Figure B-8.3 shows the gas permeability between each pair of adjacent pressure taps, calculated from the measured pressures. Figures B-8.4 through B-8.8 show liquid saturation profiles measured during transient displacement of liquid. Figure B-8.9 through B-8.18 show the liquid saturation measured at 10 through 55 cm, respectively.

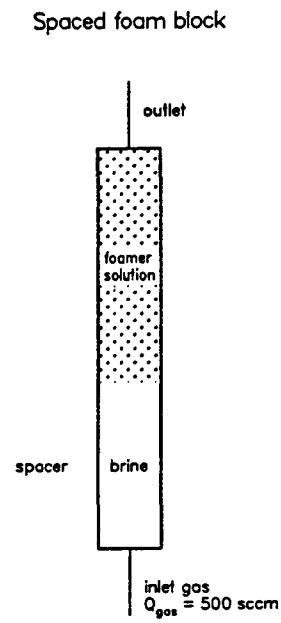

Figure B-8.1. Core at start of experiment 8, with foamer solution displaced by brine in the first 25 cm of the core.

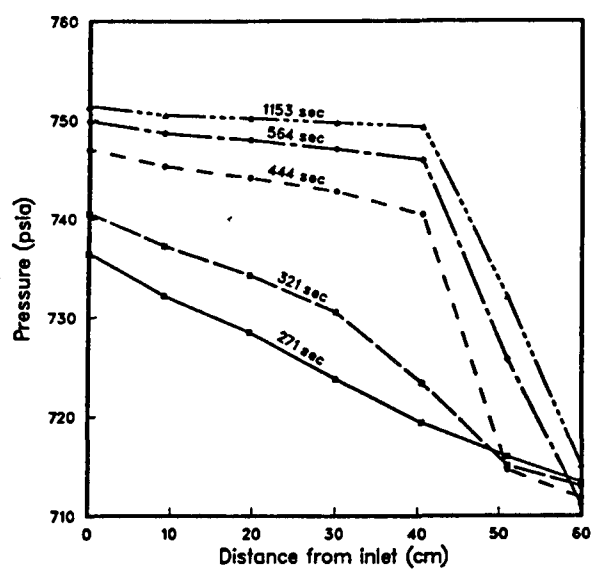

Figure B-8.2. Pressure profiles measured during injection of gas, Experiment 8.

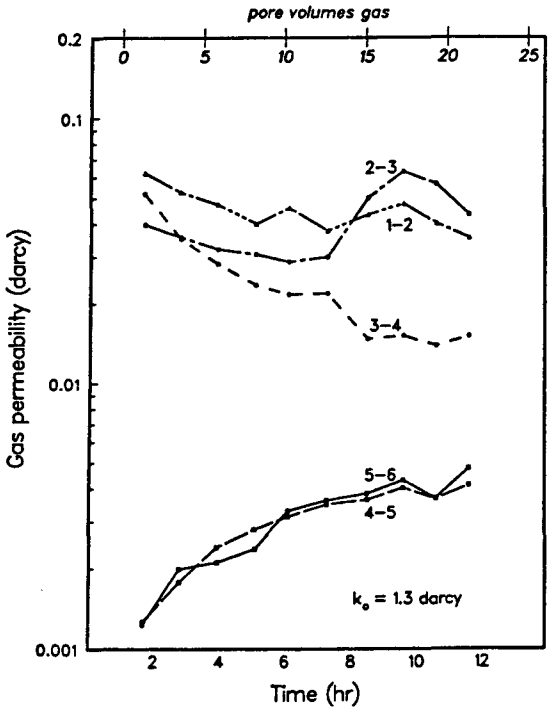

Figure B-8.3. Gas permeability between pairs of adjacent pressure taps. Key: 1-2 = gas permeability between taps at 10 and 20 cm, 3-4 = gas permeability between taps at 30 and 40 cm, etc. Permeability is lower between 40 and 60 cm where foam was formed.

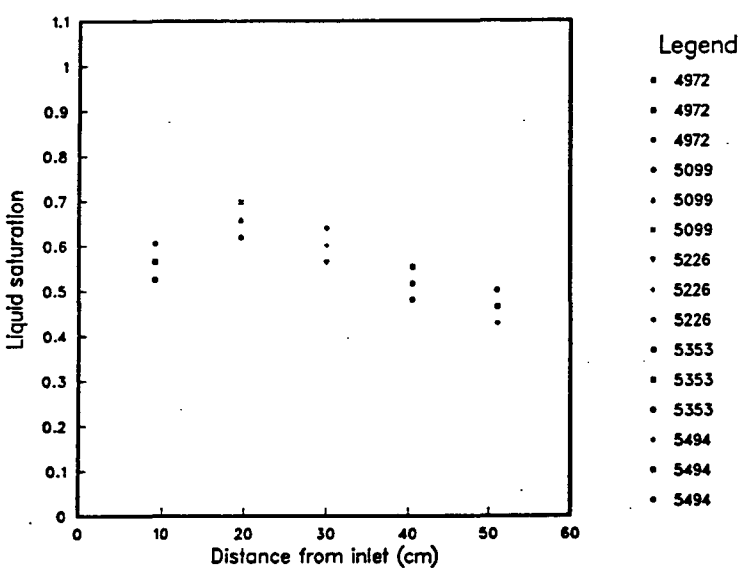

Figure B-8.4. Liquid saturation profile at 5000 sec, Experiment 8. Liquid saturation is lower where foam was formed. Three values at each station represent best value and one standard deviation based on counting error. Times under "Legend" are the mid-count times for each measurement.

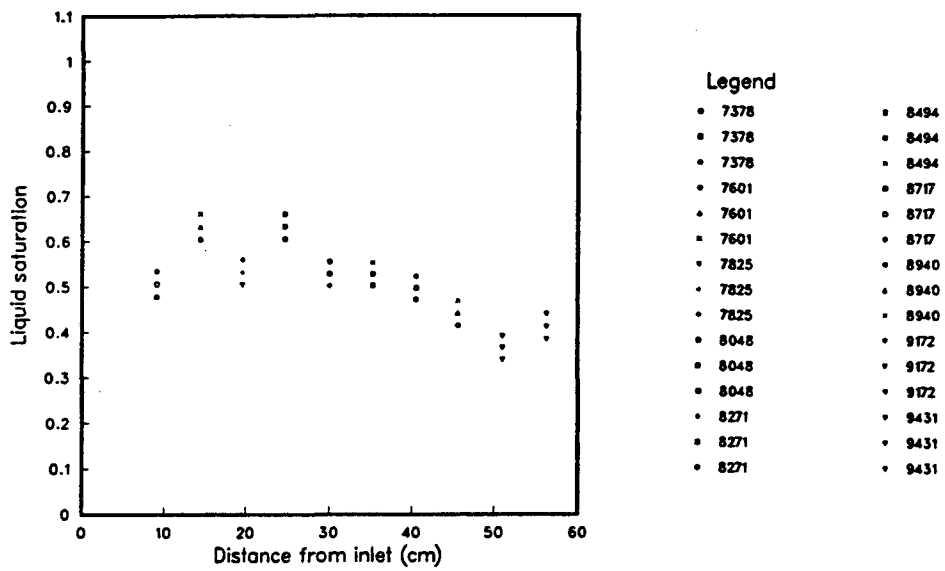

Figure B-8.5. Liquid saturation profile at 8400 sec, Experiment 8. Liquid saturation is lower where foam was formed. Three values at each station represent best value and one standard deviation based on counting error. Times under "Legend" are the mid-count times for each measurement.

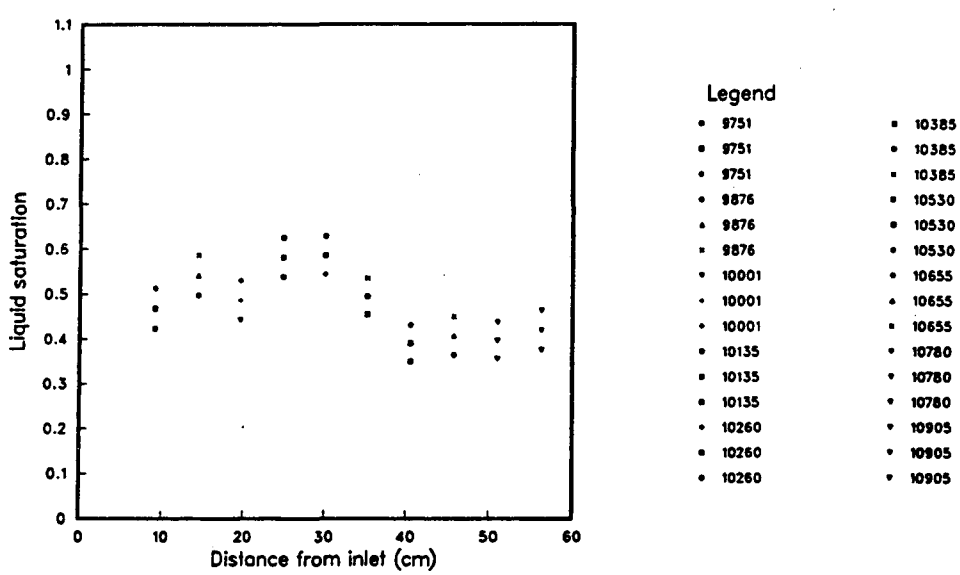

Figure B-8.6. Liquid saturation profile at 10400 sec, Experiment 8. Liquid saturation is lower where foam was formed. Three values at each station represent best value and one standard deviation based on counting error. Times under "Legend" are the mid-count times for each measurement.

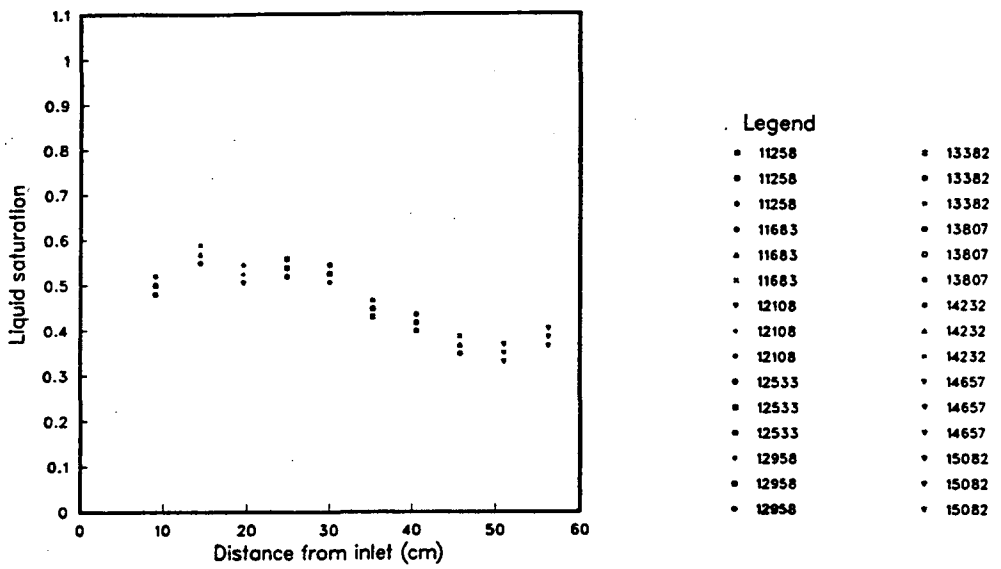

Figure B-8.7. Liquid saturation profile at 13000 sec, Experiment 8. Liquid saturation is lower where foam was formed. Three values at each station represent best value and one standard deviation based on counting error. Times under "Legend" are the mid-count times for each measurement.

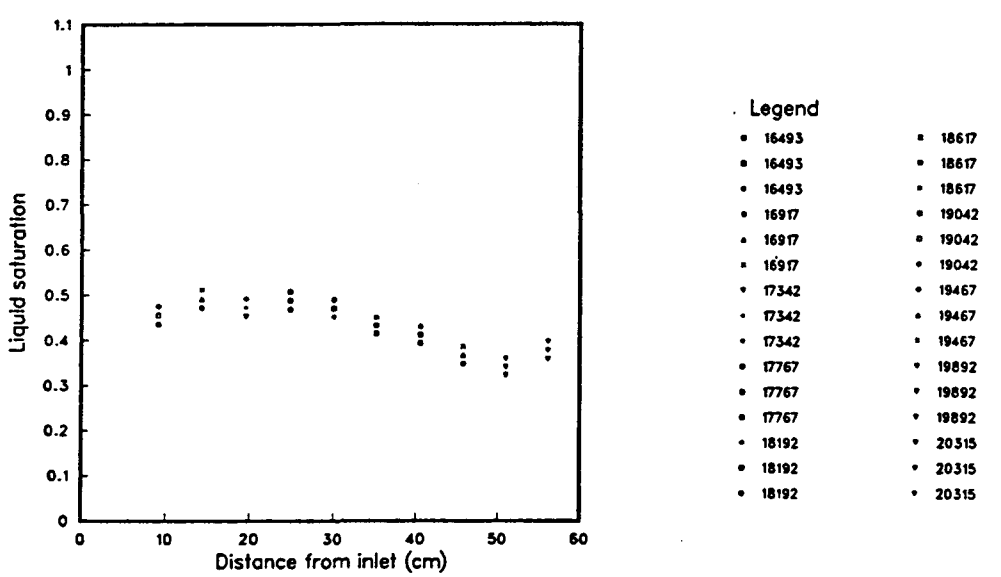

Figure B-8.8. Liquid saturation profile at 18000 sec, Experiment 8. Liquid saturation is lower where foam was formed. Three values at each station represent best value and one standard deviation based on counting error. Times under "Legend" are the mid-count times for each measurement.

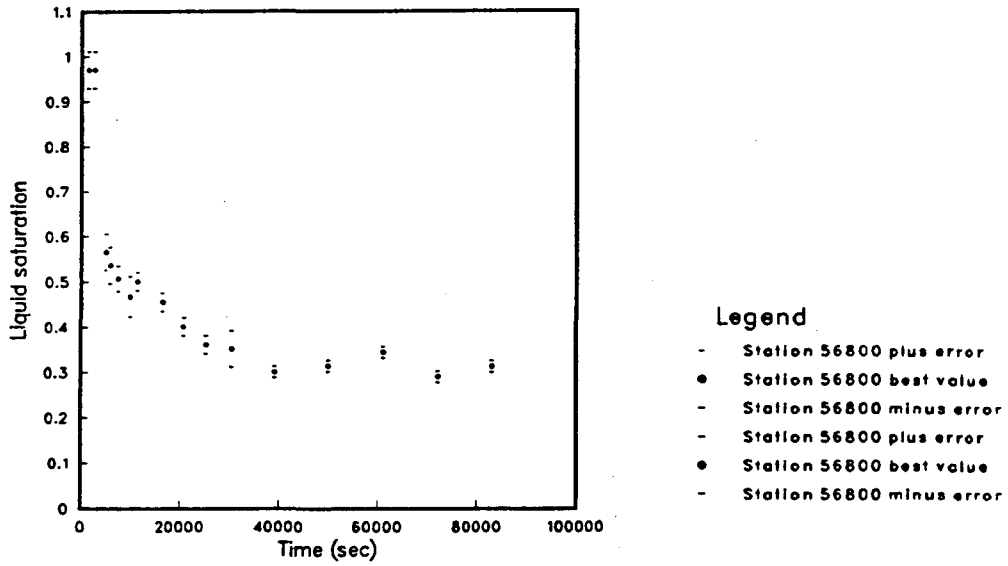

Figure B-8.9. Liquid saturation at 10 cm, Experiment 8.

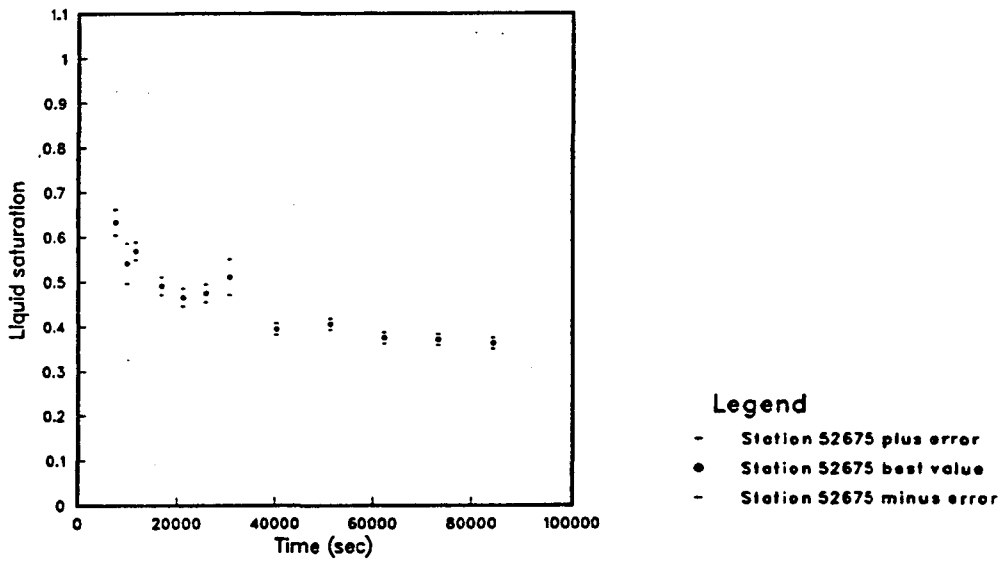

Figure B-8.10. Liquid saturation at 15 cm, Experiment 8.

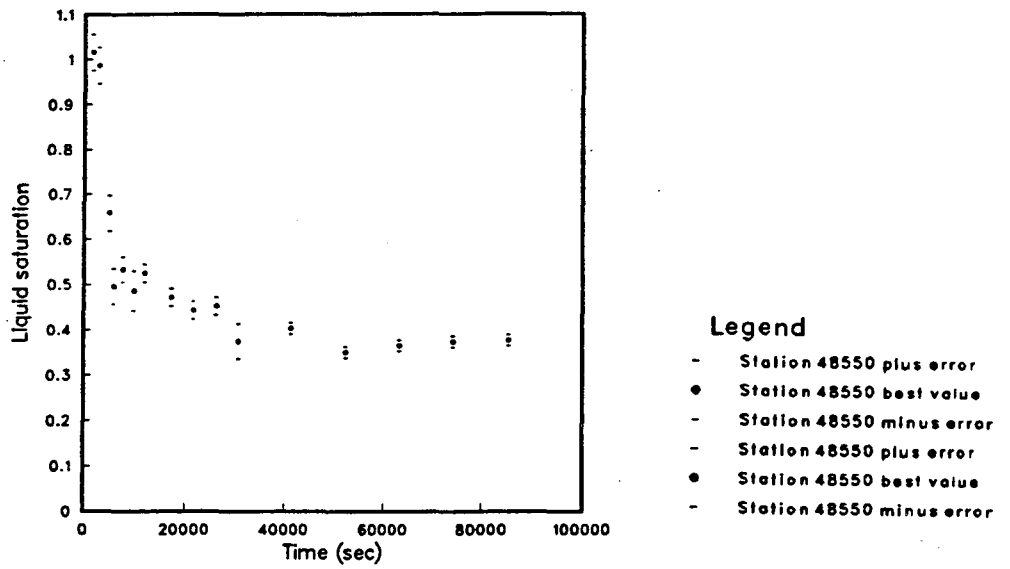

Figure B-8.11. Liquid saturation at 20 cm, Experiment 8.

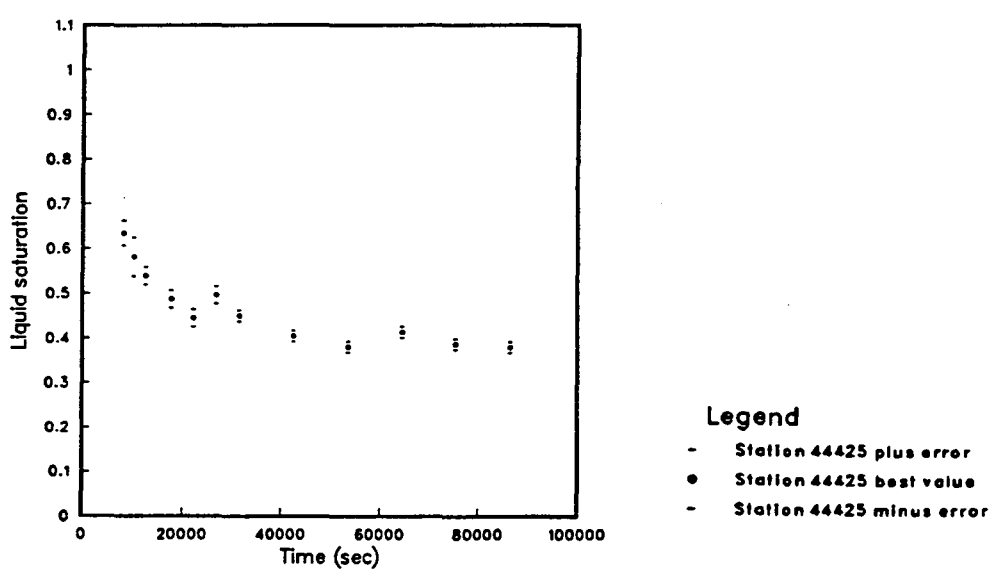

Figure B-8.12. Liquid saturation at 25 cm, Experiment 8.

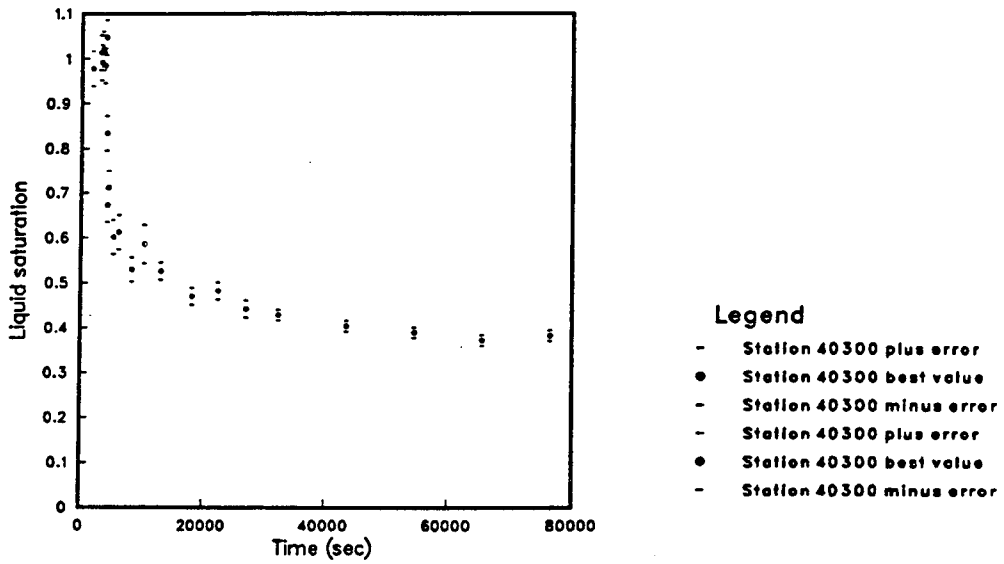

Figure B-8.13. Liquid saturation at 30 cm, Experiment 8.

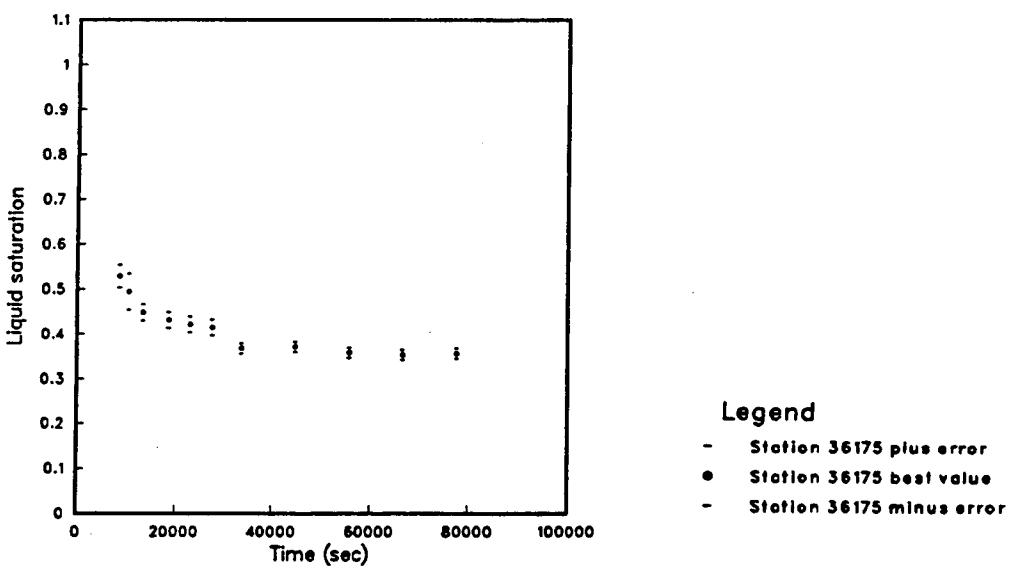

Figure B-8.14. Liquid saturation at 35 cm, Experiment 8.

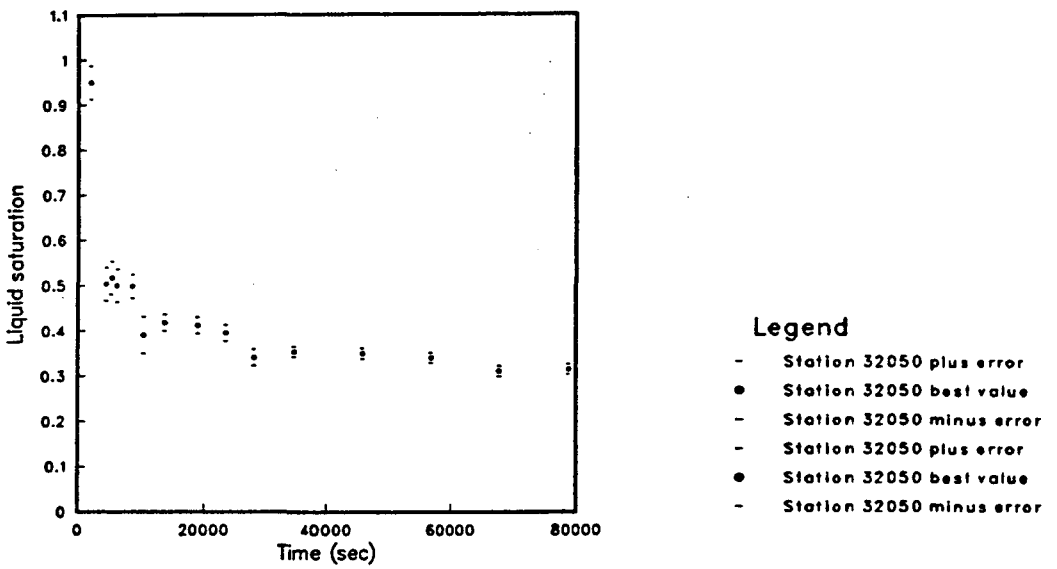

Figure B-8.15. Liquid saturation at 40 cm, Experiment 8.

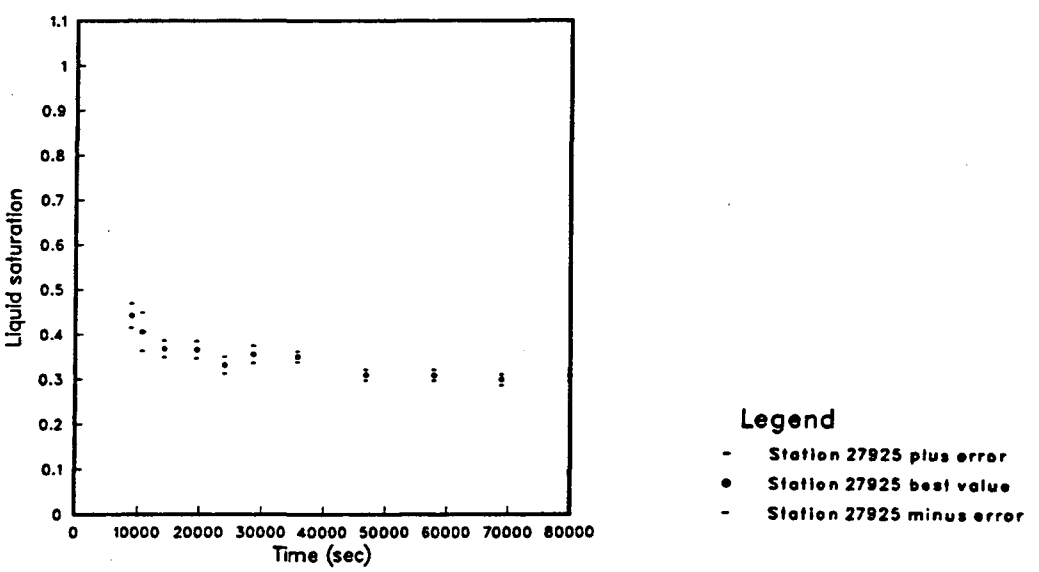

Figure B-8.16. Liquid saturation at 45 cm, Experiment 8.

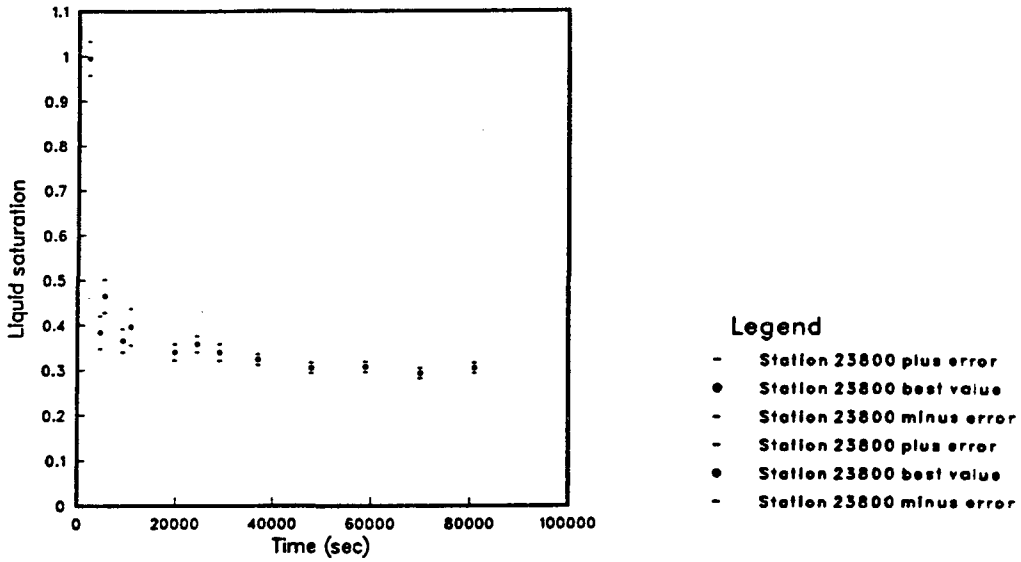

Figure B-8.17. Liquid saturation at 50 cm, Experiment 8.

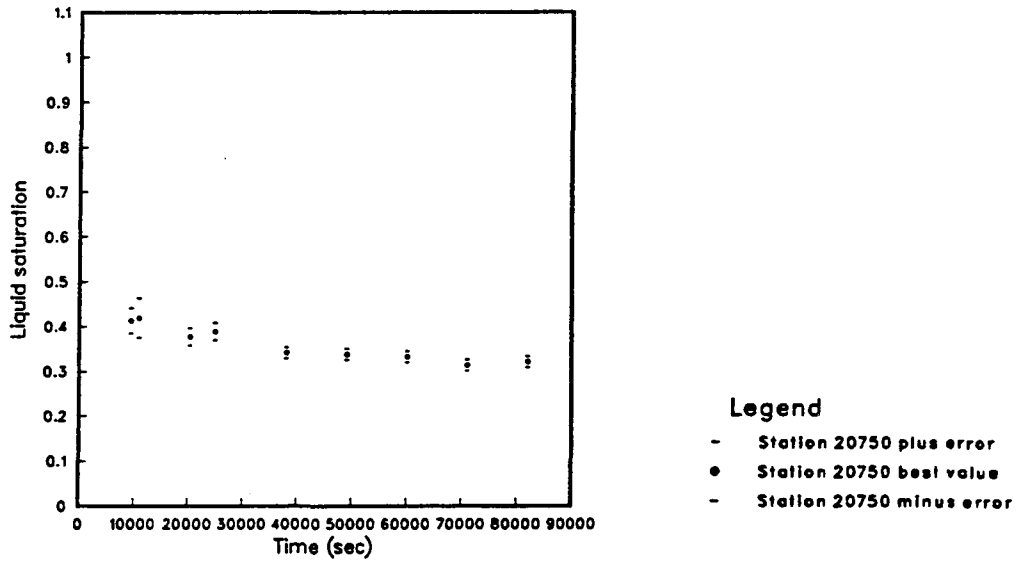

Figure B-8.18. Liquid saturation at 55 cm, Experiment 8.

Experiment 9

Experiment 9 was similar to experiment 7, except that where in experiment 7 gas was injected at constant pressure, in experiment 9 gas was injected at a constant flow rate of 500 sccm. Figure B-9.1 and B-9.2 show pressures and pressure profiles measured during transient displacement of liquid. Figure B-9.3 through B-9.7 show liquid saturations measured at 10 through 50 cm respectively. Figure B-9.8 shows the pressure recorded at pressure taps 2 through 8 (outlet = 60 cm to inlet= 0 cm), and Figure B-9.9 shows the pressures relative to the outlet pressure. Figure B-9.10 shows pressure profiles measured during the experiment.

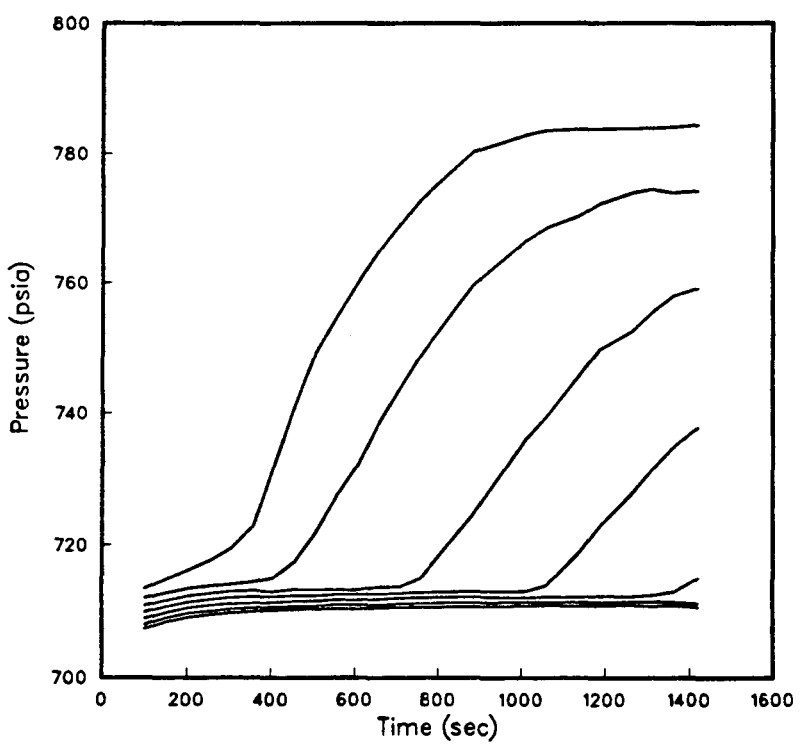

Figure B-9.1. Pressures measured at taps 8 through 2 (inlet to outlet) during initial penetration of foam, Experiment 9.

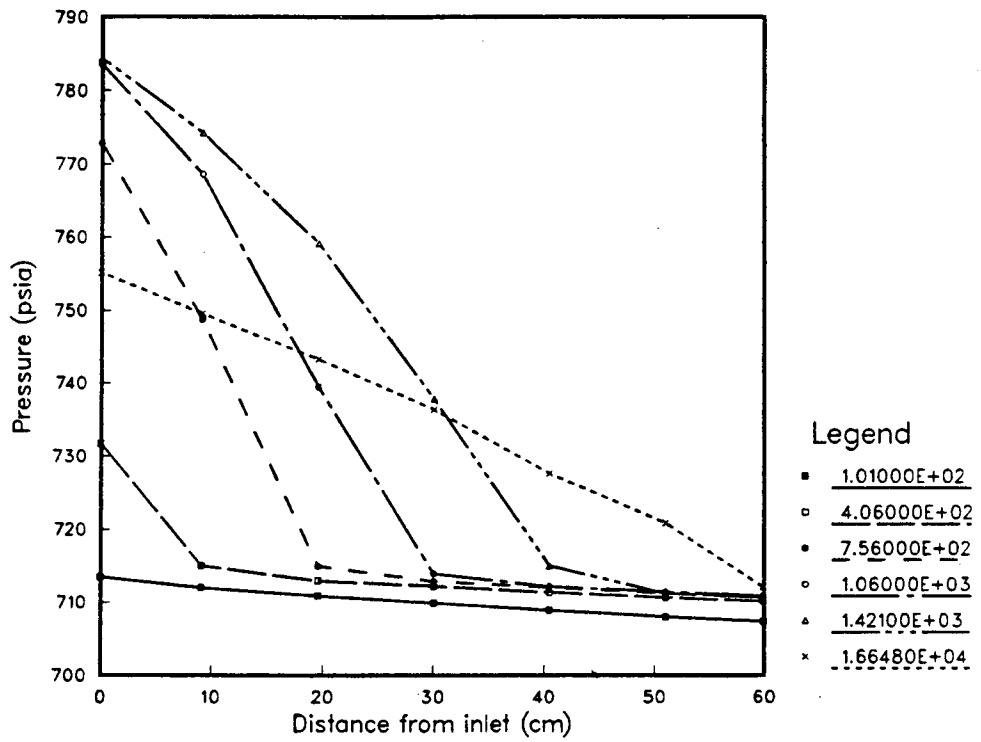

Figure B-9.2. Pressure profiles measured during foam propagation and at quasi-steady state.

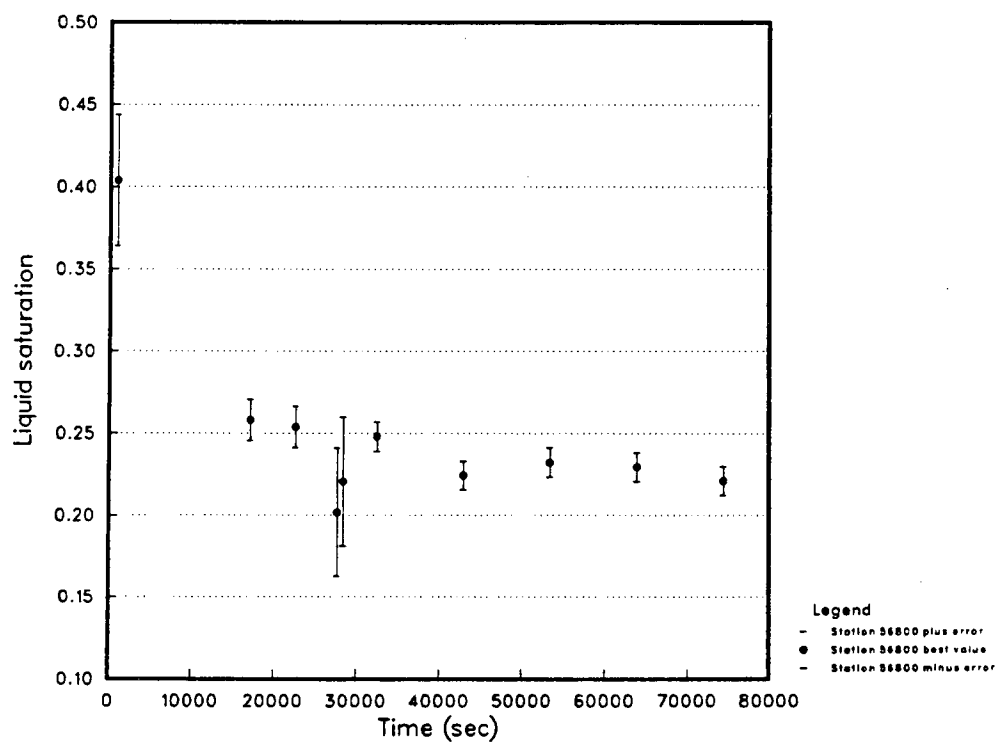

Figure B-9.3. Liquid saturation at 10 cm, experiment 9.

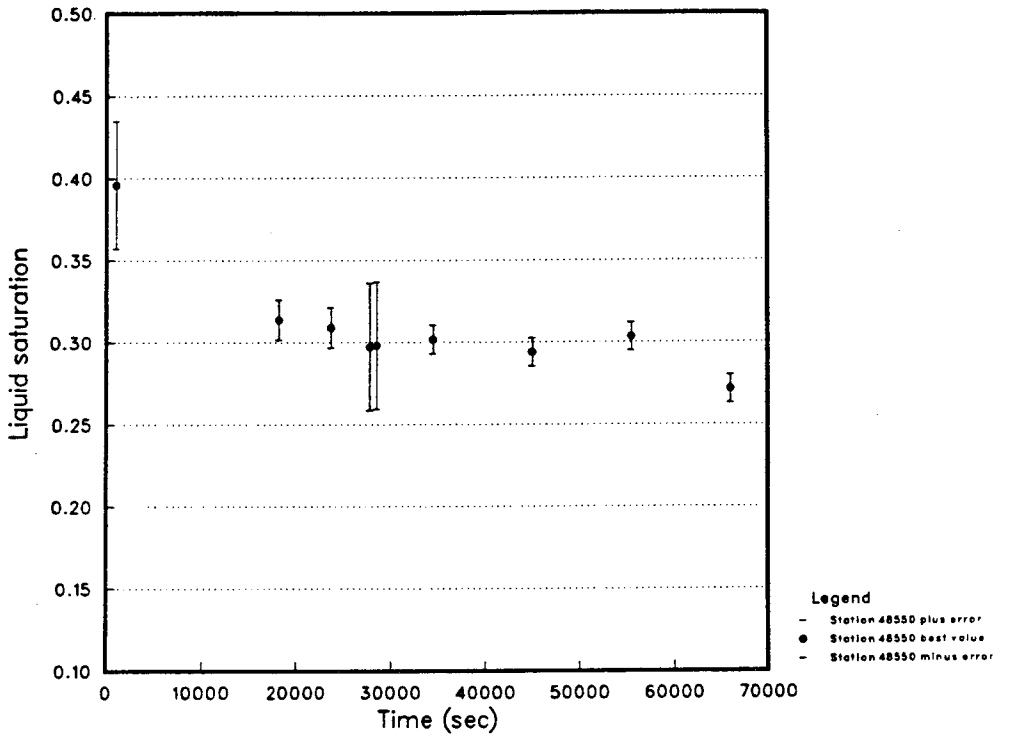

Figure B-9.4. Liquid saturation at 20 cm, experiment 9.

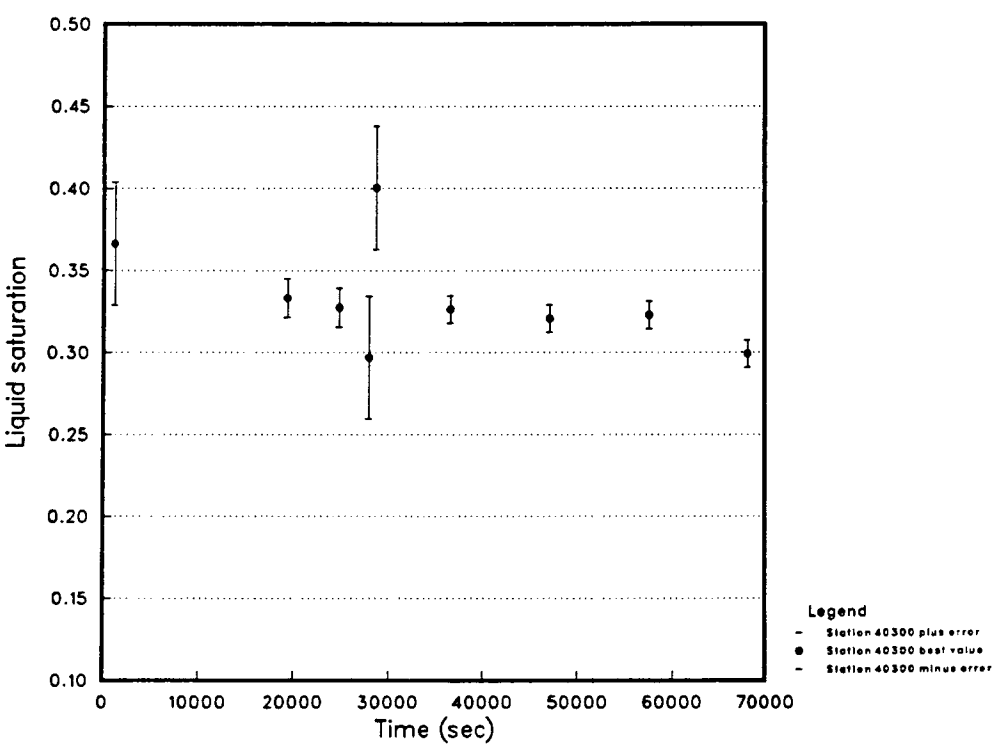

Figure B-9.5. Liquid saturation at 30 cm, experiment 9.

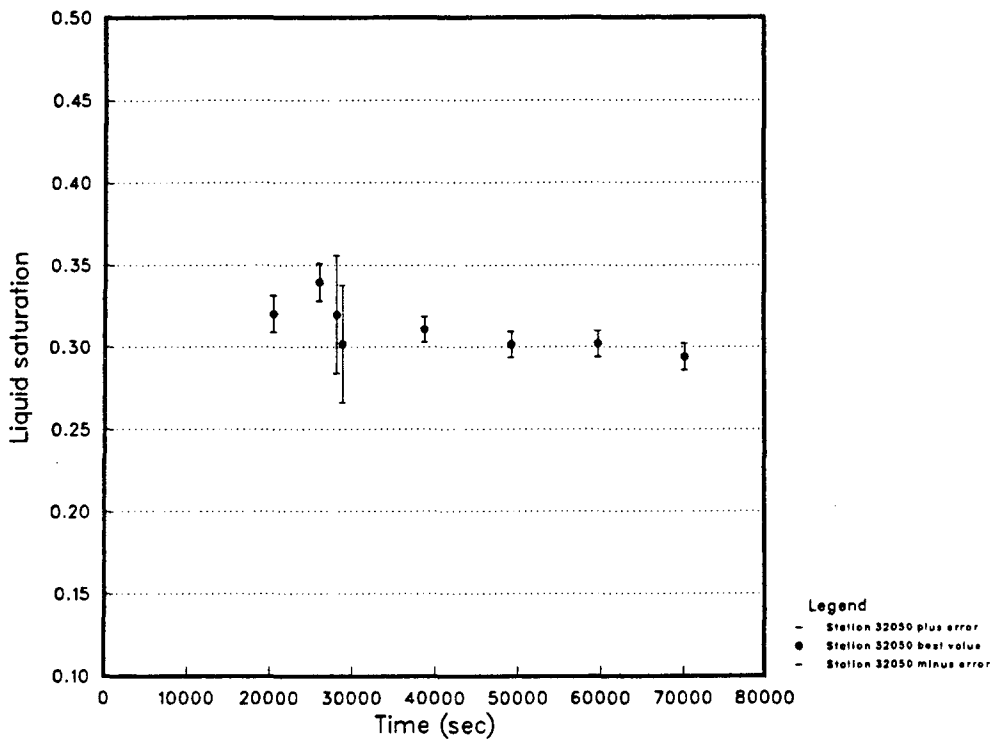

Figure B-9.6. Liquid saturation at 40 cm, experiment 9.

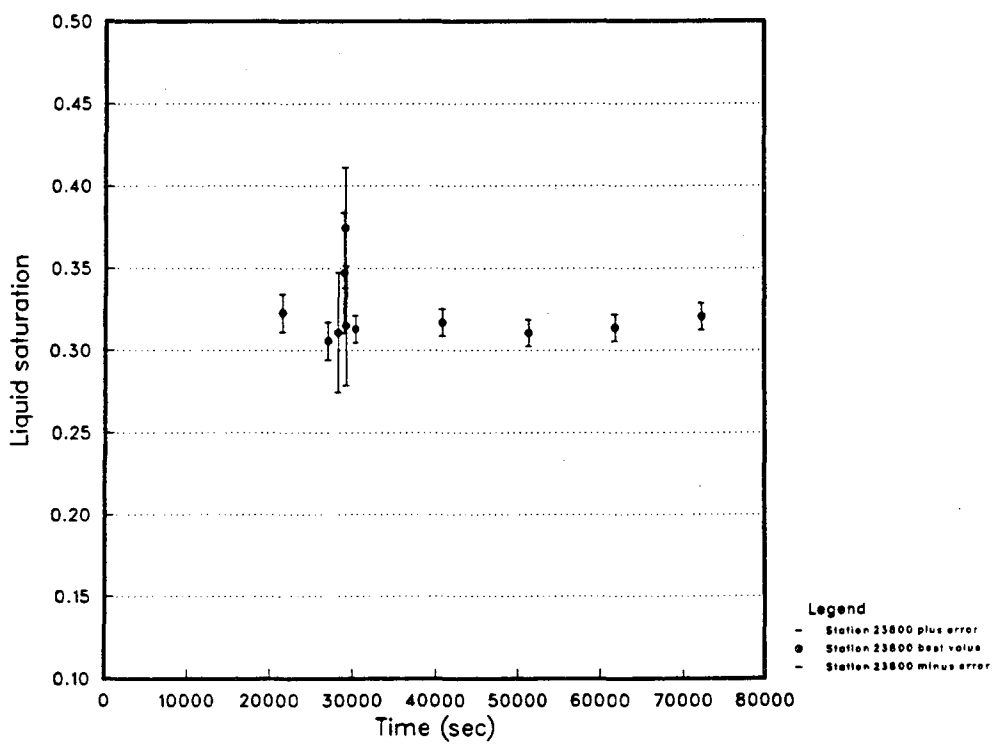

Figure B-9.7. Liquid saturation at 50 cm, experiment 9.

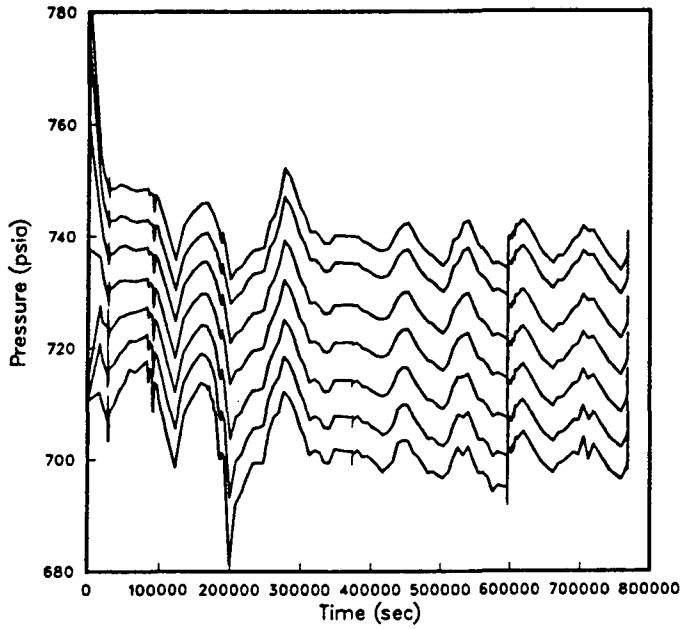

Figure B-9.8. Pressures measured at taps 8 through 2 (inlet to outlet) during experiment 9. Note that as the back pressure rose and fell with daily temperature cycles, the pressures through out the core tracked the back pressure.

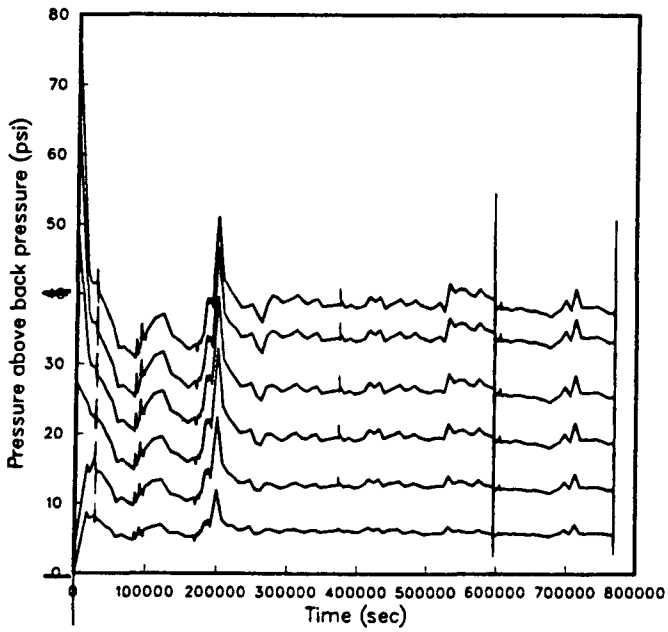

Figure B-9.9. Relative pressures above back pressure measured at taps 8 through 3 (inlet to 50 cm; outlet pressure is zero relative). Note that although all pressures rose and fell the pressure gradient through the core (and the permeability) was constant. Experiment was terminated after 9 days because of loss of control over back pressure.

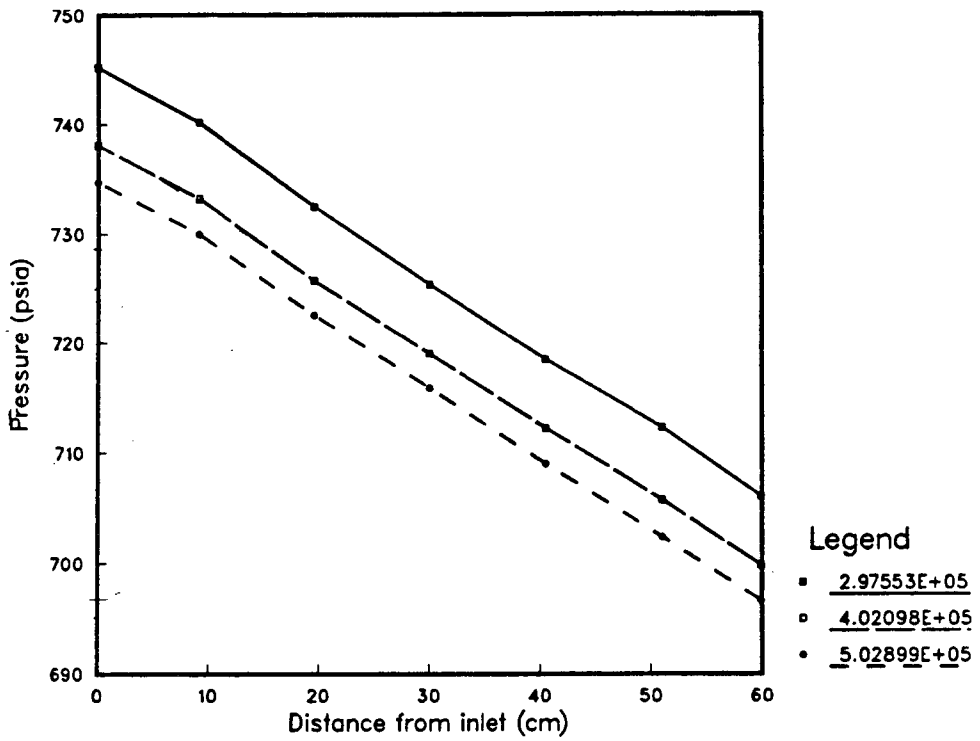

Figure B-9.10. Pressure profiles measured during experiment 9, showing that the pressure gradient was constant.

Experiment 12

This experiment was intended to determine the effect of changing the liquid flow rate upon the pressure gradient, with the gas flow rate held constant. The experiment had been tried earlier in the first part of experiment 6, but experimental difficulties had made the data difficult to interpret. In experiment 6, there had been unexplained drifting of the pressure gradient although both gas and liquid flow rates were held constant, and the inlet pressure sometimes became too great for gas delivery to continue at the set rate. To avoid these problems in experiment 12, the back pressure was reduced from 700 psi to 400 psi, and the foamer solution was made without long-chain alcohol, as it was suspected that the long chain alcohol contributed to the changes in pressure gradient, possibly by separating from the liquid phase and forming temporary obstruction of flow. A planned additional feature of this experiment was the use of a gas tracer to measure the volume of trapped gas. For gas tracer experiments, the injected gas was suddenly changed from nitrogen to air (i.e., a step change in oxygen concentration), with oxygen detection at the exit of the back-presure regulator.

An unexpected effect of changing the injected gas was that the pressure gradient through the core became steeper when the injected gas was air, and less steep when it was nitrogen. This effect is shown in Figure B-12.3. According to the manufacturer, the response of the mass flow controller to air is essentially the same as to nitrogen; no adjustment in the calibration is needed when the gas is changed from one to the other. Even if the gas flow rate changed at the same time as the gas changed, that should not have caused a change in the pressure gradient according to the results shown for experiment 3 and presented in Appendix E. Careful examination of the liquid flow rate during the experiment showed that the rate was constant and could not be the cause of the changes in the pressure gradient. When gas switching was stopped, the changes in pressure gradient stopped. The rest of the experiment was done using nitrogen as the gas, with no further changes.

Table B-12.1 shows the changes in gas and liquid flow rate during experiment 12. The first seven points have been plotted in Appendix E, Figure 9.

One effect that was observed during experiment 12 that was never observed in any other experiment was regular cycling of the pressure gradient. Above a certain minimum liquid flow rate, regular spikes in the pressure gradient appeared. When pressure measurements were sufficiently frequent, these spikes were seen to appear suddenly and at regular intervals, and to decay slowly, as shown in Figures B-12.5 through B-12.8. Note that the height and frequency of the pressure spikes are both correlated with the liquid flow rate. The pressure gradients reported in Appendix E, Figure 9 were calculated by averaging through several cycles during a period of constant liquid and gas flow rate. Figures B-12.9 through B-12.16 show liquid saturations measured at locations from 9 to 54 cm.

Table B-12.1. Gas and Liquid Flow Rates during Experiment 12

Time (sec) from		to	Liquid flow rate (mL/min)	Gas flow rate (sccm)	Point in App. E, Figure 9
879,232	→	912,000	0.18	347	A
912,000	→	996,000	0.60	347	B
996,000	→	1,052,000	1.04	347	C
1,052,000	→	1,090,000	1.24	347	D
1,090,000	→	1,172,000	1.24	120	E
1,172,000	→	1,233,000	0.215	120	F
1,233,000	→	1,254,000	0.215	347	G
1,254,000	→	1,285,000	0.0577	347	-
1,285,000	→	1,300,000	0.0577	120	-
1,300,000	→	1,343,000	0.0577	60	-
1,343,000	→	1,373,000	0.0577	200	-
1,373,000	→	1,397,000	0.0577	347	-
1,397,000	→	1,410,000	0.0577	600	-
1,410,000	→	1,427,500	0	600	-
1,427,500	→	1,471,000	0	347	-
1,471,000	→	1,600,000	0	600	-

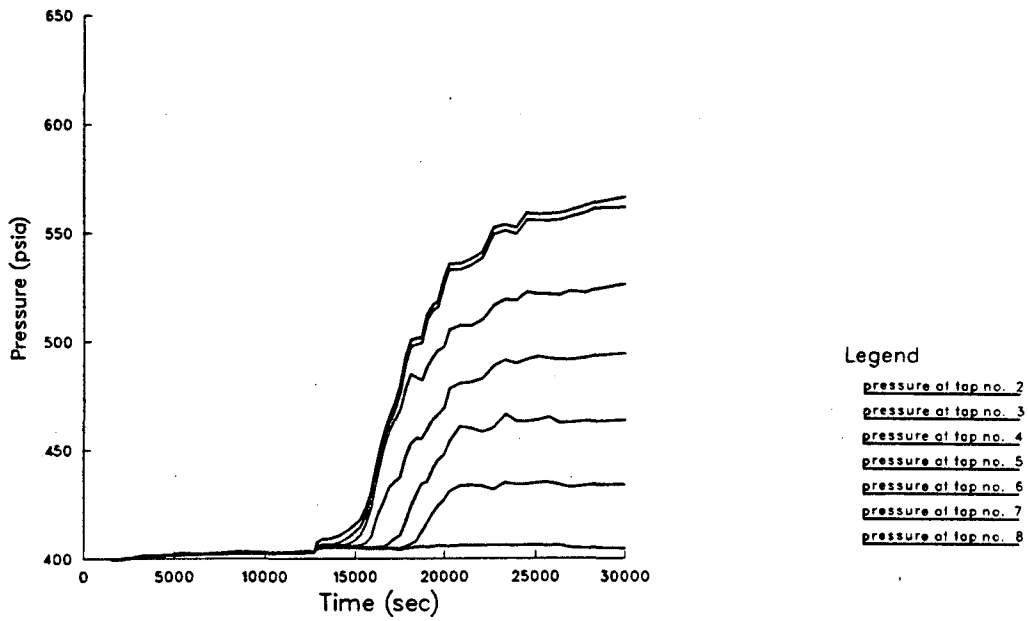

Figure B-12.1. Pressures measured at taps 2 through 8 (outlet to inlet) during initial displacement of liquid by foam. The liquid flow rate was 0.45 mL/min, gas flow rate 60 sccm. Gas flow started at 12820 sec.

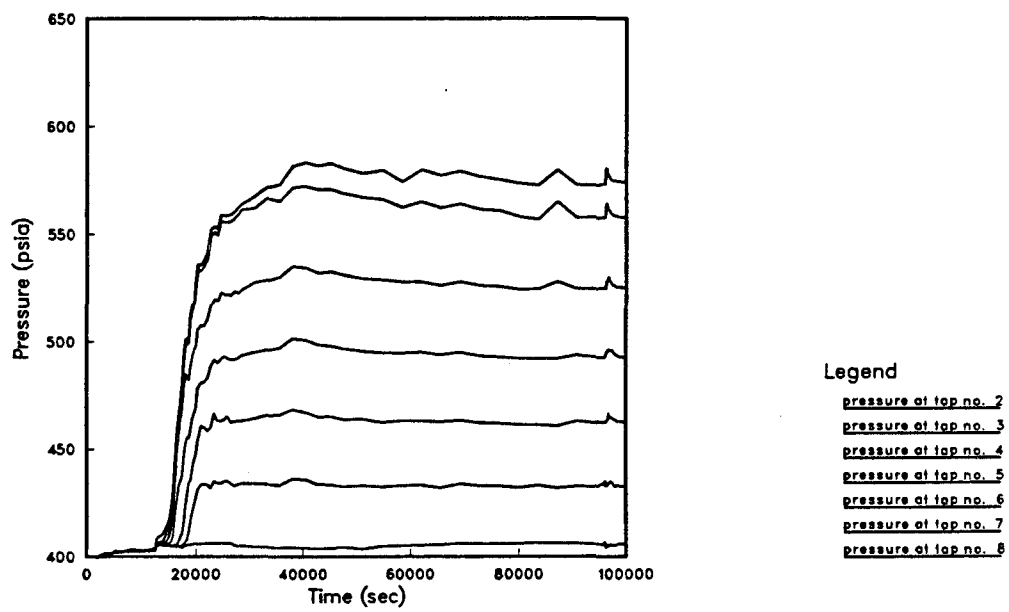

Figure B-12.2. Pressures measured at taps 2 through 8 (outlet to inlet) during and following initial displacement of liquid by foam. The initial liquid flow rate was 0.45 mL/min, and the initial gas flow rate (starting at 12820 sec) was 60 sccm. At 96105 sec the gas flow rate was doubled to 120 sccm.

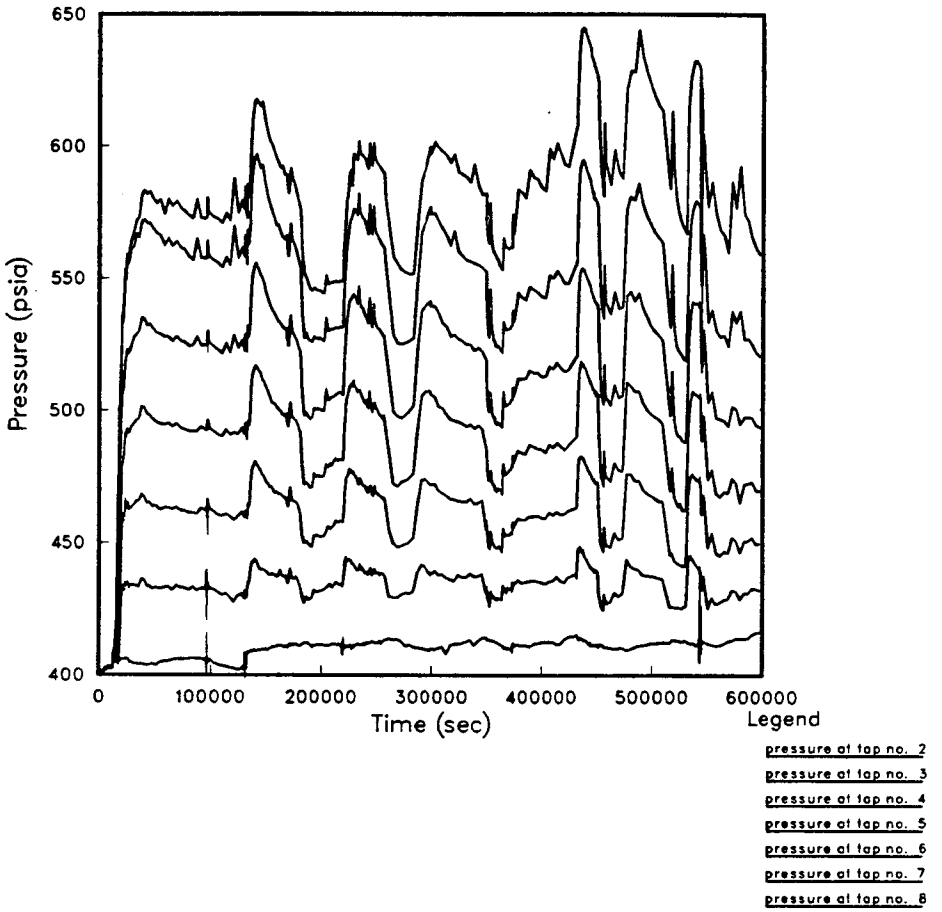

Figure B-12.3. Pressures measured during experiment 12. During this part of the experiment the liquid flow rate was constant and 0.45 mL/min and the gas flow rate was constant at 60 sccm. At 96105 sec, the gas flow rate was doubled, with no change in the pressure gradient, confirming the results obtained earlier in Experiment 3 and discussed in Appendix E. In gas tracer experiments the injected gas was changed from nitrogen to air at 133664, 219495, 284599, 432651, 474540, and 532000 seconds; and from air to nitrogen at 178859, 257433, 347000, 452000, and 516000 seconds. This figure shows that the pressure gradient through the core was always steeper when air was flowing than when Nitrogen was flowing. (In later experiments, this problem was resolved by adding a small air flow to the nitrogen so that the oxygen concentration changed from 0 to 2 % instead of from 0 to 20%.)

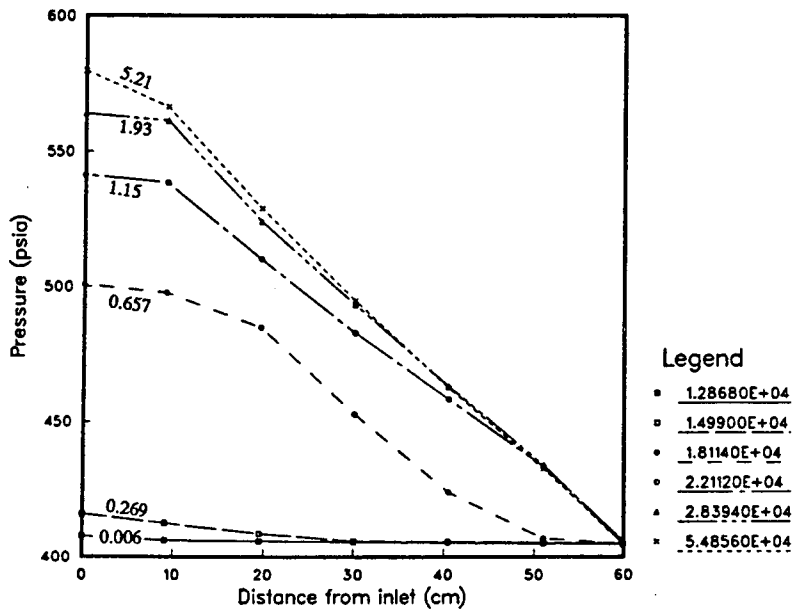

Figure B-12.4. Pressure profiles measured during initial transient displacement of liquid by foam. Each curve is identified in the legend at the right by the time in seconds (gas flow started at 12820 sec), and numbers at each curve in the figure indicate the number of pore volumes of fluid that flowed through the core.

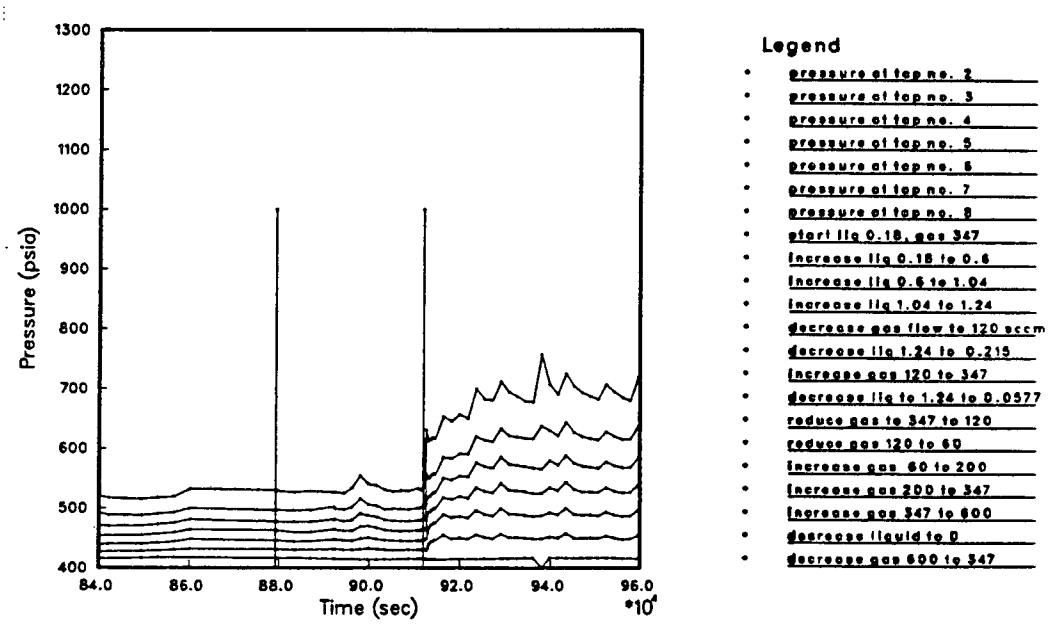

Figure B-12.5. Pressures measured at taps 2 (outlet) through 8 (inlet) during experiment 12, The period between 879,232 and 912,000 sec corresponds to point A in Figure 9 of Appendix E. Note pressure spike.

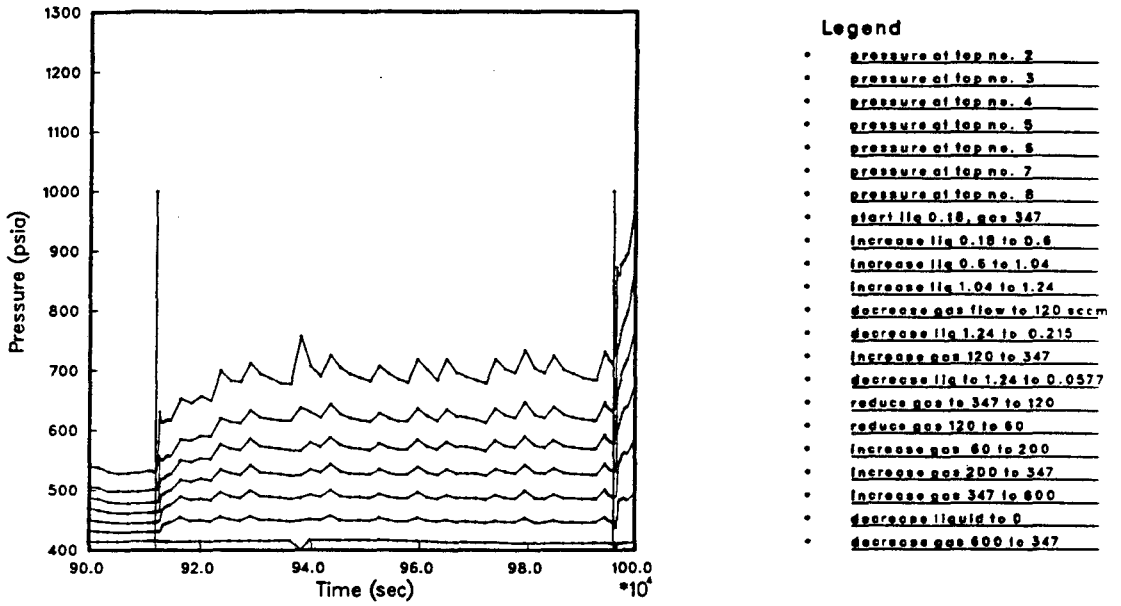

Figure B-12.6. Pressures measured at taps 2 (outlet) through 8 (inlet) during experiment 12, The period between 912,000 and 996,000 sec corresponds to point B in Figure 9 of Appendix E. Note pressure spikes.

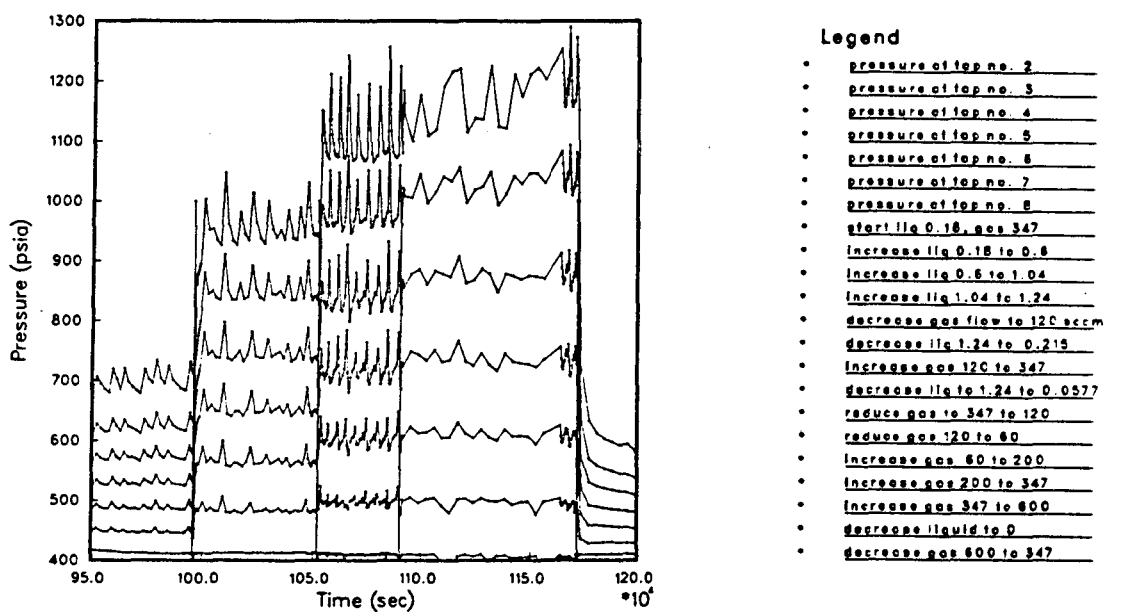

Figure B-12.7. Pressures measured at taps 2 (outlet) through 8 (inlet) during experiment 12, The period between 996,000 and 1,052,000 sec corresponds to point C in Figure 9 of Appendix E. The period between 1,052,000 and 1,090,000 sec corresponds to point D in Figure 9 of Appendix E. The period between 1,090,000 and 1,172,000 sec corresponds to point E in Figure 9 of Appendix E. Note pressure spikes.

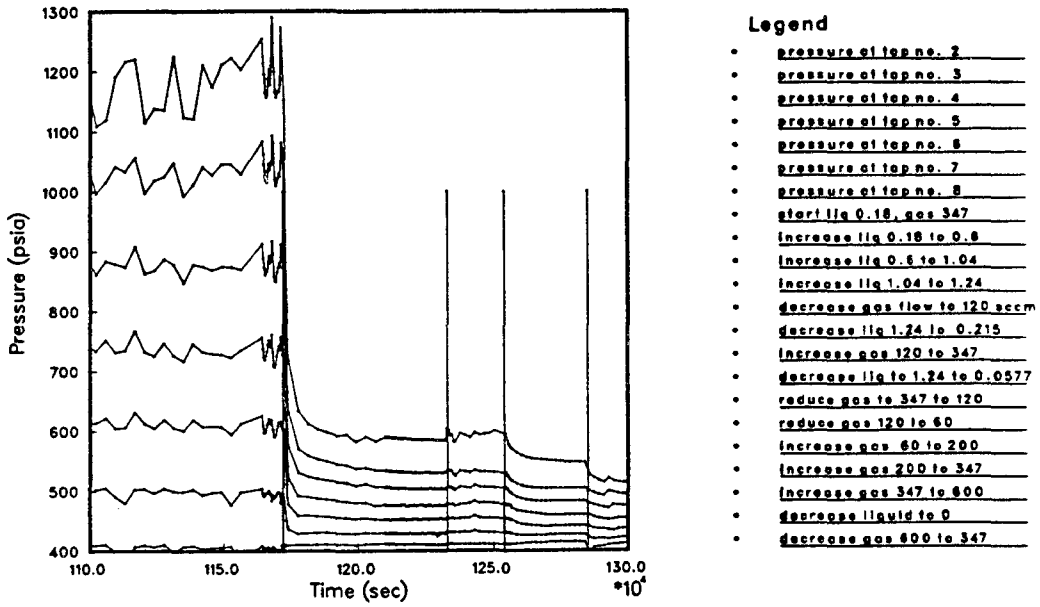

Figure B-12.8. Pressures measured at taps 2 (outlet) through 8 (inlet) during experiment 12, The period between 1,172,000 and 1,233,000 sec corresponds to point F in Figure 9 of Appendix E. The period between 1,233,000 and 1,254,000 sec, corresponds to point G in Figure 9 of Appendix E. For flow rates at later intervals, see Table B-12.1. Note lack of pressure spikes at low liquid flow rates.

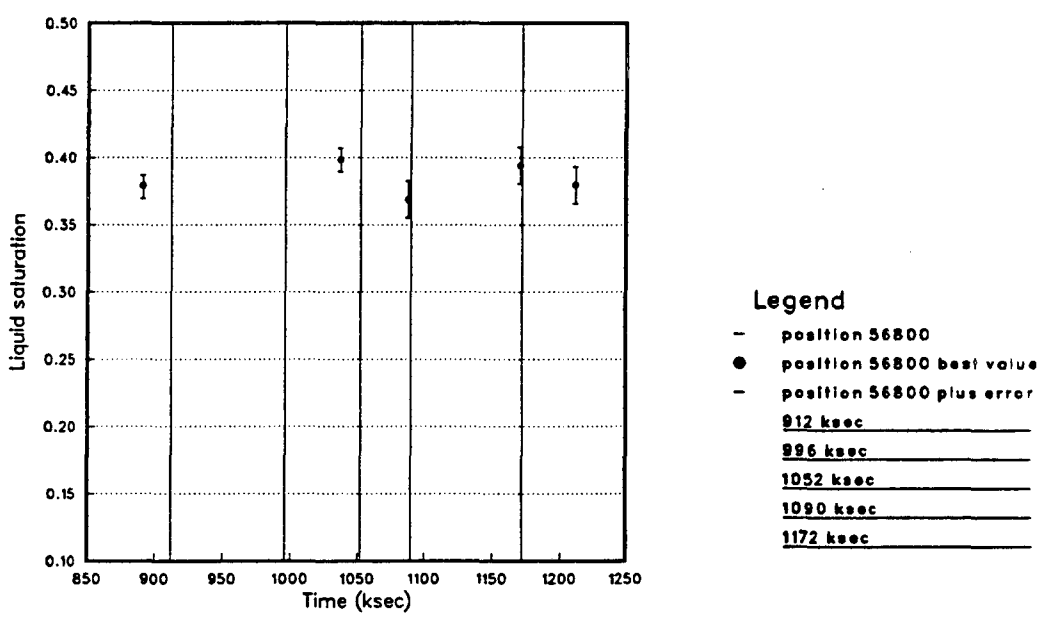

Figure B-12.9. Liquid saturation at 9.1 cm, during changes in gas and liquid flow rates (see Table B-12.1).

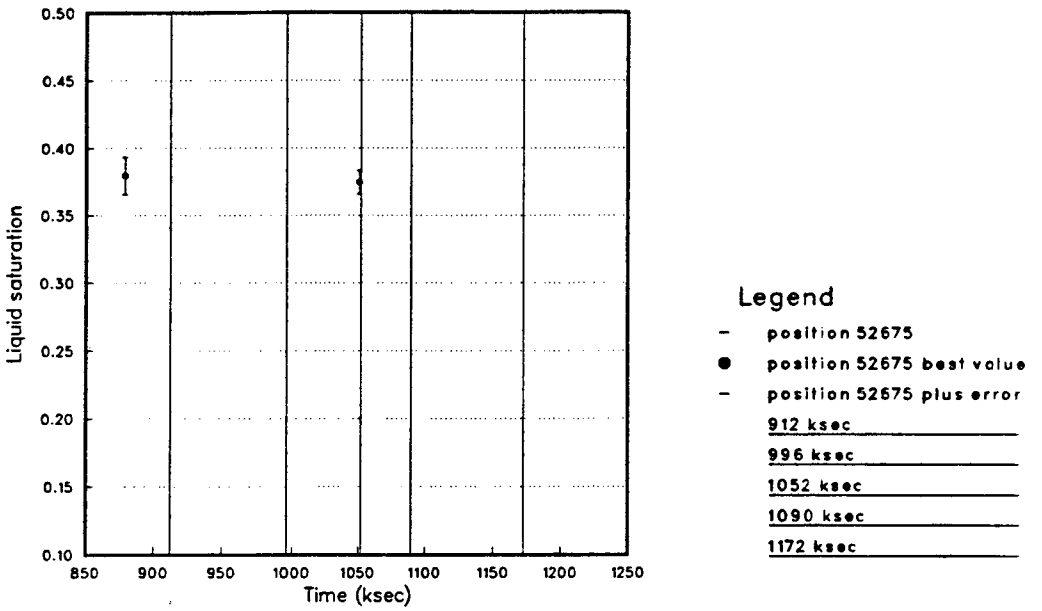

Figure B-12.10. Liquid saturation at 14.4 cm, during changes in gas and liquid flow rates (see Table B-12.1).

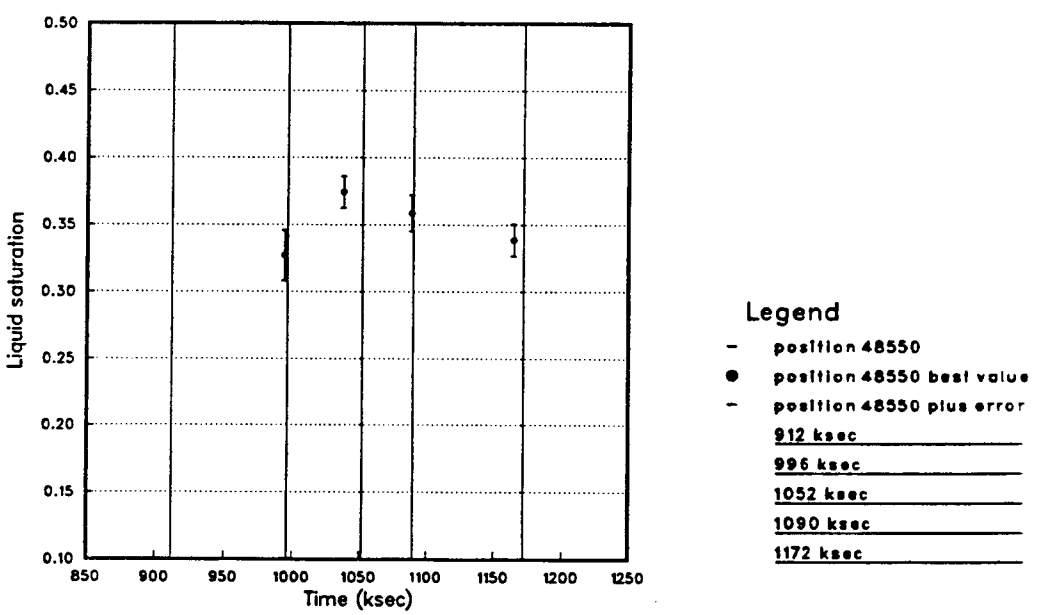

Figure B-12.11. Liquid saturation at 19.6 cm, during changes in gas and liquid flow rates (see Table B-12.1).

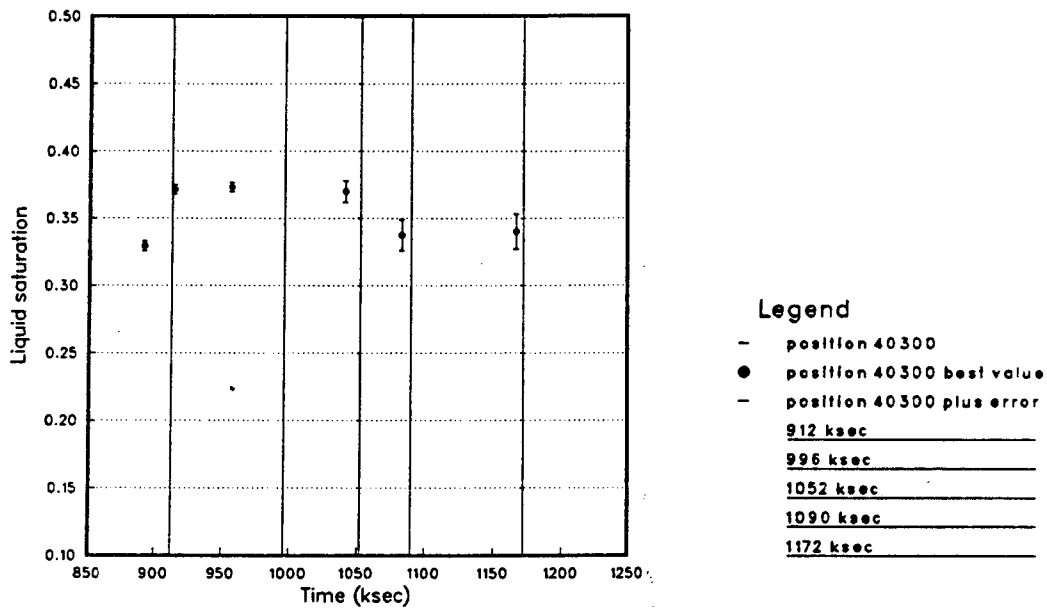

Figure B-12.12. Liquid saturation at 30.1 cm, during changes in gas and liquid flow rates (see Table B-12.1).

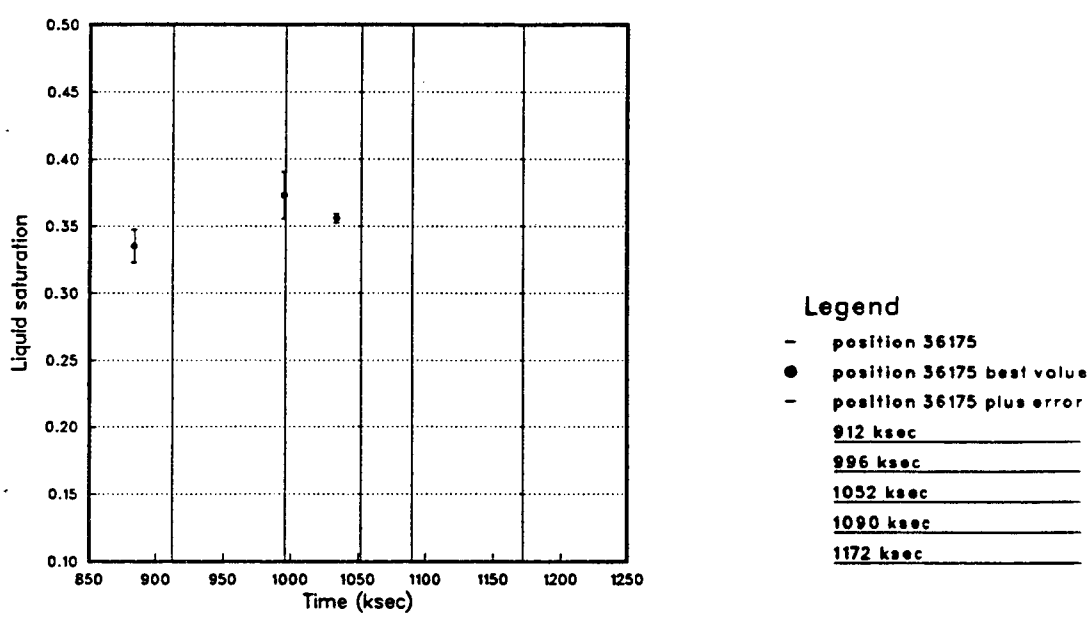

Figure B-12.13. Liquid saturation at 35.3 cm, during changes in gas and liquid flow rates (see Table B-12.1).

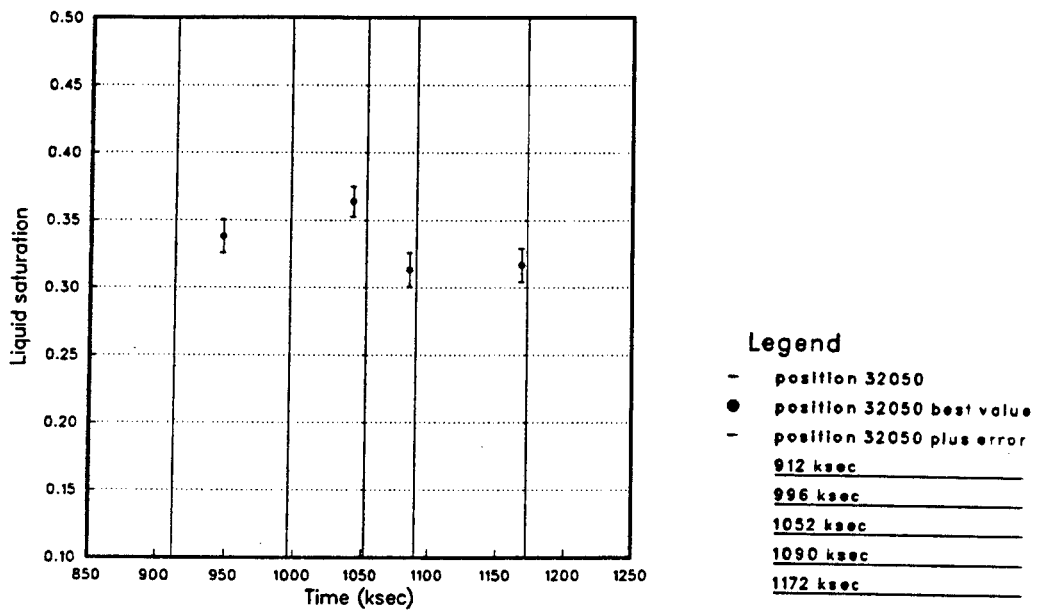

Figure B-12.14. Liquid saturation at 40.6 cm, during changes in gas and liquid flow rates (see Table B-12.1).

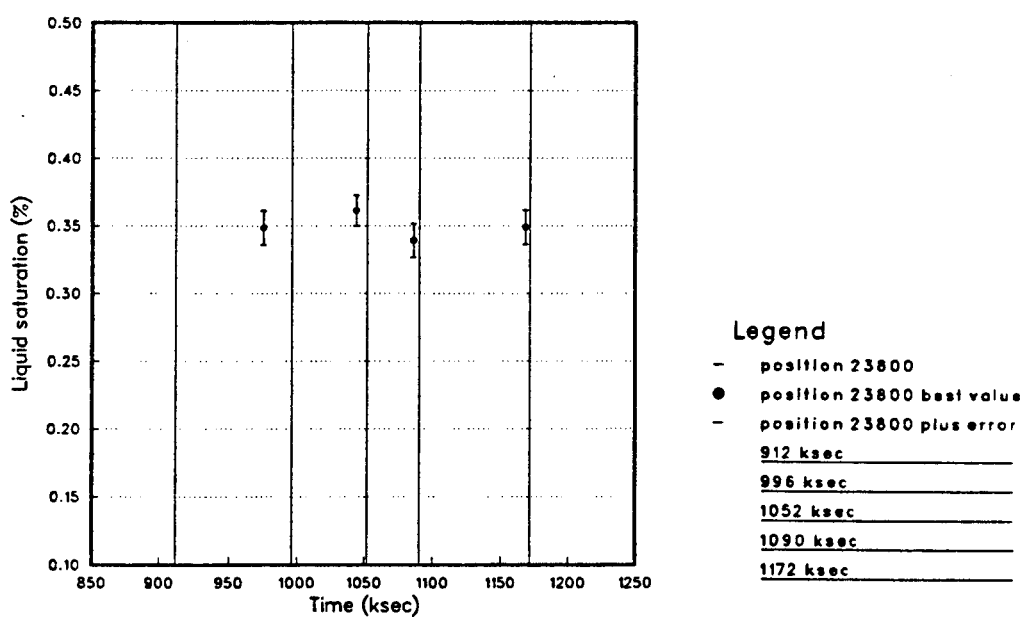

Figure B-12.15. Liquid saturation at 51.0 cm, during changes in gas and liquid flow rates (see Table B-12.1).

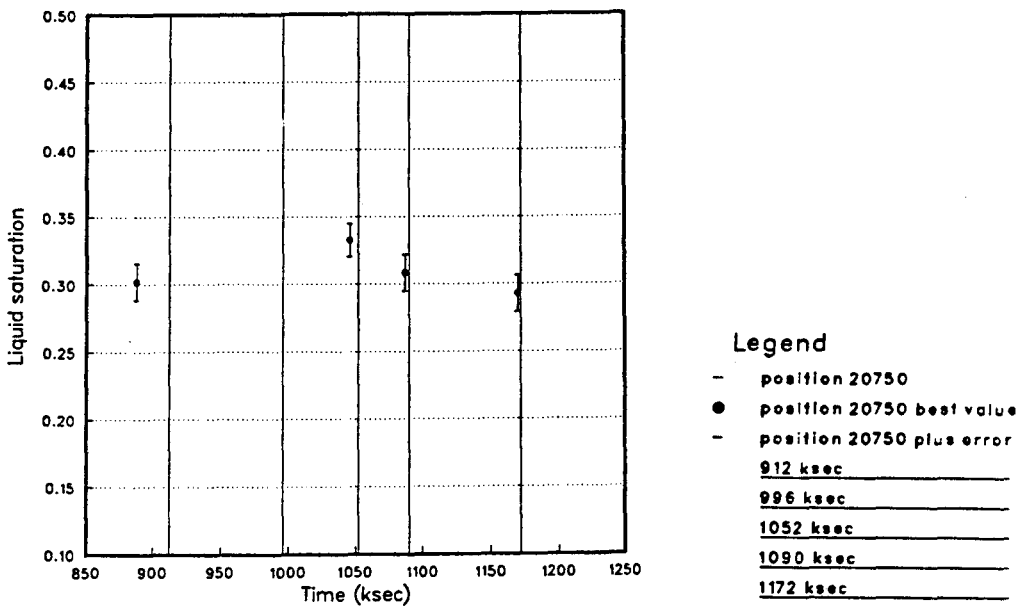

Figure B-12.16. Liquid saturation at 54.0 cm, during changes in gas and liquid flow rates (see Table B-12.1).

Experiment 15

In experiments 3 through 12, we had found that foam can be formed in a high-permeability (1.3 darcy) sandstone core by injecting gas into the core saturated with a foamer solution. The foam reduces the permeability to gas to approximately 1 millidarcy (mD). Upon recommendation of the Gas Storage Steering Committee of the Gas Research Institute, we conducted experiment 15 to demonstrate generation of a strong foam in a core of significantly lower permeability (190 mD).

The core used in this experiment was 2-in. diameter, 22-in. long Berea sandstone, cored parallel to the bedding plane. The core was coated with epoxy and then epoxy-mounted into a stainless-steel core holder. The core holder was fitted with seven pressure taps along the core length and mounted in a gamma-ray densitometry system for liquid saturation measurement. Gas flow was controlled and measured by a mass flow controller. Gas tracer measurements were made by mixing a small amount of air with the nitrogen gas and monitoring the oxygen concentration at the core exit.

Permeability measurements were made by flowing gas through the dry core. The core was found to have a permeability of 190 mD, and gas tracer measurements did not reveal any leaks. The core was evacuated and saturated with 1% NaCl brine; liquid permeability measurements confirmed the gas permeability measurements. The brine was then displaced by five pore volumes of foamer solution, which was 1% NaCl containing 1% active Steol 7-N (commercially available dodecyl ethoxysulfate) and 0.2% dodecyl alcohol. The foamer solution was turbid when prepared, and was allowed to separate into clear and turbid layers; the clear layer was used for the experiment. This was done to avoid blocking the pores with micelles of insoluble alcohol.

The first part of the experiment was conducted similar to experiment 9. Gas was then injected at a controlled rate of 200 standard cm^3/min, against a back pressure of 500 psia. Both pressures and liquid saturation were automatically monitored at seven locations along the core.

After one day, an additional 8 mL slug of foamer solution was injected into the core while gas injection continued. The pressures recorded during the experiment are shown in Figure B-15.1. The pressure gradient required to inject gas through the core gradually decreased after injection of the slug. The overall core permeability calculated from the measured pressures is shown in Figure B-15.2.

Gas tracer measurements made during this part of experiment showed that the apparent volume of mobile gas in the core was about 40 cm^3, while the total gas volume was about 160 cm^3. The apparent mobile gas measures not only the gas which is actually flowing but also a fraction of the trapped gas bubbles which exchange tracer gas by diffusion. Therefore this result indicates that at least 75% of the gas in the core is trapped bubbles. The rest of the gas consists of either mobile bubbles or (more likely) connected flow paths.

The results of the experiment in low-permeability sandstone confirmed the results of previous experiments in high-permeability sandstone. The principal difference is the degree of permeability reduction. Whereas a 1000-fold permeability reduction was observed in the Boise sandstone, in this case the factor of permeability reduction was about 100. This suggests that if foam is used to block gas flow in storage applications, the greatest effect will occur in high-permeability streaks where it is needed most.

Table B-15.1. Gas and Liquid flow rates during experiment 15

Time (sec) from		to	Liquid flow rate (mL/min)	Gas flow rate (sccm)	Point in Figure F-15-14
0	→	1,226,142	0	200	-
1,226,142	→	1,285,547	varies	200	-
1,285,547	→	1,427,121	0.019	200	A
1,472,121	→	1,659,479	0.027	200	B
1,659,479	→	1,812,238	0.036	200	C
1,812,238	→	1,991,001	0.043	200	D
1,991,001	→	2,129,268	0.047	200	E
2,129,268	→	2,482,183	0.050	200	F

During the second part of the experiment, liquid was injected along with gas to confirm the results of experiments 3 and 12, as discussed in Appendix E. The liquid flow rate was varied stepwise as shown in Table B-15.1, while the pressure was measured at seven points along the length of the core. Figure B-15.14 shows the pressure gradient plotted against the liquid flow rate. The results presented in Figure B-15.14 show that, at constant gas flow rate, the pressure gradient is proportional to the liquid flow rate. This is the same results that was obtained for the 1300-millidarcy Boise sandstone core, as reported in Appendix E. As explained in Appendix E, $1/k_{rl}$ is uniform through the core, and constant through changes in gas and liquid flow rates. The value of $1/k_{rl}$ in this experiment was approximately 3000, compared with a value of approximately 1000 found for the Boise core. The difference apparently results from the different relative permeability curves for the two sandstones. In both experiments, the observation that $1/k_{rl}$ was constant agreed with the independent observation that the liquid saturation in the core was uniform and constant over order-of-magnitude changes in gas and liquid flow rates.

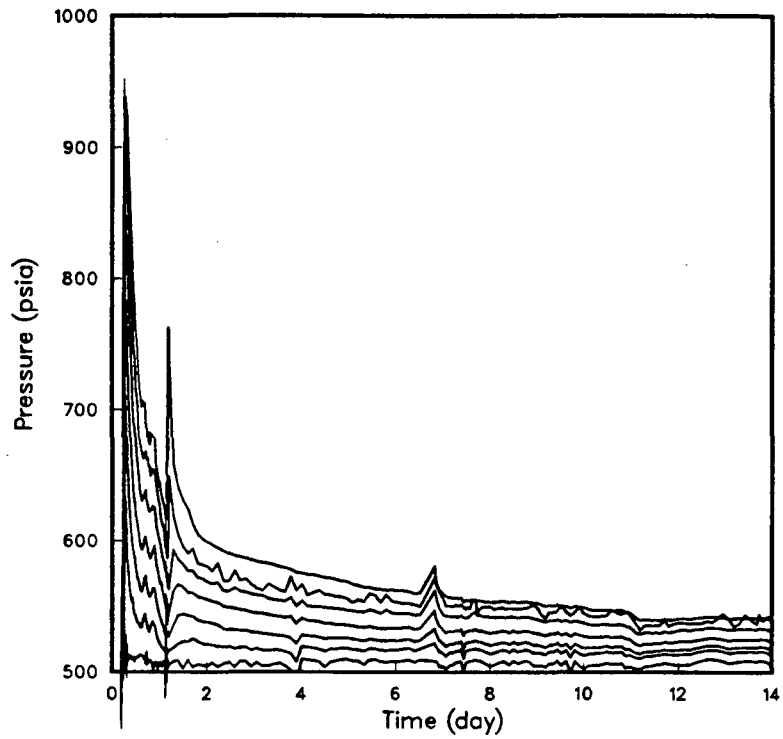

Figure B-15.1. Pressures measured at taps 2 (outlet) through 8 (inlet) during Experiment 15. An additional slug of foamer solution was injected at 1 day.

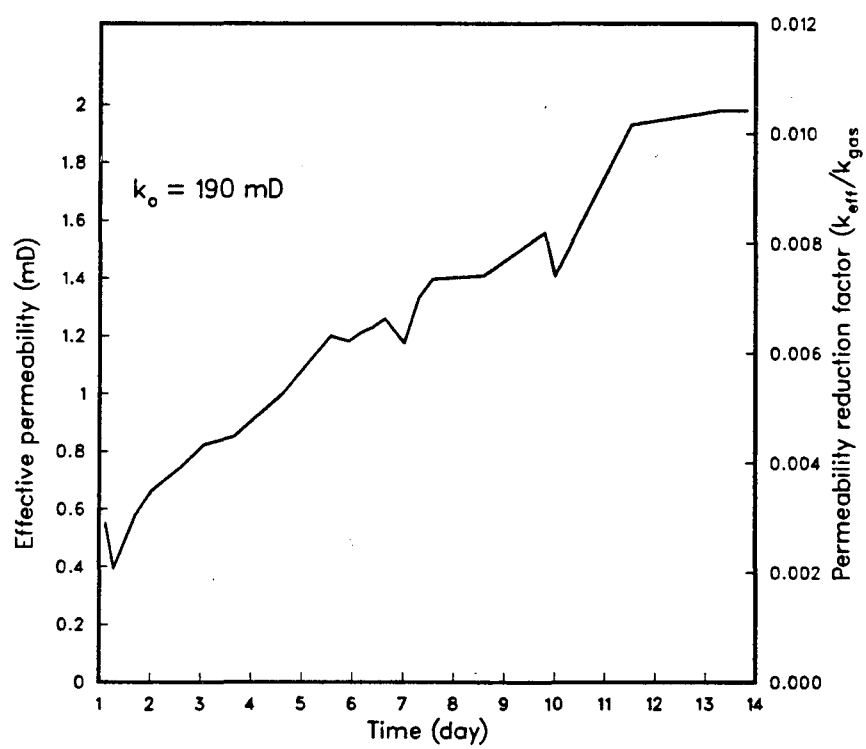

Figure B-15.2. Overall permeability measured during Experiment 15.

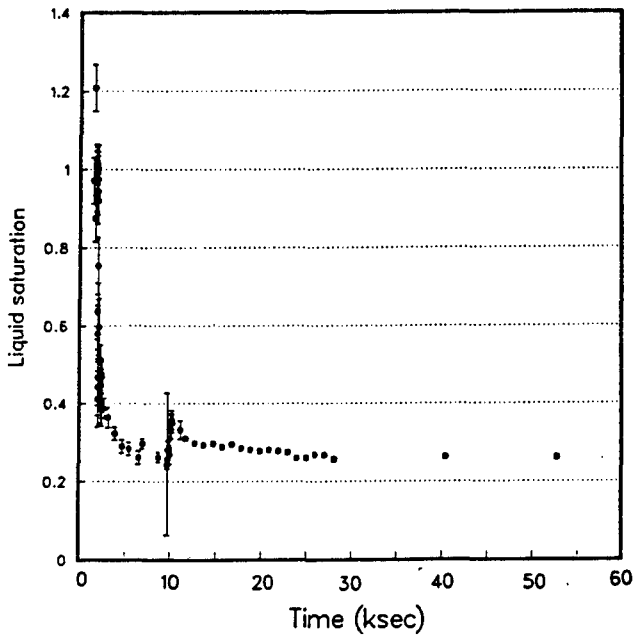

Figure B-15.3. Liquid saturation measured at 5.5 cm, showing transient displacement of liquid by foam. Note each tick mark on the x-axis is 50,000 sec. Note liquid saturation approaching connate.

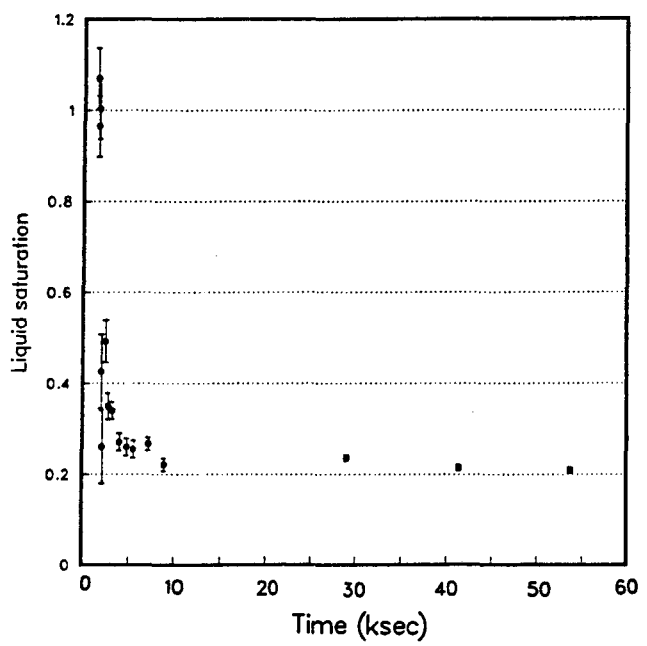

Figure B-15.4. Liquid saturation measured at 9.4 cm, showing transient displacement of liquid by foam. Note each tick mark on the x-axis is 50,000 sec. Note liquid saturation approaching connate.

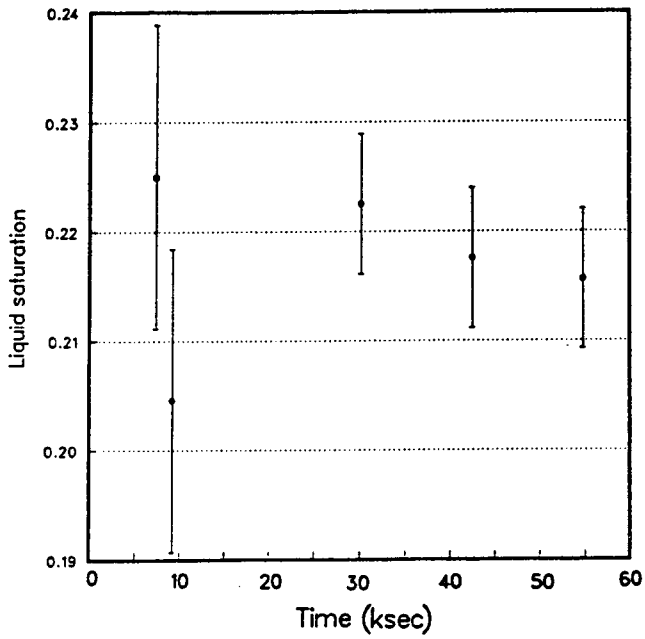

Figure B-15.5. Liquid saturation measured at 13.9 cm, showing transient displacement of liquid by foam. Note each tick mark on the x-axis is 50,000 sec. Note liquid saturation approaching connate.

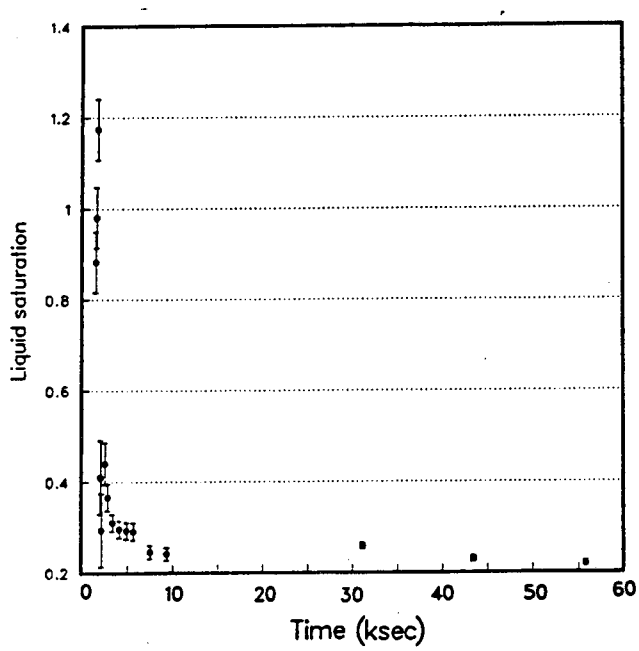

Figure B-15.6. Liquid saturation measured at 18.5 cm, showing transient displacement of liquid by foam. Note each tick mark on the x-axis is 50,000 sec. Note liquid saturation approaching connate.

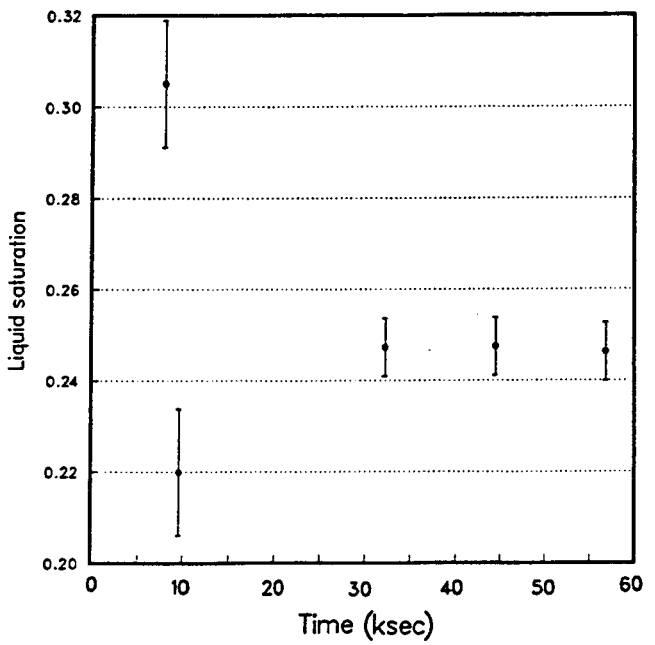

Figure B-15.7. Liquid saturation measured at 23.1 cm, showing transient displacement of liquid by foam. Note each tick mark on the x-axis is 50,000 sec. Note liquid saturation approaching connate.

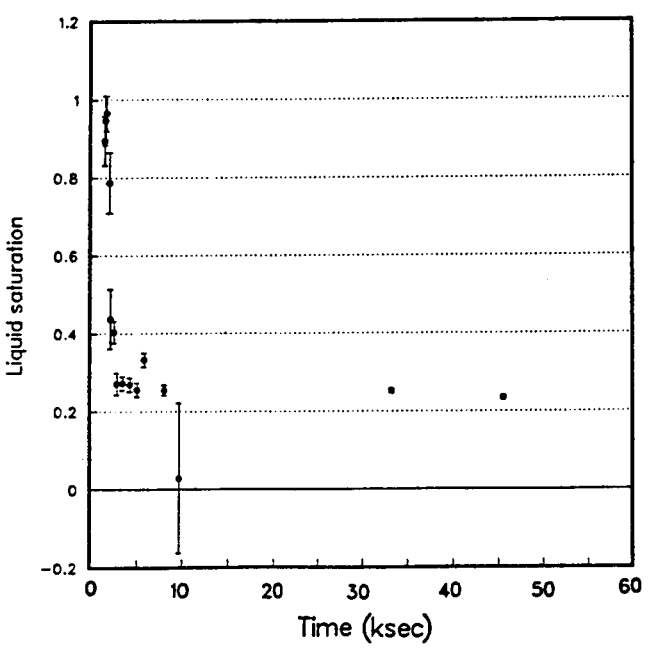

Figure B-15.8. Liquid saturation measured at 27.6 cm, showing transient displacement of liquid by foam. Note each tick mark on the x-axis is 50,000 sec. Note liquid saturation approaching connate.

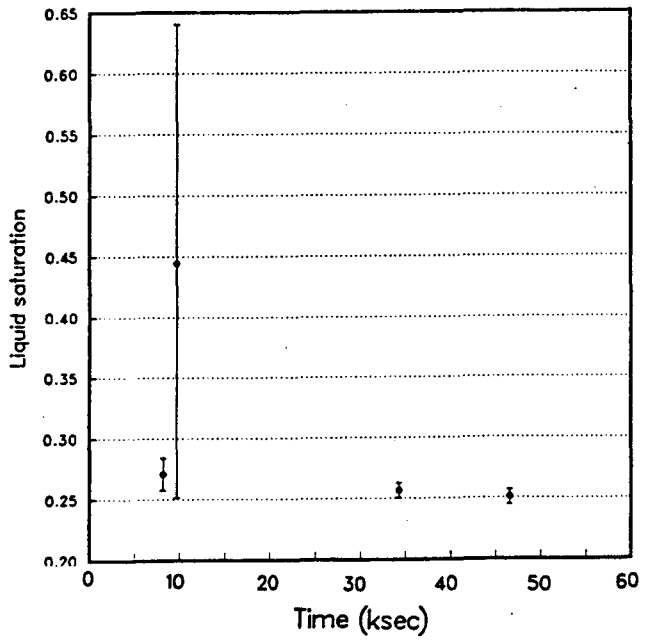

Figure B-15.9. Liquid saturation measured at 32.2 cm, showing transient displacement of liquid by foam. Note each tick mark on the x-axis is 50,000 sec. Note liquid saturation approaching connate.

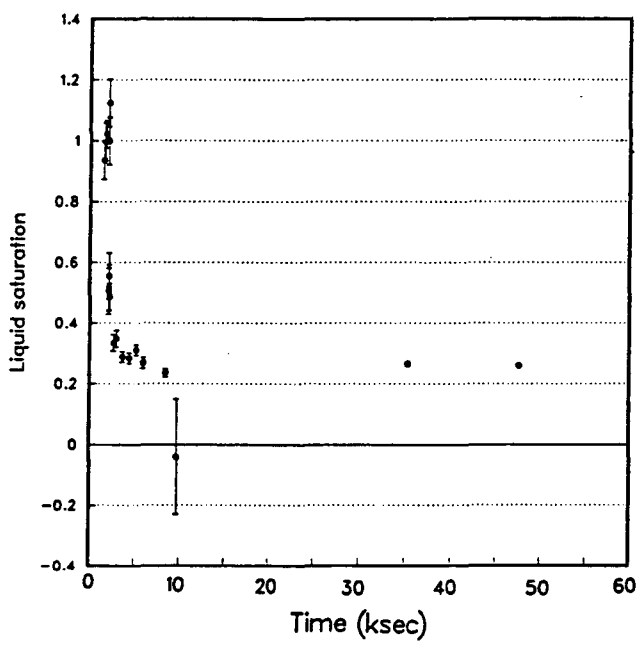

Figure B-15.10. Liquid saturation measured at 36.8 cm, showing transient displacement of liquid by foam. Note each tick mark on the x-axis is 50,000 sec. Note liquid saturation approaching connate.

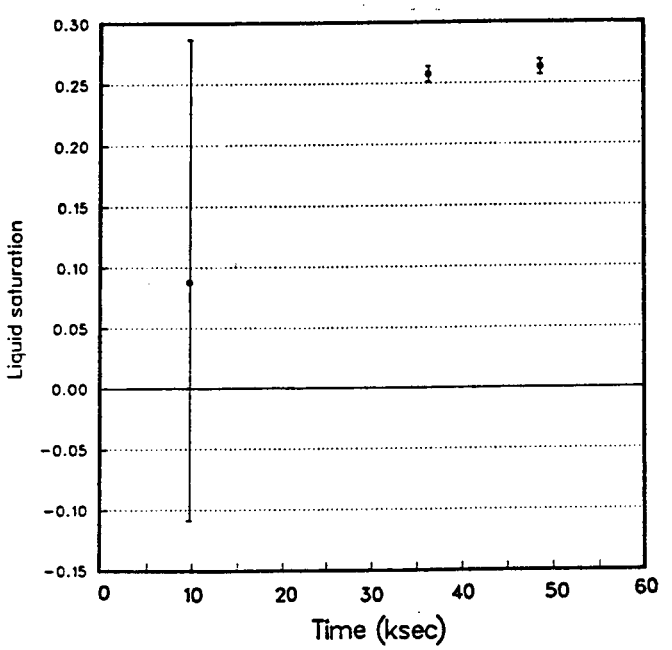

Figure B-15.11. Liquid saturation measured at 41.3 cm, showing transient displacement of liquid by foam. Note each tick mark on the x-axis is 50,000 sec. Note liquid saturation approaching connate.

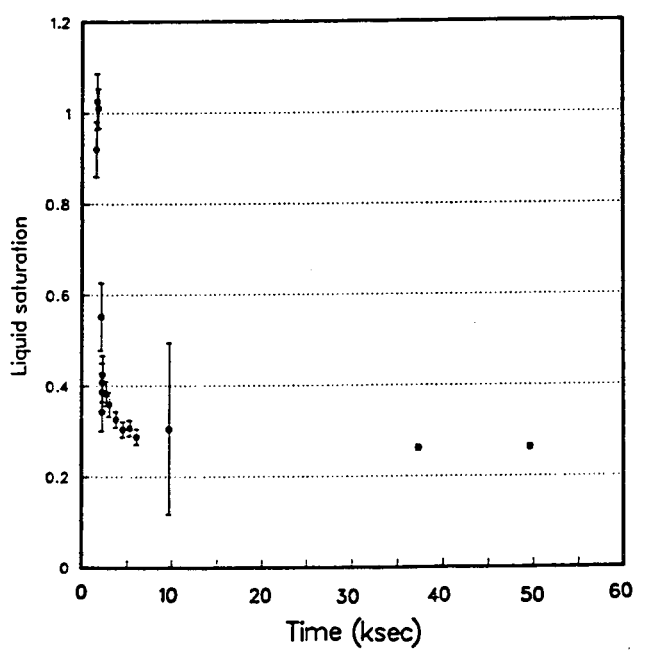

Figure B-15.12. Liquid saturation measured at 45.9 cm, showing transient displacement of liquid by foam. Note each tick mark on the x-axis is 50,000 sec. Note liquid saturation approaching connate.

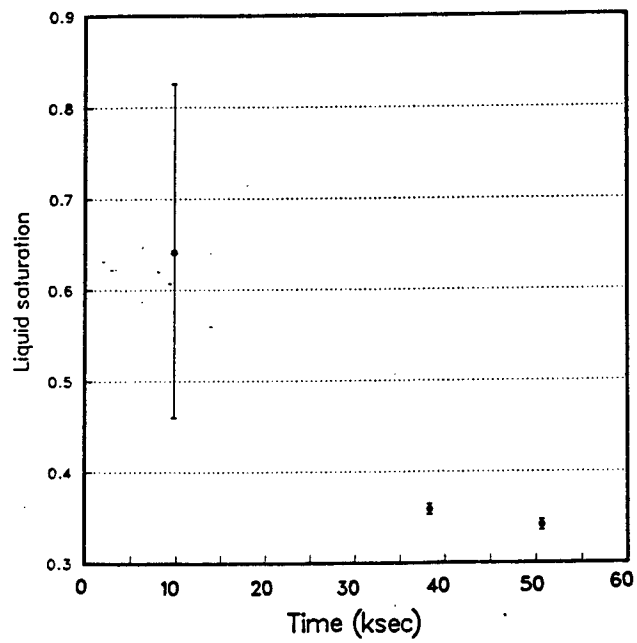

Figure B-15.13. Liquid saturation measured at 49.8 cm, showing transient displacement of liquid by foam. Note each tick mark on the x-axis is 50,000 sec. Note liquid saturation approaching connate.

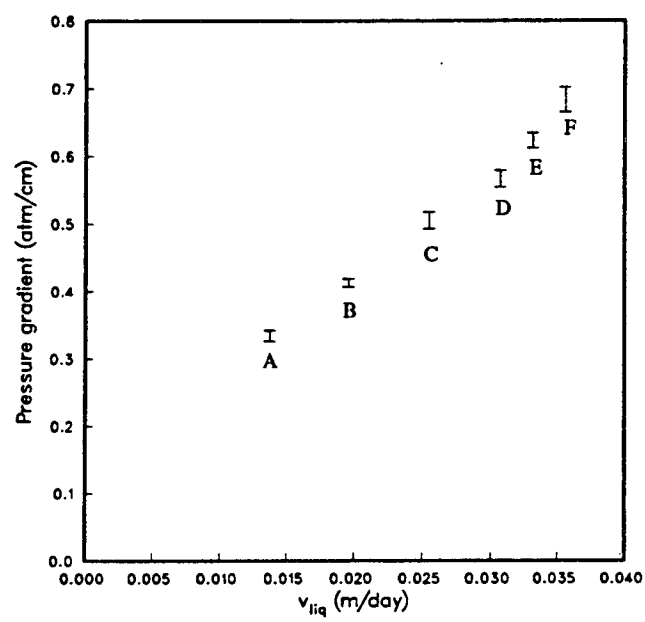

Figure B-15.14. Pressure gradient during changes in liquid flow rate (see Table B-15.1). Each symbol represents the range of pressure gradients measured during a period of constant liquid flow rate.

Appendix C.

Feasibility Analysis and Development of a Foam-Protected Underground Natural Gas Storage Facility

Proceedings AGA Operating Section
paper #87-DT-110, pp. 539-549

1987

87-DT-110

Feasibility Analysis and Development of a Foam-Protected Underground Natural Gas Storage Facility

P. A. WITHERSPOON, Professor of Geological Engineering
C. J. RADKE, Professor of Chemical Engineering
University of California, Berkeley

Y. SHIKARI, Manager, Storage Research
Gas Research Institute

K. PRUESS, P. PERSOFF, S. M. BENSON, and Y. S. WU, Earth Sciences Division
Lawrence Berkeley Laboratory

ABSTRACT

Underground storage of natural gas has been practiced for over 40 years as a cost-effective means of meeting peak demand. However, the volume of gas that must remain in the storage aquifer (base gas) is typically large compared to the quantity that is available for withdrawal (working gas). One way of improving the efficiency of gas storage operations is to keep the working gas closer to the withdrawal wells and to create a thicker gas saturated region. To achieve this, the mobility of the injected gas must be controlled. We are investigating the feasibility of using foam as a mobility control agent for gas storage operations. Specific concepts for using foam to improve gas storage operations range from improved injection/withdrawal well performance to the potential for creating isolated underground storage regions. This paper describes the efforts of the first year of the three-year research program that is being sponsored by the Gas Research Institute. Laboratory studies for identifying suitable foams and for improving our knowledge of foam behavior are being carried out. In addition, a mathematical model for simulating "foam-protected" gas storage operations and for designing "foam-protected" storage operations is being developed. Preliminary economic analyses indicate a signficant reduction in gas storage costs in a successfully implemented "foam-protected" aquifer gas storage operation.

INTRODUCTION

The transmission and distribution segments of the gas industry share a common interest in gas storage. To meet peak loads and to ensure dependable delivery of gas to all end-users, gas storage has become a vital link in the supply, transport, and distribution network. Of the various forms of natural gas storage technologies being employed to meet different market and application needs, large-scale seasonable storage by utilities in underground formations is perhaps the most prevalent. Since the cost of meeting seasonal and peak demands has increased considerably in recent years, a significant amount of research and development has been carried out by the gas industry to improve storage technologies and methods. These have ranged from methods for increasing reservoir capacity (overpressuring and porosity enhancement) to techniques for reducing base gas requirements (mined hard-rock caverns and salt domes).

The Gas Research Institute (GRI) is currently involved in the development of concepts aimed at an enhancement of natural gas service to the consumer. To maintain the attractiveness of the gas options to industrial customers and to reinforce the "value-in-use" of natural gas to present and potential residential as well as commercial customers, it is essential to develop efficient, economical, and safe means of reducing the "cost of service," including that of natural gas storage in underground formations.

One specific aspect of undergound storage of natural gas merits further research: migration of gas beyond the designated storage area during the gas injection cycle. During the formation of the initial storage volume in an underground aquifer, some of the injected gas will finger away from the main bubble, sometimes for long distances, because of the adverse mobility ratio between water and gas. This migrated gas is often difficult to recover, thus, leading to a reduced percentage of working gas. It is, therefore, important to devise effective means of controlling such migration in underground natural gas storage facilities. For storage in underground aquifers, gas must displace water from the porous medium. Unfortunately, gas does not invade a water-saturated zone in a uniform piston-like fashion. Rather, the gas front breaks up and "fingers" through the water, leading to a very inefficient displacement mechanism. Also, because of its low density, the gas tends to rise to the top of the system, where it migrates as a thin layer (gravity override). More importantly, high mobility of gas compared to that of water results in formation of thin gas zones far from the main bubble. During gas withdrawal, these far-removed zones can be trapped as off-site and isolated gas, which is practically unrecoverable.

Extensive experience of oil recovery practice points out the fact that stable, efficient displacement requires the mobility of the drive fluid to be equal to, or only slightly less than, that of the displaced fluid. In the case of water displacing a more viscous oil, aqueous polymer solutions are used for "mobility control." Because of its exceptional flow properties and its cost, foam is currently undergoing extensive field testing in oil recovery processes, notably steam flooding. A considerable body of information is also growing to aid in detailed understanding of foam flow behavior in porous media.

The economic and market factors that influenced the development of gas storage technologies and methods in the past have changed. The cost of base gas has now become a major cost element, making a high turn-over ratio critically vital. Thus, there exists a need to examine critically relevant research programs in oil recovery processes to assess the feasibility of employing similar technologies and/or techniques to reduce migration of natural gas in underground storage facilities.

One possible solution would be to use natural gas/water foam as a mobility control agent. Because the foam would contain over 95 percent by volume of natural gas, it would provide a compatible and an easily applied source of mobility control. Specifically, a number of analytic and technical questions must be answered before foam barriers can be applied successfully in the field. These questions include, but are not necessarily limited to, the following:

- What is the applicable state of the art as far as the use of foam as a mobility control agent is concerned?
- What are the desirable properties of foam stabilizing chemicals? What are the selection criteria governing the choice of a given foam stabilizer?
- How is the foam generated in the porous media? How does it actually flow? How can this behavior be simulated mathematically?
- Is the foam barrier concept technically feasible? If yes, how can it be verified or validated experimentally?
- What are the preliminary economics of foam-protected natural gas storage reservoirs?
- What criteria should be used to select a field test site?
- What are the initial market penetration opportunities for foam-protected natural gas storage reservoirs?

To answer these and other pertinent questions, GRI is sponsoring a comprehensive research program at Lawrence Berkeley Laboratory (LBL) to assess technical feasibility and economics of using foam barriers for controlling the migration of flow behavior in porous media; to develop foams that have long-term stability; and to verify their performance in actual applications via selected field tests in the United States.

FOAM PROTECTED STORAGE CONCEPTS

The ability of foam to control the mobility of the injected gas and to block undesired gas flow can be used to improve the efficiency of underground gas storage operations with several different concepts. The earliest documentation of the concept of using foam for this purpose was presented by Bernard (1967), who proposed to take advantage of the ability of foam to block undesired gas flow and to create better closure of the natural structure of the storage aquifer. Later, Bernard and Holm (1970) proposed to take advantage of the ability of foam to block gas flow to seal natural leaks in the storage facility. In the current study, we are investigating the potential for exploiting the ability of foam to achieve mobility control and its ability to block undesired gas flow to improve the efficiency of gas storage operations. The general concepts currently being pursued were outlined by Radke et al. (1983) and are reviewed briefly below.

The first of these concepts, which is illustrated in Figure 1, relies on the ability of foam to achieve mobility control during the injection phase of the storage operation. By injecting a slug of surfactant solution before the gas is injected, a foam blanket acts to stabilize the interface between the gas and water during the injection phase, thereby improving the displacement efficiency, minimizing gravity override, and counteracting the effects of geologic heterogeneity. This concept can be used to achieve a deeper, more compact gas bubble around the injection well, which results in improved gas recovery during the withdrawal phase.

A more elaborate version of this concept (illustrated in Figure 2), which provides even better "protection" of the stored gas, could be achieved by creating a permanently emplaced "foam barrier" around the injection well. The barrier would be created by injecting a mixture of gas and surfactant solution into the aquifer until a sufficient volume of foam is emplaced. The barrier is then driven away from the injection well by the working gas. This procedure creats a cylindrical, water-free storage volume that can be used for repeated injection and withdrawal cycles. If sufficiently stable foams are developed, creation of the barrier need only be done once. Otherwise, periodic regeneration of the barrier may be required.

A larger storage volume can be created by the "skirt well" concept illustrated in Figure 3. In this concept, foam is injected through a ring of wells to form a continuous blanket of foam that surrounds the designated storage volume. This technique would allow for creating storage facilities in aquifers that do not have adequate

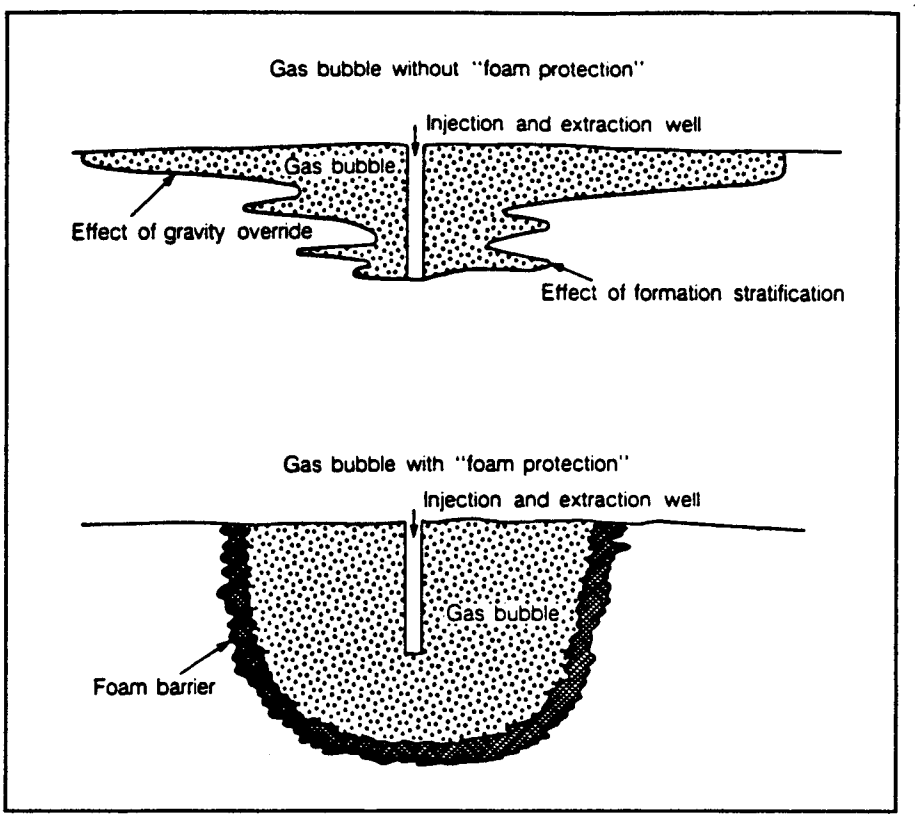

Figure 1. Schematic of gas injection with and without mobility control.

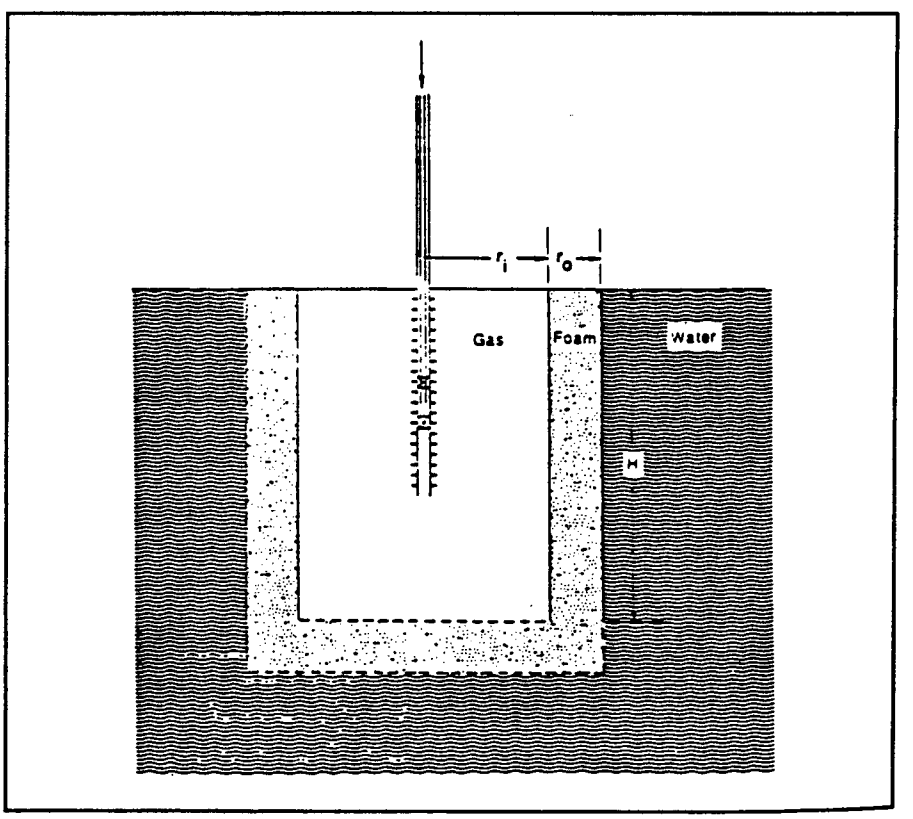

Figure 2. Single well "foam protected" storage facility.

natural closure. The multi-well barrier concept can also be used to lower the "spill point" in an existing storage aquifer, thereby creating a larger storage volume and preventing leakage of gas beyond the designated storage volume. This concept is illustrated in Figure 4.

TECHNOLOGICAL DEVELOPMENT

During an initial survey of the previous studies on the rheological properties and blocking ability of foam, several areas were identified that needed additional development prior to field-scale tests of "foam protected" aquifer gas storage [Radke et al. (1983)]. These include identification of aquifer-brine compatible surfactants; development of stable foams; improved understanding of foam flow and blocking phenomena; and improved techniques for mathematical simulation of foam behavior. Thus far, we have concentrated our efforts on two areas: laboratory studies and development of a mathematical simulation capability. The results of these efforts, which represent the first year of a three-year program, are presented below.

LABORATORY STUDIES OF FOAM PROPERTIES

Foam has been demonstrated to retard or block the flow of gas in porous media. Most of the previous work in this area has been done to evaluate using foam as a driving fluid for enhanced oil recovery. The use of foam to displace oil from porous media was motivated by observations that it has greater viscosity than either its gas or liquid phase. Fried (1961) found that foam drive could displace oil from sandpacks that remained after alternating gas and water drives. In some tests, when foam was injected at constant pressure, the flow rate decreased and flow eventually was blocked.

The ability of foam to completely block gas flow in porous media was demonstrated by Bernard and Holm (1964), who also conducted additional experiments to measure the duration of the period that permeability was reduced. Foam blocks lasted up to 30 days in 30-ft sandpacks. Reduced permeability lasted longer in longer sandpacks and in less permeable sandpacks.

Bernard and Holm (1970) conducted a study to evaluate foam for sealing leaks in gas storage reservoirs. Surfactant solution was injected into a partially saturated sandstone slab through which gas was flowing, simulating efforts to seal a leak. In one trial, the permeability to gas was reduced from 294 to 15 mD and maintained at that level for over 1000 hours, suggesting that foam blockage or at least reduced permeability can be maintained for months in low-permeability rocks.

Albrecht and Marsden (1970) formed foam by injecting gas at constant pressure into a porous medium that was initially saturated with a foamer solution. When foam emerged from the porous medium at apparent steady state, they reduced the gas injection pressure and observed that foam flow stopped. With sandpacks (beach sands, apparently with a narrow particle size range), only a small decrease in injection pressure was needed to block flow, but

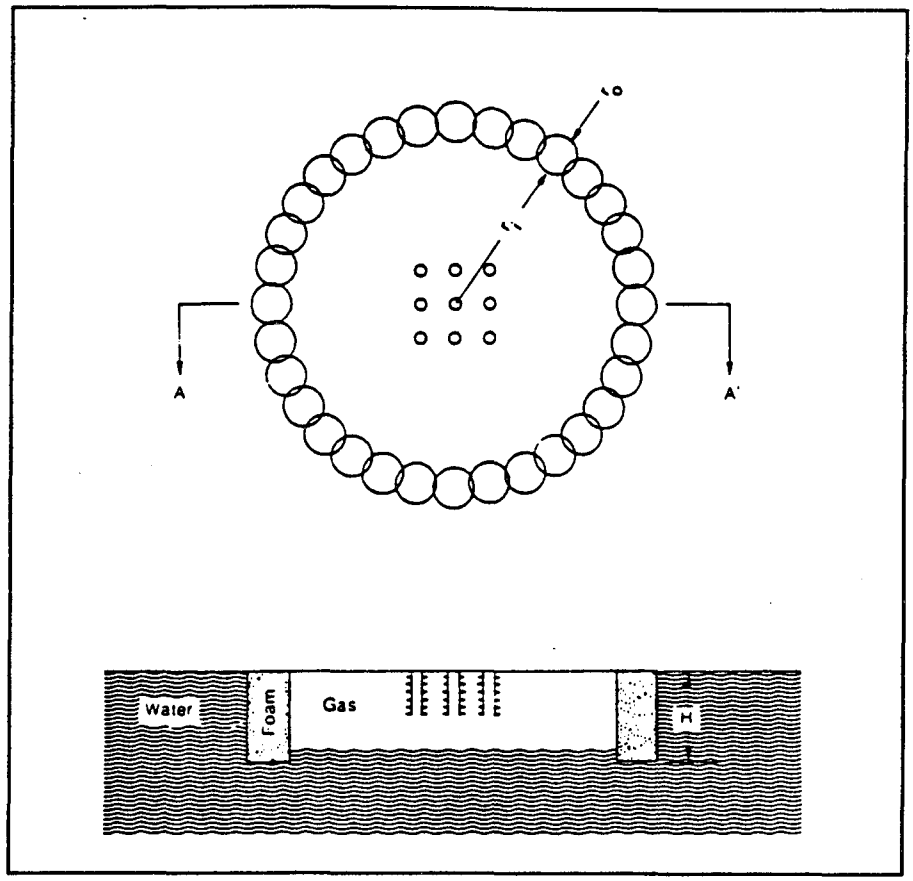

Figure 3. Skirt well "foam protected" storage facility.

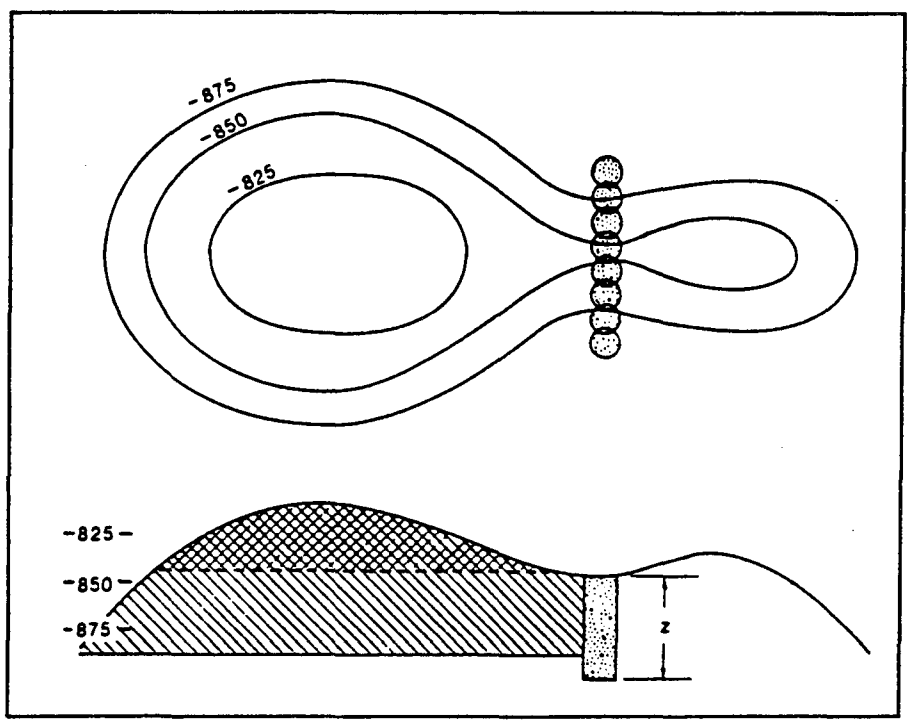

Figure 4. Spill-point lowering with a "foam-barrier."

in sandstones (presumably with a wider range of pore sizes) a larger decrease in injection pressure was needed to stop the flow of foam. No measurements were reported of how long the blocked condition lasted. The proposed mechanism of blocking is that when gas pressure decreases, the bubbles expand in the pores until the pressure gradient needed to push them through the pore throats exceeds the available gradient.

The above-mentioned studies, among others, lead to the conclusion that foam has a good potential for use in aquifer gas storage operations. However, prior to field scale testing, additional investigations are required. During the first year of this research effort, we have concentrated on screening surfactants for aquifer brine compatibility, stabilizing foams with various chemical additives, measuring foam flow behavior, and studying foam blocking. The results of these studies are summarized below.

Surfactant Screening

Brines in gas storage reservoirs commonly have high salinity and hardness. A synthetic brine was used in this work; it contained 5410 mg/L Ca, 1260 mb/L Mg, 66700 mg/L total dissolved solids, and 18750 mg/L as $CaCo_3$ hardness. Four classes of oil field surfactants were screened for brine compatibility: Shell Enordet AOS (alpha olefin sulfonate), AE (alcohol ethoxylate), AES (alcohol ethoxysulfate), and Chevron Chaser (alkylsulfonate) products. Of these, the AOS and Chaser products were eliminated because they formed precipitates with the Ca ions. The AES surfactants were selected for further tests because, being anionic, they were expected to be less susceptible to sorption on reservoir rocks than the nonionic AE surfactants.

Measurement and Enhancement of Foam Stability

Previous work has shown foam stability to be a key element in achieving blocking of gas flow, and foam stability would also be necessary to maintain blocked conditions for a period of months during a gas storage cycle. Foam is a collection of gas bubbles separated by liquid lamellae. Foams decay by liquid drainage, which thins the lamellae; by spontaneous rupture of thinned lamellae; and by pressure-driven diffusion of gas from small bubbles to larger ones.

Foam stability is enhanced by stabilizing the lamellae against spontaneous rupture. Lamellae rupture spontaneously when thin spots, which are ever present due to thermal motion of the molecules, deepen and become holes in the lamella instead of being restored. Lamellae are stabilized against spontaneous rupture by forming a dense, coherent layer of surfactant molecules at the gas-liquid interface. Ionic surfactants align themselves like matchsticks at the gas-liquid interface, with their charged ends penetrating the water. These charged ends repel each other, preventing the formation of a dense, stable surfactant layer. A denser packing of molecules at the interface is possible if a nonionic surfactant is added. The molecules of the nonionic surfactant are hypothesized to pack between the ionic molecules, thus allowing a denser and more stable surfactant layer to form (see Figure 5). The surfactant layers at opposite sides of the lamella are of like charge, so they repel each other, thus preventing the collapse of thin spots.

Nonionic surfactants used for this purpose have included long-chain alcohols [Schick and Fowkes (1957), Sharma et al. (1984)]. We evaluated several series of foamer solutions containing various AES surfactants (1 percent by weight in synthetic brine) and straight-chain alcohols (weight concentrations ranging from 0 to 0.8 percent). These commercially available materials are not single compounds but contain a range of carbon chain lengths, e.g., C_{12} to C_{15}. The carbon chain lengths of the AES molecules and the alcohols were matched as closely as possible.

Foam stability was evaluated by use of a variant of the Ross-Miles pour test, in which a volume of liquid is dropped from a pipette through a specified distance into a graduated cylinder. The volume of foam formed is measured initially and at intervals to determine both the foam-fitting ability of the solution and the stability of the bulk foam formed in the test. This test does not duplicate the survival of foam in a porous medium, but does discriminate among foamer solutions to select those that form stable lamellae (liquid films).

Results of a typical series of tests are shown in Figure 6. Here the surfactant was AES 1213 -6.5S i.e., $CH_3(CH_2)_{11-12}-(O-CH_2CH_2)_{6.5\ av.}-OSO_3^-NA^+$), and the alcohol was Neodol 25 (i.e., $CH_3(CH_2)_{(11-14)}OH$). As shown in Figure 6, without addition of the alcohol, the foam collapsed rapidly, but addition of Neodol 25 up to 0.2 percent increased the stability of the foam markedly. Addition of Neodol 25 beyond this level mainly increased the viscosity of the solution and thereby reduced the volume of foam initially formed in the test. Similar results were obtained with other AES surfactants.

Rheological Properties of Foam in Porous Media

Rheological properties of foam in porous media are needed to design the emplacement of a foam barrier. The apparent viscosity of foam flowing in a sandpack was measured by use of the apparatus shown in Figure 7. For this experiment, a low-stability foam (1 percent Triton X-100 in distilled water) was used, because this reduced the flow history effects and permitted repetition of measurements without excessive waiting for steady-state conditions. The sandpack was Ottawa flint shot 3.0 sand, with a permeability of 92.6 darcy. Gas was injected at a constant pressure and liquid at constant flow rate. The flow rates of gas and liquid were measured by timing and weighing the flow of foam exiting the sandpack into a pre-weighed graduated cylinder. Results of this experiment are shown in Figures 8 and 9. The results in Figure 8 are counterintuitive. Ordinarily, relative permeability relationships require that, at a constant injection pressure, when the flow of one phase is increased, the flow of the other decreases. In the presence of foam, however, as the liquid flow rate was

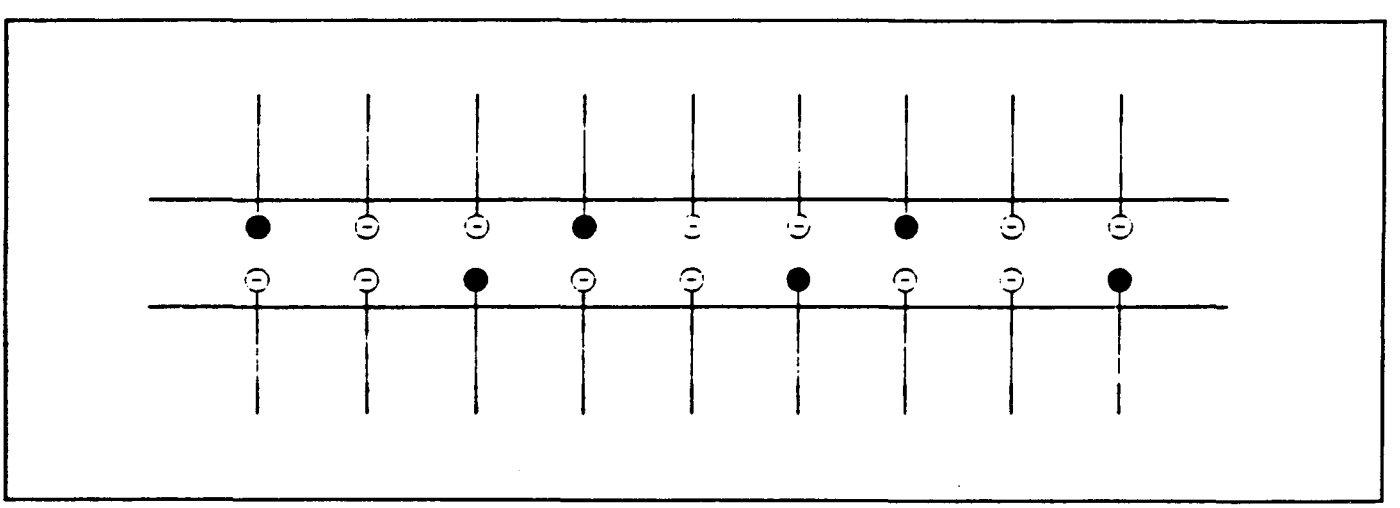

Figure 5. Anionic and nonionic surfactant molecules aligned at opposite gas-liquid interfaces of a lamella.

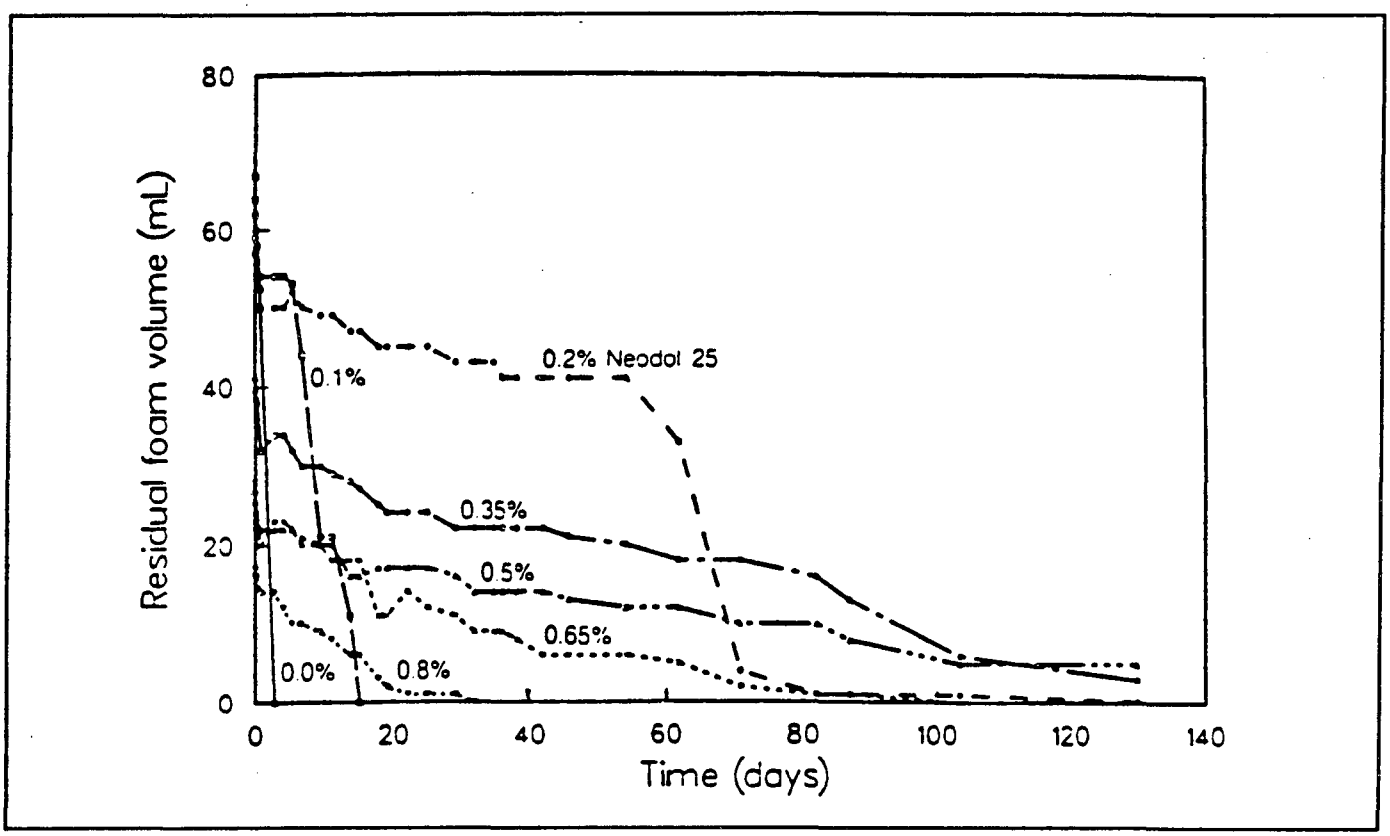

Figure 6. Static foam longevity measured in drop tests, 1 percent Shell Enordet AES 1213-6.5S in synthetic Mt. Simon brine, with varying amounts of Neodol 25.

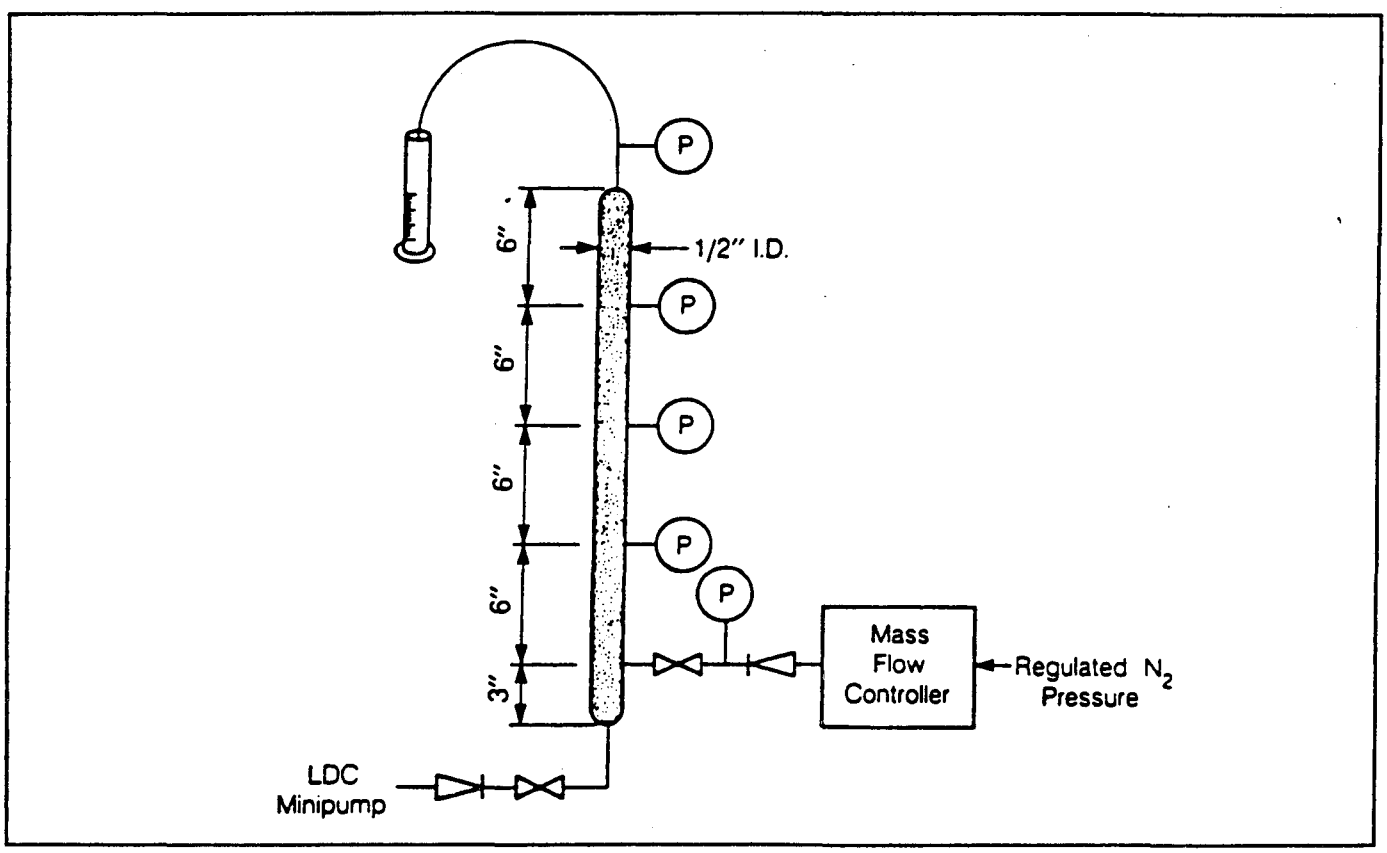

Figure 7. Apparatus for foam rheology study in sandpacks; schematic.

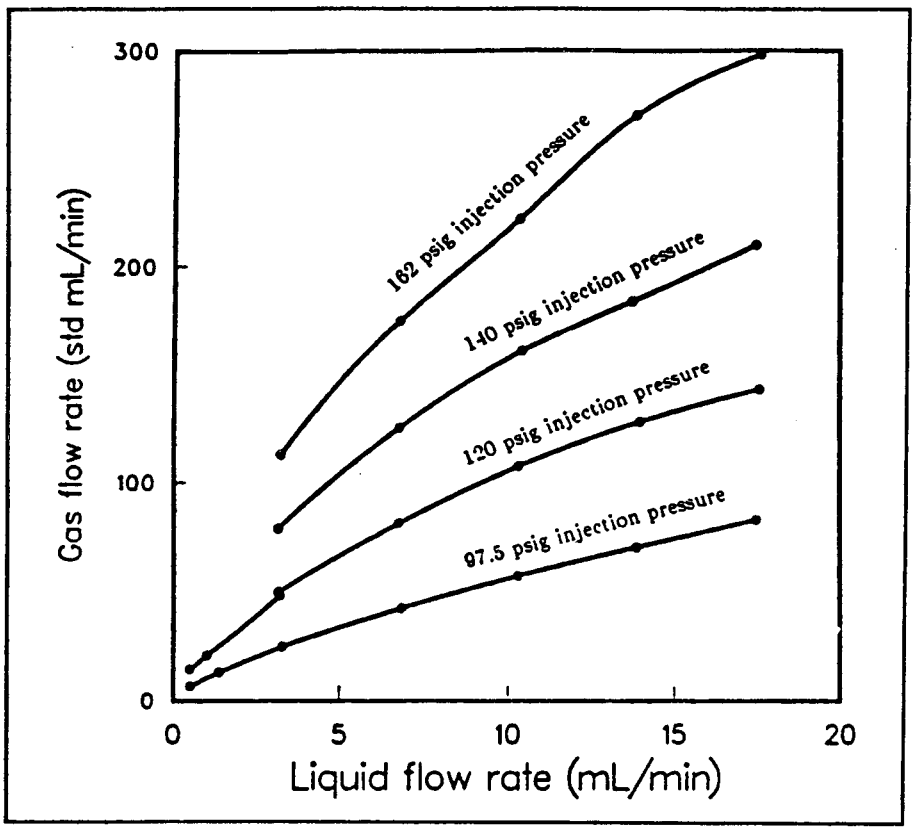

Figure 8. Foam rheology in sandpack. Plot of gas and liquid flow rates; gas injected at controlled pressure and liquid at controlled flow rate.

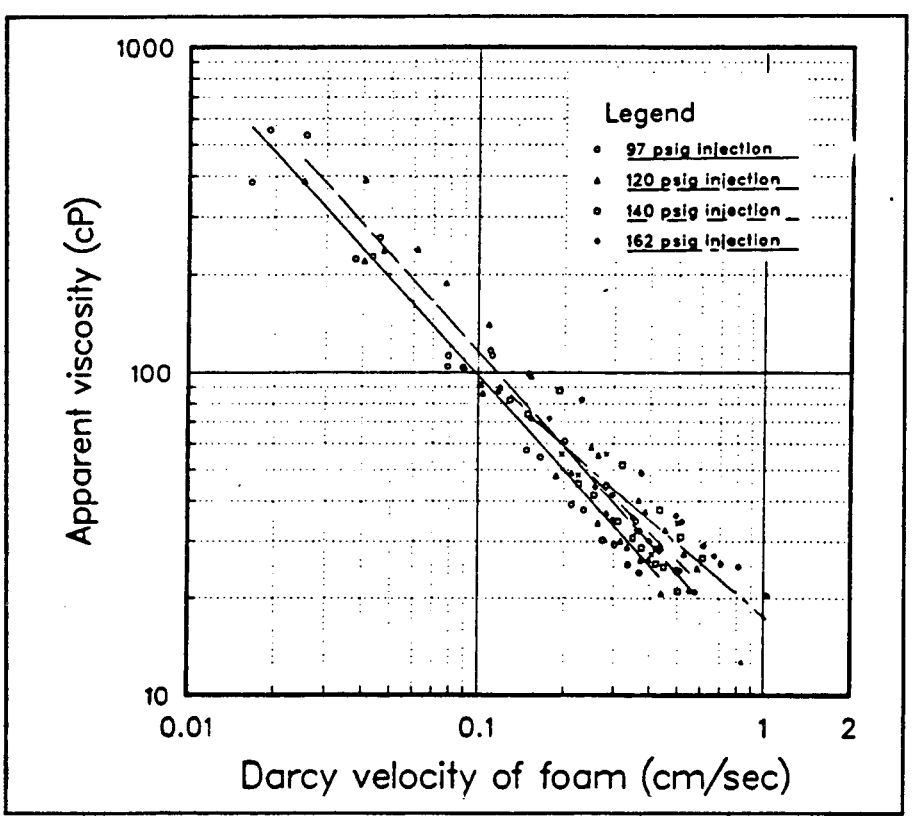

Figure 9. Foam rheology in sandpack. Plot of calculated apparent viscosity against Darcy velocity.

increased, the gas flow rate also increased. The ratio of gas to liquid flow rate was almost completely determined by the gas injection pressure.

The volumetric flow rate of gas varied through the length of the sandpack as the pressure decreased from injection to exit. The sum of the volumetric flow rates of gas and liquid is defined as the volumetric flow rate of foam (also varying through the length of the sandpack), and these data were used with the measured pressures and permeability to calculate the apparent viscosity of foam. The calculated apparent viscosity varied with the foam flow rate as shown in Figure 9. This non-Newtonian flow behavior has been observed for foam both in porous media [Treinen (1985)] and in bulk foams [Fried (1961) and many since; see review by Persoff et al. (1987)]. Description of foam flow in terms of apparent viscosity is a convenience for macroscopic modeling of foam flow in porous media and does not imply that foam flows as foam through pores. Rather, liquid is believed to flow through smaller channels, while gas bubbles separated by liquid lamellae flow through larger pores. No continuous gas phase is believed to exist. The gas bubbles and liquid continually recombine to form the observed foam.

Blockage of Gas Flow by Foam

Laboratory demonstrations of gas flow blocking by foam in sandpacks were conducted to obtain greater understanding of the blocking mechanism and to measure the durability of blocked conditions. For these experiments, a stable foamer solution consisting of 1.0 percent AES 1213-6.5S and 0.2 percent Neodol 25 in brine was used. The apparatus was similar to that shown in Figure 7 but with only one pressure gauge at the inlet. Foam was formed by injecting gas at constant pressure and liquid at constant flow rate. After steady-state conditions were reached, the gas flow was blocked by stopping the liquid flow and rapidly reducing the gas injection pressure from the "injection" pressure to the "holding" pressure. When this was done, flow of foam and gas through the sandpack stopped. Complete blocking of gas flow was obtained in all experiments in which the absolute holding pressure was less than 74 percent of the absolute injection pressure. An explanation of this observed blocking phenomenon is that when the gas injection pressure is reduced, gas bubbles throughout the sandpack expand. Trapped bubbles expand laterally, forming new lamellae, which cut off continuous gas paths, blocking the flow of gas. The duration of the blocked condition in 93 darcy sand was highly variable in these experiments, ranging from less than 1 day to 48 days. Such variability apparently results from the difficulty of reproducing the same conditions at blocking (number and location of lamellae) and the spontaneous rupture of the metastable lamellae, which is a random process.

Previous work has shown that foam blocks last longer in less permeable media, therefore, additional experiments were done using Ottawa F-75 sand, which has a permeability of 20 D. In these experiments the stability of the foam was further enhanced by addition of 0.5 percent guar (Galactasol 253, Henkel Corp., Houston, TX). This increases the viscosity of

the liquid phase, retarding thinning of the lamellae. It is also suspected that the guar strengthens the lamellae by forming a network of gel-like structure in the liquid phase. Two foam blocks have now supported a pressure gradient of 5 psi/ft with no gas flow for 50 and 70 days. A similar test in 93-D flint shot 3.0 sand lasted for 5 days, so the greater longevity of the blocked condition appears to have resulted from the lower permeability of the sand. In less-permeable media, the lamellae that block gas flow are smaller, and smaller lamellae are less vulnerable to spontaneous rupture.

MATHEMATICAL MODELING

Foam is a discontinuous fluid, comprised of gas bubbles separated by thin liquid lamellae. The flow and behavior of foam in permeable media involve complex gas liquid-solid interactions on the pore level. The quantitative aspects of these are incompletely understood at the present time, although considerable progress has been made in recent years. [Hirasaki and Lawson (1985); Falls et al. (1986a,b); Ransohoff and Radke (1986)].

While a detailed pore-level understanding of foam behavior in permeable media would be desirable, it is not necessarily a prerequisite for the formulation of quantitative models for foam flow on a continuum macroscopic scale. We propose to describe the porous flow of gas, water, and foam in a phenomenological way, using established concepts of multi-phase flow [Peaceman (1977)]. In analogy to "black oil" models used in the petroleum industry [Fanchi et al. (1982)] we write mass balances for the gas, water, and foam "components" as follows (symbols defined at end of paper):

$$\frac{d}{dt}\int_{V_n} M^{(\kappa)}dV = \int_{\Gamma_n} \underline{F}^{(\kappa)}\cdot\underline{n}\,d\Gamma + \int_{V_n} q^{(\kappa)}dV \quad (1)$$

where $\kappa = 1 - \text{gas},\ 2 - \text{water},\ 3 - \text{foam}$

The accumulation terms represent the mass of the components preset per unit formation volume and are given by

$$M^{(\kappa)} = \phi \sum_{\beta} S_\beta\, \rho_\beta\, X_\beta^{(\kappa)} \quad (2)$$

The sum in equation 5 extends over all phases, β, and in general the components may be present in more than one phase. However, a reasonable first approximation may be obtained by setting $X_\beta^{(\kappa)} = \delta_{\beta\kappa}$, i.e., by assuming a one-to-one correspondence between components and phases. Mass flux is given by the multi-phase extension of Darcy's law

$$\underline{F}_\beta = -k\frac{k_{r\beta}}{\mu_\beta}\,\rho_\beta\,(\nabla P_\beta - \rho_\beta \underline{g}) \quad (3a)$$

so that

$$\underline{F}^{(\kappa)} = \sum_{\beta} X_\beta^{(\kappa)}\,\underline{F}_\beta \quad (3b)$$

The equations given above are applicable to the simultaneous flow of several phases [in the thermodynamic sense; Lewis and Randall (1961)]. The peculiar flow properties of foam in porous media can be represented by appropriate constitutive relationships. It has been observed experimentally that foam will flow in a porous medium only if the applied pressure gradient exceeds a certain threshold value, the magnitude of which depends on the medium and and the flow history [Albrecht and Marsden (1970)]. Furthermore, the resistance of foam to flow tends to diminish with increasing pressure gradient [or flow velocity; Treinen et al. (1985); Falls et al. (1986b)]. Following the recent work by Hirasaki and Lawson (1985) and Falls et al. (1986b), this effect is represented by an effective viscosity that depends on pressure gradient:

$$\mu = \mu_\infty + \frac{\alpha}{[\max(0, |\nabla P_F| - P_b')]^\beta + \delta} \quad (4)$$

Here μ_∞ is the asymptotic viscosity for large gradients, α and β are rheological constants, and P_b' is the threshold or blocking pressure gradient that must be exceeded for foam to start flowing. δ is a very small number introduced to avoid a singularity in effective viscosity at small gradients. We have expressed effective foam viscosity as a function of pressure gradient rather than flow velocity because this makes it possible to describe the transition from blocked to flowing condition. Our model presently does not account for hysteresis.

The pressure-density relationship for foam has been investigated by Ross (1969), Lord (1981), and Morrison and Ross (1983). Based on this work we use the real gas law to describe foam compressibility

$$PV = ZnRT \quad (5)$$

With suitable dependence of the compressibility factor Z on pressure and temperature, Equation 5 can describe a great variety of fluid behavior. However, it appears that by neglecting all contributions to foam compressibility except for that of the gas, a satisfactory description can be made for a wide range of conditions.

No information is available presently on the relative permeability behavior of gas-water-foam systems. Based on wettability properties of the different phases, one might expect that the relative permeability characteristics of gas-foam flow may be very similar to those of gas-water flow and that foam-water may behave similarly to gas-water. An important issue in multi-phase flow involving foam, which is intimately related to relative permeability as well as capillary pressure effects, is the nature of the displacement process (piston-like versus broad transition zones). If foam displacement is piston-like, as it well may be, special numerical techniques will be needed for an adequate description of the process.

Numerical Model

The governing equations given above are nonlinear and strongly coupled. For purposes of numerical solution we discretize these equations using integral finite differences in space (Narasimhan and Witherspoon, 1976) and first-order finite differences in time. For stability all flux terms are evaluated implicity, and all discretized equations are solved simultaneously using Newton-Raphson iteration. The linear equations arising at each iteration step are solved with a sparse version of LU-decomposition (Duff, 1977).

The numerical model has been applied to aid in the design of the laboratory experiments and for exploratory calculations of foam injection into aquifers. Of major interest are the space- and time-scales that would be involved in the emplacement of foam plumes or banks in a foam-protected gas storage scheme. An important operational constraint for foam injection is that overpressures at the injection well need to be limited to 300–500 psi so that formation fracturing will be avoided. As an example, Figure 10 shows predictions for the growth of a foam plume and the time-dependence of foam injection rate for foam injection at constant pressure of 1800 psi into an aquifer initially at 1500 psi. Problem parameters are given in Table 1, and Figure 11 shows the simulated pressure profile and the pattern of effective foam viscosity after 388.3 days of injection. Additional studies are underway to examine gas storage reservoir performance (injection and production rates and pressures, water coning) in the presence of hypothetical foam banks.

Analytical Model

Simplified versions of the governing flow equations were studied with a view to obtaining approximate analytical solutions in closed form. Such solutions can be useful for showing overall trends, and for verifying complex numerical simulators.

Using a somewhat simplified form for the relationship between effective viscosity and pressure gradient (setting $\mu_\infty = P_b' = \delta = 0$ in Equation (4)), we have applied an integral technique (Ozisik, 1980) to obtain approximate analytical solutions for one-dimensional linear and radial flow of foam (with no other phases present). The pressure solution for constant rate mass injection into a semi-infinite medium with 1-D linear flow is:

$$P(x,t) = P_i + \frac{1}{3}\left(\frac{Q_m\alpha}{Ak\rho_o}\right)^{1/\beta+1}\delta(t)\left(1 - \frac{x}{\delta(t)}\right)^3 \quad (6)$$

The function $\delta(t)$ has the meaning of a pressure disturbance penetration length and is given by

$$\delta(t) = \sqrt{\frac{12Q_m t}{A\phi\rho c}\left(\frac{AK\rho_o}{Q_m\alpha}\right)^{1/\beta+1}} \quad (7)$$

PRELIMINARY ECONOMIC ANALYSIS

We have attempted to carry out a preliminary analysis of the economics of foam-protected gas storage. The benefits should result from the increased recoverability of the total gas in storage, that is, an improvement in the ratio of working gas to base gas. Another possible benefit is the more efficient use of existing storage reservoirs by limiting the migration so as to avoid parts of a structure. To illustrate the possible economic benefits that might be realized, two examples are presented: (a) a foam-protected storage reservoir created by using a ring of "skirt wells" to develop a continuous curtain of foam (see Figure 3), and (b) a storage reservoir with a lowered spill point created by

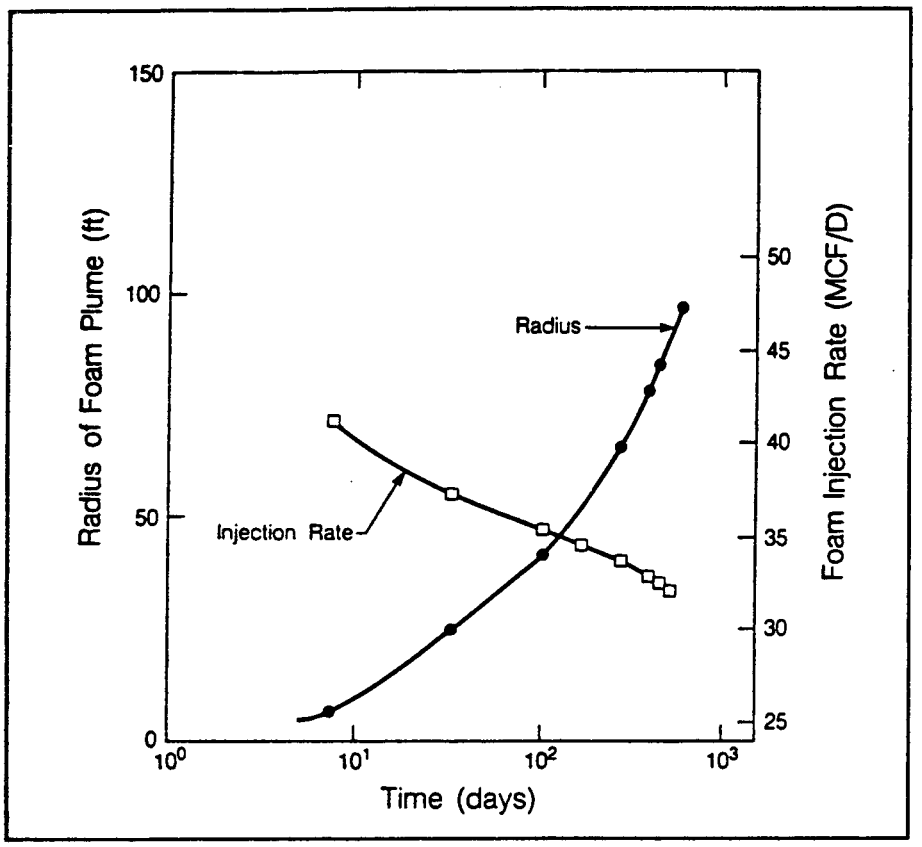

Figure 10. Foam injection rate and the radial distance to the foam "front" as a function of time.

Table 1
Parameters for Foam Injection Problem with 1-D Radial Flow

Aquifer		
	thickness	H = 100 ft
	outer radius	r = 25,000 ft
	porosity	ϕ = 10 %
	permeability	k = 400 md
	formation compressibility	c = 5.e-6 psi^{-1}
	initial pressure	P = 1,500 psi
	initial temperature	T = 86 °F
Well		
	fully penetrating	
	wellbore diameter	d = .667 ft
	skin factor	s = 0
Foam		
	density at standard temperature and pressure	ρ_F = 0.4173 lb/ft^3
	quality at standard temperature and pressure	Q = 99.4% gas by volume
	rheological parameters:	P_b' = 0 psi/ft
		μ_∞ = 20 cp
		α = 110 cp $(psi/ft)^{1/3}$
		β = .333
		δ = 1.e-10 $(psi/ft)^{1/3}$

injecting foam through a line of wells at an intermediate spill point (see Figure 4).

Table 2 summarizes the assumptions that were adopted in developing the economics of a foam protected storage reservoir using "skirt wells." The basic assumption was made that the storage project should be capable of withdrawing 10 Bcf working gas per season, and it was further assumed that this would require 40 Bcf base gas in a conventional aquifer project. Since the costs of wells, pipelines, compressors, etc. will not change significantly, these items can be excluded, and the investment costs were therefore estimated to be $120 million.

By comparison, a foam-protected storage reservoir would be created using 50 wells to form a barrier with an internal diameter of 1500 ft, that is 200 ft wide, and has a vertical height of 300 ft. Since this would create a very large gas volume around the well field, the system should be capable of recovering a much higher fraction of the total gas in storage. We assumed that the base gas requirement could be reduced to 10 Bcf, and on this basis the investment cost for 10 Bcf working gas would be $72.5 million. This is almost $50 million less than the cost of the conventional approach and serves to illustrate the possibilities.

Table 3 summarizes the assumptions that were adopted in expanding the use of a conventional storage aquifer by lowering the spill point by use of a foam barrier as shown in Figure 12. In this case, it is desired to limit the migration of gas past the intermediate spill point at −3110 ft. As is shown in Table 3, conventional use of the structure would be limited to −3080 ft and 28.5 Bcf. If one assumes 20 percent working gas, the seasonal withdrawal would be 5.7 Bcf and would require 40 injection-withdrawal wells.

By comparison, the use of 32 wells to create a foam barrier as shown in Figure 12, could lower the spill point by 50 feet, allowing storage of an additional 43.1 Bcf within the same structure. The greater thickness of the gas-saturated region is assumed to improve the working gas as a percent of total gas from 20 percent to 30 percent. Due to the larger size of storage facility and the increased rate of gas withdrawal, we estimate new costs associated with the lowered spill point facility include a 46 percent increase in the cost of land, injection-withdrawal wells, compressors, pipelines, etc. As a basis of comparison, we have evaluated the cost of storage per Bcf of working gas, for the two cases. As shown in Table 3, lowering the spill point of the structure decreases the cost per Bcf of gas from $18.5 to $10.2 million. An additional benefit from spill point lowering is the possibility of increasing the storage capacity of an existing facility, rather than having to develop new ones.

SUMMARY AND FUTURE WORK

This paper summarizes the results of the first year of a three year research program for evaluating the feasibility of using surfactant-gas foams for improving the efficiency of underground natural gas storage facilities. To date, we have concentrated on investigating the behavior of foam in the laboratory and on developing a suitable mathematical model for simulating a "foam-protected" aquifer gas

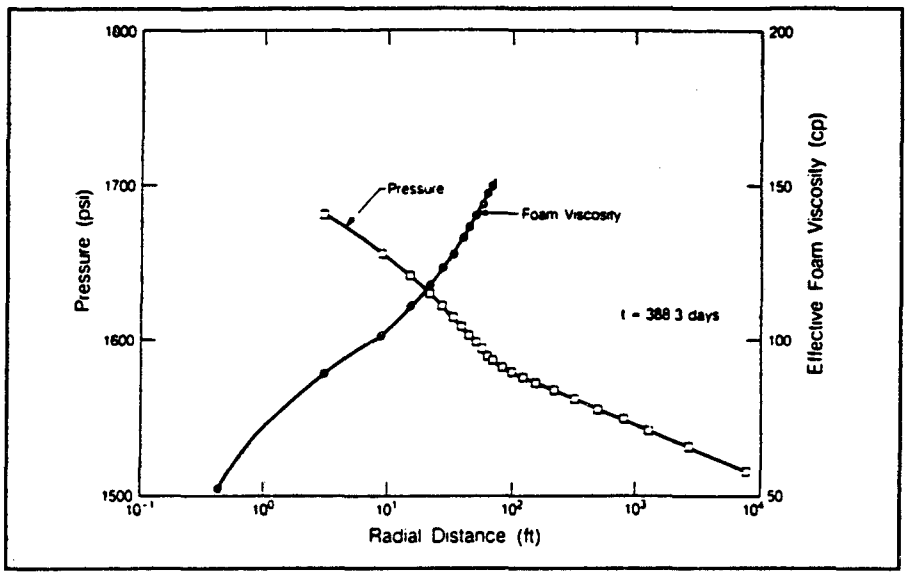

Figure 11. Formation pressure and foam viscosity as a function of distance from the foam injection well.

Table 2
Assumptions and Costs for the Prelimary Economic Comparison Between a 10 Bcf "Foam-Protected" Storage Facility and a Conventional Storage Project

I. CONVENTIONAL STORAGE		
A. Assumptions		
1. Nominal depth	3,000	ft
2. Porosity	11	%
3. Residual water saturation	20	%
4. Storage pressure	1,400	psig
5. Total gas required	50	BCF
6. Cost of gas	$3.00	per MCF
B. Costs Excluding Working Gas		
1. Base gas, 40 BCF	$120.0	M
2. Other costs*		
Total	$120.0	M
II. SKIRT WELL FOAM STORAGE		
A. Assumptions		
1. Nominal depth	3,000	ft
2. Porosity	11	%
3. Residual water saturation	20	%
4. Storage pressure	1,400	psi
5. Total gas required	20	BCF
6. Cost of gas	$3.00	per MCF
7. Skirt thickness	200	ft
8. Skirt height	300	ft
9. Skirt inner radius	1500	ft
10. Foam quality	90	% gas
11. Surfactant concentration	1	%
12. Cost surfactant	$2.00	per pound
13. Cost per well	$400	K
14. Well spacing	200	ft
B. Costs Excluding Working Gas		
1. Base gas, 10 BCF	$30.0	M
2. Foam gas, 5.3 BCF	15.9	
3. Surfactant, 3.3 M pounds	6.6	
4. Skirt wells, 50	20.0	
5. Other costs*		
Total	$72.5	M

Note: * Costs of land, injection-withdrawal wells, compressors, pipelines, etc. assumed to be approximately the same for either method.

storage operation. During the second year of this project, we will conduct a series of laboratory experiments to study the behavior of foam in a typical aquifer sandstone, at realistic aquifer pressures. These data, along with mathematical predictions of the dynamics of the foam emplacement process, will allow us to design a suitable demonstration project, where one or more of the "storage concepts" can be tested. During the final year of the project, after choosing a suitable field test site, we plan to carry out a field demonstration.

ACKNOWLEDGMENT

This work was supported through U.S. Department of Energy Contract No. DE-AC03-76SF00098 by the Gas Research Institute, Chicago, Illinois.

NOMENCLATURE

A	Area (L^2)
c	Total compressibility (LT^2/M)
d	Well diameter (L)
$\underline{F}_\beta$	Mass flux of β-phase (β-gas, water or foam)
$\underline{g}$	Acceleration of gravity (L/T^2)
H	Formation thickness (L)
k	Absolute permeability (L^2)
$M^{(x)}$	Mass of x component (x = gas, water or foam) present per unit formation volume (M/L^3)
n	Number of moles
$\underline{n}$	Normal inward unit vector
P	Pressure (M/LT^2)
P_b'	Blocking pressure gradient (M/L^2T^2)
q	Source rate (M/L^3T)
Q	Foam quality (gas volume/foam volume)
Q_m	Foam mass injection rate (M/T)
q	source rate (M/L^3T)
r	Radial distance (L)
R	Universal gas constant
S	Saturation
t	Time (T)
T	Temperature (°K)
V	Volume (L^3)
x	Length coordinate (L)
$X_\beta^{(x)}$	Mass fraction of component x in phase β
Z	Compressibility factor
α	Rheological constant of foam $[(M/L^2T^2)^\beta]$
β	Rheological exponent of foam
δ	Small number
$\delta(t)$	Pressure disturbance penetration length (L)
$\delta_{\beta x}$	1 if $\beta = x$; O if $\beta \neq x$
μ	Viscosity (M/LT)
μ_∞	Foam viscosity at large pressure gradient (M/LT)
ρ	Mass density (M/L^3)
ϕ	Porosity
Γ_n	Surface of volume element n

Subscripts:

F	foam
i	Initial
m	Mass

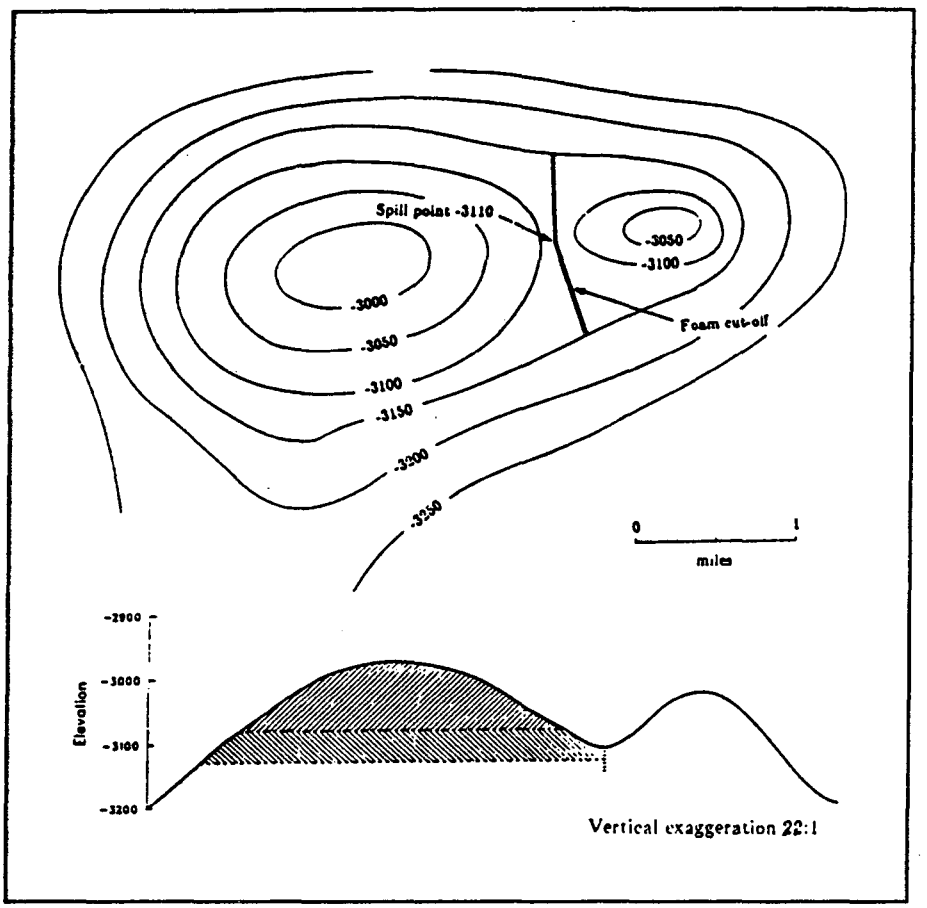

Figure 12. A schematic of the dome structure used for economic analysis of the spill-point lowering concept.

22. Sharma, M. K., D. O. Shah, and W. E. Brigham, "Correlation of chain length compatibility and surface properties of mixed foaming agents with fluid displacement efficiency and effective air mobility in porous media, *I&EC Fundamentals, 23,* pp. 213–220, 1984.
23. Treinen, R. J., W. E. Brigham, and L. M. Castanier, Apparent Viscosity Measurements of Surfactant Foam in Porous Media, Stanford Petroleum Research Institute, Report SUPRI TR–48, October 1985.

Table 3
Data, Assumptions, and Costs for the Preliminary Economic Comparison Between a Conventional Project and One With a Foam-Blocked Spill Point

CONVENTIONAL STORAGE		
A. Assumptions		
1. Surface elevation	620	ft above MSL
2. Depth	3080	ft below MSL
3. Porosity	11	%
4. Residual water saturation	20	%
5. Storage pressure	1600	psig
6. Total gas	28.5	BCF
7. Working gas, 20%	5.7	BCF
B. Costs Excluding Working Gas		
1. Base gas, 22.8 BCF	$68.4	M
2. Other costs *	37.5	
Total cost	$105.9	
Total cost per BCF working gas	$ 18.5	M
LOWERED SPILL POINT		
A. Assumptions		
1. Depth	3130	
2. Porosity	11	%
3. Residual water saturation	20	%
4. Storage pressure	1600	psig
5. Total gas	71.6	BCF
6. Working gas, 30%	21.5	BCF
7. Cut off dimensions (ft) L × W × H	6400 × 200 × 25 ave.	
8. Foam quality	90	% gas
9. Surfactant concentration	1	%
10. Cost of surfactant	$2	per pound
11. Cost per well	$400	K
12. Well spacing	200	ft
B. Costs Excluding Working Gas		
1. Base gas, 50.1 BCF	$150.3	M
2. Surfactant, 0.17 Million lb	0.3	
3. Cut-off wells, 32	12.8	
4. Foam gas, 0.36 BCF	1.1	
5. Other costs *	54.6	
Total cost	$219.1	M
Total cost per BCF working gas	$10.2	M

* Costs of land, injection-withdrawal wells, compressors, pipelines increased 46% to allow for increased area and increased withdrawal rate.

n For volume element n
o Standard temperature and pressure
r Relative
β Phase (gas, water or foam)

Superscript:

x Component (1-gas, 2-water, 3-foam)

REFERENCES

1. Albrecht, R. A., and S. S. Marsden, "Foams as Blocking Agents in Porous Media," *Soc. Pet. Eng. J., 51*, March 1970.
2. Bernard, G. G., Method for the subterranean storage of gas, U.S. Patent No. 3,330,352, issued July 11, 1967.
3. Bernard, G. G., and L. W. Holm, "Effect of foam on permeability of porous media to gas," *Soc. of Pet. Eng. J.*, September 1964.
4. Bernard, G. G., and L. W. Holm, "Model study of foam as a sealant for leaks in gas storage reservoirs," *Soc. of Pet. Eng. J.*, pp. 9-16, March 1970.
5. Duff, I. S., MA28- A Set of FORTRAN Subroutines for Sparse Unsymmetric Linear Equations, AERE Harwell report R 8730, July 1977.
6. Falls, A. H., P. A. Gauglitz,, G. J. Hirasaki, D. D. Miller, T. W. Patzek, and J. Ratulowski, "Development of a Mechanistic Foam Simulator: The Population Balance and Generation by Snap-Off," paper SPE-14961, presented at SPE/DOE Enhanced Oil Recovery Symposium, Tulsa, OK, April 1986a.
7. Falls, A. H., J. J. Musters, and J. Ratulowski, "The Apparent Viscosity of Foams in Homogeneous Bead Packs," submitted to *Soc. Pet. Eng. J.*, 1986b.
8. Fanchi, J. R., K. J. Harpole, and S. W. Bujnowski, BOAST: A Three-Dimensional, Three-Phase Black Oil Applied Simulation Tool. Volume 1: Technical Description and Fortran Code, report DE 83-000529, National Technical Information Service, Springfield, VA, 1982.
9. Fried, A. N., "The foam-drive process for increasing the recovery of oil," U.S. Dept. Interior, Bureau of Mines, RI-5866, 1961.
10. Hirasaki, G. J., and J. B. Lawson, "Mechanisms of Foam Flow in Porous Media: Apparent Viscosity in Smooth Capillaries," *Soc. Pet. Eng. J.*, pp. 176-190, April 1985.
11. Lewis, G. N., and M. Randall, *Thermodynamics*, McGraw-Hill, New York, 1961.
12. Lord, D. L., "Analysis of Dynamic and Static Foam Behavior," *J. Petr. Tech.*, pp. 39-45, January 1981.
13. Morrison, I. D., and S. Ross, "The Equation of State of a Foam," *J. Coll. and Interf. Sci., 95*, No. 1, pp. 97-101, September 1983.
14. Narasimhan, T. N., and P. A. Witherspoon, "An Integrated Finite Difference Method for Analyzing Fluid Flow in Porous Media," *Water Res. Res., 12*, No. 1, pp. 57-64, 1976.
15. Ozisik, M. N. *Heat Conduction*, John Wiley & Sons, New York, 1980.
16. Peaceman, D. W., *Fundamentals of Numerical Reservoir Simulation*, Elsevier, New York, 1977.
17. Persoff, P., Y. S. Wu, S. M. Benson, C. J. Radke, K. Pruess, and P. A. Witherspoon, Feasibility Analysis and Development of Foam-Protected Underground Natural Gas Storage: Part I: Literature Survey. Task Report to Gas Research Institute under GRI contract no. 5086-271-1160, Lawrence Berkeley Laboratory, 1987.
18. Radke, C., P. A. Witherspoon, and M. S. King, Foam-Protected Natural-Gas Storage Reservoirs, Proceedings of the Second Underground Storage Session, American Gas Association Transmission Conference, Seattle, Washington, May 2-4, 1983.
19. Ransohoff, T. C., and C. J. Radke, "Mechanisms of Foam Generation in Glass Bead Packs," paper SPE-15441, presented at the 61st Annual Meeting of the Society of Petroleum Engineers, New Orleans, LA, October 1986.
20. Ross, S., "Bubbles and Foam: New General Law" in *Chemistry and Physics of Interfaces-II*, American Chemical Society Publications, pp. 15-25, Washington, D.C. 1971.
21. Schick, M. J., and F. M. Fowkes, "Foam stabilizing additives for synthetic detergents. Interaction of additives and detergents in mixed micelles," *J. Phys. Chem.*, Vol. 61, pp. 1062-1068, 1957.

Appendix D.

On PVT-Data, Well Treatment, and Preparation of Input Data for an Isothermal Gas-Water-Foam Version of MULKOM

LBL-25783
UC-403

On PVT - Data, Well Treatment, and Preparation of Input Data for an Isothermal Gas - Water - Foam Version of MULKOM

by K. Pruess and Y. S. Wu

Earth Sciences Division
Lawrence Berkeley Laboratory
University of California
Berkeley, California 94720

Prepared for Gas Research Institute
GRI Contract Number 5086-271-1160

Yusuf A. Shikari, Senior Project Manager

August 1988

Table of Contents

Introduction D7
PVT Treatment D9
Well Treatment D15
Input Formats D19
Acknowledgements D36
References D37
Appendix A: Mass and Energy Balances D39
Appendix B: Space and Time Discretization D41
Tables D44
Figures D45

Introduction

MULKOM is a multi-dimensional numerical model for simulating the coupled mass and heat transport of multiphase fluids in permeable media. Originally developed for geothermal reservoir simulation, MULKOM features a modular architecture (Fig. 1) which facilitates applications to a variety of flow systems of interest in subsurface resource recovery and storage. Table 1 lists presently available fluid property modules.

Because of the diverse research applications in the engineering of geothermal, oil, and gas reservoirs, as well as in the geologic isolation of nuclear wastes, and in groundwater contamination problems, MULKOM has proliferated into different versions with special features, limited compatibility, and generally sketchy documentation. The notes assembled in this report are intended to assist in applications of a particular version of MULKOM adapted for isothermal flow of gas-water-foam mixtures. Not all of these three phases need be present; for example, systems containing only gas and water may be simulated by setting foam saturation (volume fraction of foam) to a very small value. It is emphasized that the version of MULKOM described here is under continuing development; the chief shortcoming at the present time being the treatment of foam as an indestructible phase, rather than as an emulsion of gas and surfactant solution with texture changing in response to flow.

The section on PVT treatment highlights the correlations used to calculate thermophysical properties of the foam and gas phases, and gives detailed specifications of the relative permeability treatment used. The section on well treatment describes the formulation for production and injection wells with multi-layer completions operating under combined rate and pressure constraints. Subsequently, a detailed description of

input formats for specifying simulation problems is given. The appendices include statements of the governing equations for multiphase flow solved by the MULKOM simulator in continuum as well as in discretized form.

The information in these notes is not meant as a "stand alone"; it is to be used in conjunction with the TOUGH User's Guide (Pruess, 1987), which documents a particular version of MULKOM for nonisothermal flow of water-air mixtures (saturated-unsaturated flow), and with a recent report (Pruess, 1988) on the overall design and governing equations of MULKOM. Interested users are cautioned that familiarity with the source code is required for meaningful applications of MULKOM.

PVT - TREATMENT

The treatment of thermophysical properties for gas and water is similar to that used in other versions of the MULKOM and TOUGH simulators (Pruess, 1983, 1987, 1988). Special provisions are made to take into account the effects of pressure gradients upon effective foam viscosity and to handle foam relative permeability.

Water Phase

There are no provisions for user-input water properties, as all thermophysical properties of liquid water are computed, within experimental accuracy, from the steam table equations as given by the International Formulation Committee (1967).

Foam Phase

Foam is not a "phase" in the thermodynamic sense. It is a discontinuous fluid, comprised of gas bubbles separated by thin liquid lamellae. We treat foam in a phenomenological way, using conventional concepts of multi-phase flow of continua. At the present time no provisions are made to account for generation or destruction of foam in the porous medium. It is treated as a phase distinct from gas and water which obeys a separate conservation law.

1. Equation of State

The pressure dependence of foam density is parametrized with the real gas law (Ross, 1971),

$$\rho_f = \frac{P_f M_f}{Z_f RT} \tag{1}$$

Here ρ_f, P_f, M_f, and Z_f are, respectively, the effective density, pressure, molar weight and compressibility factor of the foam phase. R is the universal gas constant, and T is temperature. M_f is defined as:

$$M_f = \frac{1}{\frac{W_f}{M_g} + \frac{1 - W_f}{M_l}} \tag{2}$$

where M_g and M_l are, respectively, the molar weights of the gaseous and liquid phases making up the foam. W_f is the foam mass quality, i.e., the mass fraction of gas in the foam phase. It is defined in terms of the gas and liquid masses per unit volume of foam, m_g and m_l, as follows

$$W_f = \frac{m_g}{m_g + m_l} \tag{3}$$

Applying the real gas law to the gas phase inside the foam bubbles, and neglecting contributions from liquid compressibility and from surface effects, the foam compressibility factor Z_f in (1) can be expressed as (Lord, 1981)

$$Z_f = M_f P_f Z_g \left[W_f + (1 - W_f) \frac{\rho_g}{\rho_l}\right] / M_g P_g \tag{4}$$

Values for the foam compressibility factor Z_f can either be supplied from tabular input data obtained from laboratory experiments, or default values calculated internally from Equation (4) can be used.

2. Capillary Pressure

Capillary pressure between water and foam phases is defined as:

$$P_{cwf} = P_f - P_w = f(S_w, S_f) \tag{5}$$

being a function of water saturation S_w and foam saturation S_f, (no hysteresis), which is obtained by interpolation from user-supplied input data.

3. Viscosity

Effective foam viscosity is represented as a function of pressure gradient as follows:

$$\mu_f = \mu_\infty + \frac{\alpha}{[\max(0, |\nabla P_f| - P_b')]^\beta + \delta} \tag{6}$$

where μ_∞ is the asymptotic viscosity for large presure gradient. α and β are rheological constants of foam, to be supplied from measured data and P_b' is the threshold or blocking pressure gradient which must be exceeded before foam begins to flow. δ is a very small number (10^{-10}) introduced to avoid a singularity in effective viscosity for numerical calculations at small pressure gradient.

Gas Phase

The gas phase consists of methane and is assumed to obey the real gas law.

$$\rho_g = \frac{P_g M_g}{Z_g RT} \tag{7}$$

The gas compressibility factor Z_g is calculated internally as function of presure and temperature, based on tabulated properties of methane, (Vargaftik, 1975)

$$Z_g = Z_g\ (T, P_g) \tag{8}$$

Capillary pressure between water and gas phases

$$P_{cwg} = P_g - P_w = f(S_g) \tag{9}$$

is a single-valued function of gas saturation, (no hysteresis), which is obtained by interpolation from user-supplied input data or by the internal formulation of Leveretts' function [TOUGH User's Guide, Pruess (1987)]. Viscosity is calculated internally as function of temperature and pressure, using interpolation from tabulated data for

methane (Vargaftik, 1975)

$$\mu_g = \mu_g(T, P_g) \tag{10}$$

Relative Permeability

It is assumed that all three phases (gas, foam, and water) are present in all volume elements at all times. When dealing with two-phase flow problems of gas-water, foam-water, or gas-foam flow, a very small value is specified for the saturation of the absent phase ($S = 10^{-5}$).

To prevent any of the three phases from disappearing, relative permeabilities are interpolated to zero at small values of saturation (see Figure 2). The following formulation is used.

When $S_\beta \leq S_{cut2}$ (β = gas, liquid, foam),

$$k_{r\beta} = \begin{cases} k^*_{r\beta} + (S_\beta - S_{cut2})/(S_{cut2} - S_{cut1})\, k^*_{r\beta} & \text{for } S_\beta \geq S_{cut1} \\ 0 & \text{for } S_\beta < S_{cut1} \end{cases} \tag{11}$$

The parameters S_{cut1} and S_{cut2} are taken as 5×10^{-6} and 10^{-5}, respectively. Water and gas relative permeabilities for water-gas two-phase flow are obtained as single-valued functions of water and gas saturation, respectively, by interpolating from user-supplied input data:

$$k_{rw} = k_{rw}(S_w) \tag{12}$$

$$k_{rg} = k_{rg}(S_g) \tag{13}$$

As an alternative, analytical expressions given by Fatt and Klikoff (1959) can be used. When dealing with three-phase flow, we have two options for foam relative permeability. One is to use Stone's second method (Stone, 1973) with the renormalization of Aziz and Settari (1979). The other is a sharp-front tracking technique which is discussed in the next section. For the former, foam relative permeability is specified in the foam-water and foam-gas two-phase systems:

$$k_{rfw} = k_{rfw}(S_w) \tag{14}$$

$$k_{rfg} = k_{rfg}(S_g) \tag{15}$$

Then foam relative permeability in three-phase conditions is:

$$k_{rf} = k_{rfcw} \left[\left(\frac{k_{rfw}}{k_{rfcw}} + k_{rw} \right) \left(\frac{k_{rfg}}{k_{rfcw}} + k_{rg} \right) - (k_{rw} + k_{rg}) \right] \tag{16}$$

where k_{rfcw} is (two-phase) foam relative permeability at connate water saturation.

Treatment of Sharp Displacement Fronts

In order to model sharp fronts which may arise at gas-foam or foam-water interfaces, an optional front-tracking technique is available for one-dimensional flow, in which a suitable adjustment of relative permeabilities is performed to maintain the moving gas-foam or foam-water interfaces sharp. The relative permeabilities are considered as functions not only of saturations at the node, but also of those at the upstream and downstream nodes:

$$k_{rf} = k_{rf}(S_f, S_{up}, S_{down}) \tag{17}$$

$$k_{rw} = k_{rw}(S_w, S_{up}, S_{down}) \tag{18}$$

$$k_{rg} = k_{rg}(S_g, S_{up}, S_{down}) \tag{19}$$

Consider a process in which a foam bank is driven by gas to displace water. The foam-water interface is identified by $S_{f,\,up} \approx 1$ and $S_{w,\,down} \approx 1$. (For the "sharp interface" option irreducible saturations are ignored. If necessary, non-zero irreducible saturations can be accounted for by a suitable adjustment in porosity.) At the grid block boundary downstream from the foam-water interface relative permeability to water should be reduced and foam relative permeability should become non-zero only when upstream foam saturation approaches 1. The gas-foam interface is identified by $S_{g,up} \approx 1$ and $S_{f,\,down} \approx 1$. At the grid block boundary downstream from this interface, only foam can flow until gas saturation in the upstream node approaches 1.

The "sharp front " constraints on phase mobilities are implemented by means of appropriate relative permeability functions. We introduce two parameters, S_1 and S_2 ($S_2 > S_1$), which typically are of order 0.01. The relative permeability at the grid block boundary downstream from the sharp front is then varied from 0 to 1 as the saturation of the invading phase in the upstream block increases from 1 - S_2 to 1 - S_1. Denoting the relative permeability of the invading phase by $k_{r,in}$, we perform a linear interpolation as follows.

$$k_{r,in} = \begin{cases} 0 & S_{in,up} \leq 1-S_2 \\ [S_{in,up} - (1-S_2)]/(S_2-S_1) & 1-S_2 < S_{in,up} < 1-S_1 \\ 1 & S_{in,up} > 1-S_1 \end{cases} \tag{20}$$

The relative permeability of the displaced phase, denoted by $k_{r,dis}$, is simply given by

$$k_{r,dis} = 1 - k_{r,in} \tag{21}$$

The "sharp front" treatment can be applied at grid block boundaries where foam is either the invading phase (sweeping the upstream block) or the displaced phase (being swept from the downstream block).

WELL TREATMENT

The code does not contain a separate wellbore model which would permit modeling of the flow in the tubing between wellhead and sandface. Therefore, wells must be represented in terms of sandface conditions, such as pressure or flow rate from production wells (sinks), and flow rate or injection pressure for injection wells of gas, foam or water. Well operating conditions can be time-dependent, i.e., wells can be injected into, produced from, or shut in according to arbitrary user-specified schedules.

Production Wells

The code allows production wells to produce on deliverability by producing against a specified bottomhole pressure or under water or gas rate constraints. For specified bottomhole pressure P_{wb}, the mass production rate for a well from grid layer l is expressed as (Fanchi, et al., 1982):

$$q_l = (PI)_l \sum_{\beta=1}^{NPH} \left(\frac{k_\beta \rho_\beta}{\mu_\beta}\right)_l (P_l - P_{wb} - f_l) \tag{22}$$

where $(PI)_l$ is the the well productivity index in layer l; P_l is the pressure in the well grid block; f_l is a gravity correction for the flowing wellbore pressure; and β is a phase index (β = 1: gas; 2: water; 3: foam). For a pseudo-steady state radial flow, the productivity index is given by (Coats, 1977):

$$(PI)_l = \frac{2\pi\,(k\Delta Z)_l}{\ln\left(\frac{r_e}{r_w}\right) + s - 1/2} \tag{23}$$

where $(k\Delta Z)_l$ is the permeability-thickness product in layer l; r_e is well grid block radius; r_w is well radius; and s is the van Everdingen skin factor. If the well is producing from a grid block which does not have cylindrical shape, an approximate productivity index can be computed by using an effective radius

$$r_e = \sqrt{A/\pi} \tag{24}$$

The gravity correction f_l in the rate expression (22) is obtained as follows (Pruess, 1987). Assume the production well is open from layer $l = 1$ (bottom) to $l = L$ (top). The gravity correction in layer l, f_l, is then calculated from the gravity correction in layer $l + 1$ immediately above it by means of the following recursion formula:

$$f_l = f_{l+1} + \frac{g}{2} (\rho_l^f \, \Delta Z_l + \rho_{l+1}^f \, \Delta Z_{l+1}) \tag{25}$$

where ρ_l^f is the flowing density in the tubing opposite layer l. The gravity correction vanishes in the top layer, i.e., $f_L = 0$. Flowing densities ρ_l^f are computed using a phase volume-weighting procedure. If wellbore pressure were zero, we would obtain the following volumetric flow rate of phase β from layer l:

$$r_{l,\beta} = \left(\frac{k_\beta}{\mu_\beta}\right)_l (PI)_l \, P_l \tag{26}$$

The total volumetric flow rate of phase β opposite layer l is, at zero wellbore pressure:

$$r_{l,\beta}^T = \sum_{m=1}^{l} r_{l,\beta} \tag{27}$$

Then flowing densities are obtained from the following approximate expression:

$$\rho_l^f = \frac{\sum_{\beta=1}^{NPH} \rho_{l,\beta} \, r_{l,\beta}^T}{\sum_{\beta=1}^{NPH} r_{l,\beta}^T} \tag{28}$$

It is possible to specify target rates (constraints) on water-production or gas production. If either target production is specified, the code computes a flowing wellbore pressure opposite the topmost open layer:

$$P_{wbc} = \frac{-Q_{con} + \sum_l (PI)_l \left(\frac{k_\beta \rho_\beta}{\mu_\beta}\right)_l \left(\frac{P_l - f_l}{\rho_\beta^o}\right)}{\sum_l (PI)_l \left(\frac{k_\beta \rho_\beta}{\mu_\beta}\right)_l \frac{1}{\rho_\beta^o}} \tag{29}$$

where phase β is water or gas according to which rate constraint is in effect; Q_{con} is the target rate; ρ_β^o is the density of phase β at standard conditions. After obtaining the

wellbore pressure P_{wbc} from (29) for a rate constraint, the code compares it to the input minimum flowing wellbore pressure P_{wb}. If $P_{wbc} > P_{wb}$ the well is able to deliver the target rate(s), and P_{wbc} is used as flowing bottomhole pressure in (22). For $P_{wbc}<P_{wb}$ the target rate(s) cannot be achieved, and the well is placed on deliverability with bottomhole pressure P_{wb}. The code has the capability to switch from rate to pressure constraints (or vice versa) in the course of a simulation, as required in response to changing reservoir conditions.

Injection Wells

The treatment for injection wells is similar to that for production wells, except that no gravity correction is made for flowing wellbore pressure. For specified injection pressure P_{in}, the mass rate of injection of phase β (β = gas, water or foam) into layer l is given by:

$$W_l = (WI)_l \; \rho_l \; (P_{in} - P_l) \sum_{\beta=1}^{NPH} \left(\frac{k_\beta}{\mu_\beta}\right)_l \tag{30}$$

where the injectivity index $(WI)_l$ is defined exactly like the productivity index $(PI)_l$. Note that the fluid mobility for injection is based on total mobility of all phases, as is customary when injecting into multi-phase systems (Fanchi et al., 1982). ρ_l is the density of injected fluid at reservoir conditions. When injecting foam, a viscosity corresponding to the largest velocity is used in (30). When a target injection rate is specified, a flowing injection wellbore pressure is calculated as:

$$P_{in,c} = \frac{W_o + \sum_l (WI)_l \rho_l P_l \sum_\beta \left(\frac{k_\beta}{\mu_\beta}\right)_l}{\sum_l (WI)_l \rho_l \sum_\beta \left(\frac{k_\beta}{\mu_\beta}\right)_l} \tag{31}$$

where W_o is the specified target mass injection rate. If $P_{in,c} > P_{in}$ the target rate cannot be achieved, and a rate will be calculated from (30) for injection pressure P_{in}. For $P_{in,c} \leq P_{in}$ the target rate can be achieved, and injection pressure is equal to $P_{in,c}$. As in the case of production wells, the code has a capability to switch from pressure to rate

constraint (or vice versa) in the course of a simulation.

All well equations given above are coded fully implicitly in the program, except for the gravity correction equation (25), which is obtained just once at the beginning of each time step. All derivative terms arising from the well equations are taken into account in the Jacobian matrix. The rate constraints are embedded in the source terms, so that they are automatically satisfied when solving the mass-balance equations.

INPUT FORMATS

The blocks ROCKS, ELEME, CONNE, GENER, and INCON can have a variable number of records, depending upon how many items the user wishes to specify. The end of these variable-length blocks is indicated with a blank record. (For CONNE, GENER, and INCON it is possible to have, instead of the blank record, a record with "+++" written in columns 1-3, followed by some element and source cross-referencing information in the case of CONNE and GENER, and followed by restart-information in the case of INCON; see below.)

We shall now explain the records and variables in detail.

All the input and output can be specified either in standard metric units, or in field units.

TITLE

is the first record of the deck, containing a header of up to 80 characters, to be printed on every page of output. This can be used to identify a problem. If no header is desired, leave this record blank.

ROCKS

introduces material parameters and initial conditions for up to 27 different reservoir domains

Record ROCKS.1

Format (A5, I3, I2, 5E10.4)

MAT, NADF, NAD, DM, POR, (PER(I) I = 1,3)

MAT material (domain) name.

NADF sequence number of relative permeability and capillary pressure function.

NAD = 0: will only read one data record per domain.

1: will read one additional record per domain with pore compressibility.

2: will read another record per domain with initial conditions.

DM rock grain density; lb/cuft (kg/m^3).

POR default porosity (void fraction) for all grid blocks belonging to domain "MAT", for which no other porosity has been specified in block INCON.

PER(I), I = 1, 2, 3 absolute permeability along three principal axes, as specified by ISOT in block CONNE: md (m^2).

Record ROCKS.1.1 (optional, NAD ≥ 1 only)

Format (1E10.4)

COM

COM pore compressibility; 1/psi (1/Pa).

Record ROCKS.1.2 (optional, NAD ≥ 2 only)

This record introduces a set of primary variables which are used as default initial conditions in the domain specified in "MAT" (Record ROCKS.1) for all elements for which no other values are specified in block INCON (with option START only).

Format (3E20.14)

X1, X2, X3

X1 water pressure; psi (Pa).

X2 gas saturation.

X3 foam saturation.

Repeat records 1, 1.1, and 1.2 for up to 27 reservoir domains.

Record ROCKS.2 A blank record closes the ROCKS data bock.

PARAM introduces computation parameters

Record PARAM.1

Format (2I2, 3I4, 24I1, E10.4).

NOITE, KDATA, MCYC, MSEC, MCYPR, (MOP(I), I = 1, 24), T.

NOITE specifies the maximum number of iterations per time step (default value is 8).

KDATA specifies amount of printout (default = 1).

0 or 1: print a selection of the most important variables.

2: print fluxes.

3: print primary variables and their changes.

If the above values for KDATA are increased by 10, printout will occur after each iteration (not just after convergence).

MCYC maximum number of time steps to be calculated.

MSEC maximum duration, in machine seconds, of the simulation (default is infinite).

MCYPR printout will occur for every multiple of MCYPR steps (default is 1).

MOP(I), I = 1,24 allows choice of various options.

MOP(1) if ≠ 0, short printout for non-convergent iterations will be suppressed.

MOP(2) through MOP(6) generate additional printout in various subroutines, if set ≠ 0. The amount of printout increases with MOP(I).

MOP(2) CYCIT (main subroutine).

MOP(3) MULTI (flow- and accumulation-terms).

MOP(4) QU (sinks/sources).

MOP(5) EOS (equation of state).

MOP(6) LINEQ (linear equations).

MOP(7) if $\neq 0$, a printout of input data will be provided.

MOP(8) not used.

MOP(9) not used.

MOP(10) not used.

Calculational choices are as follows:

MOP(11) determines evaluation of mobilities at interfaces.

0: mobilities are upstream weighted with WUP (default is WUP = 1.).

1: mobilities are spatially interpolated between adjacent elements.

MOP(12) not used

MOP(13) if $\neq 0$, perform new matrix decomposition only when the number of pivot failures is a multiple of MOP(13). This option is available only with MOP(14) = 2.

MOP(14) determines handling of pivot failures in matrix decomposition.

0: perform new decomposition.

1: reduce time step, stay with old decomposition.

2: ignore pivot failure and proceed (MOP(13) = 0, or number of pivot failures not a multiple of MOP(13)).

MOP(15) not used.

MOP(16) permits to choose time step selection option.

0: use time steps explicitly provided in INPUT.

>0: Increase time step by at least a factor 2, if convergence is achieved in a number of iterations not exceeding MOP (16)

MOP(17) permits to scale the matrix solved in MA28.

0: No scaling.

1: Scale after encountering a singular matrix.

2: Scale after pivot failure.

3: Scale after pivot failure or matrix singularity.

>4: Scale on first iteration in each time step.

>6: Scale all the time.

MOP(18) used to perform a permutation (reordering) of the Jacobian matrix.

0: no pre-ordering of Jacobian matrix.

1: Jacobian matrix is pre-ordered for block lower triangular form.

MOP(19) Permits to choose relative permeability data and front-tracking techniques.

0: k_{rw}, k_{rg}, and k_{rf} are provided from tabular INPUT data.

1: k_{rw} and k_{rg} are calculated from the internally installed formulation [Fatt and Klikoff (1959)], only dealing with water-gas two phase flow.

2: relative permeabilities are calculated internally by the sharp-front technique. No capillary pressure data are needed, regardless of the choice of MOP(20).

MOP(20) permits to choose capillary pressure data.

0: P_{cwg} and P_{cwf} are provided from tabular INPUT data.

1: Use Leverett's function [TOUGH User's Guide, Pruess (1987)] to calculate capillary pressure P_{cwg}. P_{cwf} is set to zero.

MOP(21) -
MOP(24) not used.

T reservoir temperature; °F (°C)

Record PARAM.2

Format (4E10.4, A5, 5X, 2E10.4)
TSTART, TIMAX, DELTEN, SCALE, ELST, GF, REDLT

TSTART starting time of simulation; seconds.

TIMAX time in seconds at which simulation should stop (default is infinite).

DELTEN length of time steps in seconds. If DELTEN is a negative integer, DELTEN = -NDLT, the program will proceed to read NDLT records with time step information.

SCALE scale factor to change the size of the mesh (default = 1.0).

ELST set equal to the name of one element to obtain a short printout after each time step.

GF magnitude (ft/sec^2 or m/sec^2) of the gravitational acceleration vector. Blank or zero gives "no gravity" calculation.

REDLT factor by which time step is reduced in case of convergence failure (default is 4.).

Record PARAM.2.1, 2.2, etc.

Format (8E10.4)
(DLT(I), I = 1, 100)

DLT(I) length (in seconds) of time step I.

This set of records is optional for DELTEN = − NDLT, a negative integer: Up to 13 records can be read, each containing 8 time step sizes. If the number of simulated time steps exceeds the number of DLT(I), the simulation will continue with time steps equal to the last non-zero

DLT(I) encountered.

Record PARAM.3

Format (8E10.4)
RE1, RE2, FOR, WUP, WNR, DFAC, SING, U

RE1 convergence criterion for relative error (default = 1.E-5)

RE2 convergence criterion for absolute error (default = 1.)

FOR weighting factor for time differencing (it is strongly recommended to use *only* default value = 1., i.e., fully implicit). Generally, $0 \leq FOR \leq 1$.

WUP upstream weighting factor for mobilities at interfaces (default = 1.0). $0 \leq WUP \leq 1$.

WNR weighting factor for increments in Newton/Raphson iteration (default = 1.0). $0 < WNR \leq 1$.

DFAC increment factor for computing derivatives (default = 1.E-8).

SING correction for matrix elements which are numerically zero (default = 0.).

U pivoting parameter (default = 0.1). $0 \leq U \leq 1$; increased value for U will make criterion for pivot selection more stringent, resulting in better numerical stability at the expense of more storage for matrix decomposition.

Record PARAM.4

Format (3E20.14)

DEP(I), I = 1, 3

This record holds a set of primary variables completely analogous to record ROCKS.1.2. These variables are used as default initial conditions for all elements for which no other values are prescribed either in block ROCKS or in block INCON (with option START only).

DEP(1) water pressure; psi (Pa).

DEP(2) gas saturation.

DEP(3) foam saturation.

FIN (optional).

A record with FIN punched in columns 1-3 indicates that all data are input in field units. In this case the file SAVE, holding thermodynamic parameters at the end of a MULKOM run, will also be written in field units, to permit restarting with the same input deck. If FIN is absent, input data and file SAVE are in SI units.

FOUT (optional)

A record with FOUT punched in columns 1-4 will cause the main printed output to be written in field units. If FOUT is absent, printed output will be in SI units. In either case, dimensioned parameters are printed with their units displayed.

FIVEP (optional)

A record with FIVEP punched in columns 1-5 will cause patterned printout to be generated for single- or multi-layer grids corresponding to 1/8 of a five- or nine-spot pattern.

Record FIVEP.1 (only for option "FIVEP")

Format (2I5)

NROW, LAY

NROW number of grid block rows in the 1/8 five-spot mesh.

LAY number of grid layers.

TIMES (optional)

This data block specifies desired printout times.

Record TIMES.1

Format (2I5, 2E10.4)

ITI, ITE, DELAF, TINTER

ITI — is the number of explicitly provided times at which printout is to be generated (restriction: ITI ≤ 100).

ITE — is the total number of times at which printout is desired (restriction: ITE ≥ ITI).

DELAF — is the maximum time step, in seconds, to be taken after any of the printout times have been reached (default is infinite).

TINTER — is the time increment, in seconds, to be applied for printout times with index ITI+1, ITI+2,... , ITE.

Record TIMES.2, 3, 4, etc.

Format (8E10.4)

TIS(I), I = 1, ITI

TIS(I) — Printout times, in seconds.

A maximum of 100 printout times can be specified, in ascending order. Time steps will be automatically adjusted to let the program reach the desired printout times.

ELEME — introduces element information.

Record ELEME.1

Format (A3, I2, 2I5, A3, A2, E10.4)

EL, NE, NSEQ, NADD, MA1, MA2, VOLX

El, NE — 5-character code name of an element. The first three characters are arbitrary, the last two characters must be numbers.

NSEQ — number of additional elements having the same volume and belonging to the same reservoir domain.

NADD — increment between the code numbers of two successive elements. (Note: the maximum permissible code number NE + NSEQ * NADD is <99.).

MA1, MA2 — a five character material identifier corresponding to one of the reservoir domains as specified in block ROCKS. If the first three characters are

blanks, the last two characters must be numbers in which case they would indicate the sequence number of the domain as entered in ROCKS.

VOLX element volume, ft^3 (m^3).

Repeat record ELEME.1 for the number of elements desired.

Record ELEME.2 A blank record closes the ELEME data block.

CONNE introduces information for the connections (interfaces) between elements.

Record CONNE.1

Format (A3, I2, A3, I2, 3I5, I5, 4E10.4)

EL1, NE1, EL2, NE2, NSEQ, NAD1, NAD2,

ISOT, D1, D2, AREAX, BETAX

EL1, NE1 code name of the first element.

EL2, NE2 code name of the second element.

NSEQ number of additional connections in the sequence.

NAD1 increment of the code number of the first element between two successive connections.

NAD2 increment of the code number of the second element between two successive connections.

ISOT set equal to 1, 2, or 3; specifies absolute permeability to be PER(ISOT) for the materials in elements (EL1, NE1) and (EL2, NE2), where PER is read in block ROCKS. This allows assignment of different permeabilities, e.g., in the horizontal and vertical direction.

D1, D2 distance ft (m) from center of first and second element, respectively, to their common interface.

AREAX interface area ft^2 (m^2).

BETAX cosine of the angle between the gravitational acceleration vector and the line between the two elements. GF x BETAX > 0 (<0) corresponds to first element being above (below) the second element.

Repeat record CONNE.1 for the number of connections desired.

Record CONNE.2 a blank record closes the CONNE data block.

GENER provides specifications for multilayer production and injection wells. It is possible to specify arbitrary well schedules, by providing up to 20 data blocks beginning with a record having GENER written in columns 1-5, followed by specifications of all production and injection well feeds, and terminated by a blank record. Subsequent GENER blocks will be read at times as specified in block GENTI (see below).

Record GENER.1.1 (production wells)

Format (2A5, E10.4, 5X, I5, 5X, A4, 1X, 4E10.4)

ELEG, SOURCE, WAT, LTABG, TYPE, PI, PWB, HG, QGAS

ELEG code name of element containing well feed (bottommost layer must be specified first).

SOURCE code name of the well. The first three characters are arbitrary; the last two characters are numbers.

WAT rate constraint (target rate) of water production from well (to be specified for record with bottommost feed only); STB/D (m^3/s).

LTABG number of open layers (to be specified for bottommost feed only).

TYPE set equal to "DELV", to indicate a production well is being specified.

PI productivity index for the particular layer; RB·cp/D/psi (m^3).

PWB flowing bottomhole pressure opposite topmost open layer (to be specified for last -top- layer only); psi (Pa).

HG vertical thickness of layer in which the well is open; ft (m).

QGAS gas target rate from well (to be specified for bottommost feed only); MMCF/D, (m^3/D).

Repeat record GENER.1.1 for all LTABG open layers of a multilayer well. The feeds must be entered sequentially, going from bottom up. After all feeds of one production well have been entered, additional production well data may be specified.

Record GENER.1.2 (gas, foam or water injection wells)

Format (2A5, E10.4, 5X, I5, 5X, A4, 1X, E10.4, 20X, E10.4)

ELEG, SOURCE, WI, LTABG, TYPE, G, PIN

ELEG — code name of element containing an open interval of the injection well (open layers can be specified in arbitrary order).

SOURCE — code name of the well. The first three characters are arbitrary; the last two characters must be numbers.

WI — injectivity index of the well (to be specified separately for each layer); RB·cp/D/psi (m^3).

LTABG — number of open layers (to be specified on first record for each injection well).

TYPE — set equal to "GASI", "FOAM", "WATI" to indicate that an injection well for gas, foam or water, respectively, is being specified.

G — total (maximum) rate of entire injection well (to be specified on first record for each injection well); STB/D (kg/s) for foam or water injection, MMCF/D (kg/s) for gas injection.

PIN — injection pressure; psi (Pa).

Repeat record GENER.1.2 for all LTABG open layers of a multi-layer injection well. The feeds can be entered in arbitrary order. After all feeds of one well have been entered, injection data for additional wells may be specified.

Record GENER.2

A blank record closes a set of generation data. Additional sets of generation data may be specified, which will be read at times specified in block GENTI, below.

GENTI (optional)

This data block introduces information on times at which new generation data will be read. If GENTI is absent, only one GENER block will be read, and the well data provided in that block will be used throughout the entire run.

Record GENTI.1

Format (I5)

IGEN

IGEN number of generation data sets.

Record GENTI.2

Format(8E10.4)

GENT(I), I = 1, IGEN

GENT(I) times, in seconds, at which generation data will be read.

A maximum of 20 times can be specified, in ascending order. For each of these times, a new data block GENER will be read.

START (optional)

A record with START punched in columns 1-5, allows a more flexible assignment of initial conditions.

INCON introduces initial conditions.

Record INCON.1

Format (A3, I2, 2I5, E15.9)

EL, NE, NSEQ, NADD, PORX

EL, NE code name of element.

NSEQ number of additional elements with same initial conditions.

NADD increment between the code numbers of two successive elements with identical initial conditions.

PORX porosity (void fraction); if zero or blank, porosity will be taken as specified in block ROCKS if option START is used.

Record INCON.2

Format (3E20.14)

X1, X2, X3

Set of primary variables for the element specified in record INCON.1.

X1 water pressure; psi (Pa).

X2 gas saturation.

X3 foam saturation.

Record INCON.3 A blank record closes the INCON data input block. (For an alternative, see note below).

Note on closure of blocks CONNE, GENER, and INCON.

The "ordinary" way to indicate the end of any of the above data blocks is by means of a blank record. There is an alternative available if the user makes up an input deck from the files MESH, GENER, or SAVE, which have been generated by a previous MULKOM run. These files are written exactly according to the specifications of data blocks ELEME and CONNE (file MESH), GENER (file GENER), and INCON (file SAVE), except that the blocks CONNE, GENER, and INCON terminate with a record with "+++" in columns 1-3 followed by some cross-referencing and restart information. MULKOM will accept this type of input, and in this case there is no blank record at the end of the indicated data blocks.

PVT Data Input.

RELATive permeability

A record with RELAT written in columns 1-5 indicates beginning of relative permeability and capillary pressure information. Up to ten data sets can be specified, each of which provides two-phase water-foam and

foam-gas relative permeability data, and optional capillary pressure data. A data set can be attached to a certain reservoir domain by setting the parameter NADF in record ROCKS.1 for that domain equal to the sequence number of the data set.

Record RELAT.1

Format (2(I1,I4))

NCW, NSW, NCG, NSG

NCW = 0: no water-foam-capillary pressure data will be read; P_{cfw} is assumed to be zero.

1: water-foam capillary pressure data will be read.

NSW number of water saturations provided in data set (restriction: NSW ≤ 20).

NCG = 0: no gas-water-capillary pressure data will be read; P_{cwg} is assumed to be zero.

1: gas-water-capillary pressure data will be read.

NSG number of gas saturations provided in data set (restriction: NSG ≤ 20).

Record RELAT.2

Format (8E10.4)

ASW(I), I = 1,NSW

ASW(I), I = 1,NSW specifies an array of NSW water saturations, in ascending order, for which relative permeability and (optional) capillary pressure data will be tabulated. ASW(1) is irreducible water saturation for MOP(19) ≠ 2. ASW(1) and ASW(2) are the two parameters S_1 and S_2 for performing an interpolation of "sharp front" relative permeabilities for water and foam if MOP(19) = 2.

Record RELAT.3

Format(8E10.4)

AKRW(I), I = 1,NSW

AKRW(I), I = 1,NSW provides water relative permeabilities in two-phase water-foam system at the water saturations read in array ASW, above.

Record RELAT.4

Format (8E10.4)

AKRFW(I), I = 1,NSW

AKRFW(I), I = 1, NSW provides foam relative permeabilities in two-phase water-foam-system at the water saturations read in array ASW, above.

Record RELAT.4.1 (optional, NCW ≥ 1 only)

Format (8E10.4)

PCFW(I), I = 1,NSW

PCFW(I), I = 1,NSW provides foam capillary pressures in two-phase water-foam-system at the water saturations read in array ASW, above.

Record RELAT.5

Format (8E10.4)

ASG(I), I = 1,NSG

ASG(I), I = 1,NSG specifies an array of NSG gas saturations, in ascending order, for which relative permeability and (optional) capillary pressure data will be tabulated. ASG(1) is irreducible gas saturation for MOP(19) ≠ 2. ASG(1) and ASG(2) are the two parameters S_1 and S_2 used for performing an interpolation of "sharp front" relative permeabilities for gas and foam if MOP(19) = 2.

Record RELAT.6

Format (8E10.4)

AKRG(I), I = 1,NSG

AKRG(I), I = 1,NSG provides gas relative permeabilities in two-phase foam-gas system at the gas saturations read in array ASG, above.

Record RELAT.7

Format (8E10.4)

AKRFG(I), I = 1,NSG

AKRFG(I), I = 1,NSG provides foam relative permeabilities in two-phase foam-gas system at the gas saturations read in array ASG, above

Record RELAT.7.1 (optional, NCG ≥ 1 only)

Format (8E10.4)

PCOG(I), I = 1,NSG

PCOG(I), I = 1,NSG provides gas capillary pressures in two-phase gas-water system at the gas saturations read in array ASG, above.

Repeat records RELAT.1 through RELAT.7.1 for up to ten data sets.

Record RELAT.8 a blank record closes the RELAT data block.

REOLG introduces information on rheological properties of foam

Record REOLG.1

Format (8E10.4)

ALPHA, BETA, VISI, DPB, QF, RMWF

ALPHA rheological constant of foam, cp·(psi/ft)^{BETA} (Pa·s(Pa/m)^{BETA})

BETA rheological exponent of foam

VISI foam viscosity at large pressure gradient; cp (Pa·s)

DPB blocking pressure gradient; psi/ft (Pa/m)

QF foam mass quality (gas mass fraction)

RMWF effective molecular weight of foam

ENDCY closes the MULKOM input file and initiates the simulation.

Acknowledgement

The authors appreciate a review of the manuscript by P. Persoff and P. Witherspoon. Much of the support for developing the MULKOM simulator was provided by the Geothermal Technology Division, U. S. Department of Energy, under Contract No. DE-AC03-76SF00098. Additional funding came from the Office of Basic Energy Sciences. The development of gas-water-foam simulation capabilities was supported by the Gas Research Institute under Contract No. 5086-271-1160

References

Aziz, K. and Settari, T., *Petroleum Reservoir Simulation,* Applied Science Publishers, London, 1979.

Coats, K. H., Geothermal Reservoir Modelling, paper SPE-6892, presented at the 52nd Annual Fall Technical Conference and Exhibition of the SPE, Denver, CO, October 1977.

Duff, I. S., MA28 - A Set of FORTRAN Subroutines for Sparse Unsymmetric Linear Equations, AERE Harwell report R8730, July 1977.

Edlefsen, N. E., and Anderson, A. B. C., Thermodynamics of Soil Moisture, *Hilgardia,* Vol. 15, No. 2, pp. 31-298, 1943.

Edwards, A. L., TRUMP: A Computer Program for Transient and Steady State Temperature Distributions in Multidimensional Systems, National Technical Information Service, National Bureau of Standards, Springfield, Virginia 1972.

Fanchi, J. R., Harpole, K. J., and Bujnowski, S. W., BOAST: A Three-Dimensional, Three-Phase Black Oil Applied Simulation Tool, Volume 1: Technical Description and Fortran Code, report DE 83-000529, National Technical Information Service, Springfield, VA, 1982.

Fatt, I., and Klikoff, W. A., Effect of Fractional Wettability on Multiphase Flow through Porous Media, *AIME Transactions, 216,* 246, 1959.

International Formulation Committee, A Formulation of the Thermodynamic Properties of Ordinary Water Substance, IFC Secretariat, Düsseldorf, Germany, 1967.

Lord, D. L., Analysis of Dynamic and Static Foam Behavior, *J. Petr. Tech.,* 39-45, January 1981.

Narasimhan, T. N. and Witherspoon, P.A., An Integrated Finite Difference Method for Analyzing Fluid Flow in Porous Media, *Water Resources Research,* Vol. 12, No. 1, pp. 57-64, 1976.

Peaceman, D.W., Fundamentals of Numerical Reservoir Simulation, Elsevier, Amsterdam 1977.

Pruess, K., Development of the General Purpose Simulator MULKOM, Annual Report 1982, Earth Sciences Division, report LBL-15500, Lawrence Berkeley Laboratory, 1983.

Pruess, K., SHAFT, MULKOM, TOUGH: A Set of Numerical Simulators for Multiphase Fluid and Heat Flow, *Geotermia, Rev. Mex. Geoenergia, 4,* 185-202, 1988 (also: Lawrence Berkeley Laboratory Report LBL-24430).

Pruess, K., TOUGH User's Guide, Nuclear Regulatory Commission, Report NUREG/CR-4645, June 1987, (also: Lawrence Berkeley Laboratory Report LBL-20700, Berkeley, CA, June 1987).

Pruess, K., and Narasimhan, T. N., A Practical Method for Modeling Fluid and Heat Flow in Fractured Porous Media, *Society of Pet. Engr. Jour.,* Vol. 25, No. 1, pp.

14-26, February 1985.

Ross, S., Bubbles and Foam: New General Law, in: Chemistry and Physics of Interfaces II, American Chemical Society Publications, 15-25, Washington, D. C., 1971.

Stone, H. L., Estimation of Three-Phase Relative Permeability and Residual Oil Data, *J. Canadian Pet. Tech., 12,* (4) 53-61, 1973.

Vargaftik, N. B., Tables on the Thermophysical Properties of Liquids and Gases, Second Edition, John Wiley and Sons, New York, 1975.

Appendix A. Mass and Energy Balances

The basic mass- and energy-balance equations(*) solved by MULKOM can be written in the following general form:

$$\frac{d}{dt} \int_{V_n} M^{(\kappa)} dV = \int_{\Gamma_n} \mathbf{F}^{(\kappa)} \cdot \mathbf{n} \, d\Gamma + \int_{V_n} q^{(\kappa)} \, dV \qquad (A.1)$$

The integration here is over an arbitrary subdomain V_n of the flow system under study, which is bounded by the closed surface Γ_n. The quantity M appearing in the accumulation term denotes mass or energy per unit volume, with $\kappa = 1, \ldots, NK$ labeling the mass components, and $\kappa = NK + 1$ for the heat "component".

The mass accumulation term is written in a general way, to allow for the presence of several components (chemical species) in the fluid.

$$M^{(\kappa)} = \phi \sum_{\beta=1}^{NPH} S_\beta \, \rho_\beta \, X_\beta^{(\kappa)} \qquad (A.2)$$

The total mass of component κ is obtained by summing over all fluid phases $\beta = 1, \ldots, NPH$. S_β is the saturation (volume fraction) of phase β, ρ_β is density of phase β, and $X_\beta^{(\kappa)}$ is the mass fraction of component κ present in phase β. Similarly, the heat accumulation term in a multi-phase system is(*)

$$M^{(NK+1)} = \phi \sum_{\beta=1}^{NPH} S_\beta \, \rho_\beta \, u_\beta + (1-\phi) \, \rho_R \, C_R \, T \qquad (A.3),$$

where u_β denotes internal energy of fluid phase β.

The mass flux term is a sum over phases

$$\mathbf{F}^{(\kappa)} = \sum_{\beta=1}^{NPH} X_\beta^{(\kappa)} \, \mathbf{F}_\beta \qquad (A.4)$$

for $\kappa = 1, \ldots, NK$. Individual phase fluxes are given by a multi-phase version of

(*) The heat balance equation is ignored in the isothermal gas-water-foam version of MULKOM.

Darcy's law:

$$F_\beta = - k \frac{k_{r\beta}}{\mu_\beta} \rho_\beta (\nabla P_\beta - \rho_\beta g) \tag{A.5}$$

Here k is absolute permeability, $k_{r\beta}$ is relative permeability of phase β , μ_β is viscosity, and

$$P_\beta = P + P_{cap,\beta} \tag{A.6}$$

is the pressure in phase β, which is the sum of the pressure P of a reference phase, and the capillary pressure of phase β relative to the reference phase. In addition to Darcy flow, MULKOM also includes binary diffusion in the gas phase for fluids with two gaseous (or volatile) components κ, κ'

$$f_{\beta = gas}^{(\kappa)} = - \phi S_g \tau D_{\kappa\kappa'} \rho_g \nabla X_g^{(\kappa)} \tag{A.7}$$

$D_{\kappa,\kappa'}$ is the coefficient of binary diffusion which depends on the nature of the gaseous components and on pressure and temperature. τ is a tortuosity factor. When binary diffusion is present the flux-term (A.7) simply gets added to that of (A.4).

Heat flux contains conductive and convective components (no dispersion)

$$F^{(NK+1)} = -K\nabla T + \sum_\beta h_\beta F_\beta \tag{A.8}$$

where K is thermal conductivity of the medium, and $h_\beta = u_\beta + P/\rho_\beta$ is the specific enthalpy of phase β.

MULKOM can model vapor pressure lowering due to capillary and phase adsorption effects. This is represented by Kelvin's equation (Edlefsen and Anderson, 1943):

$$P_v (T, S_l) = P_{sat} (T) \cdot \exp \left\{ \frac{m_l \cdot P_{cap}(S_l)}{\rho_l R(T + 273.15)} \right\} \tag{A.9}$$

where P_{sat} is saturated vapor pressure of bulk liquid, P_{cap} is the difference between liquid and gas phase pressures, m_l is the molecular weight of the liquid, and R is the universal gas constant.

Appendix B. Space and Time Discretization

The continuum equations (A.1) are discretized in space using the "integral finite difference" method (Edwards, 1972; Narasimhan and Witherspoon, 1976). Introducing appropriate volume averages, we have

$$\int_{V_n} M dV = V_n M_n \tag{B.1}$$

where M is a volume-normalized extensive quantity, and M_n is the average value of M over V_n. Surface integrals are approximated as a discrete sum of averages over surface segments A_{nm}:

$$\int_{\Gamma_n} \mathbf{F} \cdot \mathbf{n} \, d\Gamma = \sum_m A_{nm} F_{nm} \tag{B.2}$$

Here F_{nm} is the average value of the (inward) normal component of **F** over the surface segment A_{nm} between volume elements V_n and V_m. This is expressed in terms of averages over parameters for elements V_n and V_m. For the basic Darcy flux term, Eq. (A.5), we have

$$F_{\beta,nm} = - k_{nm} \left[\frac{k_{r\beta} \, \rho_\beta}{\mu_\beta} \right]_{nm} \left[\frac{P_{\beta,n} - P_{\beta,m}}{D_{nm}} - \rho_{\beta,nm} \, g_{nm} \right] \tag{B.3}$$

where the subscripts (nm) denote a suitable averaging (interpolation, harmonic weighting, upstream weighting). D_{nm} is the distance between the nodal points n and m, and g_{nm} is the component of gravitational acceleration in the direction from m to n.

The discretized form of the binary diffusive flux in the gas phase is

$$f^{(\kappa)}_{\beta=gas,nm} = - \phi_{nm} \, S_{g,nm} \, \tau_{nm} \, (D_{\kappa\kappa'})_{nm} \, \rho_{g,nm} \, \frac{X_{g,n} - X_{g,m}}{D_{nm}} \tag{B.4}$$

Substituting Eqs. (B.1) and (B.2) into the governing Eq. (A.1) a set of first-order ordinary differential equations in time is obtained.

$$\frac{dM_n^{(\kappa)}}{dt} = \frac{1}{V_n} \sum_m A_{nm} F^{(\kappa)}_{nm} + q_n^{(\kappa)} \tag{B.5}$$

Time is discretized as a first order finite difference, and the flux and sink and source terms on the right hand side of Eq. (B.5) are evaluated at the new time level, $t^{k+1} = t^k + \Delta t$, to obtain the numerical stability needed for an efficient calculation of multi-phase flow. This treatment of flux terms is known as "fully implicit," because the fluxes are expressed in terms of the unknown thermodynamic parameters at time level t^{k+1}, so that these unknowns are only implicitly defined in the resulting equations; see e.g. Peaceman (1977). The time discretization results in the following set of coupled non-linear, algebraic equations:

$$R_n^{(\kappa)k+1} \equiv M_n^{(\kappa)k+1} - M_n^{(\kappa)k} - \frac{\Delta t}{V_n}\left\{\sum_m A_{nm}\, F_{nm}^{(\kappa)k+1} + V_n\, q_n^{(\kappa)k+1}\right\}$$

$$= 0 \qquad \text{(B.6)}$$

The entire geometric information of the space discretization in Eq. (B.6) is provided in the form of a list of grid block volumes V_n, interface areas A_{nm}, nodal distances D_{nm}, and components g_{nm} of gravitational acceleration along nodal lines. There is no reference whatsoever to a global system of coordinates, or to the dimensionality of a particular flow problem. The discretized equations are in fact valid for arbitrary irregular discretizations in one, two or three dimensions, and for porous as well as for fractured media. This flexibility should be used with caution, however, because the accuracy of solutions depends upon the accuracy with which the various interface parameters in equations such as (B.3, B.4) can be expressed in terms of average conditions in grid blocks. A sufficient condition for this to be possible is that there exists approximate thermodynamic equilibrium in (almost) all grid blocks at (almost) all times (Pruess and Narasimhan, 1985). For systems of regular grid blocks referenced to global coordinates (such as r - z, x - y - z), Eq. (B.6) is identical to a conventional finite difference formulation (e.g. Peaceman, 1977).

For each volume element (grid block) V_n there are NK+1 equations (κ=1, . . ., NK, NK+1), so that for a flow system with N grid blocks (B.6) represents a total of $N \cdot (NK+1)$ coupled non-linear equations. The unknowns are the $N \cdot (NK+1)$

independent primary variables x_i [i = 1, ..., N · (NK+1)] which completely define the state of the flow system at time level t^{k+1}. These equations are solved by Newton/Raphson iteration, which is implemented as follows. We introduce an iteration index p and expand the residuals $R_n^{(\kappa)k+1}$ in Eq. (B.6) at iteration step p+1 in a Taylor series in terms of those at index p:

$$R_n^{(\kappa)k+1}(x_{i,p+1}) = R_n^{(\kappa)k+1}(x_{i,p}) + \sum_i \frac{\partial R_n^{(\kappa)k+1}}{\partial x_i}\bigg|_p (x_{i,p+1} - x_{i,p}) + \ldots = 0 \tag{B.7}$$

Retaining only terms up to first order, we obtain a set of N · (NK+1) linear equations for the increments $(x_{i,p+1} - x_{i,p})$:

$$-\sum_i \frac{\partial R_n^{(\kappa)k+1}}{\partial x_i}\bigg|_p (x_{i,p+1} - x_{i,p}) = R_n^{(\kappa)k+1}(x_{i,p}) \tag{B.8}$$

All terms $\partial R_n/\partial x_i$ in the Jacobian matrix are evaluated by numerical differentiation. Eq. (B.8) is solved with the Harwell subroutine package "MA28" (Duff, 1977). Iteration is continued until the residuals $R_n^{(\kappa)k+1}$ are reduced below a preset convergence tolerance.

Table 1. MULKOM fluid property modules.

components	number of components
water	1
water at near-critical conditions	1
two waters*	2
water, CO_2†	2
water, NaCl	2
water, air	2
water, SiO_2‡	2
water, volatile hydrocarbon, non-volatile hydrocarbon	3
water, natural gas, foam	3

*water with tracer

† with mineral buffer

‡ includes dissolution and precipitation, as well as associated changes in porosity and permeability.

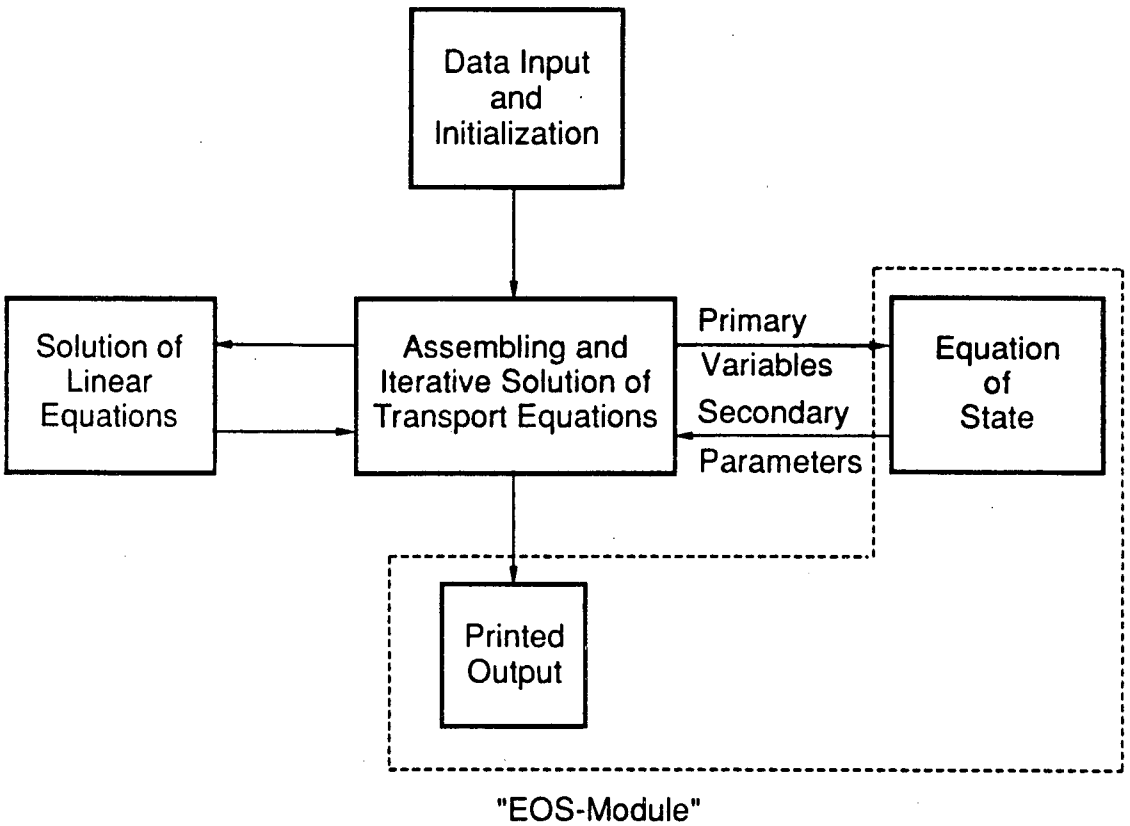

Figure 1. Modular architecture of MULKOM and TOUGH.

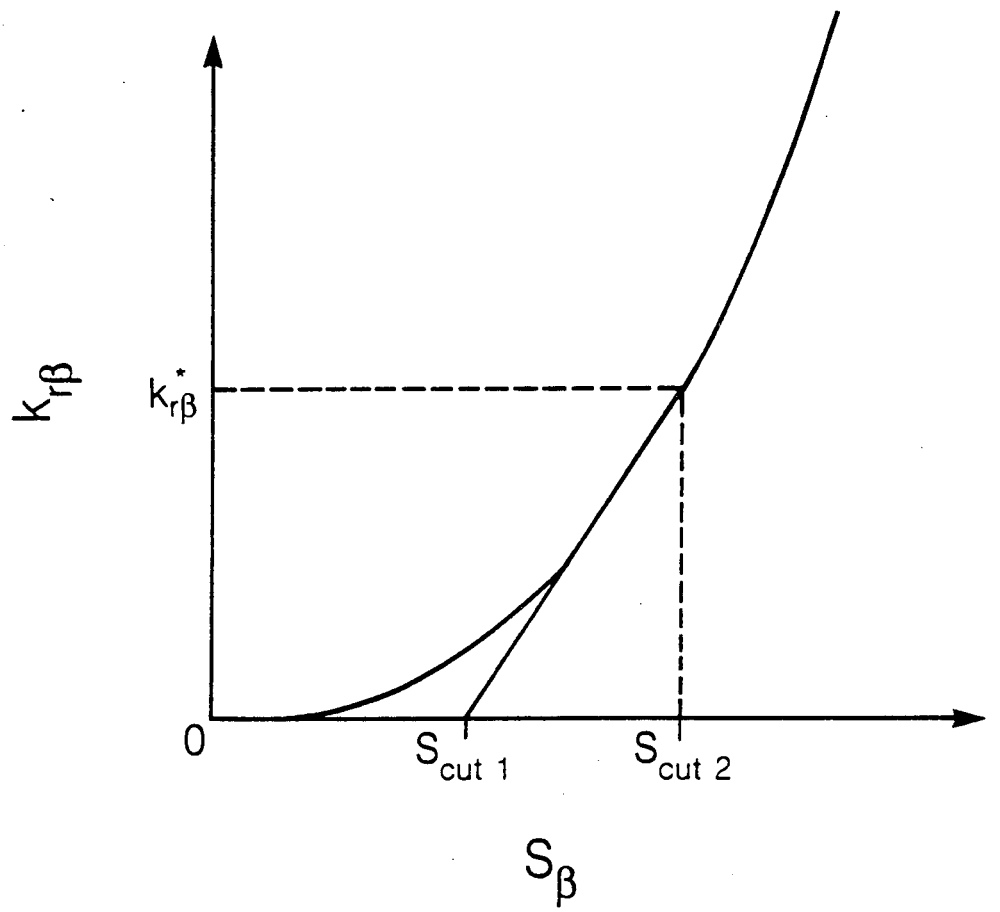

Figure 2. Schematic of linear interpolation of relative permeability for a phase with small saturation.

Appendix E.

A Laboratory Investigation of Foam Flow in Sandstone at Elevated Pressure

SPE
Society of Petroleum Engineers

SPE 18781

A Laboratory Investigation of Foam Flow in Sandstone at Elevated Pressure

by P. Persoff, Lawrence Berkeley Laboratory; C.J. Radke, U. of California; K. Pruess and S.M. Benson, Lawrence Berkeley Laboratory; and P.A. Witherspoon, U. of California

SPE Members

This paper was prepared for presentation at the SPE California Regional Meeting held in Bakersfield, California, April 5-7, 1989.

This paper was selected for presentation by an SPE Program Committee following review of information contained in an abstract submitted by the author(s). Contents of the paper, as presented, have not been reviewed by the Society of Petroleum Engineers and are subject to correction by the author(s). The material, as presented, does not necessarily reflect any position of the Society of Petroleum Engineers, its officers, or members. Papers presented at SPE meetings are subject to publication review by Editorial Committees of the Society of Petroleum Engineers. Permission to copy is restricted to an abstract of not more than 300 words. Illustrations may not be copied. The abstract should contain conspicuous acknowledgment of where and by whom the paper is presented. Write Publications Manager, SPE, P.O. Box 833836, Richardson, TX 75083-3836. Telex, 730989 SPEDAL.

ABSTRACT

Use of foam as a mobility-control fluid in underground applications such as enhanced oil recovery and natural gas or air storage in aquifers requires quantitative information on its flow behavior in porous media at relevant conditions. Little information is currently available in consolidated sands and at pressures characteristic of reservoir depths. We study the flow of foam through a 1.3 μm^2 Boise sandstone core at ambient temperature and at back pressures up to 5.2 MPa (750 psia). Total superficial velocities range from 1 to 45 m/day, and inlet foam qualities range from 0.70 to 0.996. Sequential pressure taps and gamma-ray attenuation are used to measure local flow resistances and liquid saturations during transient displacement and in the steady state.

We find that foam in the unsteady state is rheopectic; in the steady state it is shear thinning with respect to increasing gas flow but Newtonian with respect to increasing liquid flow. That is, steady pressure gradients for foam are sensibly independent of gas velocity but increase nearly linearly with increasing liquid velocity. No hysteresis in foam flow resistance is noted. Also at steady state, the pressure profile is linear and the liquid saturation is uniform and constant between 30 and 35%, a value that is about 10 saturation units above connate. The steady-state liquid saturation is practically independent of flow rate and inlet foam quality. Hence, foam flow resistance is not a unique function of liquid saturation.

Steady-state flow behavior of foam is rationalized in terms of changes in bubble texture. We also suggest a unique way of plotting foam flow behavior such that all our data collapse to a single constant which is characteristic only of the porous medium and the stabilizing surfactant package. If proven general, this correlation should be very useful for estimating foam mobilities as input to numerical simulations of possible field applications.

References and illustrations at end of paper.

INTRODUCTION

Foam is a promising fluid for achieving mobility control in a variety of underground processes including enhanced oil recovery by steam, CO_2, or enriched hydrocarbon flooding, and aquifer storage of natural gas or air. Because of its dispersed nature, foam exhibits low flow mobilities which may possibly overcome gravity override and viscous fingering through the permeable streaks always present in underground porous media.

Unfortunately, the flow behavior of foam is very complicated; there is a plethora of results that are directly contradictory. For example, Huh and Handy [1] report increasing foam mobility with increasing liquid velocity while Nahid [2] and Sanchez and Schechter [3] report the opposite. Also, Sanchez and Schechter [3] and Treinen, Brigham, and Castanier [4] observe hysteresis in foam mobility whereas Huh and Handy [1] do not. Both Huh and Handy [1] and Sanchez and Schechter [3] show that foam mobility (plotted as foam relative permeability) varies with the liquid saturation in the core. But De Vries and Wit [5] find a constant liquid saturation in the porous medium; they measure varying foam mobilities at this fixed saturation value.

Clearly, additional experiments are needed to resolve some of these discrepancies. Particularly needed are data in reservoir sandstones and at pressures close to reservoir conditions. Our goal is to understand foam flow behavior under these conditions in both the steady and unsteady states. Because of the contradictory results noted above, we desired a direct measure of the in-situ liquid saturations, and we wished to probe the possible separate effects of gas and liquid flow rates and hysteresis on foam flow behavior. Our experiments to meet these goals are described below.

EXPERIMENT

Apparatus

The experimental flow apparatus is shown in Fig. 1. A 5.1-cm (2-in.) diameter, 60-cm (24-in.) long core of Boise sandstone was epoxy-mounted into a 316 stainless steel cylinder designed for 20 MPa (3000 psia). The core porosity was 0.25 and one pore volume (PV) corresponded to 300 cm^3. Swagelok O-seal pressure taps were drilled through the epoxy to the core, and liquid-filled tubes were connected from each pressure tap to a multiplexing valve. Pressure was measured using a single Paroscientific 43KT piezoelectric quartz-crystal pressure transducer (Paroscientific, Redmond, WA) and a Scanivalve 12L7 multiplexing valve (Scanivalve, San Diego, CA) set to visit sequentially all the taps. Back pressure was maintained by a Mity-mite dome-loaded back-pressure regulator (Grove Valve and Regulator Co., Emeryville, CA). Aqueous liquid was injected at a controlled rate by an LDC minipump, Model 2396 (Milton Roy Corp., Riviera Beach, FL). Nitrogen gas was injected at controlled mass flow rate through a Brooks 5850-TRP mass flow controller (Emerson Electric, Hatfield, PA).

Liquid saturation was measured by gamma-ray densitometry [6], using a 47 mCi Cs-137 source collimated to a 0.32-cm (1/8-in.) diameter beam, with detection by a Harshaw 5.1-cm (2-in.) NaI(Tl) scintillation counter and an NB-15X plug-on preamplifier (Harshaw Chemical Co. Solon, OH). Actual counting was done on a Norland IT-5300 multichannel analyzer (Norland Corp., Ft. Atkinson, WI), with a digital gain stabilizer to compensate for drift. The intensity of the gamma ray (counts/s falling within a 662 keV peak) was premeasured at selected stations when the core was at 0% and again at 100% liquid saturation. Liquid saturation was calculated from observed beam intensity using the relationship $S_{liq} = [\ln(I_d/I)]/[\ln(I_d/I_w)]$, where I_d and I_w are the intensity of the gamma ray premeasured at 0% and 100% liquid saturation, respectively, and I is the intensity measured at any unknown intermediate saturation. This relationship follows from the Beer-Lambert law [7]. The gamma-ray source and detector were mounted on a carriage which could be moved sequentially to each of the stations by a Slow-syn stepper motor and Model DPF107 motor controller (Anaheim Automation, Anaheim, CA). The greatest source of error in measurement of liquid saturation is the measurement of gamma-ray intensity. When counting radioactive decay, the standard deviation of the number of events counted is the square root of the number of events counted. Therefore the longer the counting period, the more precise is the measurement of liquid saturation. Because of the trade-off between counting time and precision in monitoring liquid saturation, it was necessary in transient measurements to choose between monitoring at one location with good time resolution or sweeping the length of the core with poorer resolution. Generally, we counted long enough to keep the standard deviation in liquid saturation to less than 5 saturation units during transient measurements and 2 saturation units during steady-state measurements. Pressure sweeps could be made without loss of time resolution. All measurements were controlled and data recorded by an HP-9000 series computer.

Steady-state relative permeabilities of the core to gas and liquid were measured in the drainage mode, with local effective permeabilities calculated between each pair of adjacent pressure taps. The measured relative permeabilities are shown in Fig. 2. An arrow indicates the location of connate water saturation where it was not possible to gauge any liquid weepage.

The foamer solution was a brine containing 18.2 g/L Na, 1.3 g/L Mg, 5.4 g/L Ca, and 40.3 g/L Cl, with 1% by weight active surfactant. The surfactant was either of two chemically similar alkylethoxysulfates: Enordet AES 1215-9S (Shell Chemical Co.) or Steol 7N (Stepan Chemical Co., Northridge, IL). The surface tension, measured by the Wilhelmy plate method, was 29 mN/m; the viscosity, measured with a Contraves rotational viscometer, Model 15T, was 1.2 mPa·s. In some runs, 0.2 wt % of long chain alcohol of average carbon number 14 (Neodol 25) was added, which increased the liquid viscosity to 1.7 mPa·s.

Procedure

The core was initially vacuum-saturated with brine and displaced by at least 10 PV of foamer solution. In all runs, liquid was injected at constant volumetric rate and gas was injected at constant mass flow rate. The progress of gas and foam through the core was monitored by frequent pressure sweeps and by monitoring of liquid saturation at a single station, with occasional saturation sweeps. After foam had propagated through the length of the core and steady state was reached, the gas and liquid flow rates were varied independently to reach a series of steady states.

Gas flow velocity was calculated by converting the measured flow rate, in volume at standard conditions, to the average pressure in the core, and then dividing by the cross-sectional area of the core. The fractional flow of gas (also referred to as inlet foam quality) and the time per pore volume were also based on the average gas pressure in the core.

RESULTS

In this section we first report on the transient behavior when gas and liquid are injected and foam is propagated through the core. Then we examine the steady-state behavior as gas and/or liquid flow rates are changed stepwise. Here the goal is to determine the effects of changing flow rates upon foam mobility and liquid saturation.

Transient Behavior

Figures 3 through 5 show displacement results for simultaneous injection of aqueous surfactant solution and nitrogen at a fractional gas flow or inlet foam quality of 96% and a total superficial velocity of 4.2 m/day into the Boise sandstone core initially saturated with the surfactant solution. Transient liquid saturations in the sandstone are seen in Figs. 3 and 4 while Fig. 5 reports the corresponding pressure profiles.

From Fig. 3, which shows the liquid desaturation history at the 9.1-cm core location ($x/L = 0.15$), we observe monotonic decline to a steady value of 30% for times between 0.3 and 0.7 PV. For other positions we find an initial rather sharp decline to a saturation of about 65% followed by a gradual decline to the steady value. This is reminiscent of the two-step displacement process hinted at by Mohammadi, Van Slyke, and Ganong [8].

Figure 4 indicates that after the 65% liquid saturation front passes, desaturation occurs from the front of the core.

Gas breakthrough is observed near 1.0 PV. Sometime after 13 PV steady state is attained. The final liquid saturation in the core is about 30%, which from Fig. 2 is about 5 saturation units above connate saturation.

An important finding from Fig. 5 is that the transient pressure profiles exactly track the liquid-saturation history in that high pressure gradients (i.e., large foam flow resistances) occur where liquid saturations are lowest. For example, at the 1.03 PV time, which is close to gas breakthrough, the effective flow resistance is highest near the core inlet where the liquid saturation is 30%, while near the core outlet, where the liquid saturation is 65%, pressure gradients are quite small. The finding of low transient foam mobility at low liquid saturation is general for all core locations during the entire time of the displacement process. Mohammadi, Van Slyke, and Ganong [8] also indicated high foam mobility initially, followed by lower foam mobility during the latter stages of the displacement process. Again from Fig. 5, steady state is reached after 13 PV. The final pressure profile is linear, reflecting a constant foam mobility along the core.

In our transient studies, which are not extensive, we find that liquid displacement does not always behave in exactly the same fashion at each location in the core for different experiments. Likewise, the time to reach steady state varies. Usually several PV are sufficient, but in some experiments tens of PV are required. However, the following trends are invariably seen. There is a relatively rapid desaturation front at 65% liquid saturation, followed by a gradual displacement to near 35% commencing from the core inlet. Most of the time to reach steady state is during the second slow desaturation stage. During the transient displacement foam mobility is low where liquid saturation is low, and high where liquid saturation is high. Finally, a steady state is reached in which the pressure gradient and liquid saturations are practically uniform along the core. The final low foam mobilities and low liquid saturations indicate clearly that the minimum critical velocity necessary to generate a fine-textured, strong foam [9,10] was exceeded in all our experiments.

Steady Behavior

Figures 6 through 9 report the liquid saturation profiles and the relationship between pressure drop and flow rate in the steady state. The data cover a range of total superficial velocity between 1 and 45 m/day; the gas fractional flow at core average conditions ranges from 70 to over 99%. In these figures any numbers shown in parentheses refer to the gas fractional flow, or equivalently, to the inlet foam quality. Likewise, lines simply connect data points.

Figure 6 indicates that at a fixed liquid velocity and for a wide range in gas velocity, the liquid saturation in the core is constant. Except for the very lowest gas velocity, at which steady state has possibly not been reached, the liquid saturation is fixed at 30-35%. Clearly with foam flow there is not a 1 to 1 correspondence between fractional flow and liquid saturation.

Figure 7 shows the fascinating result that, for a fixed liquid velocity, the pressure drop is essentially independent of gas flow rate over a change of almost two orders of magnitude. De Vries and Wit find the same rheological behavior for foam flow in both sandstone and sandpacks at elevated pressure [5]. Conversely, Friedmann, Chen, and Gauglitz ascertain a 2/3 power dependence of pressure drop on flow rate, although they consider much higher velocities than in this work [10].

Results for the effect of liquid velocity at constant gas velocity are shown in Figs. 8 and 9. Similar to Fig. 6, the steady-state saturation profiles in Fig. 8 are uniform and constant independent of liquid velocity down to a quality of 70%. This trend of constant liquid saturation for changing foam mobility needs to be studied for even wetter foams, but it again emphasizes that the mobility of foam is not a unique function of saturation.

Figure 9 displays the role of liquid velocity on foam pressure drop for two fixed gas velocities. Except at the lowest velocities, there is an almost linear increase in the foam pressure gradient with increasing liquid velocity. Again, Nahid [2] and Sanchez and Schechter [3] find a similar decrease in foam mobility with increasing liquid flow, but Huh and Handy [1] report just the opposite trend. Note that the two data points for the lower gas velocity fall on the same line as those for the higher gas velocity. This confirms the results of Fig. 7 that gas velocities do not have a major impact on the foam pressure drop.

The letters in alphabetic order labeling the points in Fig. 9 indicate consecutive steady states. Either raising or lowering gas or liquid flow to the same final state produces identical flow behavior. We do not observe hysteresis in steady-state foam mobilities.

DISCUSSION

Foam in porous media is a gas (or internal nonwetting phase) dispersed in an interconnected wetting liquid comprised of liquid bridges and lamellae [9,11]. During flow, the injected gas and liquid phases, whether initially dispersed or not, separate near the core inlet. Wetting liquid occupies the smallest pores and transports separately from the foam phase. The amount of wetting liquid conducted by flowing lamellae and liquid bridges and through and along static lamellae is very small compared to that conducted by the completely liquid-filled pore channels [12,13]. Consequently, the quality of the foam phase inside a porous medium is higher than that injected. Further, the wetting liquid-flow resistance obeys the classic two-phase Darcy's law. At a given wetting-liquid saturation, the relative permeability to the liquid is the same as that in two-phase flow of immiscible Newtonian fluids, independent of the presence of a discontinuous foam phase. Essentially all investigations of foam flow in porous media confirm this observation [1,3,5,13-15].

Because the wetting liquid separates into its own pore channels, the foam phase becomes the nonwetting phase and transports in the large pores not occupied by the continuous wetting liquid. The foam phase can be classified according to three regimes: trapped bubble trains, flowing bubble trains, and possibly, for weakly stabilizing surfactants or high gas velocities, free continuous gas. The three regimes are listed qualitatively in increasing order of the pore sizes in which they reside. From visual observations of etched-glass micromodels, nonflowing foam is trapped at pore constrictions [16] and therefore occupies the intermediate size pores. Tracer [2,10,13] and micromodel [16] experiments provide estimates of the fraction of the foam phase that is trapped between 30 and 90%. Flowing bubbles are located in the next largest pore channels, with

any free gas likely occupying the very largest pores.

The most important property that determines the amount of trapped (versus flowing) foam and the effective flow resistance of each regime is the texture (i.e., the bubble size and size distribution) [11]. Micromodel studies [9,16-18] and core effluent observations [15,19] of texture indicate that the bubble size distribution exhibits a wide spread. Bubbles can be significantly smaller or larger than pore bodies but generally they are on the order of one to several pore body volumes (see, for example, Fig. 1 of [20]). The discontinuous gas bubbles essentially span the pores channels in which they reside, and, when flowing, they slide over thin films and crevices of wetting liquid adjacent to mineral grain surfaces [16,20,21]. Considerable success has been achieved in predicting flowing bubble resistance based on elongated bubbles flowing in a single capillary and a linear dependence on local bubble density [10,19,21,22]. Similarly, initial attempts at understanding bubble trapping and the pressure gradients necessary to release bubbles also involve the bubble texture [23]. Foam microstructure in the porous medium directly determines its flow resistance.

Bubbles do not maintain their identity during transport through a porous medium. Whether externally generated or produced inside the core, they are shaped according to the nature of the porous medium in which they find themselves by "making" and "breaking" processes [4]. Foam texture arises from a balance among varied and complicated mechanisms which give rise to bubble birth and death. Lamellae and bubbles are generated primarily by snap-off in intermittently liquid-filled germination sites [9,16,17,24] (two other generation mechanisms are leave-behind and bubble division [9]). Conversely, lamellae break from capillary suction at Plateau borders [20,25], from fast and extensive stretching near pore bodies of termination sites [20] and from gas diffusion between adjacent bubbles of different mean curvatures [15,26].

For an effectively incompressible foam generated inside a linear core, the bubble texture diminishes over quite small distances to a constant steady-state size where the rates of generation and collapse are equal [10]. At this state even the trapped bubble trains should not be viewed as completely static. Ever-present pressure fluctuations and flow-path alterations release some trapped bubble trains. These are subsequently replaced from the flowing bubble regime at equal frequency.

The kinetics of foam generation and collapse obviously depend upon surfactant structure, composition, and concentration, but they also depend upon liquid saturation [9,20], and separately on gas and liquid flow rates [10,15,19,20]. Because of the velocity rate effects and the redistribution of the wetting liquid into its own flow paths, foam mobility is not in general expected to be a unique function of fractional flow or saturation. Additionally, because the foam making and breaking kinetics vary with velocity, the foam texture does also. This re-emphasizes how strongly foam texture and foam rheology are coupled.

Based on these general observations we now discuss our transient and steady-state experimental results.

Transient Behavior

To rationalize the transient displacement results of Figs. 3-5, we tentatively argue as follows. Initially, unfoamed gas fingers into the larger pore channels because of extremely adverse mobility contrast. Foam bubbles and lamellae are created by leave-behind and by snap-off. However, their number density is small because germination sites are sparse in the large pore space [9] and because the locally high interstitial gas velocities may destroy some moving lamellae [20]. This rather coarse-textured, weak foam does exhibit some increased flow resistance compared to the free gas [9]; accordingly, the local pressure gradients increase (for constant imposed flow rates) enough to overcome the entrance capillary pressure of nearby liquid-filled pores. More liquid is now displaced, allowing the gas to encounter additional germination and leave-behind sites. Bubble and lamellae density further increase, which again raises local pressure gradients, and so on in a cascading fashion.

Wetting-fluid displacement is faster early at high liquid saturation compared to that later at low liquid saturation because the capillary entrance pressures at high liquid saturations (i.e., those reflecting larger pore throats) change much more gradually per unit of desaturation compared to those at low liquid saturations. Relatively larger flow pressure gradients are therefore demanded for desaturation at low liquid saturation. These higher pressure gradients require a finer-textured foam, which takes longer to evolve. This reasoning also explains why the high pressure gradients in Fig. 5 correspond directly to the low liquid saturations in Fig. 4. Finally, at steady state a strong foam [9] of constant and fine texture (i.e., high flow resistance) develops throughout the core, forcing the liquid saturation down to a low and uniform value and establishing a uniform pressure gradient (i.e., a linear pressure profile).

Of course, even at steady state there must be a net bubble generation near the core inlet and a decline in bubble size. Apparently, the region where the rates of bubble birth and death are out of balance is confined to a region so near the core inlet that it does not affect the overall linearity of the pressure profile. De Vries and Wit state a similar conclusion [5], although Minssieux detected a region of high liquid saturation near the inlet of a sandpack [27].

The lack of precise reproducibility for transient displacement by foam may be due to the chaotic nature of the initial gas-fingering process. Somewhat different gas flow paths are likely established for each separate experiment. Foam evolution is therefore somewhat statistical. Fortunately, steady-state behavior does appear to be reproducible.

The foam-flooding process is unique in that the drive fluid becomes more flow resistant or thickens with time. In the unsteady state, foam may thus be classified as rheopectic. Near the flood front free gas exists, behind the front coarse or weak foam exists, and still further behind the front a strong, fine-textured foam evolves. According to this scenario, use of the Johnson-Bossler-Naumann technique [28] to calculate unsteady relative permeabilities of foam from dynamic displacement data seems ill-advised. Not only is the rheopectic nature of foam ignored, but the Johnson-Bossler-Naumann procedure implicitly presumes that both the drive and displaced fluids exhibit flow resistances that are unique functions of local saturation. This presumption is not correct even for foam

flowing at steady state, as discussed below.

Steady Behavior

Over the range of flow velocities and fractional flows that we have investigated, once a strong foam evolves at steady state, the liquid saturation is driven down to about 35%. This value is independent of fractional flow and velocity. Foam mobility varies at this constant saturation. Figures 10 and 11 show the separate dependences of foam resistance on gas and liquid velocities, respectively. We choose to report our results in terms of a nondimensional foam flow resistance, FFR, defined by

$$FFR \equiv \frac{k}{\mu_{liq} v_{gas}} \left[\frac{-dp_{gas}}{dx} \right] , \qquad (1)$$

where k is the absolute permeability, p_{gas} is the gas pressure, v_{gas} is the gas superficial velocity, x is the axial distance along the core, and μ_{liq} is the wetting-liquid viscosity. FFR may be considered either as a foam flow resistance or as an inverse foam mobility, both made nondimensional by the absolute permeability and the liquid-phase viscosity. Figures 10 and 11 replot the data of Figs, 7 and 9, respectively, in terms of FFR.

Figure 10 indicates that at constant liquid velocity foam is a shear-thinning fluid: higher gas velocities reduce FFR. The simplest models of the flowing bubble-train regime reveal that at constant texture the pressure drop should vary with gas velocity to the 2/3 power [11,21,22], as observed by Friedmann, Chen, and Gauglitz [10]. This means that FFR should vary with gas velocity to the -1/3 power. Because of the insensitivity of gas pressure gradient to gas velocity, however, Fig. 10 reveals a -1 power dependence, or a much more strongly shear-thinning foam.

At least three explanations may be offered. First, higher gas velocities could coarsen the foam texture. The reason is that processing more gas through a fixed number of germination sites (recall that the liquid saturation is constant) of constant snap-off frequency produces larger bubbles and decreases bubble density. Further, higher gas velocities lead to faster coalescence, also coarsening the foam [20]. Second, additional fluid-mechanical resistances, such as viscous dissipation in stretching and contracting lamellae, could contribute to the foam rheology. Third, the higher pressure gradients at higher gas velocities could release trapped bubbles and open more flow channels. However, this latter effect of trapped-bubble release should not be significant because of the relatively constant pressure gradient independent of gas velocity (cf. Fig. 7).

From Fig. 11 we discover that foam flow at constant gas velocity appears to be approximately Newtonian. That is, FFR increases almost proportionally with increasing liquid velocity. The proposed explanation is that the higher liquid velocities through germination sites increase the frequency of snap-off, making more bubbles and a finer textured foam. Thus, liquid velocity influences the foam mobility indirectly through bubble density.

The observations in Figs. 7 and 9 that foam pressure gradients increase about linearly with liquid velocity and are reasonably independent of gas velocity suggest that FFR is directly proportional to v_{liq}/v_{gas}. This means also that FFR^{-1} (i.e., the effective foam flow mobility) is directly proportional to f_{gas}/f_{liq}, independent of total velocity. Thus a plot of FFR^{-1} versus total velocity should yield horizontal lines for constant values of fractional gas flow, with the spacing between the lines increasing as fractional gas flow increases. Lee and Heller [29] report plots for CO_2 foam that seem to show this behavior, except possibly at the highest gas fractional flows (see Figs. 3 and 4 of [29]).

Because we find that FFR is proportional to v_{liq}/v_{gas}, the quantity $FFR(v_{gas}/v_{liq})$ should be a constant independent of fractional flow and total velocity, as shown in Fig. 12. There does appear to be a slight upward trend toward high foam qualities, consonant both with the deviations from linearity in Fig. 9 at low liquid velocity and with the deviations seen by Lee and Heller [29]. Nevertheless, if proven general, the correlation suggested in Fig. 12 should be extremely useful for practical estimates of foam flow behavior. With only one or two measurements of foam pressure drops and flow rates in a given porous medium and with a given surfactant system (i.e., to set the absolute level of $FFR(v_{gas}/v_{liq})$), the entire steady flow behavior of foam can be predicted. We caution that a wider range of foam qualities, and different core permeabilities and surfactant types and concentrations must be studied before such a correlation can be solidified.

Finally, Fig. 13 repeats the general finding in foam-flow studies that flow studies that the liquid flow resistance obeys Darcy's law. Here the liquid relative permeability is plotted as a function of gas fractional flow for several different liquid and gas flow rates. A constant value of about 10^{-3} emerges. This value is very close to that measured independently in two-phase flow of continuous gas and surfactant-free brine in Fig. 2 at the wetting-liquid saturation of 30-35%. Hence increasing (or decreasing) liquid flow rates during steady flow of strong foam simply forces more (or less) liquid through the liquid-filled channels. The number of liquid paths is not materially changed.

The attentive reader will note that $FFR(v_{gas}/v_{liq})$ and the inverse relative permeability to the liquid phase are identical (i.e., compare the constant values in Figs. 12 and 13). This follows immediately because at steady state the identical pressure gradients in the wetting and nonwetting phases force the velocity-weighted resistances to be identical. The underlying reason why both $FFR(v_{gas}/v_{liq})$ and the inverse relative permeability to the liquid phase are constant is that the liquid saturation remains constant independent of both the gas and liquid velocity.

In summary, foam flowing in porous media is a rheopectic fluid which at steady state is pseudoplastic with respect to gas flow and Newtonian with respect to liquid flow. Foam exhibits fascinating multiple personalities. Apparently, the foam texture adjusts to set a flow resistance that is compatible with a constant and low liquid saturation in the core. Because of the strong coupling between foam flow and foam texture, progress at quantifying the rheology of this unique fluid [10] can only be made by directly measuring bubble-size distributions.

CONCLUSIONS

We make the following conclusions for foam flow in

1 μm^2 sandstone at about 5 MPa (700 psia) back pressure and for total superficial velocities between 1 and 45 m/day and foam quality between 0.7 and 0.995:

1. During transient foam flooding of a surfactant-solution-saturated core, the foam flow resistance builds in time and continuously varies from that characteristic of free gas to that of a strong, fine-textured foam.

2. Steady foam flow resistance increases with increasing liquid velocity but decreases with with increasing gas velocity. No hysteresis is observed in the steady state.

3. Although foam flow resistance varies with flow rate, liquid saturations at steady state do not. They are constant at 0.3 to 0.35 independent of flow rates and foam quality. Therefore, foam flow resistance is not a unique function of liquid saturation.

4. Liquid flow resistance during foam flow obeys Darcy's law and exhibits the standard relative permeability pertinent to the core liquid saturation, independent of liquid and gas flow rates.

5. A unique flow-resistance correlation is suggested which collapses all our data into a single value. This value is characterized only by the nature of the porous medium and the stabilizing surfactant package and is independent of foam quality and total velocity.

6. The most crucial parameter controlling foam flow resistance in porous media apparently is the bubble texture.

NOMENCLATURE

$f =$ fractional flow (dimensionless)

$FFR = \dfrac{k}{\mu_{liq} v_{gas}} \left[\dfrac{-dp_{gas}}{dx} \right]$, nondimensional foam flow resistance

$I =$ intensity of gamma-ray radiation (counts/s)

$k =$ absolute permeability (μm^2)

$L =$ core length (m)

$p =$ pressure (Pa)

$S =$ saturation (dimensionless)

$v =$ superficial velocity (m/s)

$x =$ distance along core (m)

Greek letters:

$\mu =$ viscosity (Pa·s)

Subscripts:

$d =$ 0% liquid saturation

$w =$ 100% liquid saturation

ACKNOWLEDGMENTS

This work was supported by the Gas Research Institute, Chicago, IL, under Contract No. 5086-271-1160, and by the U.S. Department of Energy, under Contract No. DE-AC03-76SF00098 to the Lawrence Berkeley Laboratory of the University of California.

REFERENCES

1. Huh, D. G. and Handy, L. L.: "Comparison of Steady and Unsteady-State Flow of Gas and Foaming Solution in Porous Media," SPE 15078, presented at the 1986 California Regional Meeting of the SPE, Oakland, CA, April 2-4.

2. Nahid, B. H.: "Non-Darcy Flow of Gas through Porous Media in the Presence of Surface Active Agents," Ph.D. Thesis, University of Southern California, Los Angeles, CA., (1971).

3. Sanchez, J. M. and Schechter, R. S.: "The Effect of Trace Quantities of Surfactant on Nitrogen/Water Relative Permeabilities," SPE 15446, presented at the 1986 Annual Technical Conference and Exhibition of the SPE, New Orleans, LA, October 5-8.

4. Treinen, R.J., Brigham, W.E., and Castanier, L.M.: "Apparent Viscosity Measurements of Surfactant Foam in Porous Media -- SUPRI TR-48," U.S. Dept. of Energy Report DOE/SF/11564-13 (DE86000260), December 1985.

5. DeVries, A. S. and Wit, K.: "Rheology of Gas/Water Foam in the Quality Range Relevant to Steam Foam," SPE 18075, presented at the 1988 Annual Technical Conference and Exhibition of the SPE, Houston, TX, October 2-5.

6. Reda, D.C. and Eaton, R.R.: "Definition of a Facility for Experimental Studies of Two-Phase Flows and Heat Transfer in Porous Material," AIAA 16th Thermophysics Conference, Paper No. AIAA-81-1190 (1981).

7. Moore, W.J.: *Physical Chemistry* 3rd ed, Prentice-Hall, Englewood Cliffs, NJ (1963) p. 820.

8. Mohammadi, S.S., Van Slyke, D.C., and Ganong, B. "Steam-Foam Pilot Project in Dome-Tumbador, Midway Sunset Field," paper SPE 16736 presented at the 1987 Annual Technical Conference and Exhibition of the SPE, Dallas, TX, September 27-30.

9. Ransohoff, T. C. and Radke, C. J.: "Mechanism of Foam Generation in Glass-Bead Packs," *SPERE* (May 1988) 573-585.

10. Friedmann, F., Chen, W. H. and Gauglitz, P. A., "Experimental and Simulation Study of High-Temperature Foam Displacement in Porous Media," SPE/DOE 17357, presented at the 1988 SPE/DOE Enhanced Oil Recovery Symposium, Tulsa, OK, April 17-20.

11. Falls, A.H., Hirasaki, G.J., Patzek, T.W., Gauglitz, P.A, Miller, D.D., and Ratulowski, T.: "Development of a Mechanistic Foam Simulator: The Population Balance and Generation by Snap-Off," *SPERE* (August 1988) 884-892.

12. Bond, D.C. and Bernard, G.G.: "Rheology of Foams in Porous Media," presented at the 1966 SPE-AIChE Joint Symposium and AIChE 58th Annual Meeting, Dallas, TX, February 7-10.

13. Holm, L. W.: "The Mechanism of Gas and Liquid Flow Through Porous Media in the Presence of Foam," *SPEJ* (December 1968) 359-369.

14. Bernard, G.G., Holm, L. W., and Jacobs, W. L.: "Effect of Foam on Trapped Gas Saturation and on Permeability of Porous Media to Water," *SPEJ* (December 1965) 295-300.

15. Friedmann, F. and Jensen, J. A.: "Some Parameters Influencing the Formation and Propagation of Foams in Porous Media," SPE 15087, presented at the 1986 California Regional Meeting of SPE, Oakland, CA, April 2-4.

16. Manlowe, D. J.: "Pore-Level Mechanisms of Foam Destabilization by Oil in Porous Media," M. S. Thesis. University of California, Berkeley (1988), Appendix 4B, p. 186-189.

17. Mast, R. F.: "Microscopic Behavior of Foam in Porous Media," SPE 3997, presented at the 1972 Annual Meeting of SPE, San Antonio, TX, October 8-11.

18. Owete, O. S. and Brigham, W. E.: "Flow Behavior of Foam: A Porous Micromodel Study," *SPERE* (August 1987) 315-323.

19. Ettinger, R.A.: "Flow Resistance of Foam in Berea Sandstone," M.S. Thesis, University of California, Berkeley, 1989.

20. Jimenez, A. I. and Radke, C. J.: "Dynamic Stability of foam Lamellae Flowing Through a Periodically Constricted Pore," presented at the Symposium on Advances in Oil Field Chemistry, Third Chemical Congress of the North American Continent and 195th National Meeting of ACS, Toronto, Canada, June 5-11 (1988).

21. Ginley, G. M. and Radke, C.J.: "The Influence of Soluble Surfactants on the Flow of Long Bubbles Through a Cylindrical Capillary," presented at the Symposium on Advances in Oil Field Chemistry, Third Chemical Congress of the North American Continent and 195th National Meeting of ACS, Toronto, Canada, June 5-11 (1988).

22. Hirasaki, G. J. and Lawson, J. B.: "Mechanisms of Foam Flow in Porous Media: Apparent Viscosity in Smooth Capillaries," *SPEJ* (April 1985) 176-190.

23. Rossen, W. R.: "Theories of Foam Mobilization Pressure Gradient," SPE/DOE 17358, presented at the 1988 SPE/DOE Enhanced Oil Recovery Symposium, Tulsa, OK, April 17-20.

24. Ransohoff, T.C., Gauglitz, P.A., and Radke, C.J.: "Snap-off of Gas Bubbles in Smoothly Constricted Noncircular Capillaries," *AIChE Journal* (May 1987) 753-765.

25. Khatib, Z.I., Hirasaki, G.J., and Falls, A.H.: "Effects of Capillary Pressure on Coalescence and Phase Mobilities in Foams Flowing Through Porous Media," *SPERE* (August 1988) 919-926.

26. Bikerman, J.J.: *Foams*, Springer-Verlag, New York, NY (1973) p. 194.

27. Minssieux, L.: "Oil Displacement by Foams in Relation to their Physical Properties in Porous Media," *JPT* (January 1974) 100-108.

28. Johnson, E.F., Bossler, D.P., and Naumann, V.O.: "Calculation of Relative Permeability from Displacement Experiments," *Trans. AIME 216* 370-372 (1959).

29. Lee, H.O. and Heller, J.P.: "Laboratory Measurements of CO2-Foam Mobility," paper SPE 17363, presented at the 1988 SPE/DOE Enhanced Oil Recovery Symposium, Tulsa, OK, April 17-20.

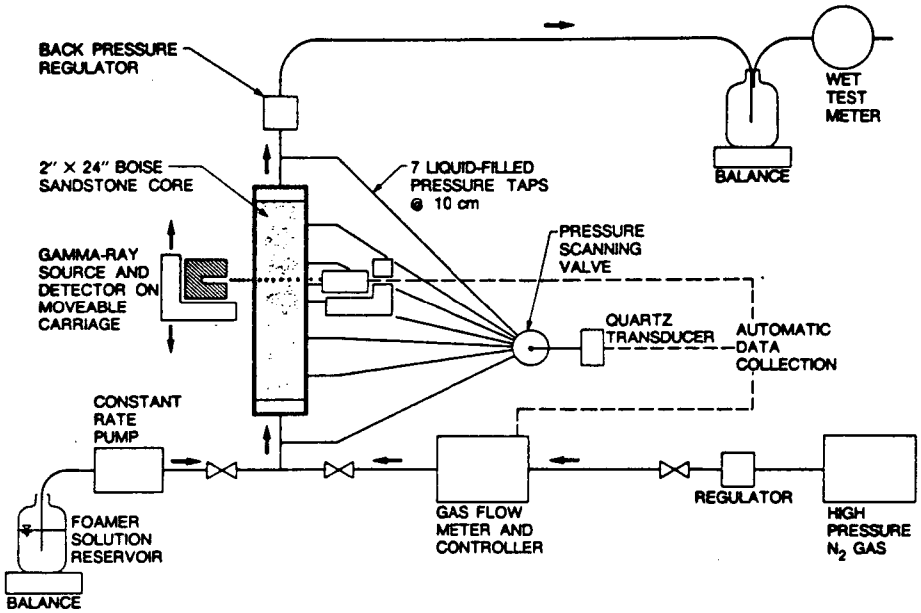

Fig. 1—Apparatus for foam flow experiments.

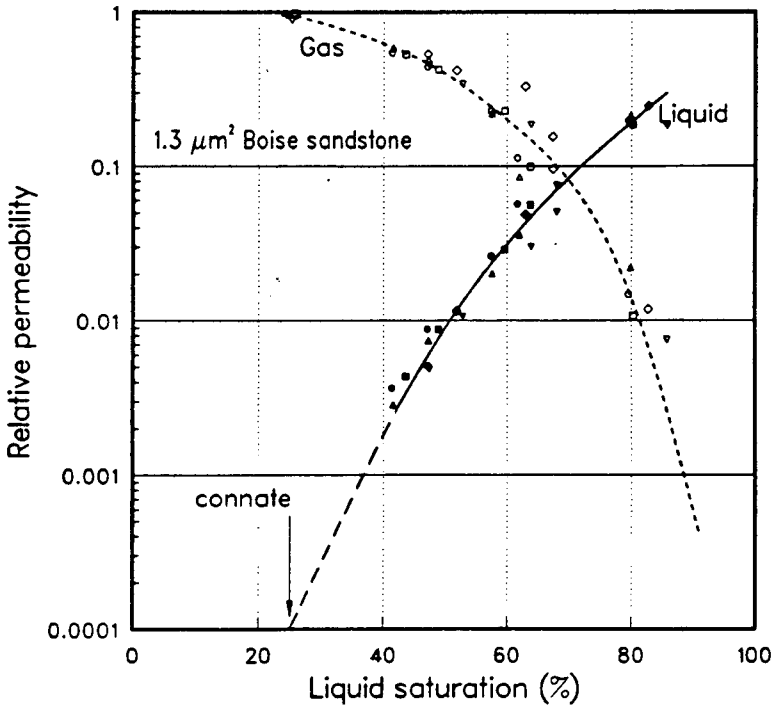

Fig. 2—Gas/brine relative permeability of Boise sandstone. Open symbols refer to gas and closed symbols to the liquid phase. Various symbols reflect individual measurements between each pair of adjacent pressure taps.

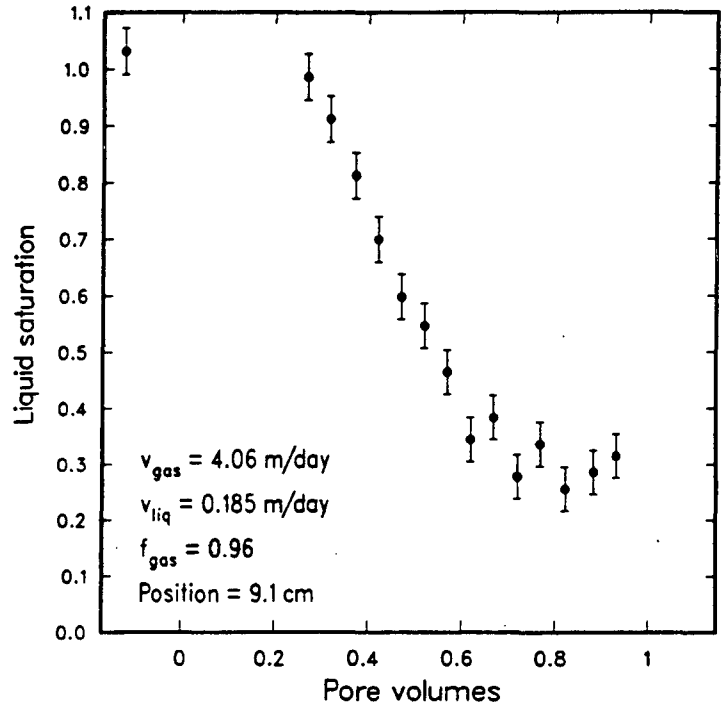

Fig. 3—Transient decrease in local liquid saturation during first pore volume of foam flooding. Liquid viscosity = 1.7 mPa·s.

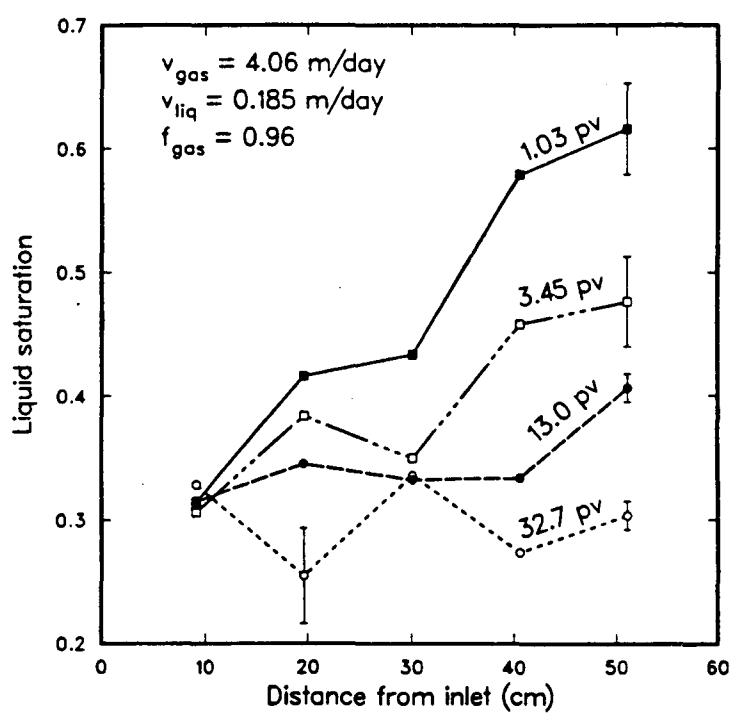

Fig. 4—Liquid saturation profiles measured during transient displacement of liquid by foam. Error bars shown at 51 cm are typical. Liquid viscosity = 1.7 mPa·s.

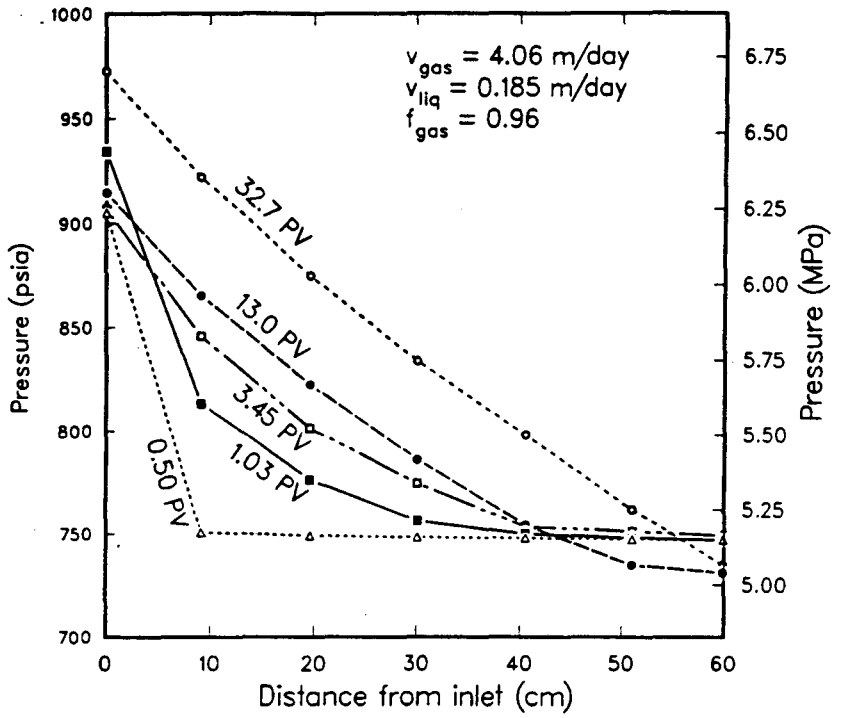

Fig. 5—Pressure profiles measured during transient displacement of liquid by foam. Liquid viscosity = 1.7 mPa·s.

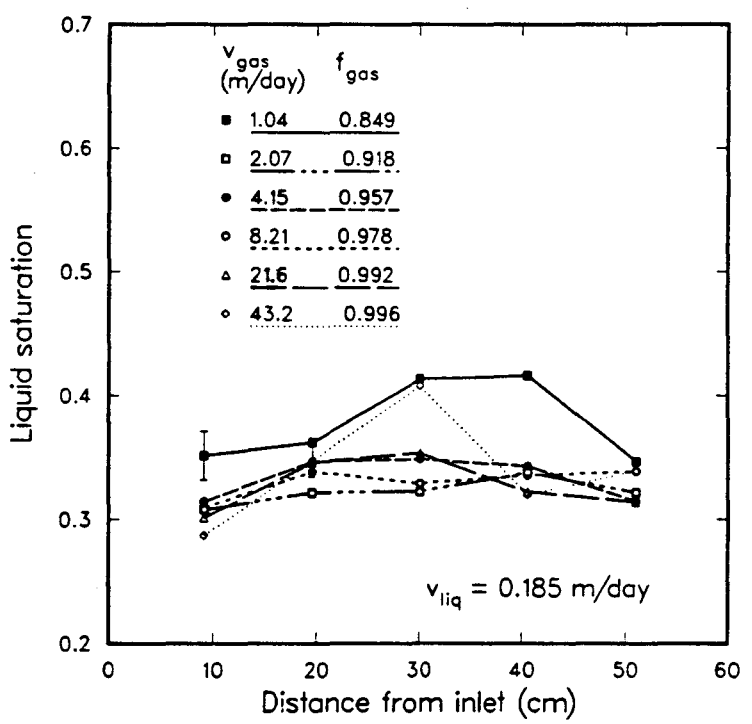

Fig. 6—Liquid saturation profiles measured during six successive steady states at different gas velocities. Liquid velocity held constant at 0.185 m/day; liquid viscosity = 1.7 mPa·s. The longer error bar is typical for measurements made with v_{gas} = 1.04 m/day; the shorter error bar is typical for measurements made at all other gas velocities.

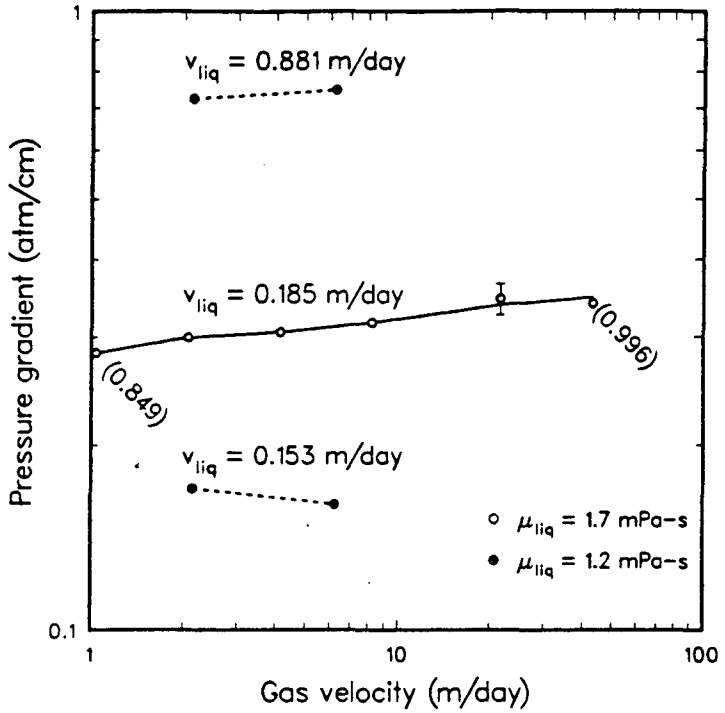

Fig. 7—Steady foam pressure gradient vs. gas velocity for three constant liquid velocities. Numbers in parentheses correspond to fractional gas flow. A typical error bar is shown.

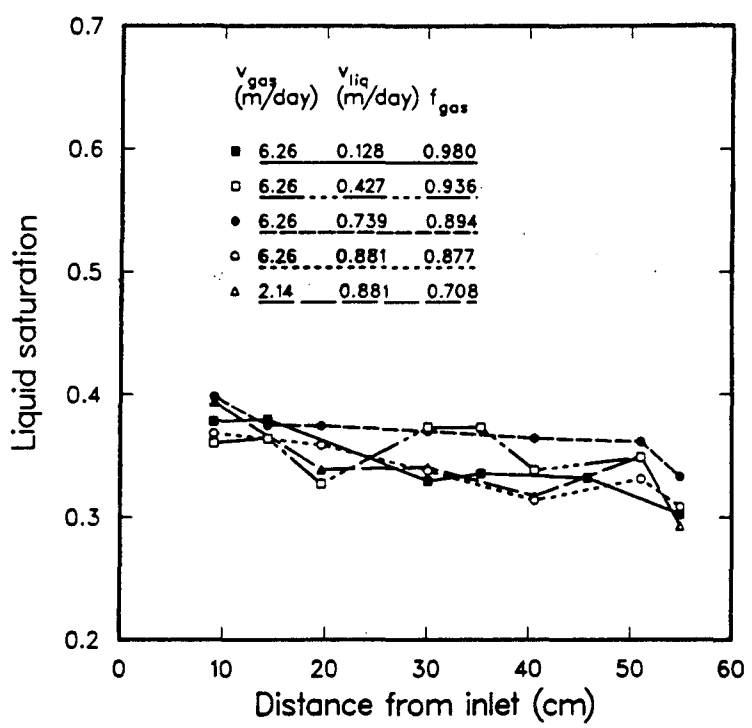

Fig. 8—Liquid saturation profiles measured during five successive steady states. These profiles correspond to points labeled A through E in Fig. 9. Uncertainty for all measurements is ±2%. Liquid viscosity = 1.2 mPa·s.

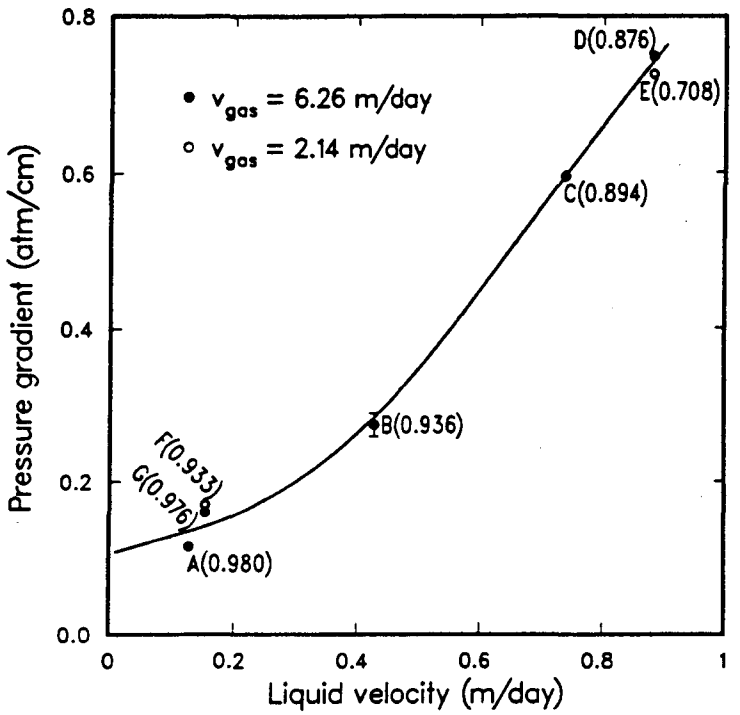

Fig. 9—Steady foam pressure gradient vs. liquid flow rate. Points labeled A through G represent consecutive steady states. Numbers in parentheses correspond to fractional gas flow. Liquid viscosity = 1.2 mPa·s. A typical error bar is shown.

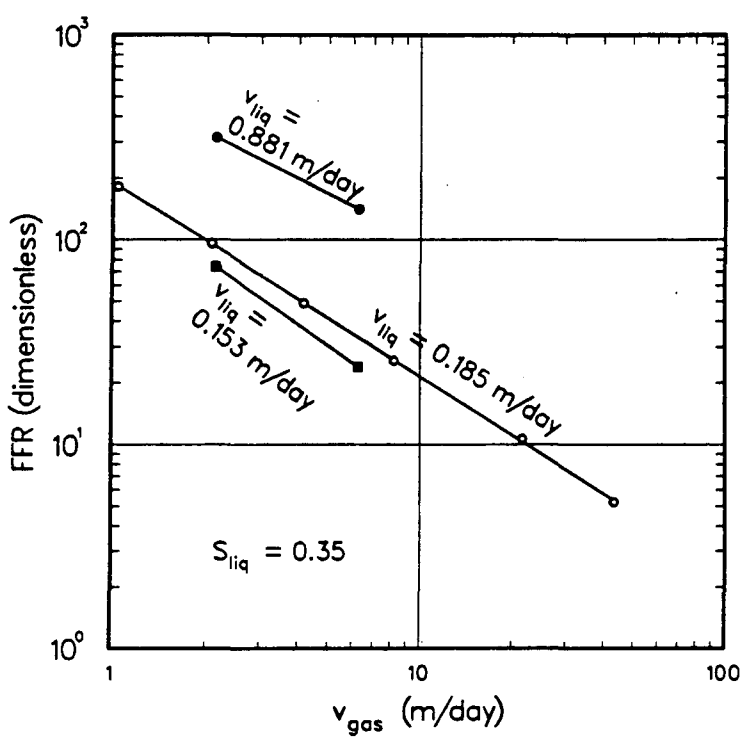

Fig. 10—Foam flow resistance vs. gas velocity.

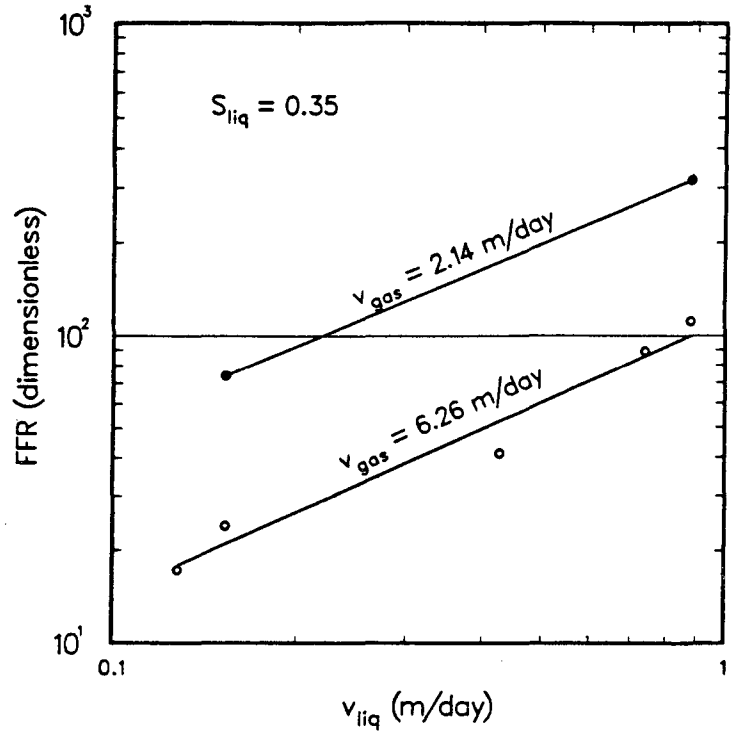

Fig. 11—Foam flow resistance vs. liquid velocity.

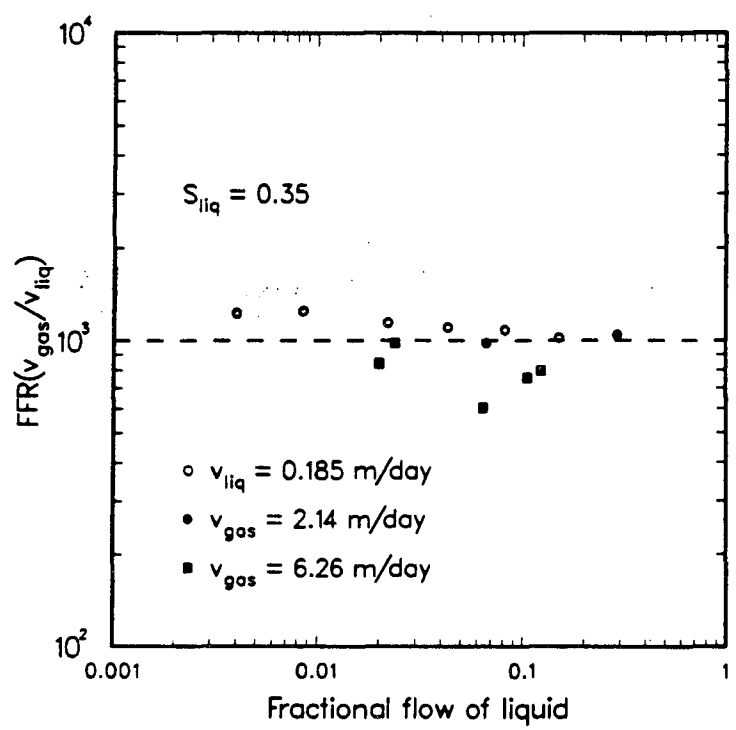

Fig. 12—FFR (v_{gas}/v_{liq}) vs. fractional flow of liquid. The dashed line is eye fit.

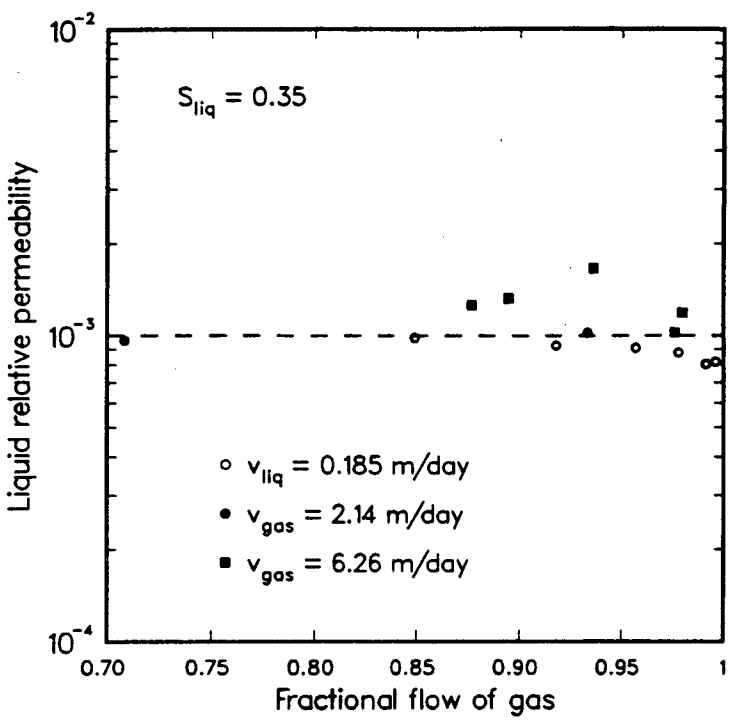

Fig. 13—Liquid relative permeability vs. fractional flow of gas. The dashed line is eye fit.

Appendix F.

Aqueous Foams for Control of Gas Migration and Water Coning in Aquifer Gas Storage

AQUEOUS FOAMS FOR CONTROL OF GAS MIGRATION AND WATER CONING IN AQUIFER GAS STORAGE

L'EMPLOI DE MOUSSES AQUEUSES POUR MAITRISER LA MIGRATION DU GAZ ET LE SOULEVEMENT EN CONE DE L'EAU DANS L'ACCUMULATION DU GAZ EN AQUIFERE

P. Persoff, K. Pruess, S.M. Benson, and Y.S. Wu
Earth Sciences Division, Lawrence Berkeley Laboratory, USA

C.J. Radke and P.A. Witherspoon
University of California, Berkeley, California, USA

Y.A. Shikari
Gas Research Institute, USA

ABSTRACT

Two causes of poor recoverability are migration of stored gas far from the injection well and upward coning of water into withdrawal wells. We conducted laboratory and numerical simulation investigation of the use of aqueous foams to block the flow of gas or liquid to ameliorate these problems. Experiments in sandstone cores at simulated reservoir conditions showed that foam reduces the permeability to gas and liquid by three orders of magnitude. A numerical simulation study showed that water coning could be significantly delayed by placing a horizontal foam lens just above the gas-water interface. We also discuss the conditions for forming foam in situ, the feasibility of emplacing a foam bank, and the durability of permeability reduction. Laboratory experiments and numerical simulation indicate potential for significantly improving the efficiency of aquifer gas storage with aqueous foams. A field trial of foam to prevent water coning is recommended.

RÉSUMÉ

Deux des causes de la mauvaise récupérabilité du gaz accumulé sont sa migration loin du puits d'injection et le soulèvement en cône de l'eau dans les puits de soutirage. Nous avons effectué des études en laboratoire et des études de simulation numérique de l'emploi des mousses aqueuses pour bloquer l'écoulement de gaz ou de liquide en vue de pallier à ces problèmes. Des expériences faites sur des carottes de grès dans des conditions simulées de réservoir ont indiqué que l'emploi de la mousse diminue de trois ordres de grandeur la perméabilité au gaz et au liquide. Une étude de simulation numérique a indiqué que la mise en place d'une lentille horizontale de mousse juste au-dessus du plan de séparation du gaz et de l'eau pourrait nettement retarder le soulèvement en cône de l'eau. Nous traitons aussi des conditions requises pour former une mousse in situ, la possibilité de mettre en place un banc de mousse, et la durabilité de la diminution de perméabilité. Les expériences en laboratoire et la simulation numérique indiquent que l'emploi des mousses aqueuses pourrait nettement améliorer l'efficacité de l'accumulation du gaz en aquifère. Il est préconisé de passer à un essai pratique de mousse pour empêcher le soulèvement en cône de l'eau.

INTRODUCTION

The transmission and distribution segments of the gas industry in the United States share a common interest in gas storage. To meet peak loads and to ensure dependable delivery of gas to all end users, gas storage has become a vital link in the supply, transport, and distribution network. Of the various forms of natural-gas-storage technologies adopted, large-scale seasonal storage by utilities in underground formations is perhaps the most prevalent.

Two aspects of underground storage of natural gas -- migration of gas beyond the designated storage area during the gas injection cycle and water coning into wells during the withdrawal cycle -- are addressed in this study. During the formation of the initial storage volume in an underground aquifer, some of the injected gas fingers away from the main bubble, sometimes for long distances, because of the adverse mobility ratio between water and gas. This migrated gas is often difficult to recover, leading to a reduced percentage of working gas (the fraction of total gas in storage that can be recovered during a withdrawal season). It is, thus, important to devise an effective means of controlling such migration. Another aspect of gas storage operation pertains to a typical wellbore problem in aquifer gas storage where water coning during gas withdrawal significantly reduces the deliverability (or well productivity). Elimination -- or significant delay -- of water coning in the production zone is, thus, highly desirable during the withdrawal season.

In the past, these problems have been dealt with by injection of large volumes of base gas (typically twice as much as the working gas, with the proportion being larger in specific reservoirs), but long-term increases in both interest rates and the value of natural gas have impelled a search for methods to control gas migration and water coning. One possible solution to these problems is the use of aqueous foam as a mobility control agent. The basic idea of foam-protected gas storage is to emplace a suitable foam barrier in an aquifer that would confine the stored gas in a compact volume around the injection wells [1]. Two possible applications are shown in Fig. 1. Because the proposed foam would contain about 65 percent by volume of natural gas, it would provide a compatible and easily applied means of mobility control.

For successful application of foam to underground storage of natural gas, it must be economical, environmentally acceptable, and technically feasible. The economics of foam protection must be calculated for each site, based upon such factors as the value of natural gas and of storage capacity, and the geology of the reservoir. Several concepts for foam application were presented, and the economics of foam protection discussed, with some example calculations, by Witherspoon et al. [1]. In general, the cost of foam injection is heavily weighted by the cost of drilling wells for foam injection, so the economics are most favorable where the volume of foam

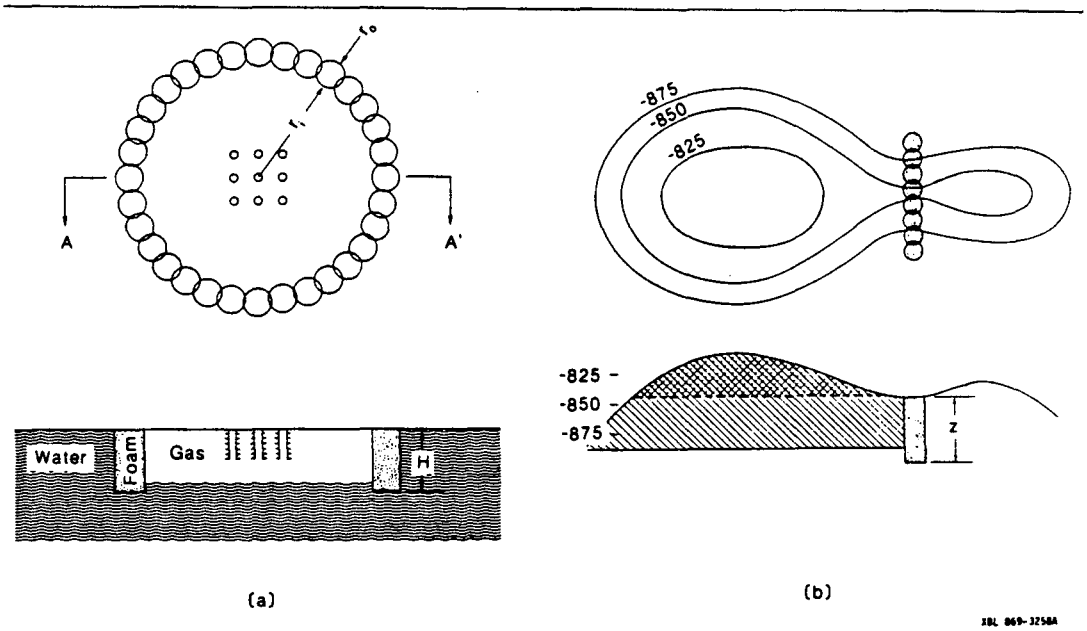

Figure 1. Application of foam to improve underground gas storage by controlling gas migration (after Witherspoon et al., 1987).
(a) Foam plumes formed at peripheral wells intersect to form a continuous barrier, containing stored gas in a more compact bubble near the injection-withdrawal wells. The use of foam obviates the need for natural closure.
(b) A small foam barrier to cut off a spill point produces a large increase in storage capacity.

to be emplaced is small relative to the increase in working gas, as in the use of a foam barrier to increase storage capacity by lowering a spill point [1], or where foam can be emplaced through an existing well, as for water-coning control. Recent improvements in horizontal-well drilling may allow a long foam barrier (as would be needed to lower a spill point) to be emplaced through a single well, also improving the economics.

Environmental acceptability also must be determined on a site-specific basis. Fortunately, the existing use of surfactants in oilfield applications suggests that if the aquifer is not classified as a potential underground source of drinking water (< 10,000 mg/L total dissolved solids), injection of non-toxic, biodegradable surfactants should be possible.

The purpose of this paper is to examine the technical questions that must be answered to make the proposed applications of foam feasible. We report results of laboratory experiments that answer some of these questions and assess our state of knowledge for others. The technical questions include:

- How is foam formed in porous media? What conditions (e.g. flow rates, liquid saturation) are necessary for the formation of foam?
- How can foam best be emplaced in a formation?
- By what mechanism does foam reduce the permeability of a porous medium to gas and to liquid? What is the degree of permeability reduction?
- How long does the permeability reduction last? How can it be made to last longer?
- What is the most effective way to use foam for underground gas storage?
- How can foam be broken, if desired?

FOAM GENERATION IN POROUS MEDIA

Foam is a mixture of gas and liquid phases such that the gas phase is not continuous but rather has been broken up into many bubbles, separated by thin liquid films called lamellae. (One or more continuous gas paths may also exist through a length of porous medium.) The question of foam formation is therefore the question of lamellae formation. Lamellae are generated when gas invades liquid-filled pores. Surfactant is not necessary for the production of lamellae, but lamellae are thermodynamically unstable because they represent extended surface area, and without surfactant they rupture immediately.

Lamellae parallel to the direction of gas flow exert a small reduction on the gas permeability, and are referred to as a "weak" foam; but lamellae perpendicular to the direction of gas flow literally block the gas flow and form a "strong" foam which typically reduces the gas permeability by orders of magnitude.

Radke and Ransohoff [2] experimentally demonstrated the existence of a critical gas velocity that must be exceeded for formation of a strong foam in initially liquid-saturated beadpacks. In our experiments in sandstone, described below, the initial liquid saturation also was 100%, and strong foam was formed in every experiment, whether only gas was injected or gas and liquid were injected simultaneously. In these experiments the minimum superficial gas velocity was 1 m/day. This suggests that the minimum velocity for strong foam formation in saturated sandstone is below this value.

EMPLACING A FOAM BANK IN A POROUS FORMATION

Emplacement of a foam barrier to block gas flow as described by Witherspoon et al. [1], or to block liquid flow as described below, requires that foam be driven some distance from an injection well. The essential problem is that foam is a non-Newtonian fluid with large apparent viscosity, and the injection pressure must be limited to avoid fracturing the formation. These factors combine to limit the distance and velocity at which foam can be driven from an injection well.

We conducted a series of experiments [3] to study the relationship of foam pressure gradient to gas and liquid flow rates. The apparatus used in those experiments, shown in Fig. 2, was also used for the experiments reported in this paper. Pressure and liquid saturation (by gamma-ray densitometry) were automatically measured at several locations along the sandstone core. Liquid was delivered by a constant rate pump, and nitrogen gas was delivered at either constant mass flow rate or constant injection pressure. Back pressure was maintained by a dome-loaded back-pressure regulator. In the work of Persoff et al. [3], the pressure gradient was found, surprisingly, to be essentially independent of the gas flow rate, and (except at the very lowest liquid flow rates) approximately proportional to the liquid flow rate. Quantitatively, this is expressed as

$$-\left(\frac{dp}{dx}\right)\frac{k}{\mu_{liq}\, v_{liq}} = \frac{1}{k_{rl}} = \text{constant (dimensionless)} \qquad (1)$$

where p is pressure, x is distance, k is the intrinsic permeability of the sandstone, v is the superficial velocity, μ is viscosity, and k_{rl} is the relative permeability to liquid. This behavior is accounted for by the separate effects of the gas and liquid flow rates on the number of lamellae flowing in the gas phase [3]. The value of the constant

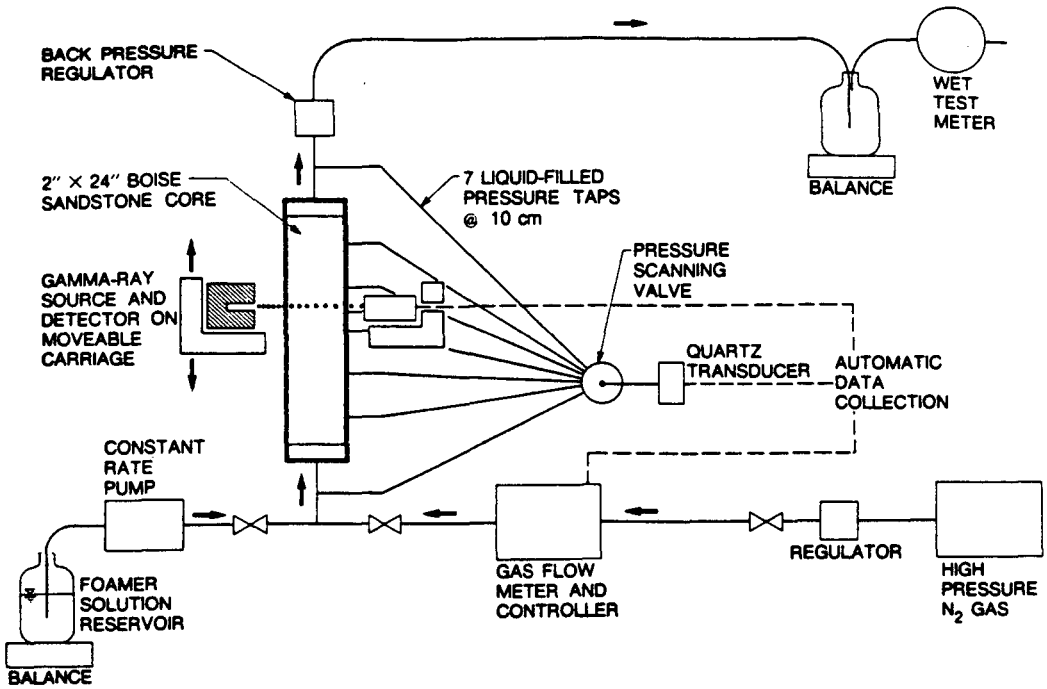

Figure 2. High-pressure apparatus for foam flow and blocking experiments in sandstone cores.

depends upon the foamer solution and porous medium. Using the foamer solution described below, we found that this value was approximately 1000 in 1.3 μm^2 (1300 millidarcy) Boise sandstone, and approximately 3000 in 0.19 μm^2 (190 millidarcy) Berea sandstone. The difference apparently results from the different relative permeability curves for the two sandstones. In both experiments, the observation that $1/k_{rl}$ was constant agreed with the independent observation that the liquid saturation in the core was uniform and constant over order-of-magnitude changes in gas and liquid flow rates. The practical implication of this finding is that, to emplace a foam barrier with minimum injection pressure, liquid velocity must be very low or zero (i.e., inject gas only).

Formation of a spaced foam block

Another approach to drive foam in-situ to a large distance, with limited injection pressures, is to create the foam block at some distance away from the injection well, rather than immediately adjacent to the borehole. This would reduce the distance through which the steep pressure gradient characteristic of foam is exerted, and in addition the region nearest the well, where pressure gradients in radial flow are normally steepest, would be free of foam. For small storage projects, a spaced foam block could also possibly allow gas to be stored inside the annular foam barrier, using the same well for foam injection and for gas injection and withdrawal. The concept of injecting a surfactant solution, displacing it with brine, and then injecting gas, was mentioned in an early patent [4], but no confirming data have been presented to show its feasibility.

We investigated experimentally the feasibility of creating a spaced foam block. The core (60-cm long, 1.3 μm^2 [1300 millidarcy] Boise sandstone) was initially saturated with foamer solution, and 0.42 pore volumes (PV) of brine were injected to displace the foamer solution 25 cm away from the injection point before injecting gas. (The specific foamer solution and brine are described in the next section.) Next, gas was injected at a constant injection pressure of 5.17 MPa (750 psi) against a back pressure of 4.91 MPa (712 psi). (All pressures are absolute.) Fig. 3 shows the pressure profiles developing over time as 0.8 PV of gas were injected. The steep pressure gradient in the region 40 to 60 cm shows that the gas mobility was low in this region, where a strong foam was formed, while the flat pressure gradient in the region 0 to 40 cm shows that the foam bank was spaced away from the inlet. Before gas was injected, the core was saturated with foamer solution from 25 to 60 cm, and with nascent brine from 0 to 25 cm. As gas displaced brine in the inlet region, the foamer solution was displaced an additional 15 cm through the core, so that the region of reduced gas mobility extended not from 25 to 60 cm but from 40 to 60 cm. Because of desorption of the surfactant and hydrodynamic dispersion, the displacement of foamer solution by brine was not complete. As a result, the region 0 to 40 cm was not completely free of foam, but actually contained a weak foam, as evidenced by the small but non-zero pressure gradient.

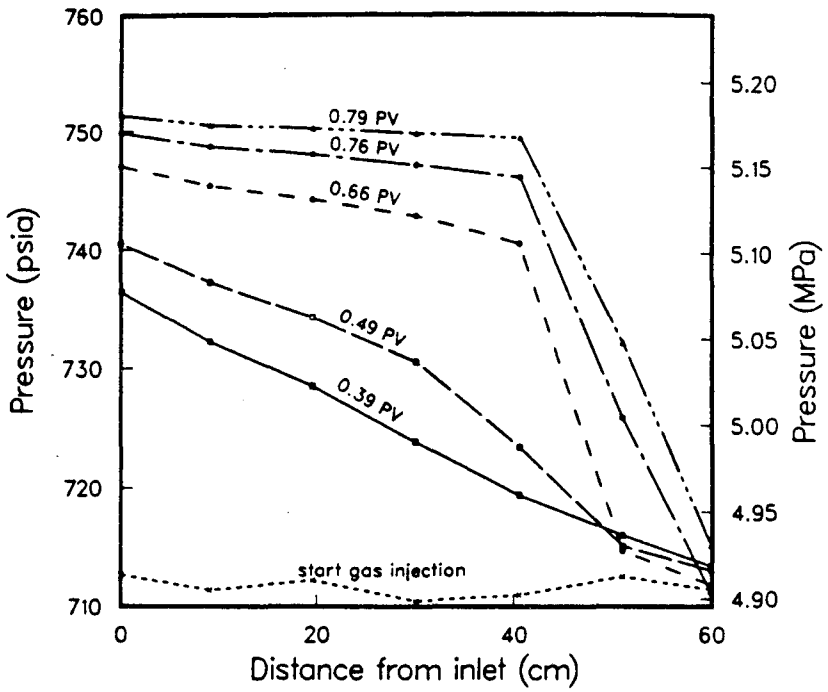

Figure 3. Pressure profiles during development of a spaced foam block.

PERMEABILITY REDUCTION BY FOAM

Foamer solution

As mentioned previously, the gas-blocking effect of foam in porous media results from numerous individual lamellae, each of which is thermodynamically unstable, but made metastable by the presence of surfactant in the liquid phase. Therefore the gas-blocking effect of foam eventually decays as individual lamellae rupture. We screened combinations of surfactants to develop a formula which was compatible with high-salinity, high-hardness brine typical of gas-storage reservoirs, and which would produce lamellae resistant to spontaneous rupture. We used a synthetic brine, representative of the Mt. Simon aquifer in Illinois where several gas-storage projects are located. The brine contained 5410 mg/L Ca; 1260 mg/L Mg; 66700 mg/L total dissolved solids; and 18750 mg/L as $CaCO_3$ hardness. Enhancement of lamella stability by combining surfactants has been reported previously [1]. The resulting foamer solution, used in all experiments, was 1 weight % alkylethoxysulfate surfactant (Shell Enordet AES 1215-9S, i.e., $CH_3(CH_2)_{11-14}-(O-CH_2CH_2)_9-OSO_4^- Na^+$, or Stepan Steol 7-N, a commercially available near-equivalent), plus 0.2 weight % lauryl alcohol. The insoluble long-chain alcohol was incorporated into the foamer solution by dissolving the surfactant in the brine, warming it to 45°C, and adding the liquid alcohol while stirring. After several days, the excess alcohol separated out from the solution and formed a buoyant turbid layer. The clear lower layer was separated and used for experiments. Failure to remove the turbid alcohol layer caused formation of a skin at the sandstone injection face in early experiments.

Gas blocking by foam

Experiments in sandpacks at low pressure. In preliminary experiments, we demonstrated foam formation, complete gas blockage by foam, and durability of foam blocks in 60-cm long, 1.3-cm diameter, 20-μm^2 (20-darcy) permeability unconsolidated sandpacks, using the apparatus and method described by Witherspoon et al. [1]. The sandpack was initially saturated with the foamer solution. Gas was injected at constant pressure and liquid at constant flow rate; gas and liquid flow rates were measured by timing and weighing foam exit flow into a graduated cylinder. Foam was formed in the sandpack and flowed at steady state conditions for about 1 hr. Then the gas injection pressure was rapidly reduced from the "injection" pressure to the "holding" pressure, and liquid flow was stopped at the same time. In a few minutes, flow of foam from the sandpack stopped, indicating that gas flow was blocked. After blocking occurred, any further gas emerging from the sandpack was collected by displacing water in an inverted graduated cylinder. In this way both the time of first gas breakthrough and the flow rate at breakthrough were monitored.

Blocking was achieved in all cases when the absolute holding pressure was less than 75% of the absolute injection pressure. We interpret this observation to mean that as the bubbles expanded due to the pressure reduction, the lamellae rearranged themselves into a configuration that completely blocked the flow of gas. Eventually, as individual lamellae ruptured, a gas flow path through the sandpack was established and flow (gas breakthrough) was observed.

Foam blocks lasted longest in experiments in which 0.5 weight percent guar (Galactosol 253, Henkel Corp., Houston, TX) was included in the foamer solution. In these experiments, extremely high injection pressure was needed to inject foam because of the high liquid viscosity. Foam was formed in the sandpacks by injecting gas at 2.17 MPa (315 psi) and liquid at 2.01 mL/min. Steady state was reached with a gas flow rate of 5.46 standard cm^3/min. The gas injection pressure was then quickly reduced to 0.17 MPa (25 psi), and the liquid flow was stopped. Gas flow was completely blocked in these experiments. Gas first broke through after two months. Fig. 4 shows the gas permeability calculated from the measured flow rates. After 100 and 250 days in duplicate tests, the permeability suddenly rapidly increased. The gas injection pressure needed to form foam in these experiments was much greater than the gas injection pressure needed in several similar experiment without guar, but the duration of permeability reduction was greater. Because of the extremely high pressure gradients (3.4 MPa/m [150 psi/ft]) needed to inject guar-stabilized foams into the sandpacks, however, we decided not to use guar in further experiments.

Experiments in sandstone cores at high pressure. For more realistic simulation of gas-storage conditions, experiments in foam formation, displacement, and blocking were conducted in 5.1-cm diameter, 60-cm long sandstone cores at elevated back pressure, using the apparatus shown in Fig. 2. Experiments were conducted in a Boise sandstone core of permeability 1.3 μm^2 (1.3 darcy) and porosity 0.25; and in a Berea sandstone sandstone core of permeability 0.19 μm^2 (190 millidarcy) and porosity 0.19.

To measure the permeability to gas, dry gas was injected through a foamed sandstone core under either constant injection pressure or constant mass-flow rate control. In none of these experiments did we observe complete blocking of gas flow, as has occasionally been reported [5; 6]. However, the permeability to gas was reduced below the intrinsic permeability of the rock by approximately three orders of magnitude, indicating that a very substantial reduction in gas leakage rate could be achieved. The permeability to gas was initially very low in all these experiments, gradually increasing to about 1 or 2×10^{-3} μm^2 (1 or 2 millidarcy) during 14 days.

In four experiments, the permeability to gas generally increased gradually with time as shown in Fig. 5. This behavior was observed whether the foam was formed by simultaneous injection of gas and liquid, or injec-

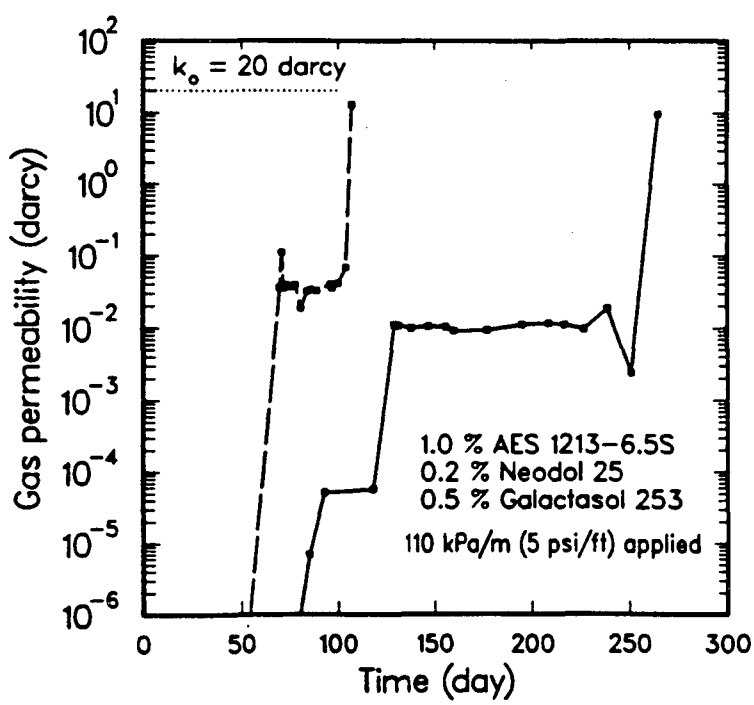

Figure 4. Duration of low permeability in duplicate sandpack experiments in which 0.5 weight % guar polymer was added to the foamer solution.

tion of gas only, whether the gas was injected at constant pressure drop or constant rate, and whether the permeability of the core was 1.3 or 0.19 μm^2 (1300 or 190 millidarcy). The details of each experiment are given in the caption of Fig. 5.

In the first experiment, we attempted to block gas flow completely, by reducing the gas injection pressure, as we had done in the low-pressure experiments. However, the same procedure at elevated back pressure in sandstone did not produce complete blockage. At steady state, the injection pressure was 6.75 MPa (980 psi) against 5.27 MPa (765 psi) back pressure. It was thus impossible to reduce the gas injection pressure far enough to completely block gas flow by bubble expansion (i.e., 25%), as had been done in the low-pressure experiments. At steady state, the gas injection pressure was suddenly reduced from 6.75 MPa (980 psi) to 5.45 MPa (790 psi) so that a 0.17 MPa (25 psi) pressure drop remained across the core. The pressure profile through the core then evolved to a uniform slope and gas continued to flow through the core at a gradually increasing rate, as shown by Fig. 5 (curve A). This experiment was discontinued after 17 days.

Because the pressure-drop/flow-rate experiments showed that the most feasible way to form a foam bank in-situ was to inject gas only, in further experiments foam was formed by injecting only gas into a core initially saturated with foamer solution (curves B - D of Fig. 5).

The increase in permeability shown in Fig. 5 (curve A) suggested that foam might need to be regenerated periodically. Therefore, a method to regenerate foam was investigated. In experiment B, gas was injected into the core at 5.17 MPa (750 psi) against a back pressure of 4.82 MPa (700 psi). Fig. 6 shows the gas flow rate at constant injection pressure. Gas initially invaded rapidly, displacing liquid from the core, and as foam advanced through the core, the flow rate decreased. Gas broke through after one hour, at a flow rate corresponding to a

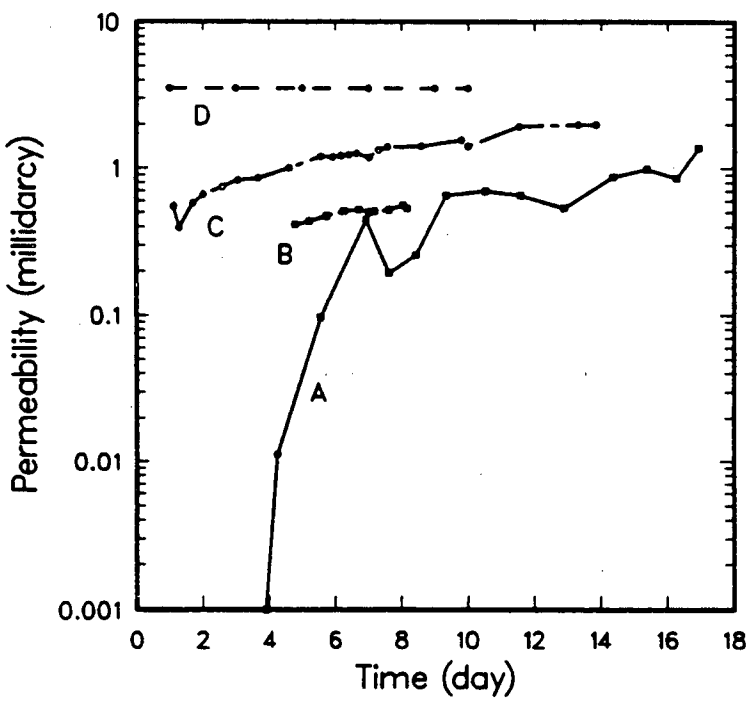

Figure 5. Gradual increase in gas permeability of foam-filled sandstone core, four experiments. In all experiments, the core was initially saturated with the foamer solution.

A = Foam generated by simultaneous injection of gas and liquid at controlled flow rates. Then liquid flow stopped and gas injection pressure reduced. Permeability measured at constant gas injection pressure. Permeability of sandstone without foam = 1.3 μm^2 (1300 millidarcy).

B = Foam generated by injection of gas at constant pressure. Additional slugs of foamer solution injected (see Figs. 5 and 6); permeability shown is after final slug. No injection pressure reduction. Permeability of sandstone without foam = 1.3 μm^2 (1300 millidarcy).

C = Foam generated by injection of gas at constant rate into 1.3 μm^2 (1300 millidarcy) core. No injection pressure reduction.

D = Foam generated by injection of gas at constant rate into 0.19 μm^2 (190 millidarcy) core. No injection pressure reduction.

permeability of 1.9×10^{-3} μm^2 (1.9 millidarcy) or a reduction by a factor of 680 compared to the initial permeability of the core. At this point, an additional 0.03 PV slug of foamer solution was injected while the inlet gas pressure was maintained. As shown in Fig. 6, the gas flow immediately dropped to almost zero and slowly recovered. Although gas permeability through the core was 1.9×10^{-3} μm^2 (1.9 millidarcy) one hour after gas invaded the initially saturated core, it took about 30 hours for the gas permeability to regain that value after the slug was injected. Fig. 7 shows the cumulative gas flow through the core at constant injection pressure. As

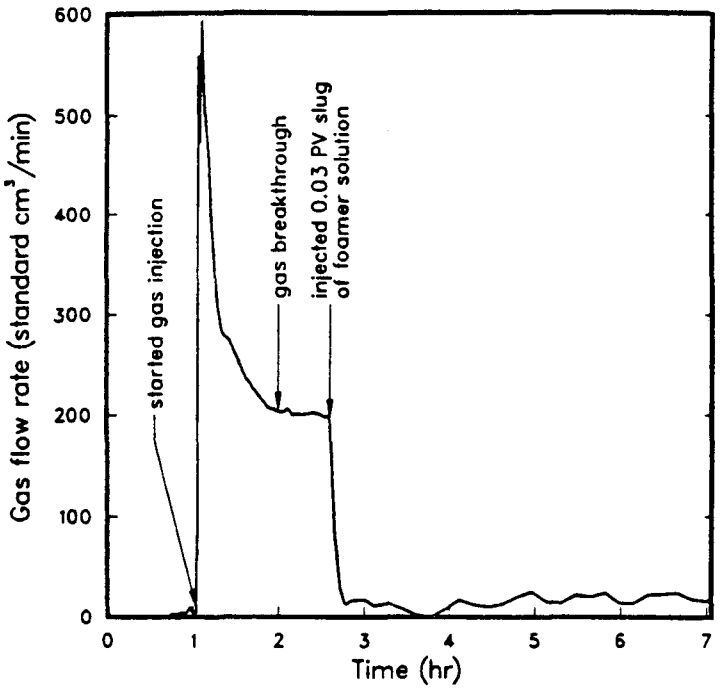

Figure 6. Gas flow rate as a function of time; gas injected at constant pressure into core initially saturated with foamer solution.

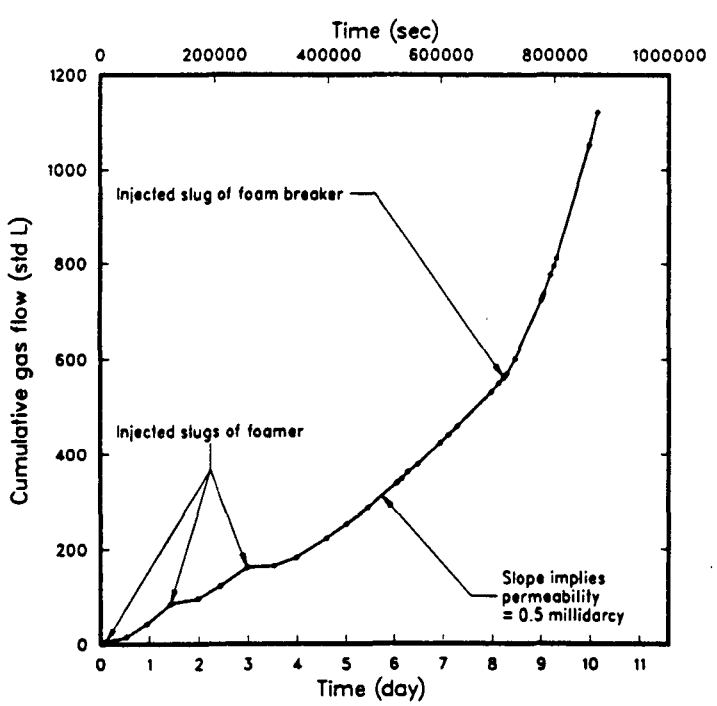

Figure 7. Cumulative gas flow as a function of time; gas injected at constant pressure drop into core initially saturated with foamer solution, showing effect of additional liquid slugs.

shown in this figure, two more slugs were injected. In each case, the permeability dropped to almost zero, and recovered gradually to less than 10^{-3} μm^2 (1 millidarcy). The gradual increase in permeability after injection of the third slug is shown in Fig. 5 (curve B). After 8 days, the foam was broken by a slug of 0.09 PV foam breaker, as described in a later section.

In two additional experiments, foam was formed by injection of gas at constant rate, one in 1.3 μm^2 (1300-millidarcy) Boise sandstone and the other in 0.19 μm^2 (190-millidarcy) Berea sandstone. Data from these experiments are plotted as curves C and D in Fig. 5. The general similarity of all the curves in Fig. 5 indicates that the permeability to gas in a 0.19 μm^2 core was similar to that in a 1.3 μm^2 core. The degree of permeability reduction was less in the lower permeability core, a phenomenon that was also observed by Bernard and Holm [7].

Liquid blocking by foam in sandstone cores at high pressure

Besides blocking gas flow, foam also blocks liquid flow, as first observed by Bernard, Holm, and Jacobs [8]. This property could be used to prevent upward coning of water into a withdrawal well. In low-permeability reservoirs, the pressure at the withdrawal well must be reduced much below the reservoir pressure to induce sufficient flow to the well. This local reduced pressure causes water to rise in a cone and to increase the liquid saturation near the withdrawal well perforations. Two-phase flow in the well results, with greatly reduced gas productivity. A strategically placed foam lens would reduce the permeability to water near the withdrawal well, thereby delaying water coning and extending the seasonal life of the withdrawal well.

In an experiment to measure the ability of foam to block liquid flow, foam was formed by injecting gas and liquid simultaneously into the 1.3 μm^2 (1300-millidarcy) Boise sandstone core. Then the injection of gas was stopped, and liquid saturation and pressure profiles were measured while the injection of liquid (foamer solution, later changed to surfactant-free brine) was continued. Fig. 8 shows the liquid saturation at 20 and 50 cm in the core during this experiment, and Fig. 9 shows the liquid permeability calculated between pairs of adjacent pressure taps. First, 9.5 pore volumes (based on the total pore volume of the core) liquid were pumped through the core. Since the liquid saturation in the core was approximately 35%, this was sufficient to replace the liquid in the core 28 times. During this part of the experiment, the liquid permeability throughout the core remained at 10^{-3} μm^2 (1 millidarcy), and the liquid saturation remained at 35% throughout the core. These values agree with the relative permeability data measured for the same core using brine and nitrogen gas (for relative permeability data see Persoff et al. [3]). Then the liquid was changed from foamer solution to brine without surfactant, and another 17 pore volumes (sufficient to replace the liquid in the core 51 times) was pumped through the core.

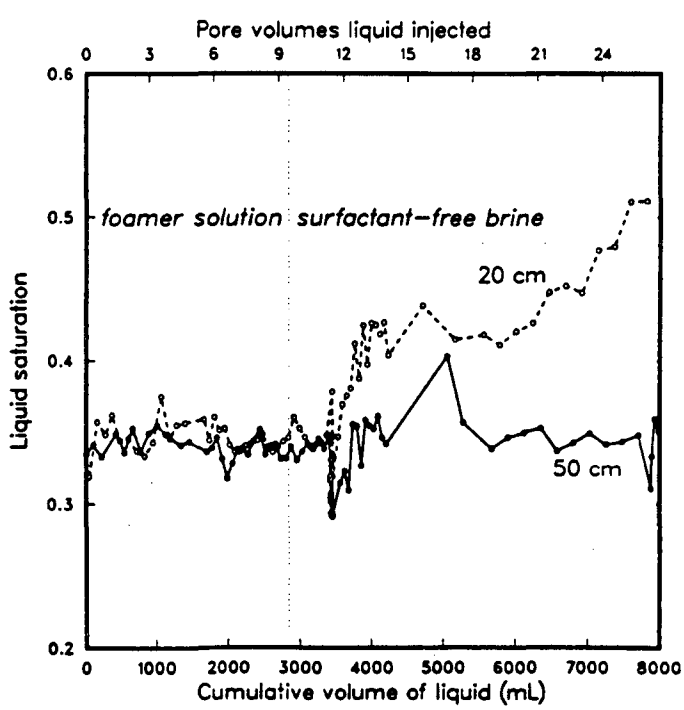

Figure 8. Liquid saturation at 10 cm and 50 cm during injection of 27 pore volumes of liquid through a foam-filled core.

Bubbles emerging from the exit of the back pressure regulator showed that lamellae broke and some of the trapped gas was released, and Figs. 8 and 9 show that both the liquid saturation and the liquid permeability increased as the surfactant was diluted in the foam, starting at the core inlet and progressing to the outlet. This agrees with the accepted view that low liquid permeability in a foamed core results from low liquid saturation [8; 3].

The results of the liquid-blocking experiment indicate that the key to controlling water coning into gas withdrawal wells is keeping the liquid saturation, and the vertical liquid permeability, at a low value in the region around the wellbore. Many foam-flow experiments reported here and elsewhere [3] show that the liquid saturation in a foam filled core is just a few units above connate, and the relative permeability to liquid is typically about 10^{-3}. This experiment demonstrated that water saturation in a foam-filled porous media remains low even though a large gradient of water pressure is imposed across it. This suggests that water coning could be controlled by strategically placing a foam "lens" near the gas-water contact so as to block the upward flow of water. Fig. 10 shows schematically the use of such a lens to block coning of water.

A three-phase gas storage reservoir simulator "MULKOM-GWF" developed for this project [9] was used to study the effectiveness of a foam lens in preventing coning and to optimize its placement. The parameters used in the simulation study are presented in Table 1. This study concluded that the effect of a low-permeability zone created by foam near a wellbore is not to prevent coning, but to diminish and delay it significantly. Since gas withdrawal is limited to a few months of the year, permanent prevention of coning is not necessary. Fig. 11 shows the calculated water production rates for a gas-withdrawal well. A foam lens placed 5 m above the gas-water contact appears sufficient to delay water coning for three months, which is a substantial improvement in the seasonal life of a withdrawal well. This application of foam appears quite promising in its economics as the advantage may be obtained without additional drilling and placement of a relatively small volume of foam.

CONTROLLED BREAKAGE OF FOAM

As part of this investigation we also demonstrated that a foam block could be broken by injection of isopropanol. Intentional breaking of a foam block might be desired if foam has been formed in a location where it interferes with gas injection or withdrawal. Isopropanol is known to break foam, and we routinely flushed cores with technical-grade isopropanol to break foam between experiments. We prepared a solution of 50 weight % isopropanol in brine for a foam-breaking demonstration following the foam-regeneration experiment. After foam had been formed and observed for 8 days, a slug of 0.09 PV (sufficient to replace one-third of the liquid in the core) of foam breaker was injected into the core at a rate slow enough not to stop the gas flow into

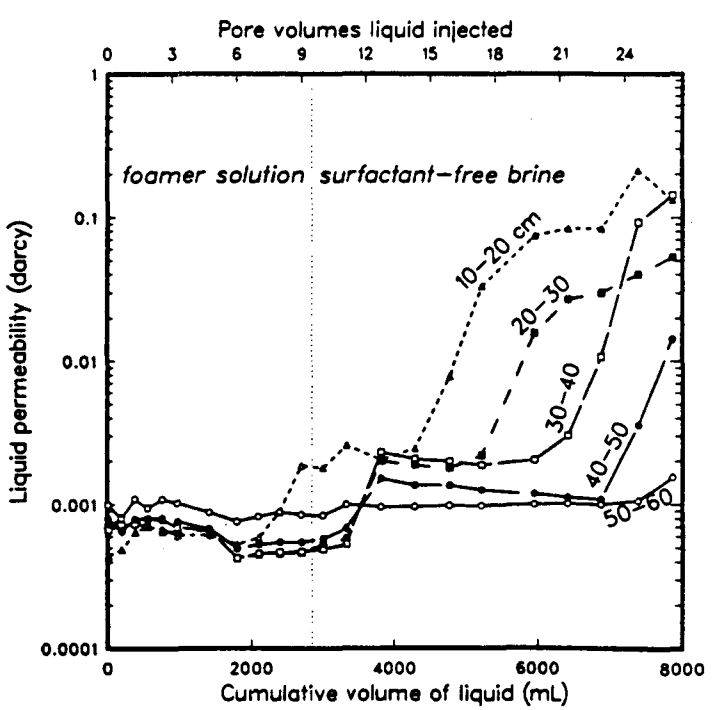

Figure 9. Liquid permeability between pairs of adjacent pressure taps during injection of 27 pore volumes of liquid through a foam-filled core.

Table 1. Parameters for Water-Coning Study

Permeability (isotropic)	3.7×10^{-2} μm^2 (37 millidarcy)
Permeability of foamed region	3.7×10^{-4} μm^2 (0.37 millidarcy)
Dimensions of foam lens: height	5 m (16.4 ft)
diameter	30.5m (100 ft)
Porosity	10%
Irreducible water saturation	20%
Irreducible gas saturation	45%
Temperature	31°C
Gas production rate	1.42×10^8 standard L/day (5×10^6 standard ft^3/day)
Perforated interval	20 m (65.6 ft)
Initial gas/water contact below reservoir top	30 m (98.4 ft)
Pressure at GWC	9.38 MPa (1360 psi)
Gas saturation at GWC	51%

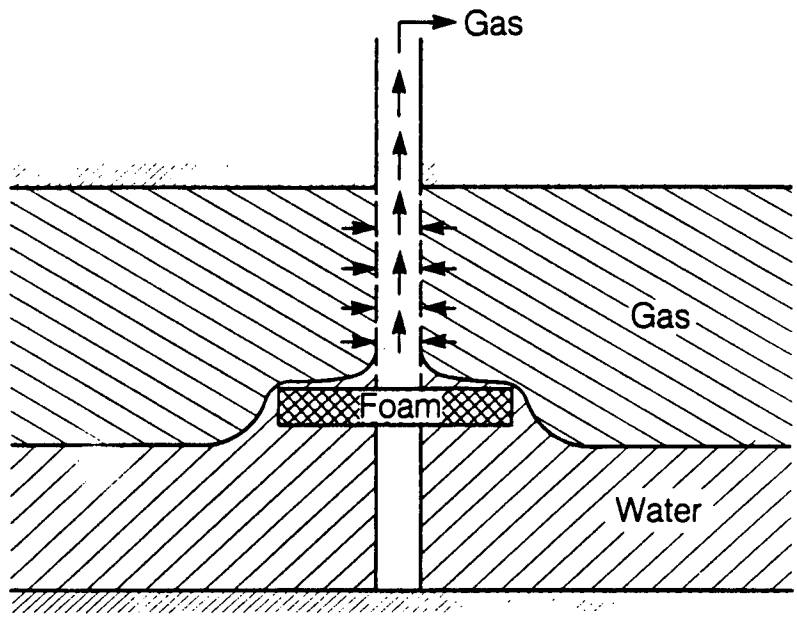

Figure 10. Use of a horizontal foam lens to reduce water coning, schematic.

the core. The pressure and liquid saturation were monitored while gas continued to flow into the core. Fig. 12 shows the pressure profiles measured during injection of the next pore volume of gas. The flat pressure gradient in the inlet region shows that the foam was broken and gas mobility restored where foam breaker displaced the foamer solution. It is clear that isopropanol is an effective foam breaker, should one be needed.

DISCUSSION

The technical issues to be resolved for foam application in aquifer gas storage are whether foam can be formed and emplaced in a formation, whether it will sufficiently reduce gas or liquid permeability, and whether the reduced permeability can be maintained for months. Our experiments, while not answering all the questions, have given favorable results to suggest that foam can be applied to increase the efficiency of underground gas storage.

The theoretical arguments and experiments of Radke and Ransohoff [2] indicate that there is a critical gas velocity that must be exceeded for generation of a strong foam. Lamellae are formed when gas invades individual liquid-filled pores, so the critical velocity presumably refers to the gas pore velocity, which is always greater than the superficial velocity. The difference between the two velocities may be large because the porosity and gas saturation are both less than unity, and some or most of the gas in the core may be trapped and immobile. We have not determined the critical pore velocity in our experiments, except to observe that it was

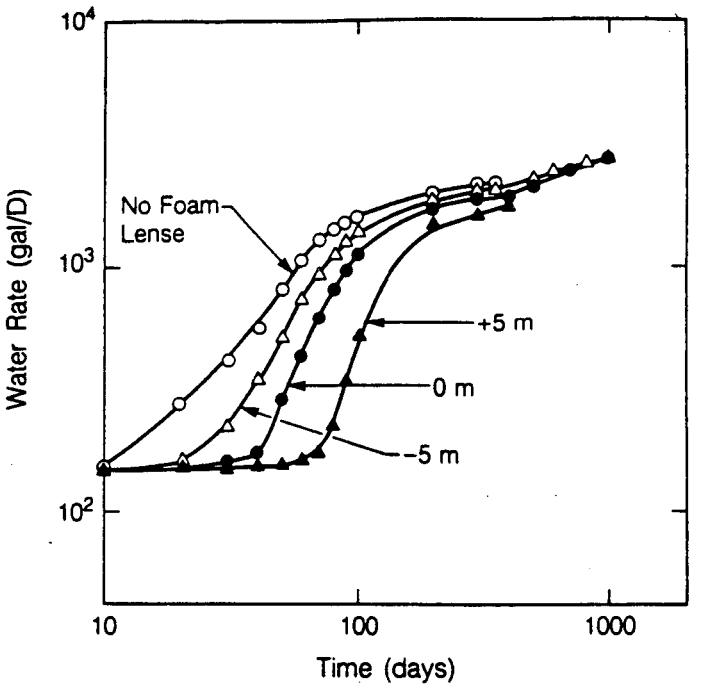

Figure 11. Numerical simulation of water production in a gas withdrawal well, using MULKOM-GWF. The parameters are listed in Table 1. Four cases are simulated: no foam lens; foam lens located at the gas-water contact; and 5 m above and below the gas-water contact. Emplacing the foam lens just above the gas-water contact provides the greatest protection against water coning. Note 1000 gal/day = 3786 L/day.

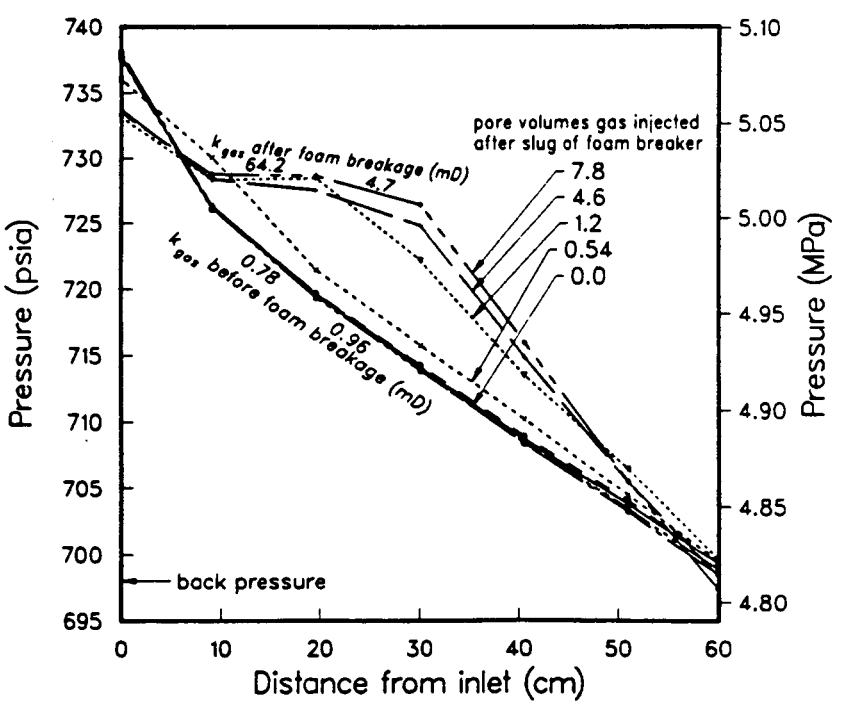

Figure 12. Increase in gas permeability, showing breakage of foam following injection of a 50 weight % isopropanol solution.

exceeded in one-dimensional experiments when the superficial gas velocity was 1 m/day.

If foam is to be formed by injecting gas from a well in radial flow, the superficial gas velocity, and possibly also the gas pore velocity, will decrease at large distances from the well. This may limit the distance at which foam can be generated in situ. Therefore better definition and measurement of the critical velocity is needed. In any case, generation of foam near a wellbore is certainly feasible.

The question of emplacement is essentially a question of how far gas can be injected above the critical velocity without exceeding the allowable injection pressure. The gas permeability of a foam-filled formation, the allowable injection pressure, the critical velocity for snap-off, and the viscosity of the liquid phase all combine to set a limit on the distance to which foam can be driven in situ. Spacing the foam bank away from the wellbore reduces the injection pressure, but also makes it more difficult to regenerate. Note also that as gas displaces liquid, the liquid is driven ahead of the foam, and its pressure drop must be added to the pressure drop through the foam. If a polymer is used in the liquid, this could also become significant.

Although one-dimensional laboratory experiments in homogeneous media have shown large reductions in gas and liquid permeability, it is necessary to determine whether this degree of permeability reduction can be achieved in the field. Radial flow may cause gas velocities to be too slow to form a strong foam at distances from the wellbore, and natural heterogeneity may interfere with emplacement of a foam bank.

The results shown in Fig. 5 suggest that for a gas-blocking application, some provision must be made to regenerate the foam. The cost of the project will depend upon the needed frequency of regeneration. It appears that additional slugs of liquid would be injected whenever the permeability of the foam block exceeds a certain limit, and the higher this limit is set, the less frequently regeneration would be needed. But even if the foam were allowed to decay, the gas saturation in the designated storage volume would be greater and more uniform than if foam had not been used, so improved recoverability of injected gas should result.

The rate of foam decay shown in Fig. 5 is likely pessimistic due to the test method. The gas injected in all these experiments was dry, and liquid saturations below connate measured during the later stages of each experiment near the inlet region indicate that liquid was removed from the core by evaporation. Low liquid saturation is known to be detrimental to foam stability [10]. The method used to conduct the experiment is therefore a severe test of foam block durability. The observation that inclusion of guar in the foamer solution increased the durability of the blocked condition might be explained by more stable lamellae being formed or by higher liquid saturation in those experiments due to greater viscosity of the displaced liquid.

Pilot-scale field testing is now needed to confirm these results in practice. The most promising application for a field trial appears to be control of water coning. Such a field trial could be done at a well where coning has been experienced in the past (the control experiment has already been done), and the foamer solution could be injected through the existing well and followed with gas. Another attractive prospect for a field trial would be the use of foam to seal a known leakage path of limited area, such as a fault zone or casing leak.

Application of foam to underground gas storage need not be limited to conventional underground storage in aquifers. Where demand is present but suitable geologic formations are absent, mined caverns in hard rock could be used as storage reservoirs. Here leakage through fractures intersecting the cavern might be controlled by foam. Another area where foam technology could be applied is compressed-air energy storage in aquifers. By controlling gas migration and water coning, foam could prevent leak-off of pressure and loss of stored energy, and ensure deliverability. Because the cycle in this application would be daily, rather than annual, requirements for foam stability might be reduced.

CONCLUSIONS

The results of these experiments support the following conclusions:

1. Foam reduces the gas permeability of a porous medium by 2 or 3 orders of magnitude. The permeability gradually increases as lamellae decay, but foam can be regenerated by injection of additional slugs of foamer solution.
2. Inclusion of 0.5 weight % guar in the foamer solution appears to enhance the stability of a foam block in a porous medium.
3. The pressure drop in foam flow through a porous medium varies directly with the liquid flow rate. Therefore, where injection pressure must be limited, the most effective way to form a foam bank is to saturate the formation with surfactant solution, and then inject gas. Alternating slugs of surfactant solution may be used to make a stronger foam.
4. Foam effectively blocks liquid flow because the liquid saturation is low. When liquid is pumped through a foam-filled core, the liquid saturation remains low as long as the surfactant concentration is not diluted. When the surfactant concentration is diluted, trapped gas is released, and liquid saturation and liquid permeability increase. In our experiment, approximately 17 pore volumes of water were pumped through the

core before the permeability increased significantly.

5. The most effective location for placement of a foam bank to prevent water coning is just above the gas-water contact.
6. Formation of a foam bank spaced away from an injection well may be feasible by injecting foamer solution, displacing it with brine, and then injecting gas. The location of the foam bank reflects displacement both by the brine and by injected gas.
7. Foam can be broken by injection of a 50 weight % isopropanol solution.

Based on the results of our experimental and theoretical studies, we conclude that application of foam to improve the efficiency of aquifer gas storage appears to be technically feasible. The logical next step would be a field trial. The most promising field trial would be an attempt to control water coning by means of a relatively small foam lens emplaced beneath the feed zone of a gas withdrawal well.

ACKNOWLEDGMENT

This work was supported by the Gas Research Institute, Chicago, IL, under Contract No. 5086-271-1160. This work was supported through U. S. Department of Energy Contract No. DE-AC03-76SF00098.

REFERENCES

1. Witherspoon, P. A., Radke, C. J., Shikari, Y., Pruess, K., Persoff, P., Benson, S. M. and Wu, Y. S., 1987. "Feasibility Analysis and Development of Foam-Protected Underground Natural Gas Storage Facility," (LBL-23500) American Gas Association, Proceedings Operating Section, paper #87-DT-110, 539-549.
2. Radke, C. J. and Ransohoff, T. C., 1988. "Mechanism of Foam Generation on Glass-Bead Packs," *SPE Reservoir Engineering, 3*, (2), 573-585.
3. Persoff, P., Radke, C. J., Pruess, K., Benson, S. M. and Witherspoon, P. A., 1989. "A Laboratory Investigation of Foam Flow in Sandstone at Elevated Pressure," presented at 1989 California Regional SPE Meeting, Bakersfield, CA, April 5-7, (SPE-18781) submitted to SPE Reservoir Engineering.
4. Bond, D. C., Bernard, G. G., 1967. "Forming Foam under Reservoir Conditions in Petroleum Recovery Process," United States patent no. 3,318,379, May 9.
5. Hanssen, J. E., 1988. "A New Method for Testing of Gas-Blocking Foams," paper SPE/DOE 17362, presented at the SPE/DOE Enhanced Oil Recovery Symposium, Tulsa, OK April 17-20.
6. Minssieux, L., 1974. "Oil Displacement by Foams in Relation to their Physical Properties in Porous Media," *Jour. Petr. Technol.*, January, 100-108.
7. Bernard G.G., and Holm, L.W., 1964. "Effect of Foam on Permeability of Porous Media to Gas," *Soc. Petr. Eng. Jour.*, September, 267-274.
8. Bernard, G. G., Holm, L. W., and Jacobs, W. L., 1965. "Effect of Foam on Trapped Gas Saturation and on Permeability of Porous Media to Water," *Soc. Petr. Eng. Jour.*, December, 295-300.
9. Pruess, K. and Wu, Y. S., 1988. "On PVT - Data, Well Treatment, and Preparation of Input Data for an Isothermal Gas - Water - Foam Version of MULKOM," (LBL-25783), prepared for Gas Research Institute under Contract No. 5086-271-1160, Lawrence Berkeley Laboratory.
10. Khatib, Z. I., Hirasaki, G. J., and Falls, A.H., 1988. "Effects of Capillary Pressure on Coalescence and Phase Mobilities in Foams Flowing Through Porous Media," *SPE Reservoir Engineering, 3*, (3), 919-926.

Appendix G.

Displacement of Newtonian Fluid by a Non-Newtonian Fluid in a Porous Medium

Submitted for publication to
Transport in Porous Media

June 30, 1989

Displacement of a Newtonian Fluid by a Non-Newtonian Fluid in a Porous Medium

by

Y.-S Wu, K. Pruess and P. A. Witherspoon

Earth Sciences Division
Lawrence Berkeley Laboratory
Berkeley, California 94720

ABSTRACT

This paper presents an analytical Buckley-Leverett-type solution for one-dimensional immiscible displacement of a Newtonian fluid by a non-Newtonian fluid in porous media. The non-Newtonian fluid viscosity is assumed to be a function of the flow potential gradient and the non-Newtonain phase saturation. To apply this method to field problems, a practical procedure has been developed, which is based on the analytical solution, and is similar to the graphic technique of Welge. Our solution can be regarded as an extension of the Buckley-Leverett method to non-Newtonian fluids. The analytical result reveals how the saturation profile and the displacement efficiency are controlled not only by the relative permeabilities, as in the Buckley-Leverett solution, but also by the inherent complexities of the non-Newtonian fluid. Two examples of application of the solution are given. One is the verification of a numerical model, which has been developed for simulation of flow of immiscible non-Newtonian and Newtonian fluids in porous media. Excellent agreement between the numerical and analytical results has been obtained using a power-law non-Newtonian fluid. Another application is to examine the effects of non-Newtonian behavior on immiscible displacement of a Newtonian fluid by a power-law non-Newtonian fluid.

Key words

Non-Newtonian fluids, Buckley-Leverett, immiscible displacement, power-law fluids, rheological models, Welge method, fractional flow theory, EOR.

Submitted for Publication to *Transport in Porous Media*, June 30, 1989.

Nomenclature

Roman Letters

A	cross-sectional area (m^2)
f_{ne}	fractional flow of Newtonian phase
f_{nn}	fractional flow of non-Newtonian phase
$\vec{g}$	gravitational acceleration vector (m/s^2)
g	magnitude of the gravitational acceleration (m/s^2)
H	power-law coefficient ($Pa \cdot s^n$)
K	absolute permeability (m^2)
k_{rne}	relative permeability to Newtonian phase
k_{rnn}	relative permeability to non-Newtonian phase
n	power-law exponential index
N_p	cumulative displaced Newtonian fluid (m^3)
P	pressure (Pa)
P_c	capillary pressure (Pa)
P_{ne}	pressure of Newtonian phase (Pa)
P_{nn}	pressure of non-Newtonian phase (Pa)
S	saturation
$q(t)$	injection rate of non-Newtonian fluid (m^3/s)
$Q(t)$	cumulative injection rate (m^3)
S_f	saturation at moving front (m)
S_{ne}	Newtonian phase saturation
S_{neir}	irreducible Newtonian phase saturation
S_{nn}	non-Newtonian saturation
$\underline{S}_{nnir}$	connate non-Newtonian saturation
S_{nn}	average saturation of non-Newtonian phase in swept zone
x	distance from inlet, coordinate (m)
x_f	distance to shock saturation front (m)
$x_{S_{nn}}$	distance of saturation S_{nn} from the inlet (m)
t	time (s)
u	Darcy velocity (m/s)
$u(t)$	total flux (m/s)
u_{ne}	Darcy velocity of Newtonian phase (m/s)
u_{nn}	Darcy velocity of non-Newtonian phase (m/s)

Greek Letters

α	angle between horizontal plane and flow direction
$\dot{\gamma}$	shear rate (s^{-1})
μ_{app}	apparent viscosity (Pa·s)
μ_{eff}	effective viscosity ($Pa \cdot s^n m^{1-n}$)
μ_{ne}	viscosity of Newtonian fluid (Pa·s)
μ_{nn}	equivalent viscosity of non-Newtonian fluid (Pa·s)
ρ_{ne}	density of Newtonian fluid (kg/m^3)
ρ_{nn}	density of non-Newtonian fluid (kg/m^3)
τ	shear stress (Pa)
ϕ	porosity of porous media
Φ	flow potential (Pa)

Subscripts

app	apparent
eff	effective
f	front
ne	Newtonian
nn	non-Newtonian
rne	relative to Newtonian phase
rnn	relative to non-Newtonian phase

Introduction

Immiscible flow of multiple phase fluids through porous media occurs in many subsurface systems. The behavior of multiple-phase flow, as compared with single-phase flow, is much more complicated and is not well understood in many areas due to the complex interactions of different fluid phases. A fundamental understanding of immiscible displacement of Newtonian fluids in porous media was contributed by Buckley and Leverett (1942) in their classical study of the fractional flow theory. The Buckley-Leverett solution gave a saturation profile with a sharp front by ignoring the capillary pressure and gravity effects. A frequently encountered property of the Buckley-Leverett method is that the saturation becomes a multiple-valued function of the distance coordinate, x. This difficulty can be overcome by consideration of a material balance. Following the work of Buckley and Leverett (1942), a simple graphic approach was invented by Welge (1952), which can easily determine the sharp saturation front without the difficulty of the multiple-valued saturation problem for a uniform initial saturation distribution. More recently, some special analytical solutions for immiscble displacement including the effects of capillary presure were obtained by Yortsos and Fokas (1983), and Chen (1983).

The Buckley-Leverett fractional flow theory has been applied and generalized by various authors to study the enhanced oil recovery (EOR) problems (Pope 1980), surfactant flooding (Larson and Hirasaki, 1978), polymer flooding (Patton, Coats and Colegrone, 1971), mechanism of chemical methods (Larson, Davis and Scriven, 1982), detergent flooding (Fayers and Perrine, 1959), displacement of oil and water by alcohol (Wachmann, 1964 ; Taber, Kamath and Reed, 1961), dispacement of viscous oil by hot water and chemical additive (Karakas, Saneie, and Yortsos, 1986), and alkaline flooding (deZabala, Vislocky, Rubin and Radke, 1982). An extension to more than two immiscible phases dubbed " coherence theory " was described by Helfferich (1981). However, no non-Newtonian behavior has been considered in any of these works.

Non-Newtonian and Newtonian fluid immiscible displacement occurs in many EOR processes involving the injection of non-Newtonian fluids, such as polymer solutions, microemusions, macroemulsions, and foam solutions. Almost all the theoretical and experimental studies performed on non-Newtonian fluid flow in porous media have focused on single non-Newtonian phase flow. Savins (1969) presented a comprehensive review of flow of a non-Newtonian fluid through porous media. Scheidegger (1974) and Bird et al. (1960) summarized many rheological models for different non-Newtonian fluids. A very important contribution to study non-Newtonian flow in porous media was made by Gogarty (1967), who showed experimentally that the effective viscosity of pseudo-plastic fluid flow in a core depends upon the average shear rate, which is a function of pore velocity only, for a given porous material. The first analytical solutions, for a power-law non-Newtonain fluid were given simultaneously by Ikoku and Ramey (1979), and Odeh and Yang (1979) by using a linearization assumption. Their solutions have been extended by many authors to more complicated problems (Gencer and Ikoko, 1984; Ikoku, 1982, Ikoku and Ramey, 1980; Lund and Ikoku, 1981; and Vongvuthipornegai and Raghavan, 1987). A numerical method was also used to model non-Newtonian flow problems (van Poolen and Jargon, 1969; McDonald, 1979).

Very little research has been published on multiple phase flow of non-Newtonian and Newtonian fluids through porous media. To the best of our knowledge, there is no analytical solution available. Even using numerical methods, very few studies have been conducted (Gencer and Ikoku, 1984). Therefore, the mechanism of immiscible displacement involving non-Newtonian fluids in porous media is still not well understood.

In this paper, an analytical solution describing the displacement mechanism of non-Newtonian / Newtonian fluid flow in porous media has been developed for one-dimensional linear flow. Our approach follows the classical work of Buckley and Leverett (1942) for immiscible displacement of Newtonian fluids. The only important difference due to non-Newtonian behavior is in the fractional flow curve, which because of the velocity-dependent effective viscosity of a non-Newtonian fluid now becomes dependent on injection rate. A practical procedure for evaluating the behavior of non-Newtonian and Newtonian displacement is provided, based on the analytical solution, which is similar to the graphic method by Welge (1952). The resulting procedure can be regarded as an extension of the Buckley-Leverett theory to the flow problem of non-Newtonian fluids in porous media. The analytical results reveal how the saturation profile and the displacement effeciency are controlled not only by the relative permeabilities, as in the Buckley-Leverett solution, but also by the inherent complexities of non-Newtonian fluids.

The analytical solution developed here will find application in two areas: 1) it can be employed to study the displacement mechanisms of non-Newtonian and Newtonian fluid in porous media, and 2) it may be used to check numerical solutions from a simulator of non-Newtonian flow.

In addition, a numerical method has been used to simulate non-Newtonian and Newtonian multiple phase flow using the integral finite difference approach (Pruess and Wu; 1988). The numerical model can take into account all the important factors which affect the flow behavior of non-Newtonian and Newtonian flluids, such as capillary pressure, complicated flow geometry and operation conditions. The different rheological models for non-Newtonian fluid flow in porous media can easily be incorporated in the code. The validity of the numerical method has been checked by comparing the numerical results with those of the analytical solution, and excellent agreement has been obtained using a power-law, non-Newtonian fluid.

Mathematical Formulation

Two-phase flow of non-Newtonian and Newtonian fluids is considered in a homogeneous and isotropic porous medium. There is no mass transfer between non-Newtonian and Newtonian phases, and disperson and adsorption on the rock are ignored. Then, the governing equations are given by

$$-\nabla \cdot (\rho_{ne} \vec{u}_{ne}) = \frac{\partial}{\partial t} (\rho_{ne} S_{ne} \phi) \tag{1}$$

for the Newtonian fluid, and

$$-\nabla \cdot (\rho_{nn} \vec{u}_{nn}) = \frac{\partial}{\partial t} (\rho_{nn} S_{nn} \phi) \tag{2}$$

for the non-Newtonian fluid. The Darcy velocities for the Newtonian and the non-Newtonian phase are described by a multiphase extension of Darcy law as

$$\vec{u}_{ne} = -K \frac{k_{rne}}{\mu_{ne}} (\nabla P_{ne} - \rho_{ne} \vec{g}) \tag{3}$$

and

$$\vec{u}_{nn} = -K \frac{k_{rnn}}{\mu_{nn}} (\nabla P_{nn} - \rho_{nn} \vec{g}) \tag{4}$$

The pressures in the two phases are related by means of the capillary pressure,

$$P_c (S_{nn}) = P_{ne} - P_{nn} \tag{5}$$

The relative permeabilities, k_{rne}, k_{rnn}, and the capillary presure P_c are assumed to be functions of saturation only. Also, from the definition of saturation, we have

$$S_{ne} + S_{nn} = 1 \tag{6}$$

Analytical Solution

For the derivation of the analytical solution, the following additional assumptions are made:

1. the two fluids and the porous medium are incompressible,
2. the capillary pressure gradient is negligible,
3. the apparent viscosity of non-Newtonian fluids is a function of the flow potential and saturation,

$$\mu_{nn} = f (S_{nn}, \nabla\Phi,) \tag{7}$$

where $\nabla\Phi$ is the flow potential gradient, a vector. Its component in the x coordinate is,

$$\frac{\partial\Phi}{\partial x} = \frac{\partial P}{\partial x} + \rho_{nn} g \sin\alpha \tag{8}$$

By definition, the viscosity of a non-Newtonian fluid is a function of the shear rate. For flow through porous media, it has been shown that the shear rate depends only on the pore velocity for a given porous material (Gogarty, 1967). The pore velocity is determined by the local potential gradient and by the local saturation within the two-phase fluid. We assume that the viscosity of the non-Newtonian fluid is described by Equation (7) for multiple-phase flow, which should be determined by experiment for the non-Newtonian fluid and the porous medium of interest.

The flow system considered is a semi-infinite linear reservoir, shown in Figure 1. It is further assumed that gravity segregation is negligible and that stable displacement exists near the displacement front. Then, Equations (1) and (2) become

$$-\frac{\partial u_{ne}}{\partial x} = \phi \frac{\partial S_{ne}}{\partial t} \tag{9}$$

and

$$-\frac{\partial u_{nn}}{\partial x} = \phi \frac{\partial S_{nn}}{\partial t} \tag{10}$$

For the Newtonian phase, the flow rate is

$$u_{ne} = -K \frac{k_{rne}}{\mu_{ne}} \left[\frac{\partial P}{\partial x} + \rho_{ne}\, g \sin \alpha \right] \tag{11}$$

and for the non-Newtonian phase,

$$u_{nn} = -K \frac{k_{rnn}}{\mu_{nn}} \left[\frac{\partial P}{\partial x} + \rho_{nn}\, g \sin \alpha \right] \tag{12}$$

To complete the mathematical description, the initial and boundary conditions must be specified. Initially, a Newtonian fluid is at its maximum saturation in the system. Thus,

$$S_{ne}(x, 0) = 1 - S_{nnir} \tag{13}$$

where S_{nnir} is the initial immobile non-Newtonian fluid saturation. For practical field problems, S_{nnir} is usually zero, which can be treated as a special case. In this problem, we are concerned with continuously injecting a non-Newtonian fluid from the inlet x=0, at a known rate $q(t)$, which can be a function of injection time, t. The boundary conditions at $x = 0$ are:

$$u_{nn}(0, t) = u(t) = \frac{q(t)}{A} \tag{14}$$

$$u_{ne}(0, t) = 0 \tag{15}$$

where A is the cross-sectional area for flow. Finally, in a semi-infinite system, the following conditions must be imposed at $x \to \infty$,

$$S_{ne} \to 1 - S_{nnir} \tag{16}$$

and

$$S_{nn} \to S_{nnir} \tag{17}$$

The governing equations (9), (10) with the boundary and initial conditions (13)-(17) can be solved to obtain the following solution (see Appendix A):

$$\left[\frac{dx}{dt} \right]_{S_{nn}} = \frac{q(t)}{\phi A} \left[\frac{\partial f_{nn}}{\partial S_{nn}} \right]_t \tag{18}$$

This is the frontal advance equation for the non-Newtonian displacement, and is the same in form as the Buckley-Leverett equation. The difference is the dependence of the fractional flow f_{nn} for the non-Newtonian displacement on saturation not only through the relative permeability, but also through the non-Newtonian phase viscosity, which is a function of both potential gradient and saturation. For a given time, a given injection rate, and given fluid and rock properties, the potential gradient can be shown using Equation (A-6) to be a function of saturation only. Equation (18) shows that a particular non-Newtonian fluid saturation profile propagates through the porous medium at a constant velocity for a given time and injection rate. As in the Buckley-Leverett theory, the saturation for a vanishing capillary pressure gradient will in general become a triple-

valued function of distance near the displacement front. Equation (18) will then fail to describe the velocity of the shock saturation front, since $\partial f_{nn}/\partial S_{nn}$ does not exist on the front. Consideration of material balance across the shock front (Sheldon, et al., 1959) provides, the velocity of the front,

$$\left[\frac{dx}{dt}\right]_{S_f} = \frac{q(t)}{A\,\phi}\left[\frac{f^{+}_{nn} - f^{-}_{nn}}{S^{+}_{nn} - S^{-}_{nn}}\right] \tag{19}$$

where S_f is the front saturation of the displacing non-Newtonian phase. The superscripts " + " and " - " refer to values ahead of and behind the shock, respectively.

The location $x_{S_{nn}}$ of any saturation S_{nn} traveling from the inlet can be determined by integrating Equation (18) with respect to time, which yields

$$x_{S_{nn}} = \frac{Q(t)}{A\,\phi}\left[\frac{\partial f_{nn}}{\partial S_{nn}}\right]_{S_{nn}} \tag{20}$$

where Q(t) is the cumulative volume of injected fluid,

$$Q(t) = \int_0^t q(\lambda)\,d\lambda \tag{21}$$

A direct use of Equation (20) , given x and t, will result in a multiple-valued saturation distribution, which can be handled by a mass balance calculation , as in the Buckley-Leverett solution. An alternative graphical method of evaluating the above solution will be discussed in the next Section.

Graphical Evaluation Method

The fractional flow of the displacing non-Newtonian phase is a function of its saturation only, after taking into account the constraint condition (A-6). Therefore, the Welge (1952) graphic method can be shown to apply for evaluation of non-Newtonian fluid displacement by an integration of the mass balance of injection into the system and incorporation of Equation (20). The only additional constraint is the need to take into account the contribution of a velocity-dependent, effective viscosity of non-Newtonian fluids on the fractional flow curve. At the moving saturation front, we have (see Appendix B),

$$\left[\frac{\partial f_{nn}}{\partial S_{nn}}\right]_{S_f} = \frac{f_{nn}|_{S_f} - f_{nn}|_{S_{nnir}}}{S_f - S_{nnir}} \tag{22}$$

and the average saturation in the displaced zone is given by,

$$\left[\frac{\partial f_{nn}}{\partial S_{nn}}\right]_{S_f} = \frac{1}{\bar{S}_{nn} - S_{nnir}} \tag{23}$$

where $\bar{S}_{nn}$ is the average saturation of the non-Newtonian phase in the swept zone. To satisfy Equations (22) and (23), a simple geometric construction can be used (see Figure 2). On a curve of fractional flow f_{nn} versus saturation S_{nn} , draw the tangent to the

fractional flow curve, from the point ($S_{nn} = S_{nnir}$, $f_{nn} = 0$). The point of tangency has coordinates ($S_{nn} = S_f$, $f_{nn} = f_{nn}|_{S_f}$), and the extrapolated tangent must intercept the line $f_{nn} = 1$ at the point ($S = S_{nn}$, $f_{nn} = 1$). Therefore, the graphic method of Welge applies if the fractional flow curves are provided for the non-Newtonian displacement process. The only difference is in the determination of the non-Newtonian fractional flow curve because we have to include the effects of the apparent viscosity of non-Newtonian fluids, which are also a function of saturation.

With given relative permeability data and the rheological model μ_{nn}, the general procedure for evaluating the flow behavior of non-Newtonian one-dimensional linear displacement is as follows:

1. Solve pressure gradients $-\partial P/\partial x$, from Equation (A-6) for different injection rates and plot the relationship between pressure gradient and saturation corresponding to the injection rate, as shown in Figure 3. This requires use of the equivalent non-Newtonian viscosity as derived in Appendix C, Equation (C-8).
2. Calculate the fractional flow, f_{nn} , by Equation (A-8), using the pressure gradients from Figure 3 to calculate the corrsponding potential gradients , then using Equation (C-8) to compute the non-Newtonian phase viscosity. An example of fractional flow curves is shown in Figure 4.
3. Calculate the derivatives of fractional flow , $\partial f_{nn}/\partial S_{nn}$, with respect to saturation from Figure 4. These are shown in Figure 5.
4. Determine the shock front saturation from Figure 4, as illustrated in Figure 2.
5. Calculate the saturation profile for $S_f < S_{nn} < 1 - S_{neir}$ from $x = 0$ to $x = x_f$ according to Equation (20) for a given injection rate and using the corresponding potential gradients from Figure 5. This profile is shown in Figure 6.
6. Determine the average saturation in the swept zone from Figure 4, as illustrated in Figure 2. This can be used to calculate the cumulative Newtonian fluid displaced, N_p ,

$$N_p = A \phi x_f (\bar{S}_{nn} - S_{nnir}) \tag{24}$$

The above procedure has been programmed for use in this work.

Comparison with Numerical Simulation

A numerical simulator (MULKOM-GWF), which is a modified version of MULKOM (Pruess, 1983; Pruess and Wu, 1988) , has been developed for modeling multiple-phase flow of non-Newtonian and Newtonian fluids in porous media under a wide range of operating conditions and with different rheological models for the non-Newtonian fluid behavior. We have programmed an equivalent non-Newtonian viscosity given by Equation (C-8) into the simulator. The validity of the numerical results from this code has been tested for immiscible displacement of a Newtonian fluid by a non-Newtonian fluid by comparison with the Buckley-Leverett-type solution obtained above. The example of interest is a one-dimensional linear flow problem of incompressible two-phase fluids in a semi-infinite, horizontal, homogeneous and isotropic porous

medium. A constant injection rate is mantained at the inlet ($x = 0$) from time $t = 0$. Initially, the reservoir is fully saturated with only the Newtonian liquid. The relative permeability curve used for both the analytical and numerical calculations is shown in Figure 7. Capillary effects are assumed to be negligible.

In order to reduce the effects of discretization in a finite system, very fine mesh spacing ($\Delta x = .0125m$) was chosen for the first 240 elements, then the mesh spacing was increased by a factor of 1.5 to the 290th element. The non-Newtonian displacement analytical solution was evaluated by using the computer-graphic method outlined in the previous section. The power-law non-Newtonian fluid has been used extensively in the study of non-Newtonian fluid flow through porous media both theoretically and experimentally. To demonstrate the applicability of the analytical solution, a power-law liquid was used as a displacing agent to drive the initially saturated Newtonian liquid in the porous medium.

The properties of rock and fluids are given in Table 1. If we assume a power-law index of $n = 0.5$, then the pressure gradients for horizontal flow can be derived from Equation (A-6) as,

$$-\frac{\partial P}{\partial x} = \frac{1}{2}\left\{\left[\frac{\left[\frac{Kk_{rne}}{\mu_{ne}}\right]^2}{\frac{Kk_{rnn}}{\mu_{eff}}} + \frac{4q}{\left[\frac{Kk_{rnn}}{\mu_{eff}}\right]^{1/2}}\right]^{1/2} - \frac{\frac{Kk_{rne}}{\mu_{ne}}}{\left[\frac{Kk_{rnn}}{\mu_{eff}}\right]^{1/2}}\right\} \tag{25}$$

Equation (25) was used in calculating the fractional flow f_{nn} to incorporate non-Newtonian flow effects in the analytical solution. A comparison of the saturation profiles from the numerical and the analytical calculations after 10 hours of non-Newtonian fluid injection into the system is given in Figure 8. This shows that the numerical results are in excellent agreement with the analytical prediction. Considering the complexity introduced when non-Newtonian fluids are involved in a multiple phase flow problem, Figure 8 provides a very encouraging indication that the numerical model is correct in describing the multiple phase immiscible displacement of non-Newtonian and Newtonian fluid flow in porous media. The viscosity profiles of the non-Newtonian fluid are given in Figure 9, and show good agreement between the analytical and numerical results over the whole non-Newtonian fluid swept region, $x < x_f$. Only at the shock advancing saturation front does the numerical solution deviate somewhat from the analytical solution, which is a typical " smearing front " effect from numerical dispersion there.

Table 1
Parameters for Linear Power-Law Fluid Displacement

Porosity	ϕ=0.20
Permeability	K=1 darcy
Cross-Sectional Area	1 m^2
Injection Rate	$q=0.8233\times10^{-5} m^3/s$
Injection Time	T=10 hrs
Displaced Phase Viscosity	μ_{ne}=5 cp
Irreducible Newtonian Saturation	S_{neir}=0.20
Initial Non-Newtonian Saturation	S_{nnir}=0.00
Power-Law Index	n=0.5
Power-Law Coefficient	H=0.01 $Pa\cdot s^n$

Discussion of non-Newtonian Displacement

For a given operating condition, non-Newtonian fluid displacement in porous media is controlled not only by relative permeability effects, as in Newtonian fluid displacement, but also by the non-Newtonian fluid rheological properties. Some fundamental behavior of power-law non-Newtonian fluid displacement will be discussed in this section by using results from the analytical solution.

1. Effects of Injection Rate

For Newtonian displacement in porous media based on Buckley-Leverett solutions, injection rate has no effect on displacement efficiency or sweep efficiency. When a non-Newtonian fluid is involved, changes in the injection rate will result in changes in the pore velocity, which will affect the viscosity of the non-Newtonian phase and fractional flow curve. The fluid and rock parameters used for the calculations in this section are similar to those used in the previous section, and any differences are indicated on the figures to follow. Figure 10 gives non-Newtonian viscosity versus saturation curves for three different injection rates in a semi-infinite linear horizontal system. Considering the constraint condition (A-6), the viscosity of non-Newtonian fluids depends only on the non-Newtonian phase saturation. The resulting saturation profiles corresponding to the injection rates are shown in Figure 11. The horizontal lines are the average saturations in the swept zone, which reflect the sweep efficiency. Since the only variable parameter in this calculation is the injection rate, the saturation distributions in Figure 11 indicate that injection rate has a significant effect on displacement. For a displacement process with this type of shear thinning fluid, the lower the injection rate, the higher the displacement efficiency becomes.

2. Effects of Power-Law Index - n

There are two parameters that characterize flow behavor of a power-law fluid, the exponential index, n, and coefficient, H. For a pseudoplastic fluid, $0 < n < 1$. If $n = 1$, the fluid is Newtonian. The effect of the power-law index , n, on linear horizontal displacement can be quite significant. Figure 12 shows that pressure gradients are changed tremendously as a function of saturation for different values of n. The apparent viscosities of several non-Newtonian fluids are given in Figure 13, and the resulting fractional flow curves are shown in Figure 14. Saturation profiles after a 10-hour injection period in the system are plotted in Figure 15. Note the significant differences in sweep effiency.

Since the power-law index, n, is usually determined from an experiment or from well test analysis, some errors cannot be avoided in determining the values of n. These results show how difficult it will be to use a numerical code to match experimental data from non-Newtonian displacement investigations in the laboratory, because of the extreme sensitivity of the core saturation distribution to n. The sensitivity of the displacement behavior to the power-index n suggests that in determining the index n, it may be helpful to match experimental saturation profiles using the analytical solution.

3. Effects of Gravity

It is expected that gravity may have more significant effects on non-Newtonian displacement than on Newtonian displacement because it influences mobility by affecting the non-Newtonian phase viscosity, in addition to the effect on the potential gradient as in Newtonian displacement. This can be demonstrated by the following example. A power-law non-Newtonian fluid is injected upwards ($\alpha=\pi/2$) , horizontally ($\alpha=0$) , and downwards ($\alpha=-\pi/2$) , to displace a heavier in-situ Newtonian fluid. The fractional flow curves are given in Figure 16. Since counterflow may occur physically at very low or very high displacing phase saturations under gravity effects, we will have the situations that $f_{nn} > 1$ for upflow and $f_{nn} < 0$ for downflow. The final saturation distributions in Figure 16 show the significance of effects of gravity on non-Newtonian displacement in porous media.

Conclusions

An analytical solution for describing the displacement of a Newtonian fluid by a non-Newtonian fluid through porous media has been developed. A general viscosity function for non-Newtonian fluids is proposed and used in the solution, which relates non-Newtonian phase viscosity to the local potential gradient and saturation, and is suitable for different rheological models of non-Newtonian fluids. The analytical solution is applicable to displacement of a non-Newtonian fluid by a Newtonian fluid or to displacement of a non-Newtonian fluid by another non-Newtonian fluid.

Two examples of application of the analytical solution are presented. First, it is used to verify a numerical simulator for multiple-phase flow involving a non-Newtonian fluid. Secondly, it is used to obtain insight into the physics of non-Newtonian displacement in porous media. The calculated analytical results reveal that non-Newtonian

dispacement is a complicated process, controlled by the rheological properties of non-Newtonian fluids used, and the injection condition, in addition to relative permeability, and is more sensitive to gravity effects as well.

Acknowledgment

For a critical review of the manuscript and the suggestion of improvements, the authors are indebted to R. Falta and C. Radke. This work was supported, in part, by the Gas Research Institute under Contract No. 5086-271-1160, and by the Office of Basic Energy Sciences, U. S. Department of Energy, under Contract No. DE-AC03-76SF00098.

Appendix A. Derivation of Buckley-Leverett Type Solution

The sum of Equations (9) and (10) gives

$$-\frac{\partial(u_{ne} + u_{nn})}{\partial x} = \phi \frac{\partial}{\partial t} (S_{ne} + S_{nn}) = 0 \qquad \text{(A-1)}$$

This means that at a given time, the total volumetric flow rate through any cross-section in the flow system is independent of the distance coordinate, x.

$$u_{ne} + u_{nn} = u(t) \qquad \text{(A-2)}$$

Physically this follows from the incompressible assumption.

The fractional flow of a phase is defined as the volume fraction of the phase flowing at a distance x and time t compared to the total flowing phase volume. For the Newtonian phase,

$$f_{ne} = \frac{u_{ne}}{u_{ne} + u_{nn}} = \frac{u_{ne}}{u(t)} \qquad \text{(A-3)}$$

and for the non-Newtonian phase,

$$f_{nn} = \frac{u_{nn}}{u_{ne} + u_{nn}} = \frac{u_{nn}}{u(t)} \qquad \text{(A-4)}$$

>From a volume balance, the sum of Equations (A-3) and (A-4) yields,

$$f_{ne} + f_{nn} = 1 \qquad \text{(A-5)}$$

Using Equations (11) and (12)), Equation (A-2) can be written as:

$$u(t) + K \left[\frac{k_{rne}}{\mu_{ne}} + \frac{k_{rnn}}{\mu_{nn}} \right] \frac{\partial P}{\partial x}$$
$$+ K \left[\frac{\rho_{ne} k_{rne}}{\mu_{ne}} + \frac{\rho_{nn} k_{rnn}}{\mu_{nn}} \right] g \sin(\alpha) = 0 \qquad \text{(A-6)}$$

Noting that μ_{nn} is a function of both flow potential gradient and saturation from Equation (7), Equation (A-6) indicates that at any given time, the potential gradient, $\partial\Phi/\partial x$, or the pressure gradient, $\partial P/\partial x$, is implicitly expressed as a function of saturation S_{nn} only (which depends on the constant angle α), or

$$\frac{\partial P}{\partial x} = \frac{\partial P}{\partial x}(S_{nn}) \qquad \text{(A-7)}$$

which is determined by the injection rate, relative permeability data, and non-Newtonian fluid behavior through Equation (A-6).

The fractional flow function for the non-Newtonian phase may be written as follows (Willhite, 1986),

$$f_{nn} = \frac{1}{1 + \left[\frac{k_{rne}}{k_{rnn}}\right]\left[\frac{\mu_{nn}}{\mu_{ne}}\right]} + \frac{\frac{K\,k_{rne}}{\mu_{ne}\,u(t)}\,(\rho_{ne} - \rho_{nn})\,g\,\sin(\alpha)}{1 + \left[\frac{k_{rne}}{k_{rnn}}\right]\left[\frac{\mu_{nn}}{\mu_{ne}}\right]} \tag{A-8}$$

which is a function of S_{nn} only after considering the constraint by Equation (A-6). Then, by the exact same procedure as for the Buckley and Leverett solution, we can obtain the analytical solution for non-Newtonian displacement, Equation (18).

Appendix B. Graphic Method

The mass conservation in the system for a given time of injection gives,

$$Q(t) = \int_0^t q(\lambda)d\lambda = \int_0^{x_f}(S_{nn} - S_{nnir})\phi A dx$$

$$= \phi A x_f(S_f - S_{nnir}) - \int_0^{x_f}\phi A x dS_{nn} \tag{B-1}$$

Substituting Equation (20) into (B-1) yields,

$$Q(t) = Q(t)(S_f - S_{nnir})\left[\frac{\partial f_{nn}}{\partial S_{nn}}\right]_{S_f} - Q(t)(f_{nn}|_{S_f} - f_{nn}|_0) \tag{B-2}$$

Noting that at $x = 0$, $S_{nn} = 1 - S_{nnir}$, and $f_{nn} = 1$, therefore,

$$1 = (S_f - S_{nnir})\left[\frac{\partial f_{nn}}{\partial S_{nn}}\right]_{S_f} - f_{nn}|_{S_f} + 1 \tag{B-3}$$

or,

$$\left[\frac{\partial f_{nn}}{\partial S_{nn}}\right]_{S_f} = \frac{f_{nn}|_{S_f} - f_{nn}|_{S_{nnir}}}{S_f - S_{nnir}} \tag{22}$$

in which $f_{nn} = 0$ at $S_{nn} = S_{nnir}$ is used, and both f_{nn} and $\partial f_{nn}/\partial S_{nn}$ are evaluated at the shock saturation S_f.

Similarly, the average saturation in the displaced zone is defined as,

$$\bar{S}_{nn} = \frac{\int_0^{x_f} S_{nn} A\phi dx}{\int_0^{x_f} A\phi dx} = \frac{\phi A}{\phi A x_f}\int_0^{x_f} S_{nn} dx \tag{B-4}$$

then

$$\phi A x_f(\bar{S}_{nn} - S_{nnir}) = \phi A\int_0^{x_f}(S_{nn} - S_{nnir})dx = Q(t) \tag{B-5}$$

Using Equation (20) again, we will have,

$$\left[\frac{\partial f_{nn}}{\partial S_{nn}}\right]_{S_f} = \frac{1}{\bar{S}_{nn} - S_{nnir}} \tag{23}$$

Appendix C. Equivalent Darcy's Law Viscosity

For a power-law non-Newtonian fluid, one describes the relationship of shear stress τ and shear rate $\dot{\gamma}$ as,

$$\tau = H\dot{\gamma}^n \tag{C-1}$$

where n and H are parameters, called power-law index and consistency of the power-law fluid. The power-law index is a dimensionless constant, and for pseudoplastic fluids ranges over $0 < n < 1$. The consistency H has units ($Pa \cdot s^n$), depending on the index n. For a Newtonian fluid, n = 1 and the viscosity equals the constant H.

" Apparent viscosity " for a power-law non-Newtonian fluid is defined as (Ikoku and Ramey, 1980),

$$\mu_{app} = H\dot{\gamma}^{n-1} \tag{C-2}$$

For single phase flow, the modified Blake-Kozeny equation for one-dimensional flow of power-law fluids gives (Savins, 1969; Bird et al, 1960; and Christopher et al, 1965),

$$u = \left[\frac{K}{\mu_{eff}}\left[-\frac{\partial P}{\partial x}\right]\right]^{\frac{1}{n}} \tag{C-3}$$

where " effective viscosity " μ_{eff} is defined as,

$$\mu_{eff} = \frac{H}{12}(9 + \frac{3}{n})^n (150K\phi)^{(1-n)/2} \tag{C-4}$$

For the two phase flow problem, we extend Equation (C-4) by replacing K by Kk_{rnn} and ϕ by $\phi(S_{nn} - S_{nnir})$, to obtain

$$\mu_{eff} = \frac{H}{12}(9 + \frac{3}{n})^n [150Kk_{rnn}(S_{nn})\phi(S_{nn} - S_{nnir})]^{\frac{1-n}{2}} \tag{C-5}$$

In the numerical simulation, we wish to relate the volumetric flow rate to the pressure gradient as is normally done in multiple-phase extension of Darcy' law, with all of the nonlinearities combined into an equivalent non-Newtonian viscosity. Thus, we write

$$u = -\frac{Kk_{rnn}}{\mu_{nn}}\frac{\partial P}{\partial x} \tag{C-6}$$

and require that this volumetric flux be equal to the expression of Equation (C-3),

$$-\frac{Kk_{rnn}}{\mu_{nn}}\frac{\partial P}{\partial x} = \left[\frac{Kk_{rnn}}{\mu_{eff}}\left[-\frac{\partial P}{\partial x}\right]\right]^{\frac{1}{n}} \tag{C-7}$$

Solving for μ_{nn}, we obtain,

$$\mu_{nn}\left[S_{nn}, \frac{\partial P}{\partial x}\right] = \mu_{eff}\left[\frac{Kk_{rnn}(S_{nn})}{\mu_{eff}}(-\frac{\partial P}{\partial x})\right]^{\frac{n-1}{n}} \tag{C-8}$$

REFERENCES

Bird, R. B. , Stewart, W. E. and Lightfoot, E. N. (1960) : *Transport Phenomena* , Wiley, New York.

Buckley, S. E. and Leverett, M. C. (1942) : " Mechanism of Fluid Displacement in Sands, " *Trans*. AIME 146, 107-116.

Chen, Z. X. (May 1988) : " Some Invariant Solutions to Two-Phase Fluid Displacement Problems Including Capillary Effect, " *SPE Reservoir Engineering,* 691-700.

Christopher, R. H. and Middleman, S. (Nov. 1965) : " Power-Law Flow through a packed Tube, " *I & EC Fundamentals,* Vol.4, No.4., 422-426.

Fayers, F. J. and Perrine, R. L. (1959) : " Mathematical Description of Detergent Flooding in oil Reservoirs, " *trans*. AIME. **216**, 277-283.

Gencer, C. S. and Ikoku, C.U. (June 1984) : " Well Test Analysis for Two-Phase flow of Non-Newtonian Power-law and Newtonian Fluids, " ASME *Journal of Energy Resources Technology,* 295-304.

Gogarty, W. B. (June 1967) : " Rheological Properties of Pseudo Plastic Fluids in Porous Media, " *Soc. Pet. Eng. J.* , 149-159.

Helfferich, F. G. (Feb. 1981) : " Theory of Multicomponent, Multiphase Displacement in Porous Media, " *Soc. Pet. Eng. J.* , 51-62.

Hirasaki, G. J. (Apr. 1981) : " Application of the Theory of Multicomponent, Multiphase Displacement to Three-Component, Two-Phase surfactant Flooding, " *Soc. Pet. Eng. J.* , 191-204.

Ikoku, C. U. (June 1982) : " Well Test Analysis of Enhanced oil Recovery Project, " ASME. *Journal Energy Resources Technology,* 142-148.

Ikoku, C. U. and Ramey, H. J. Jr. (Feb. 1980) : " Wellbore Storage and Skin Effects during Polymer Flow in petroleum reservoirs, " ASME. *Journal of Energy Resources Technology,* 149-156.

Ikoku, C. U. and Ramey, H. J. Jr. (June 1979) : " Transient Flow of Non-Newtonian Power-Law Fluids in Porous Media, " *Soc. Pet. Eng. J. , 164-174.*

Larson, R. G., Davis, H. T. and Scriven, L. E. (Feb. 1982) : " Elementary Mechanism of Oil Recovery by Chemical Methods," *Soc. Pet. Eng. J.* , 243-258.

Larson, R. G. and Hirasaki, G. J. (Feb. 1978) : " Analysis of the Physical mechanisms in Surfactant flooding, " *Soc. Pet. Eng. J.* , 42-58.

Lund, O. and Ikoku, C. U. (Apr. 1981) : " Pressure Transient Behavior of Non-Newtonian / Newtonian Fluid Composite Reservoirs, " *Soc. Pet. Eng. J.* , 271-280.

McDonald, A. E. (1979) : " Approximate Solutions for Flow of Non-Newtonian Power-law Fluids through porous Media, " Paper SPE 7690 presented at the SPE- AIME Fifth Symposium on Reservoir Simulation, Denver.

Odeh, A. S. and Yang, H. T. (June 1979) : " Flow of Non-Newtonian Power-Law Fluids through Porous Media, " *Soc. Pet. Eng. J. , 155-163.*

Patton, J. T., Coats, K. H. Colegroue, G. T. (Mar. 1971) : " Prediction of Polymer Flood Performace, " *Soc. Pet. Eng. J. , Trans.,* AIME.251, 72-84.

Pope, G. P. (June 1980) : " The Application of Fractional Flow Theory to Enhanced Oil Recovery, " *Soc. Pet. Eng. J.* , 191-205.

Pruess, K. (1982) : " Development of the General Purpose Simulator MULKOM, " *Annual Report* , Earth Sciences Division, Lawrence Berkeley Laboratory, Berkeley CA.

Pruess, K. and Wu, Y. -S (1988) : " On PVT-Data, Well Treatment, and Preparation of Input Data for an Isothermal Gas-Water-Foam Version of MULKOM, " Report LBL-25783, UC-403, Earth Sciences Division, Lawrence Berkeley Laboratory. CA.

Savins, J. G. (1969) : " Non-Newtonain Flow through Porous Media, " *Ind. Eng. Chem.* , 61, 18-47.

Scheidegger, A. E. (1974) : *The Physics of Flow through Porous Media* , University of Toronto Press.

Sheldon, J. W., Zondek, B. and Cardwell, W. T. Jr. (Aug. 1959) : " One-Dimensional,Incompressible, Noncapillary, Two-Phase Fluid Flow in a Porous Medium, " *trans,* AIME. 216, 290-296.

Taber, J. J., Kamath, I. S. K. and Reed, R. L. (Sept. 1961) : " Mechanism of Alcohol Displacement of Oil from Porous Media, " *Soc. Pet. Eng. J.,* AIME. 222, 195-209.

van Poolen, H. K. and Jargon, J. R. (Mar. 1969) : " Steady-State and Unsteaty-State Flow of Non-Newtonian Fluids through Porous Media, " *Soc. Pet. Eng. J.* , AIME. 246, 80-88.

Vongvuthipornchai, S. and Raghavan, R. (Dec. 1987) : " Pressure Falloff Behavior in Vertically Fractured Wells: Non-Newtonian Power-Law Fluids, " *SPE Formation Evaluation* , 573-587.

Vongvuthipornchai, S. and Raghavan, R. (Dec. 1987) : " Well Test Analysis of data Dominated by Storage and Skin: Non-Newtonian Power-Law Fluids, " *SPE Formation Evaluation* , 618-628.

Wachmann, C. (Aug. 1964) : " A Mathematical Theory for the Displacement of Oil and Water by Alcohol, " *Soc. Pet. Eng. J.* , 250-266.

Welge, H. J. (1952) : " A Simplified Method for Computing Oil Recovery by Gas or Water Drive, " *Trans.* , AIME 3, 108.

Willhite, G. P. : I. Waterflooding , SPE Textbook Series, Society of Petroleum Engineers, Richardson, TX. 1986.

Yortsos, Y. C. and Fokas, A. S. (Feb. 1983) : " An Analytical Solution for Linear Waterflood Including the Effects of Capillary Pressure, " *Sec. Pet. Eng. J.,* 115-124.

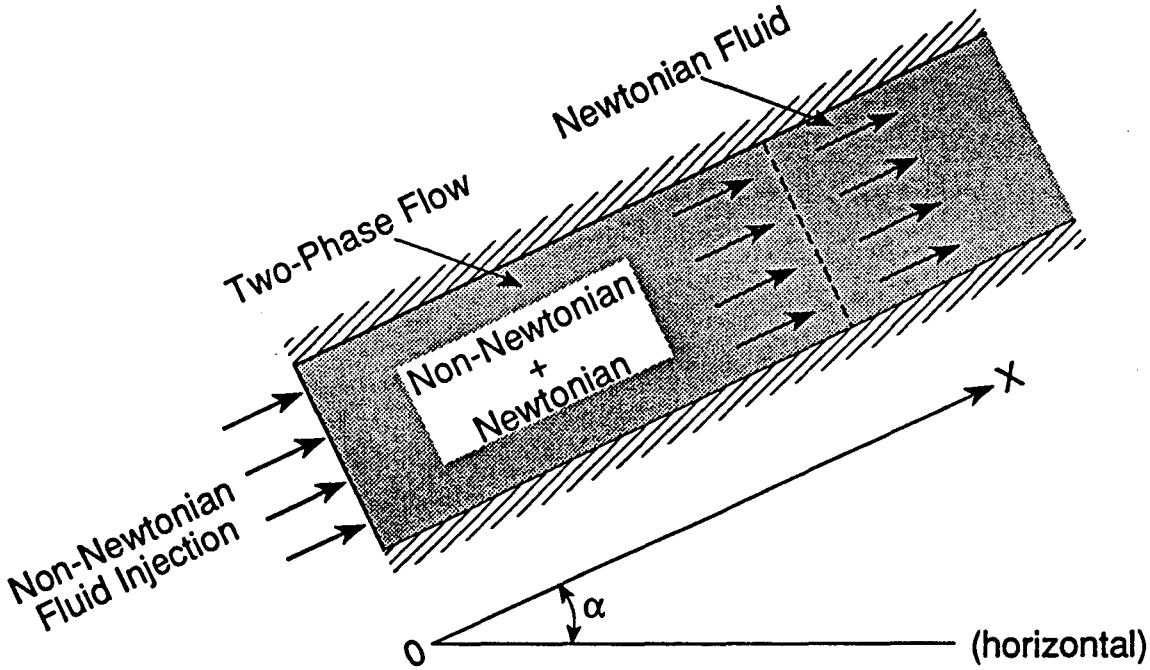

XBL 895-7624

Figure 1. Schematic of Displacement of a Newtonian Fluid by a Non-Newtonian Fluid

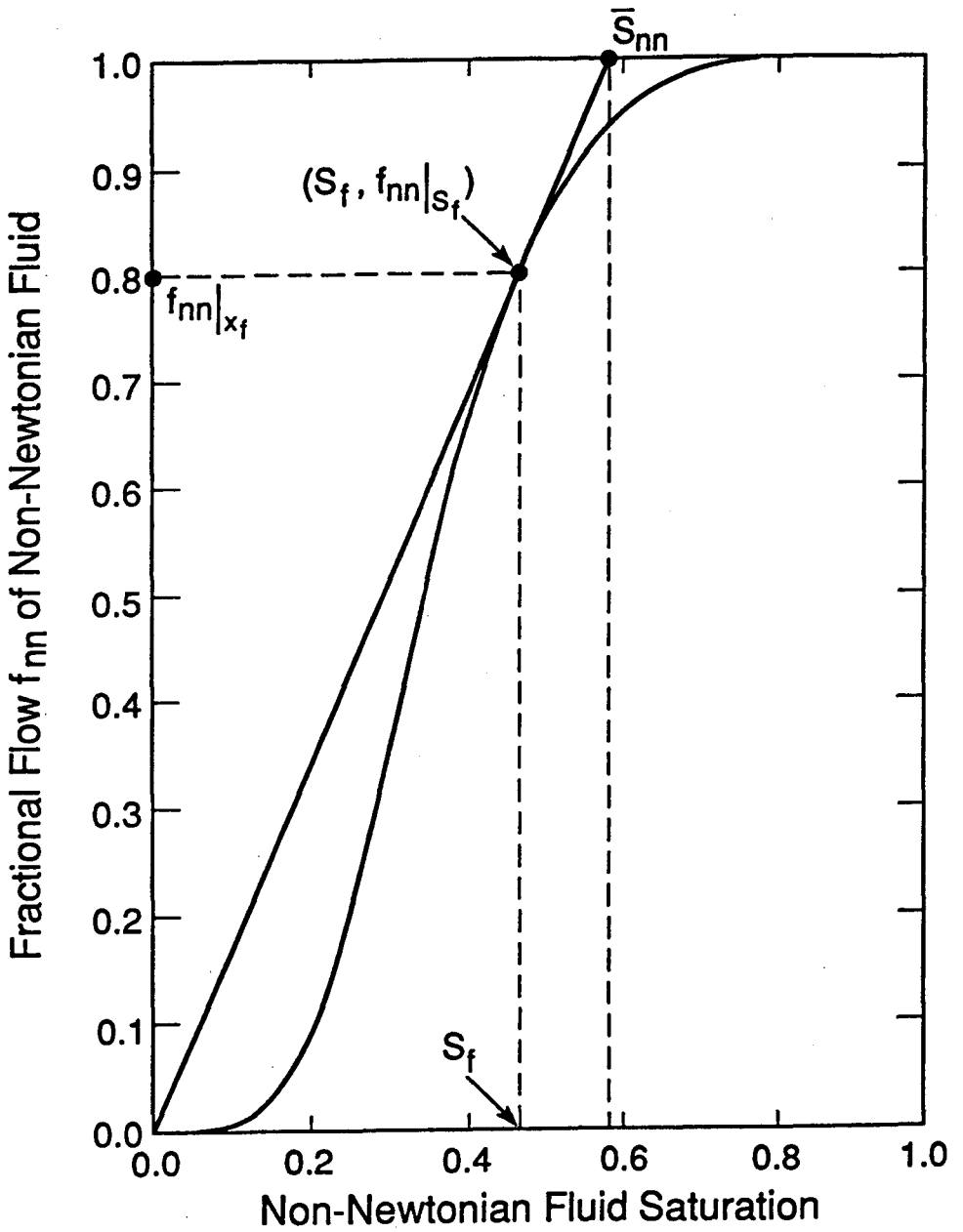

XBL 895-7621

Figure 2. Method of Determining Shock Front and Average Displacing Non-Newtonian Phase Saturations from Fractional Flow Curves

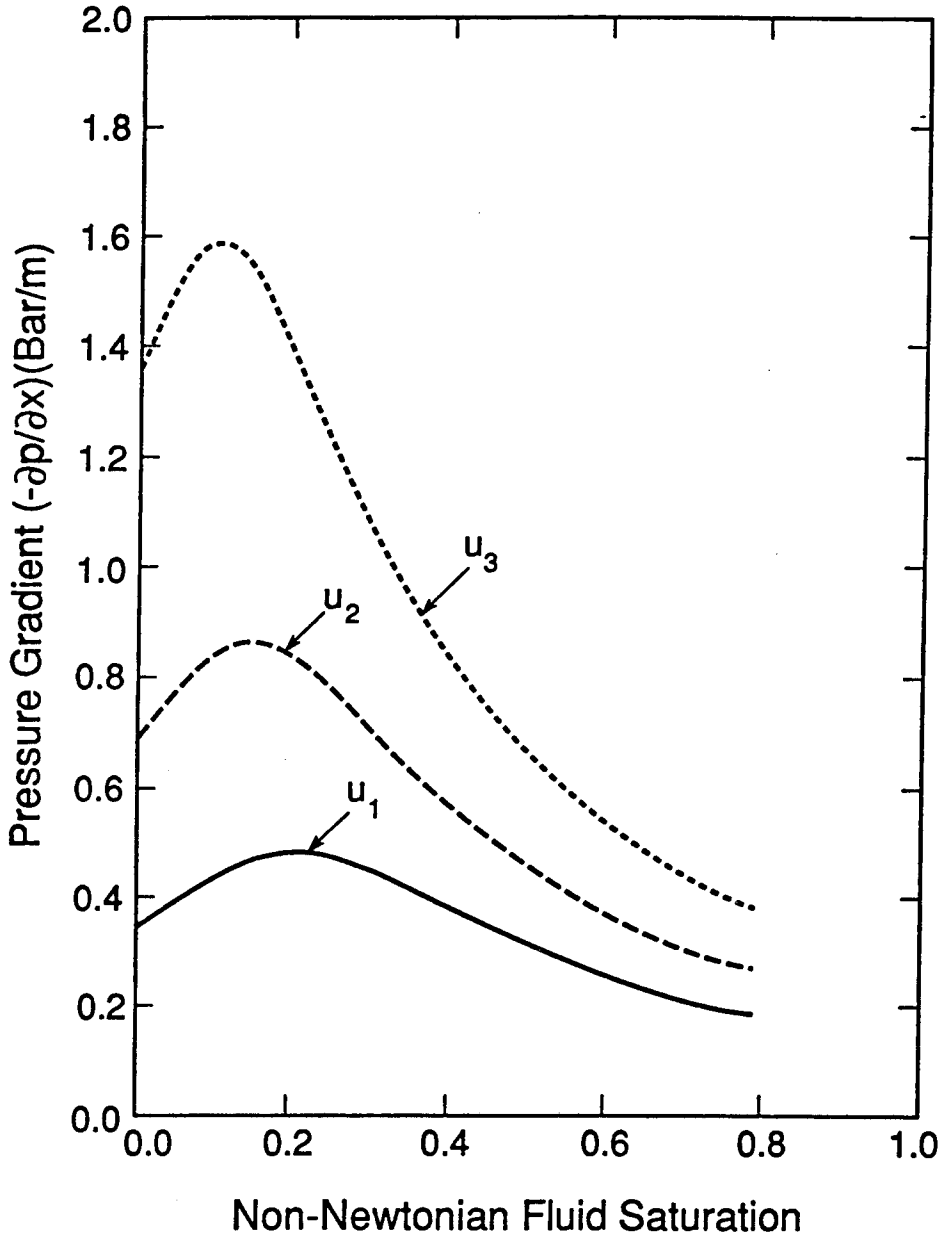

XBL 893-7618

Figure 3. Pressure Gradients versus Displacing Non-Newtonian Phase Saturation for Different Injection Rates

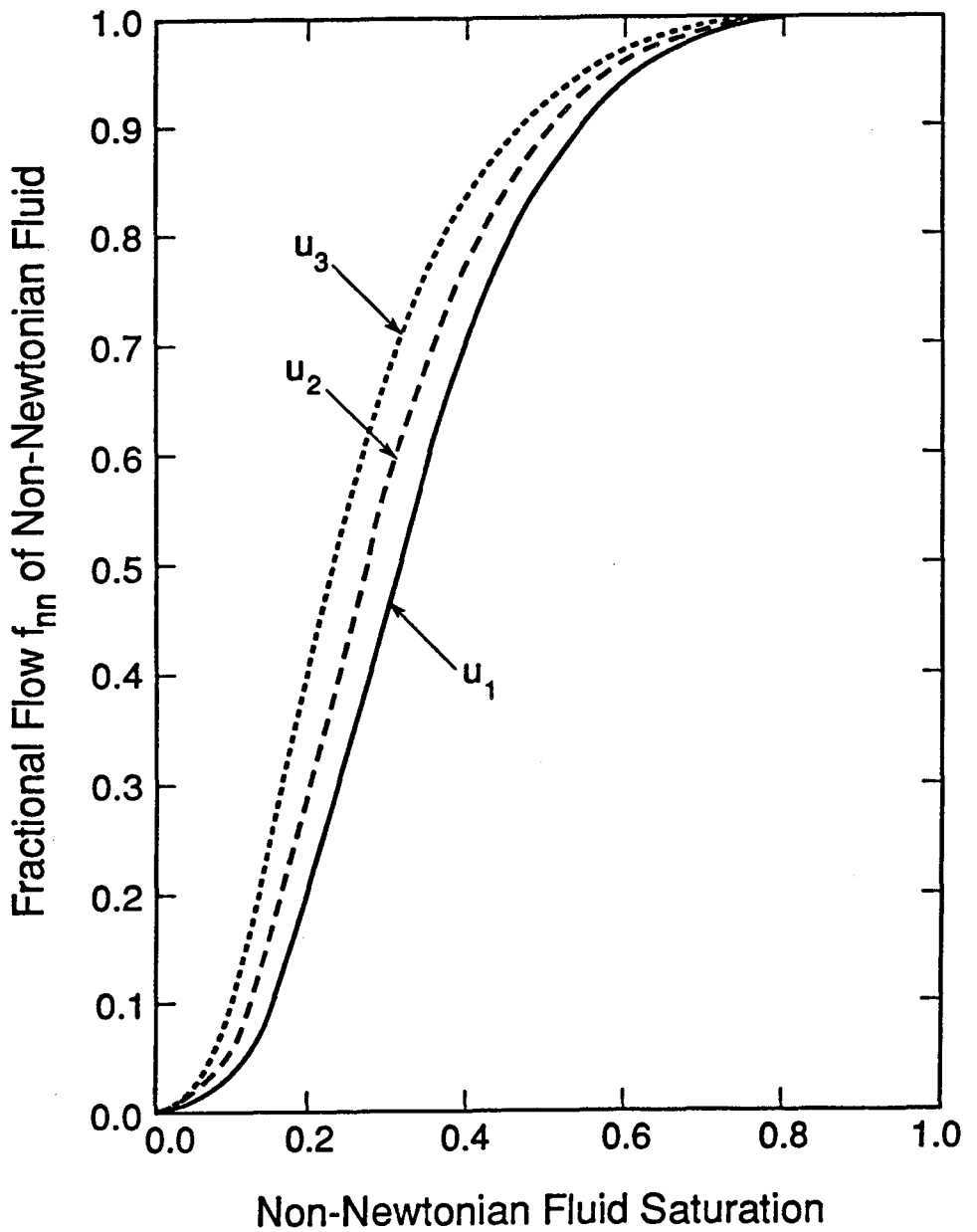

Figure 4. Fractional Flow Curves of Non-Newtonian Fluids for Different Injection Rates

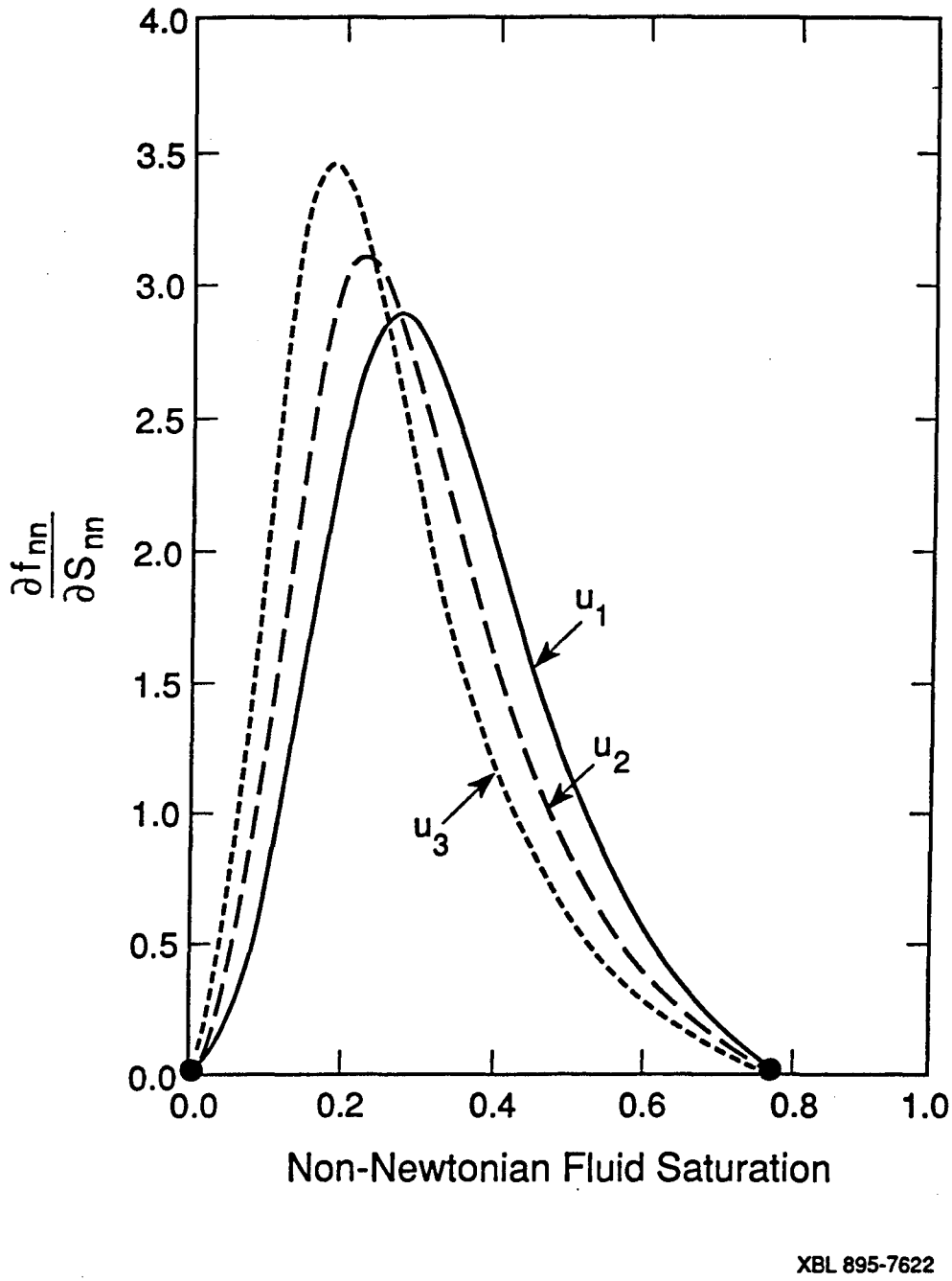

Figure 5. Derivatives of Fractional Flow with Respect to Non-Newtonian Phase Saturation for Different Injection Rates

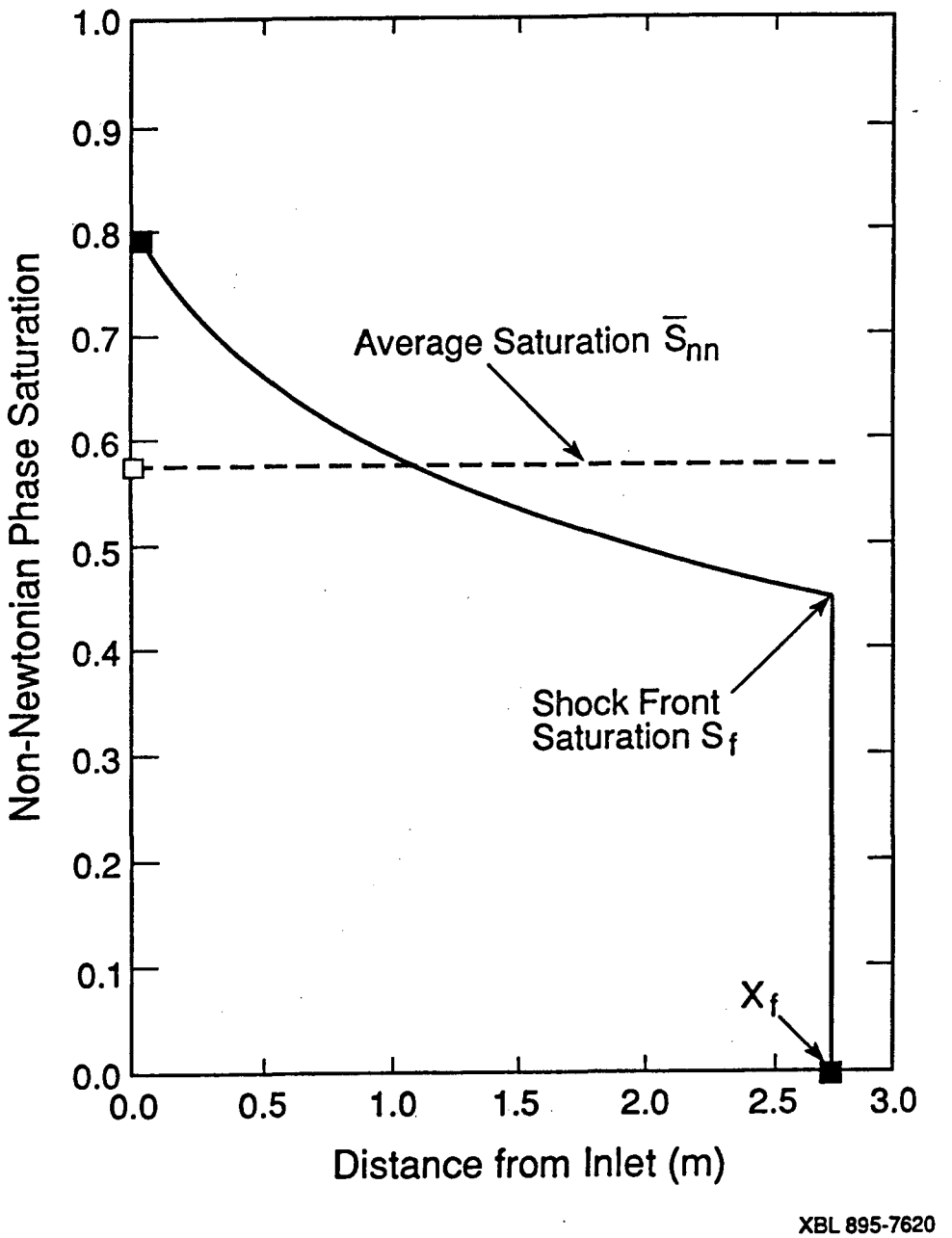

Figure 6. Saturation Distributions of Non-Newtonian Fluids in the System at a Given Injection Time

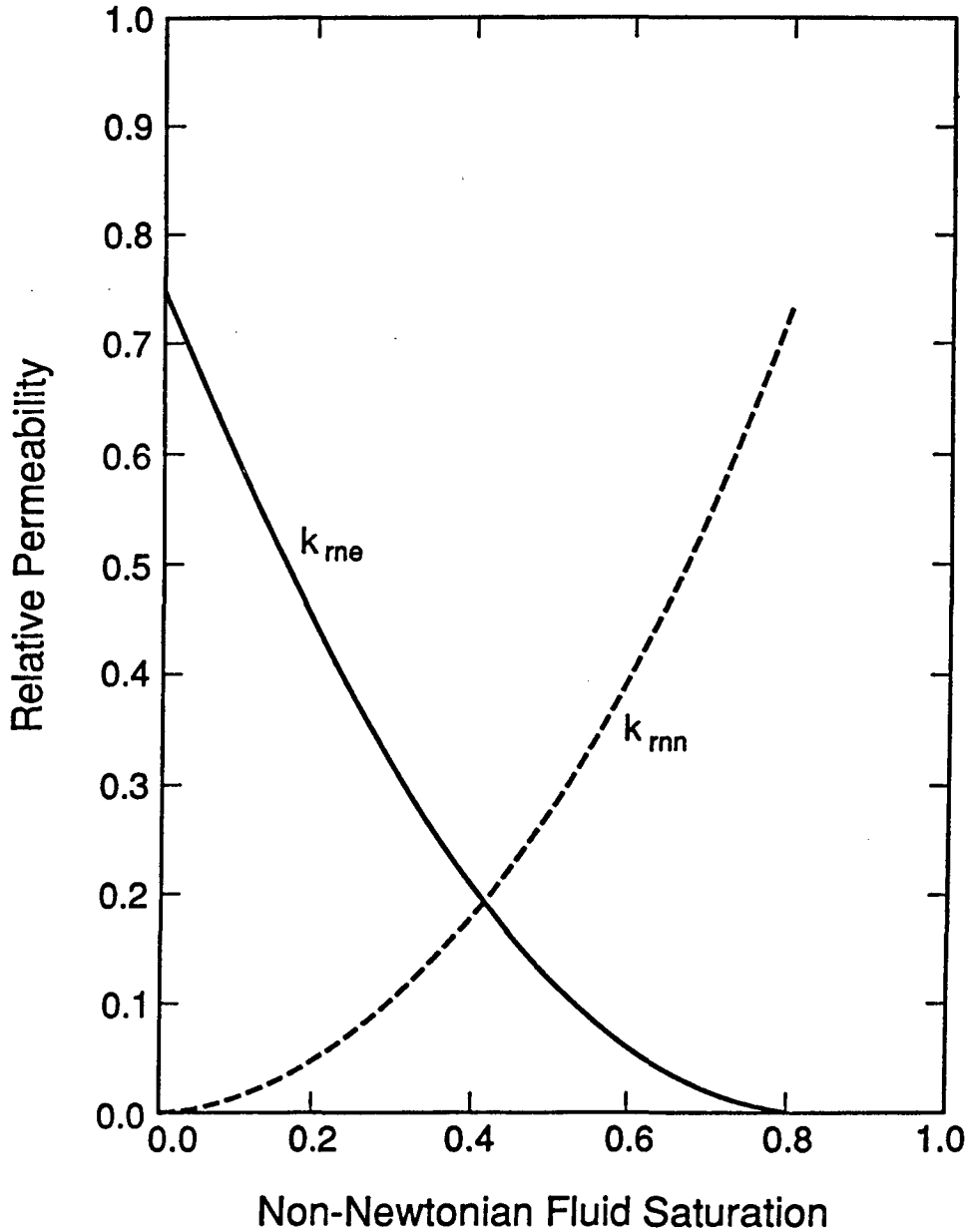

XBL 893-7521
T.I.D. Illus. 88
3/29/89

Figure 7. Relative Permeability Functions Used for All Calculations

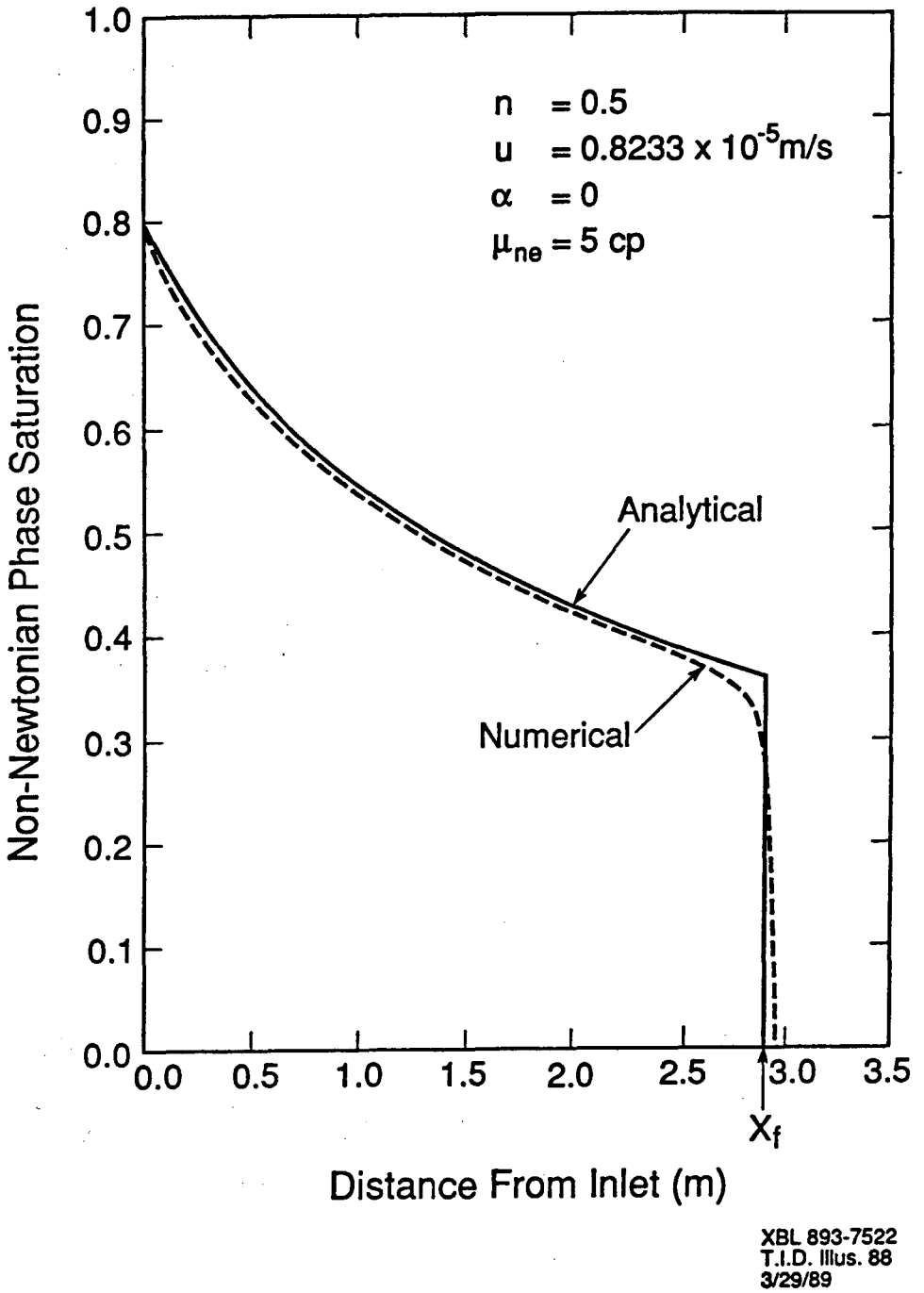

Figure 8. Comparison of Saturation Profiles Calculated from Analytical and Numerical Solutions after 10 Hours of Injection

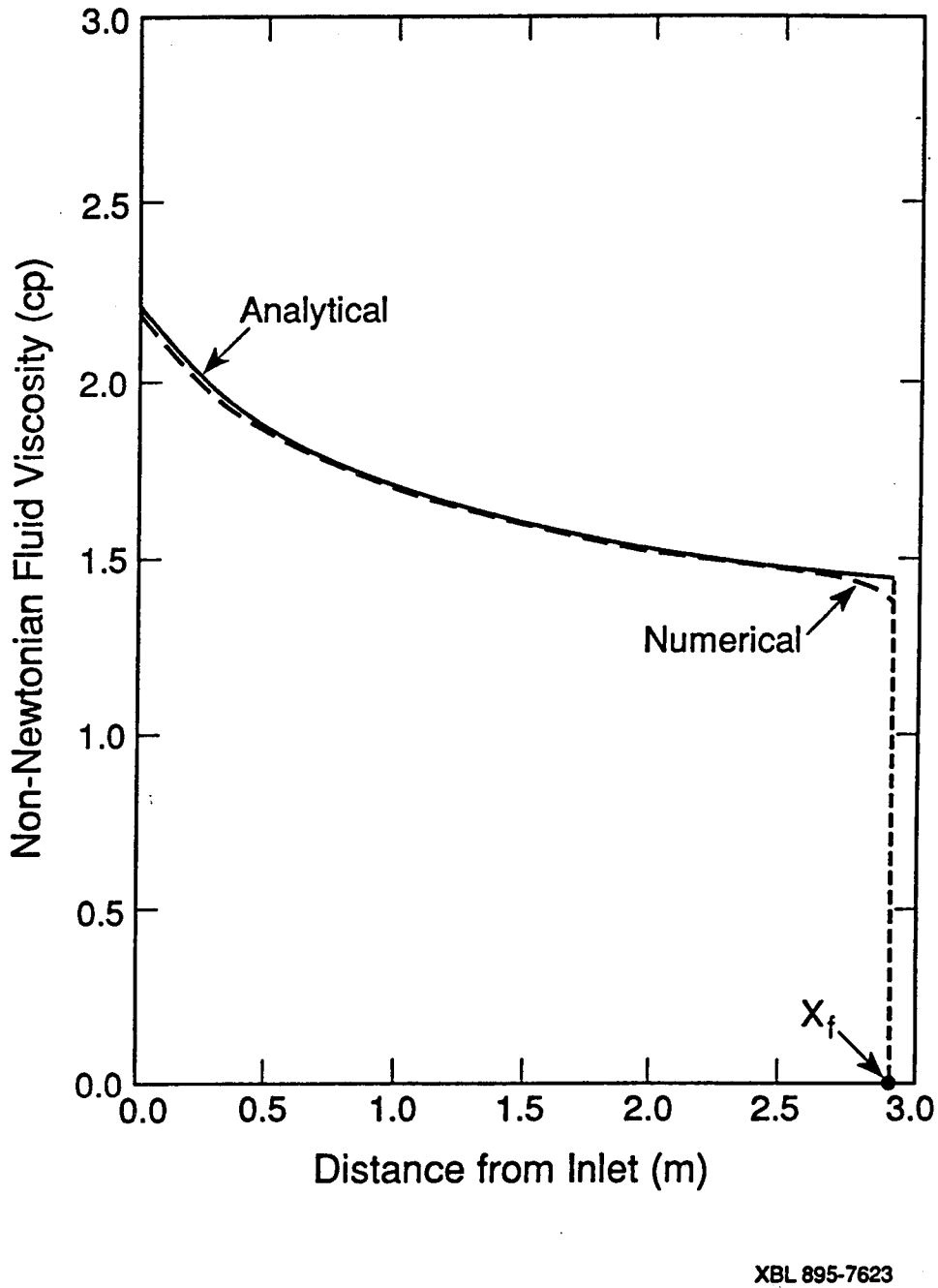

Figure 9. Comparison of Non-Newtonian Fluid Equivanlent Viscosity Profiles Calculated from Analytical and Numerical Solutions after 10 Hours of Injection

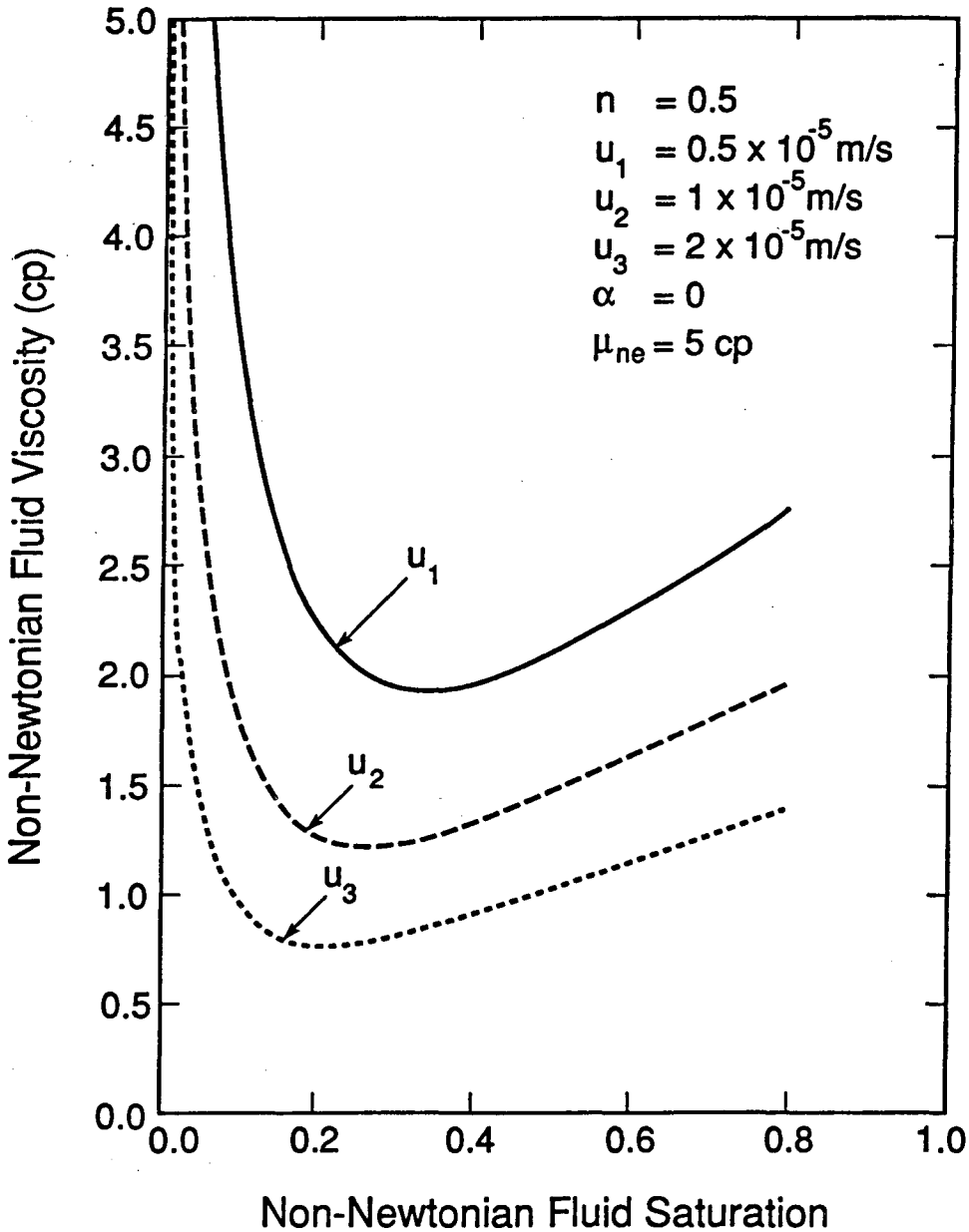

XBL 893-7513
T.I.D. Illus. 88
3/29/89

Figure 10. Non-Newtonian Phase Apparent Viscosities versus Non-Newtonian Phase Saturation for Different Injection Rates

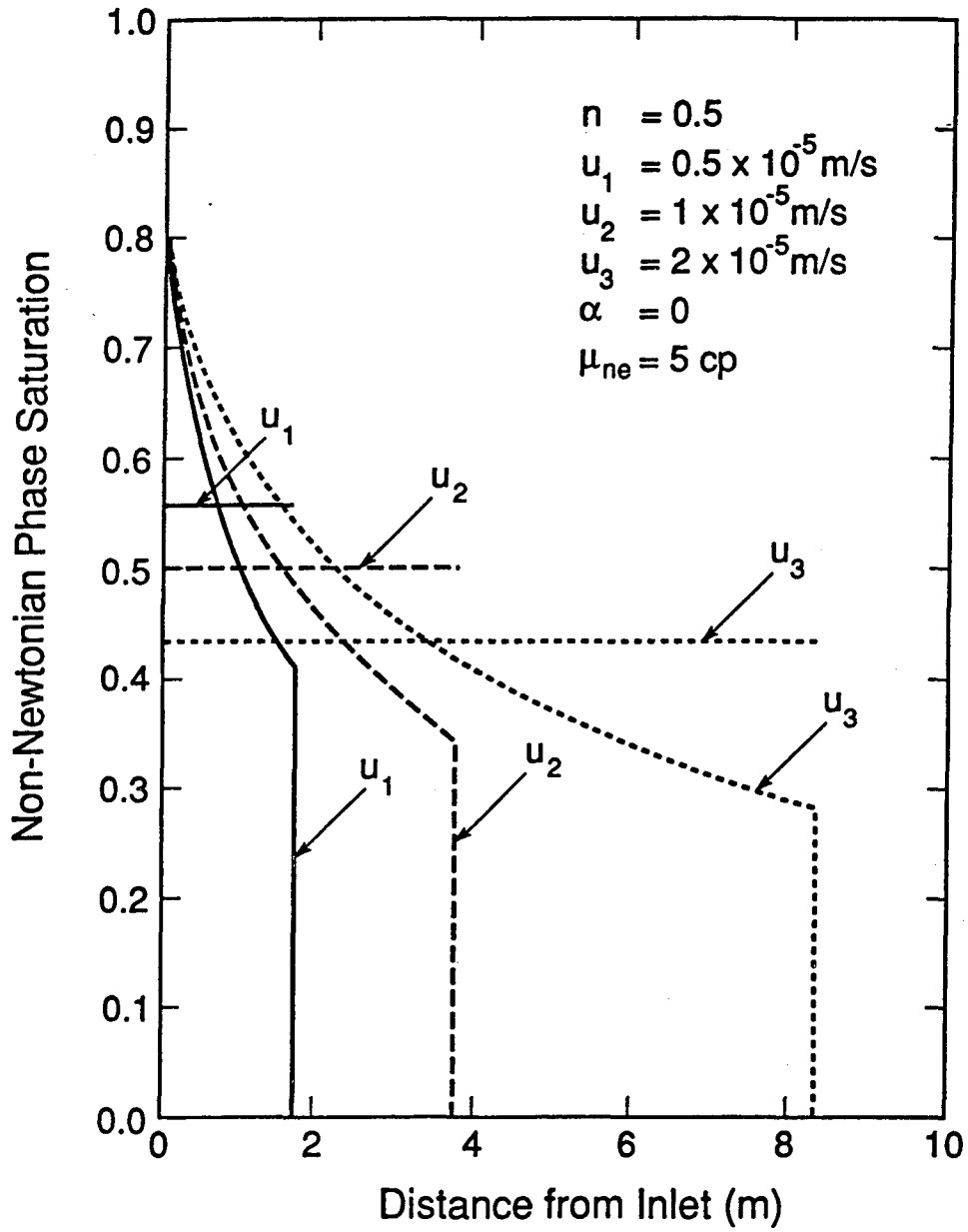

XBL 893-7514
T.I.D. Illus. 88
3/29/89

Figure 11. Non-Newtonian Phase Saturation Distributions for Different Injection Rates after 10 Hours of Injection

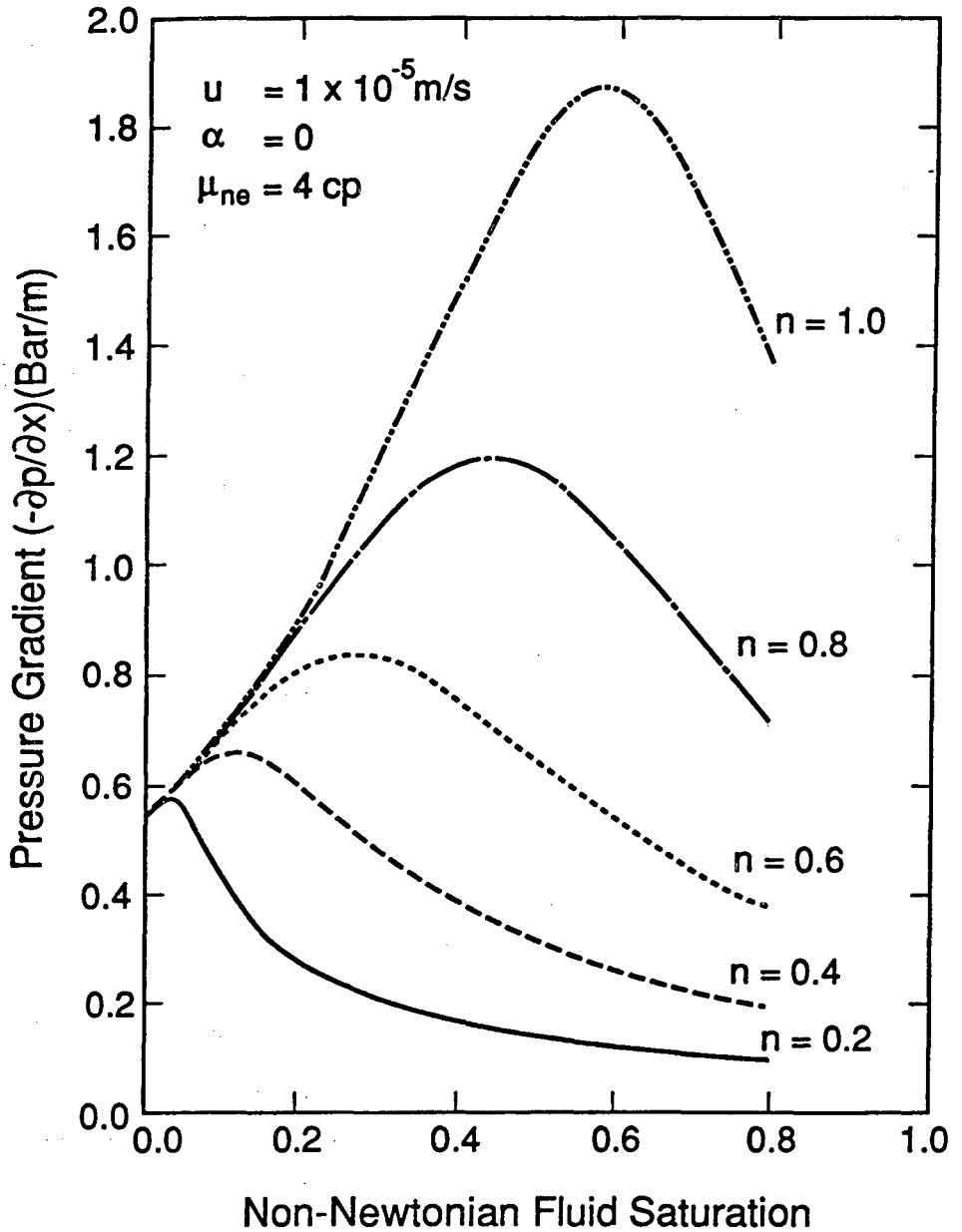

XBL 893-7519
T.I.D. Illus. 88
3/29/89

Figure 12. Effects of the Power-Law Index on Pressure Gradients

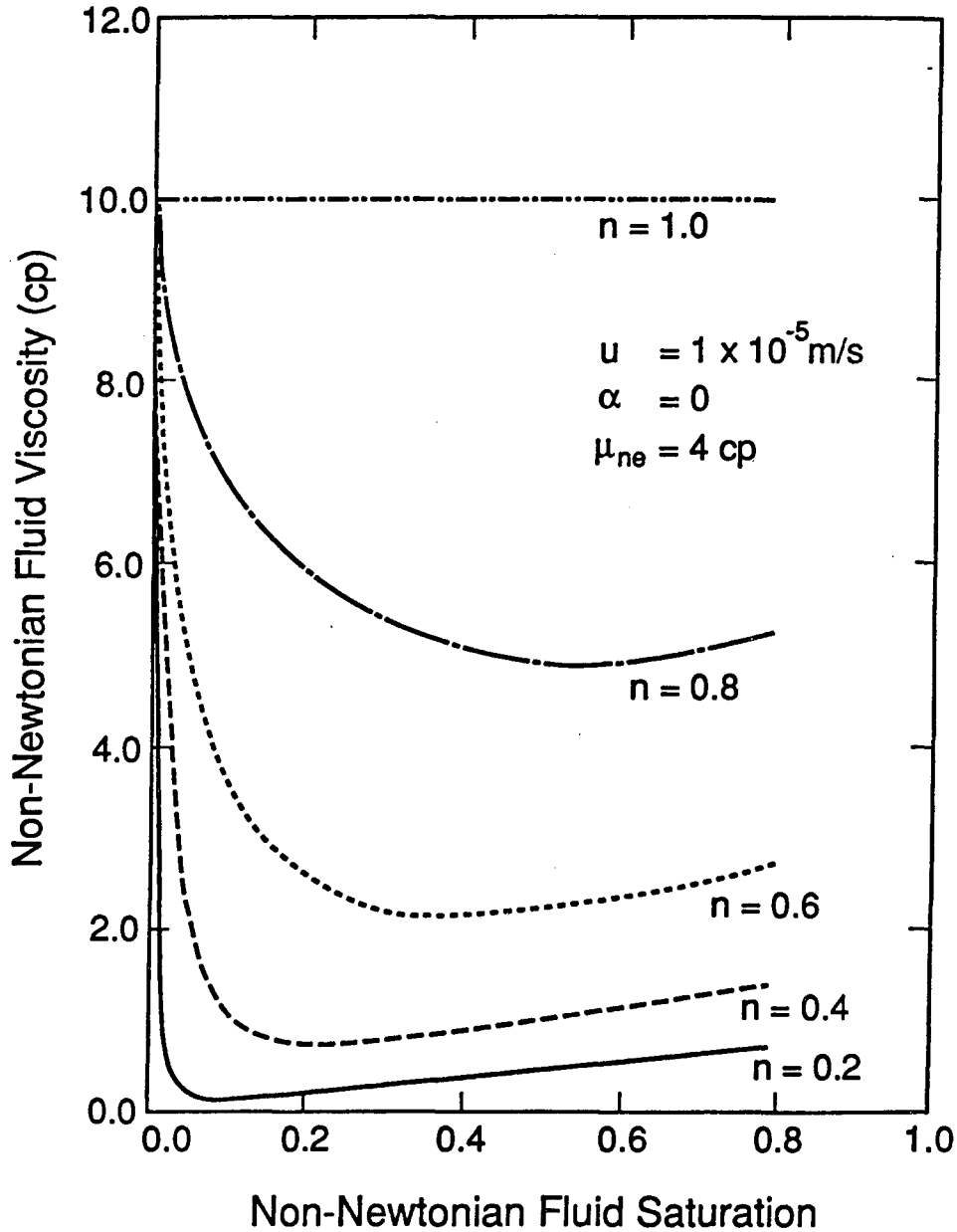

XBL 893-7517
T.I.D. Illus. 88
3/29/89

Figure 13. Effects of the Power-Law Index on Non-Newtonian Phase Equivanlent Viscosity

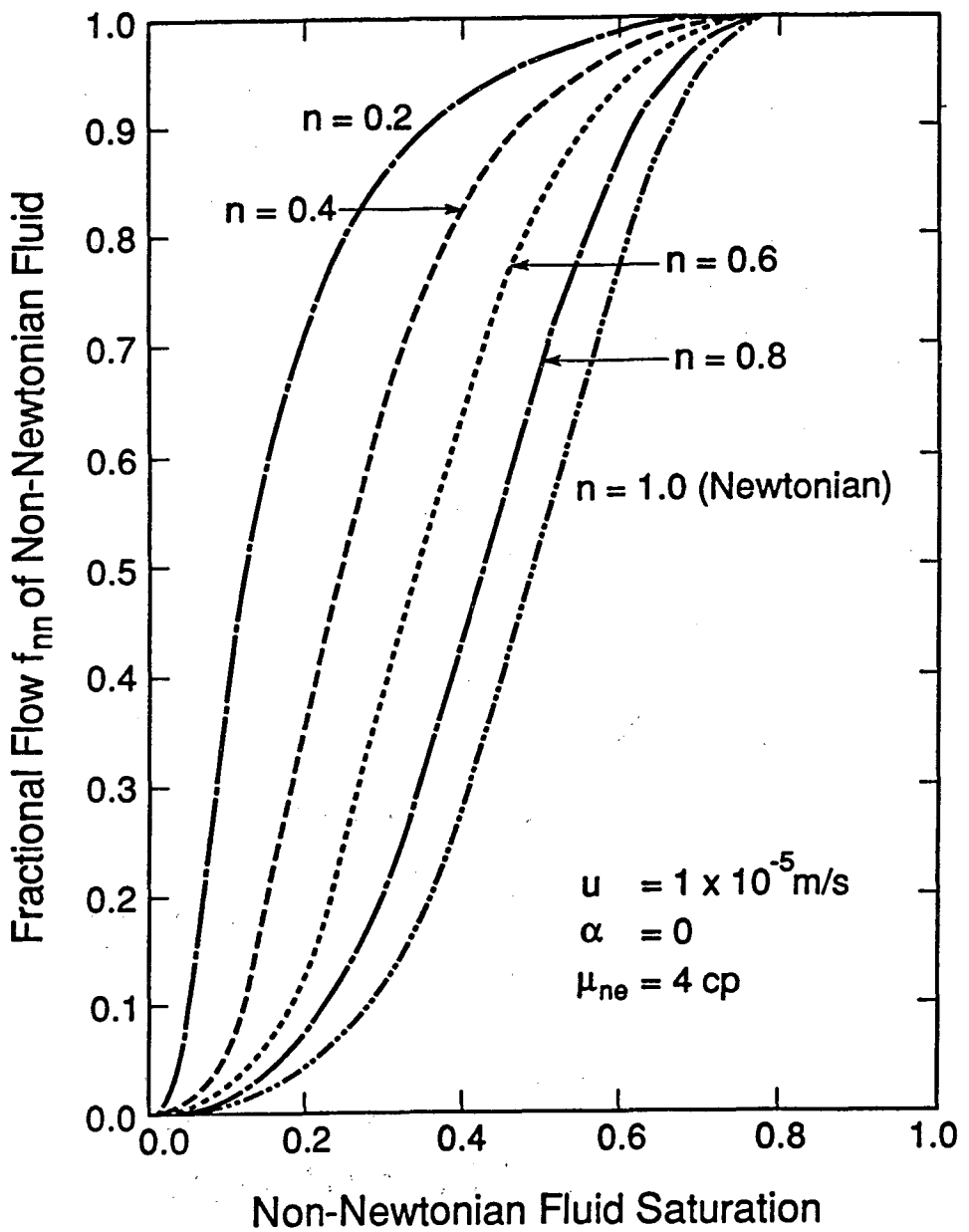

XBL 893-7518
T.I.D. Illus. 88
3/29/89

Figure 14. Effects of the Power-Law Index on Non-Newtonian Phase Fractional Flow

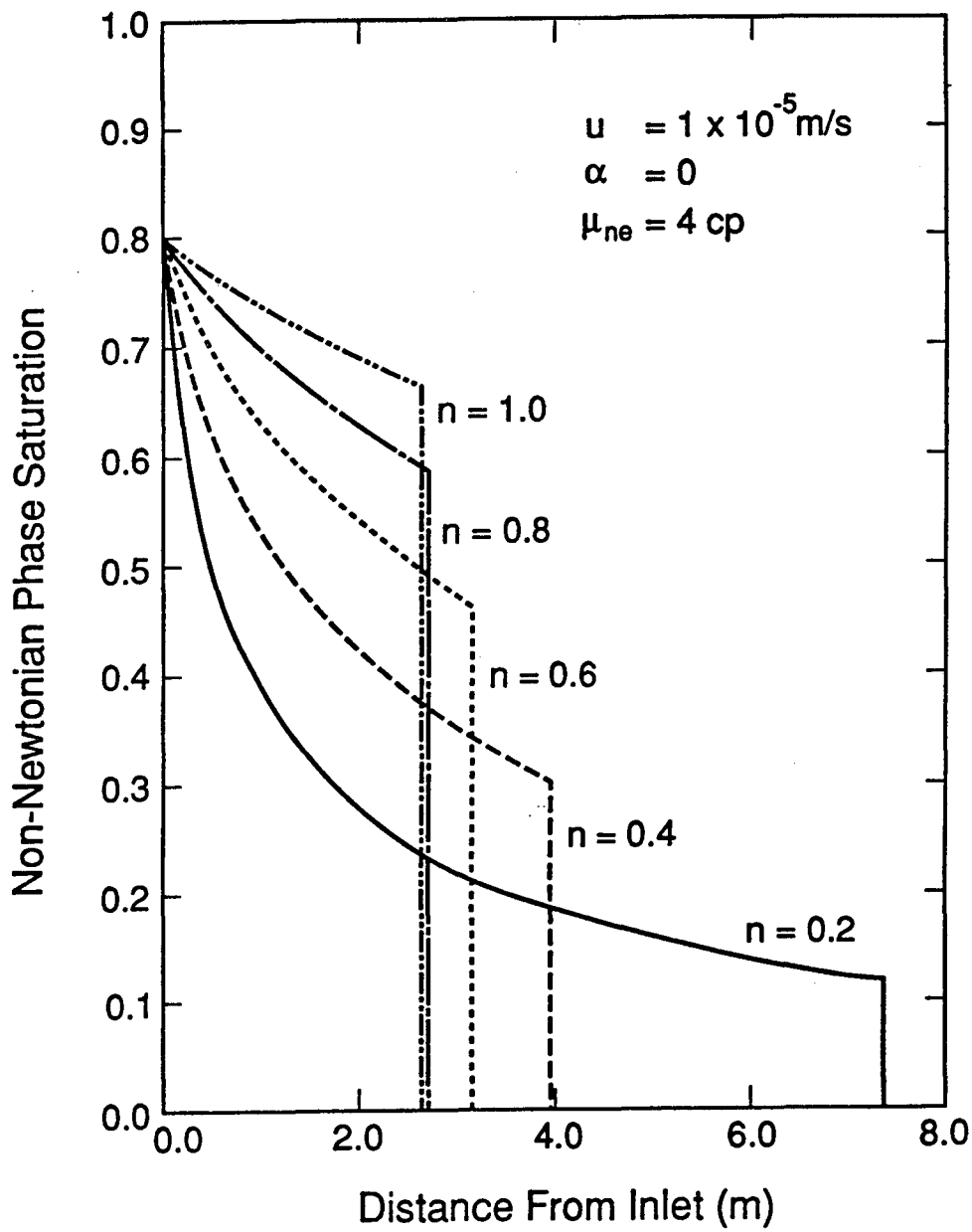

XBL 893-7520
T.I.D. Illus. 88
3/29/89

Figure 15. Non-Newtonian Phase Saturation Distributions, Effects of the Power-Law Index on Displacement Efficiency

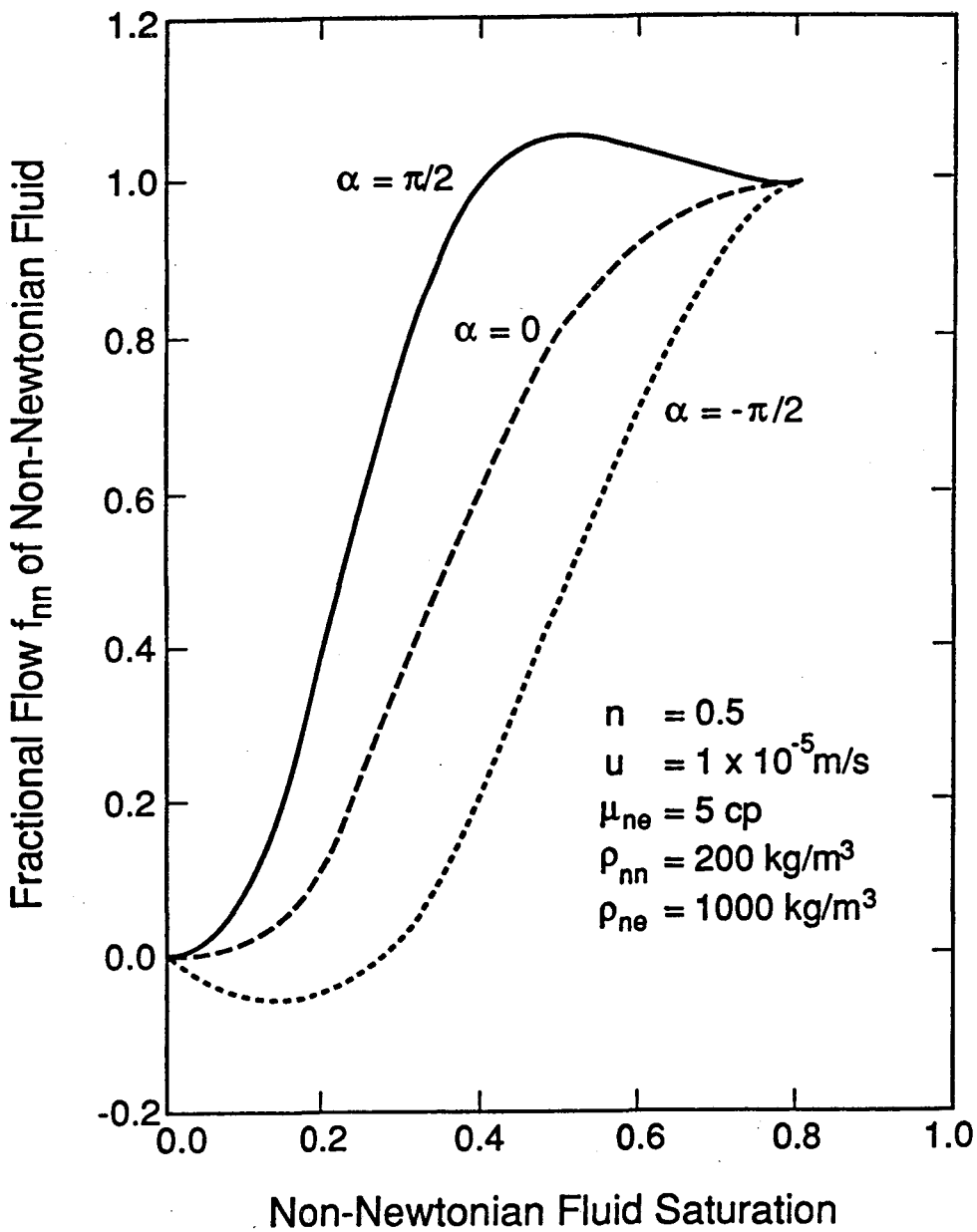

XBL 893-7515
T.I.D. Illus. 88
3/29/89

Figure 16. Fractional Flow Curves Including Gravity Effects

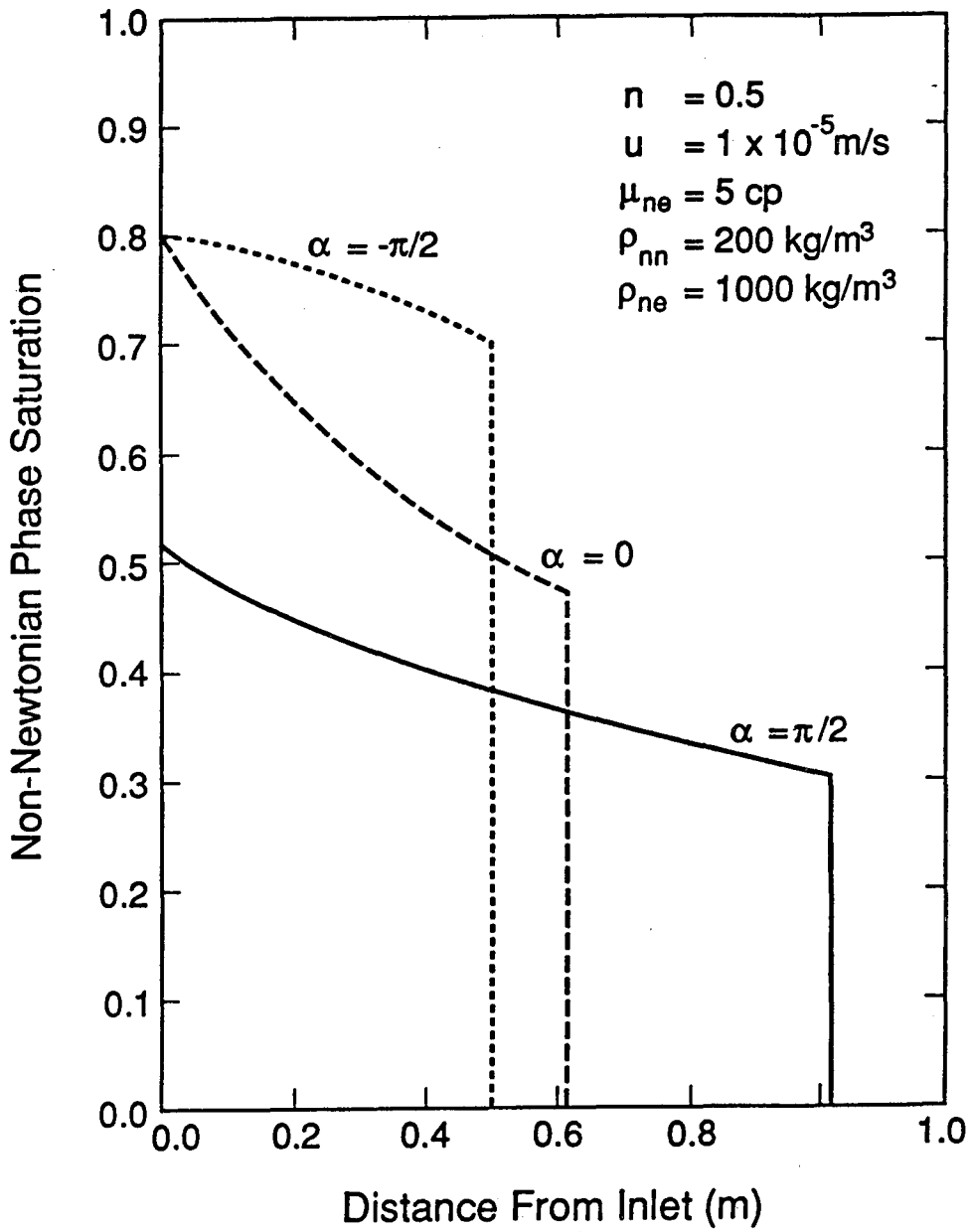

XBL 893-7516
T.I.D. Illus. 88
3/29/89

Figure 17. Non-Newtonian Phase Saturation Distributions, Effects of Gravity on Displacement Efficiency

LAWRENCE BERKELEY LABORATORY
TECHNICAL INFORMATION DEPARTMENT
1 CYCLOTRON ROAD
BERKELEY, CALIFORNIA 94720